TECHNISCHE UNIVERSITÄT MÜNCHEN

Fakultät für Medizin

The role of the long-noncoding RNA Gm12606 in irradiated and in ageing murine mesenchymal stem cells

Martina Schuster

Vollständiger Abdruck der von der Fakultät für Medizin der Technischen Universität München zur Erlangung des akademischen Grades einer Doktorin der Naturwissenschaften genehmigten Dissertation.

Vorsitz: Prof. Dr. Dr. Stefan Engelhardt

Prüfende/-r der Dissertation:

1. Prof. Dr. Michael John Atkinson

2. apl. Prof. Dr. Johannes Beckers

Die Dissertation wurde am 24.06.2021 bei der Technischen Universität München eingereicht und durch die Fakultät für Medizin am 09.11.2021 angenommen.

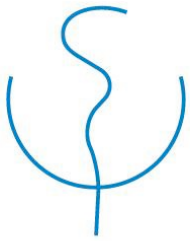

Doctoral thesis

TECHNISCHE UNIVERSITÄT MÜNCHEN

Faculty of Medicine

The role of the long-noncoding RNA Gm12606 in irradiated and in ageing murine mesenchymal stem cells

Martina Schuster

Content

I. Abbreviations

°C	Degree Celsius
β-gal	Beta-galactosidase
γ	Gamma-rays
γ-H2AX	Gamma H2A histone family member X
µg	Microgram
µL	Microlitre
ANRIL	Antisense non-coding RNA in the INK4 locus
ARF	Alternate reading frame
AS	Antisense
ASO	Antisense oligonucleotide
Bendr	Bend4-regulating effects not dependent on the RNA
BM	Bone marrow
bp	Base pair
Cas9	CRISPR associated protein 9
CCAT1	Colon Cancer Associated Transcript 1
CDK	Cyclin-dependant kinase
CDKNA2A	Cyclin-dependent kinase inhibitor 2A
cDNA	Complementary desoxyribonucleic acid
ceRNA	Competing endogenous ribonucleic acid
CFU-Fs	Colony-forming unit-fibroblastic
Chr.	Chromosome
circRNA	Circular ribonucleic acid
cM	Centimorgan

Abbreviations

CRISPR	Clustered Regularly Interspaced Short Palindromic Repeats
CVD	Cardiovascular disease
d	Day
DAPI	4',6-Diamidino-2-phenylindol
DDR	DNA damage response
DNA	Desoxyribonucleic acid
DNA-DSB	DNA double strand break
eRNA	Enhancer-derived ribonucleic acid
FBS	Fetal bovine serum
Fendrr	FOXF1 Adjacent Non-Coding Developmental Regulatory RNA
FISH	Fluorescence in-situ hybridization
g	Gram
Gm12606-1$^{+/+}$	Gm12606 transcript 1 exon1 wild-type mice
Gm12606-1$^{-/-}$	Gm12606 transcript 1 exon1 mutant mice
Gy	Gray
h	Hour
H3K27me3	Trimethylation at lysine 27 of histone H3
H19	H19 Imprinted Maternally Expressed Transcript
hMSCs	Human mesenchymal stem cells
hom	Homozygous
HOTAIR	HOX Transcript Antisense RNA)
HR	Homology directed repair
INK4	Inhibitor of CDK4
IR	Ionizing radiation
ISCT	International Society for Cellular Therapy

Abbreviations

IVF	*In-vitro* fertilization
KI	Knock-in
Klf4	Kruppel-like factor 4
KO	Knockout
l	Litre
LET	LncRNA-low expression in tumor
lincRNA	Long intergenic non-coding ribonucleic acid
LIRR1	Long intergenic radiation-responsive non-coding ribonucleic acid
lncRNA	Long non-coding ribonucleic acid
LPS	Lipopolysaccharide
M	Molar
MALAT1	Metastasis-associated lung adenocarcinoma transcript 1
MAT2A	Methionine Adenosyltransferase 2A
MDM2	Mouse double minute 2 homolog
MEG3	Maternally expressed gene 3
mg	Milligram
mGy	Milligray
MIAT	Myocardial infarction-associated transcript
min	Minute
mRNA	Messenger ribonucleic acid
MIR31HG	MicroRNA31 Host Gene
miRNA	Micro ribonucleic acid
mL	Millilitre
mM	Millimolar
mMSC	Murine mesenchymal stem cell

MSC	Mesenchymal stem cell
mOB	Mouse osteoblast
Morrbid	Myeloid RNA regulator of Bim-induced death
MOS	Mouse osteosarcoma
mut	Mutant
NEAT1	Nuclear Enriched Abundant Transcript 1
ng	Nanogram
NHEG	Non-homologous end-joining
NT	Non-transfected
NTC	No template control
p	protein
PANDA	P21-associated ncRNA DNA damage -activated
PARTICLE	Promoter of MAT2A-antisense radiation-induced circulating lncRNA
PAT	Promoter associated transcripts
PBS	Phosphate-buffered saline
PCR	Polymerase chain reaction
pmol	Picomol
Poly A	Polyadenylic acid
PRC2	Polycomb repressor complex 2
RB	Retinoblastoma
RNA	Ribonucleic acid
ROS	Reactive oxygen species
rpm	revolutions per minute
rRNA	Ribosomal ribonucleic acid
RT	Room temperature

Abbreviations

RT-qPCR	Real time quantitative polymerase chain reaction
SA- β-gal	Senescence associated β-galactosidase
sec	Second
Seq	Sequencing
SEM	Standard error of the mean
sgRNA	Single guide RNA
snRNA	Small nuclear ribonucleic acid
snRNP	Small nuclear ribonucleoprotein
snoRNA	Small nucleolar ribonucleic acid
TBE	TRIS-Borat-EDTA
TBP	TATA box binding protein
TERC	Telomerase ribonucleic acid component
TERRA	Telomeric repeat-containing ribonucleic acid
TERT	Telomerase reverse transcriptase
tRNA	Transfer ribonucleic acid
UTR	Untranslated region
Wincr	Wnt signaling-induced non-coding ribonucleic acid
Wnt	Wingless
WT	Wild-type
XIST	X-inactive specific transcript

1. Abstract

Mesenchymal stem cells (MSCs) are widely used in clinical settings as they attract beneficial immunomodulatory and regenerative properties. However, their use is difficult as *ex vivo* expansion is required to obtain sufficient numbers of MSCs, leading to an age-related loss of stem cell potency and an increasing number of senescent cells. Due to their long lifespan MSCs are suspected of accumulating radiation-induced mutations, potentially contributing to an increased involvement in age-related disease and cancer. In this study the relationship between radiation exposure and ageing of murine MSCs (mMSCs) was investigated and identified a potential regulatory pathway involving the long intergenic non-coding RNA Gm12606.

It was observed that Gm12606 is overexpressed in mMSCs during *ex vivo* ageing and after γ-irradiation. This increase parallels the epigenetic upregulation of the CDKN2A-Ink4a gene, with which it shares a genomic location. CDKN2A-Ink4a encodes the cell cycle regulator p16, whose expression is known to increase during cellular senescence and during cellular stress.

Although the expression of Gm12606 was shown to be radiation responsive, ageing had a more profound effect on Gm12606 levels. Knockdown of Gm12606 strongly influenced the transcription of the nearby entire Ink4a/Arf/Ink4b locus, suggesting that Gm12606 acts predominantly via a *cis*-mediated mechanism. *In vitro,* bone-marrow mMSCs from homozygous Gm12606-exon1 deficient C57BL/6 male mice retained a significantly lower percentage of cellular senescence than cells from wild-type littermates. In early passages of these cells, loss of Gm12606 also showed higher initial γH2AX and 53BP1 foci formation after 4 Gy. At the same time, fewer DNA double-strand breaks remained unrepaired after 24h. This indicates a more efficient recognition of DNA breaks and a better and more complete removal of the latter in mMSCs from Gm12606-exon1 mutant mice.

Abstract

This study provides evidence for the involvement of the lncRNA Gm12606 in the cellular radiation response and confirms in particular a very strong participation in the ageing process of mMSCs.

2. Zusammenfassung

Mesenchymale Stammzellen (MSCs) werden in der Klinik häufig eingesetzt, da sie vorteilhafte immunomudulatorische und regenerative Eigenschaften besitzen. Ihre Verwendung ist jedoch schwierig, da eine *ex vivo* Expansion erforderlich ist, um eine ausreichende Anzahl von MSCs zu erhalten, was zu einem altersbedingten Verlust der Stammzell-Potenz und einer zunehmenden Anzahl von seneszenten Zellen führt. Aufgrund ihrer langen Lebensdauer stehen MSCs im Verdacht, strahleninduzierte Mutationen zu akkumulieren, was möglicherweise zu einer verstärkten Beteiligung an altersbedingten Krankheiten und Krebs beiträgt. In dieser Studie wurde der Zusammenhang zwischen Strahlenbelastung und Alterung von murinen MSCs (mMSCs) untersucht und ein möglicher Regulationsweg, an dem die lange, intergene nicht-kodierende RNS (lincRNA) Gm12606 beteiligt ist, identifiziert.

Es wurde beobachtet, dass die lincRNA Gm12606 in mMSCs, während der *ex vivo* Alterung und nach γ-Bestrahlung überexprimiert wird. Dieser Anstieg verläuft parallel zur epigenetischen Hochregulierung des CDKN2A-Ink4a Gens, mit dem es sich eine genomische Position teilt. CDKN2A-Ink4a kodiert für den Zellzyklusregulator p16, von dem bekannt ist, dass seine Expression während Seneszenz und zellulärem Stress zunimmt.

Obwohl sich die Expression von Gm12606 als strahlungsabhängig erwies, hatte die Alterung eine stärkere Auswirkung auf das Expressionslevel von Gm12606. Der Knockdown von Gm12606 beeinflusste stark die Transkription des nahegelegenen Ink4a/Arf/Ink4b-Lokus, was darauf hindeutet, dass Gm12606 vorwiegend über einen *cis*-vermittelten Mechanismus wirkt. *In-vitro* behielten mMSCs aus homozygoten Gm12606-Exon1-defizienten Mäusen einen signifikant geringeren Prozentsatz an zellulärer Seneszenz als Zellen aus Wildtyp-Wurfgeschwistern. In frühen Passagen dieser Zellen zeigte der Verlust von Gm12606 auch

eine höhere initiale γH2AX und 53BP1-Foci Bildung nach 4 Gy. Gleichzeitig blieben weniger DNA-Doppelstrangbrüche nach 24h unrepariert. Dies deutet auf eine effizientere Erkennung von DNA-Brüchen und eine bessere und vollständigere Beseitigung dieser Brüche in Gm12606-exon1 mutierten mMSCs hin.

Diese Studie liefert Beweise für die Beteiligung der lincRNA Gm12606 an der zellulären Strahlungsantwort und bestätigt insbesondere eine starke Beteiligung am Alterungsprozess von mMSCs.

3. Introduction

3.1 Cellular senescence as the key driver of ageing

It is generally believed that cellular and organismal ageing is the result of the slow but continuous accumulation of damaged or dysfunctional cells, cellular debris and other waste products that gradually disrupt the normal cell function (Gems & Partridge, 2013; Kirkwood, 2005; López-Otín, Blasco, Partridge, Serrano, & Kroemer, 2013). For a long time, it was assumed that ageing of an organism is mainly due to the accumulating loss-of-function of post-mitotic cells in tissues with low cell turnover (such as the nervous system, cardiac myocytes, or skeletal muscle). This was first postulated by Miguel et al. (1980) (Miquel, Economos, Fleming, & Johnson, 1980) and widely accepted by Barja in 2004 (Barja, 2003), but was mainly motivated by studies on the most popular multicellular organism for research on ageing, namely *C. elegans*. *C. elegans* contains neurons and muscle cells, but in contrast to higher metazoans, cells cannot be replaced when they are worn out or damaged (Dimov & Maduro, 2019). In higher organism, adult stem cells provide a reservoir for the replacement of functional cells that are lost or become senescent due to the accumulation of cytotoxic or genotoxic damage. When Barja (2004) and Miquel et al (1980) postulated that mitotically active cells are not relevant for tissue or organismal ageing, they most likely referred to so-called transiently amplifying cells, which in fact represent only an intermediate stage between the long-term, slowly dividing adult stem cells and the non-dividing, post-mitotic and terminally differentiating cells. With the availability of more sophisticated single cell analysis and studies in genetically modified mice, however, the severely underestimated role of adult stem cells for a lifelong rejuvenation of organs and tissues became apparent (S. Neri & R. M. Borzì, 2020; Ren, Ocampo, Liu, & Izpisua Belmonte, 2017; Wiese, Ruttan, Wood, Ford, & Braid, 2019). This also led to the discovery of certain congenic syndromes that show progeria related to cellular defects that mainly affect stem cells (e.g., Werner-syndrome (Z. Wu et al., 2018; W. Zhang et al.,

2015) or Hutchinson-Gilford progeria (Bellantuono, Sanguinetti, & Keith, 2012; Gordon, Cao, & Collins, 2012; Scaffidi & Misteli, 2008)). Even though these rare, monogenetic disease can impressively show the importance of stem cell ageing, it is unclear to what extent the affected cellular pathways (nuclear architecture in Hutchinson-Gilford progeria and DNA repair in Werner-syndrome) are also the mechanisms that control the normal, physiological ageing of cells and tissue during the lifespan of “healthy” individuals. Genes and pathways nominated by genome-wide association studies on longevity (Igf1, FOXO3, Nrf2) could only poorly be associated with a phenotype in a defined cell type but were usually related to a “systemic” ageing phenotype (Lewis, Mele, Hayes, & Buffenstein, 2010; Morris, Willcox, Donlon, & Willcox, 2015; Reddy & Chaiban, 2017).

Not all phenotypic changes during an organisms’ lifetime are due to ageing (such as growth of the body, sexual maturation). Nevertheless, many tissues are affected by specific molecular changes that correlate with progressive ageing. Genomic instability and loss of telomere length, for example, are caused by the accumulation and transmission of this genetic damage to progeny cells (Moskalev et al., 2012). Transmissible genetic lesions can be induced by exogenous (chemicals, UV/IR radiation) and endogenous (reactive oxygen species (ROS), replication errors, spontaneous reactions) factors (López-Otín et al., 2013). Although the DNA repair machinery is capable of repairing most damage the repair capacity may not be efficient enough in the case of excessive damage, or when error-prone DNA repair pathways are used, or when chromosomal aberrations result in irreversible or even progressive genomic instability (López-Otín et al., 2013). Eventually, an accumulation of damage may trigger cell cycle stress and gene regulatory changes, that ultimately lead to cellular senescence and functional deterioration of the cell (Vijg & Montagna, 2017). The accumulation of DNA damage occurs randomly across the whole genome, as a result of exogenous genotoxic stress as well as endogenous errors during DNA replication and mitotic chromosome segregation (Scott Maynard, Evandro Fei Fang, Morten

Scheibye-Knudsen, Deborah L. Croteau, & Vilhelm A. Bohr, 2015). The integrity of the telomeric DNA, the terminal protective ends of chromosomes, however, are also affected in most somatic cells by a progressive shortening due to the incomplete replication at the termini of lagging strands (O'Sullivan & Karlseder, 2010). Telomerase, an RNA-dependent DNA-polymerase is able to replicate the chromosome ends and restore shortened sequences, but this enzyme is inactivated in most somatic cells, resulting in progressive telomere loss with every cell division. The consequence of this loss is a limited proliferative capacity, known as Hayflick limit, or replicative senescence (Hayflick, 2000; Hayflick & Moorhead, 1961). The ends of the chromosomes are protected by shelterin throughout the cell cycle (de Lange, 2005), a protective complex that hides chromosome ends from nonhomologous end joining and homology-directed repair by forming the t-loop structure to prevent their recognition as sites of double stranded DNA breaks (Palm & Lange, 2008). This prevents end-to-end chromosomal fusions that would result from attempted DNA repair at the telomeres and leads to an impairment of DNA repair ability and thus to an accumulation of persistent DNA damage in telomeres. (Doksani, Wu, de Lange, & Zhuang, 2013). The consequence is an impairment of the proliferation capacity, which further promotes the induction of cellular senescence (Fumagalli et al., 2012; López-Otín et al., 2013).

The accumulation of inadequately repaired DNA damage is only one reason for cellular ageing. Other cellular alterations that lead to the ageing phenotype (senescence) are accumulation of cellular waste (by misfolded proteins and damaged membranes) (López-Otín et al., 2013), loss of proteostasis (by impaired synthesis of chaperones) (Powers, Morimoto, Dillin, Kelly, & Balch, 2009), dysfunctional mitochondria (leading to impaired ATP production and an increase of endogenous ROS) (Green, Galluzzi, & Kroemer, 2011), deregulated nutrient sensing (by anabolic signaling that accelerates ageing and decreased nutrient signaling that extends longevity) (Fontana, Partridge, & Longo, 2010), epigenetic changes (by remodeling of the chromatin

architecture) (Pegoraro et al., 2009), or the activation of oncogenes (leading to oncogene-associated senescence) (Gorgoulis & Halazonetis, 2010).

Senescence can be defined as a proliferative stop that forces the cell cycle into a state of permanent arrest, accompanied by a characteristic set of phenotypic changes (Campisi & Di Fagagna, 2007). These are characterized by a flattened and enlarged cell morphology, increased activity of senescence activated β-galactosidase (SA-β-gal) a specific secretory phenotype and DNA damage, as well as altered gene expression (Salama, Sadaie, Hoare, & Narita, 2014). Previous studies have observed that the number of senescent cells in aged tissue increases, but not all tissues are affected equally. Whilst an increase in senescent cells has been observed in liver, skin, lung, and spleen, no changes were found in heart, skeletal muscle, and kidney (López-Otín et al., 2013; C. Wang et al., 2009).

One of the few genes with a defined relationship to cellular ageing is the CDK inhibitor CDKN2A (INK4A-p16), which shows increasing expression with the number of cell divisions and correlates with the development of cellular senescence (Melk et al., 2004; Nielsen et al., 1999). One of the most convincing mouse models of extended life span used a CDKN2A promotor driven suicide gene that causes elimination of cells as soon as they become senescent (“Ink-ATTAC” mouse) (Baker et al., 2011). The CDKN2A-INK4A (p16) is also regulated by the Bmi1 signaling pathway, which is activated in murine B-cell lymphoma but is also an important gene conferring immortality to normal and malignant stem cells (J. Lessard & G. Sauvageau, 2003). While Bmi1 activation suppresses transcription of the CDKN2A locus, p16 is overexpressed during oncogene-induced senescence (Itahana et al., 2003). This highlights the role of the CDKN2A locus in controlling cellular senescence, tumor suppression, and the proliferative capacity of stem cells (Julie Lessard & Guy Sauvageau, 2003). However, it is largely unknown which regulatory elements in the CDKN2A promotor region or in distal control elements are responsible for transcriptional control. Considering that the upstream Bmi1 pathway is closely related to the polycomb repressor

complex Prc1 (Satijn et al., 1997; H. Wang et al., 2004) it is not surprising that the CDKN2A-INK4A locus is epigenetically controlled and silenced during iPS reprogramming (Villasante et al., 2009).

3.2 Ionizing radiation indirectly affects tissue homeostasis

Humans are exposed constantly to ionizing radiation (IR) from a variety of natural and man-made sources. This background radiation includes cosmic rays, environmental radionuclides such as potassium40, uranium and its decay products including radon, as well as long-lived radionuclides released from nuclear fission (Hall, 1989). The expanding use of radiation in diagnostic imaging procedures, nuclear medicine and radiotherapy continually increases the dose received from medical procedures (Brenner & Hall, 2007).

Exposure of cells to IR can cause damage to biomolecules such as proteins, membrane lipids and DNA, either following a direct hit by a charged radiation particle, but equally relevant by the chemical attack of IR-generated free radicals. Those are the product of ionized water molecules leading to the formation of highly reactive OH^- radicals (Desouky, Ding, & Zhou, 2015). Characterized by a reactive, unpaired electron, free radicals react with DNA and proteins, and cause covalent molecular alterations, leading to their functional impairment and finally to a reduced cellular fitness (Barcellos-Hoff, Park, & Wright, 2005).

In dividing cells, the most dramatic radiation effect is the loss of clonogenic potential (Dikomey, Brammer, Johansen, Bentzen, & Overgaard, 2000; Dikomey, Dahm-Daphi, Brammer, Martensen, & Kaina, 1998; Dunne et al., 2003; McMillan, Cassoni, Edwards, Holmes, & Peacock, 1990). This can be observed in most human and rodent cells and is generally regarded as “radiation induced cell death” (Sia, Szmyd, Hau, & Gee, 2020). It results from irreversible damage to the

chromosomes or the spindle apparatus and usually causes the affected cell to undergo a permanent cell-cycle arrest at the G2/M phase, later followed by apoptosis or senescence.

3.3 Adult stem cells in life-long tissue regeneration and homeostasis

Stem cells in mammals have the ability to divide and provide daughter cells that are committed to one or more lineages. In order to maintain the pool of stem cells a stem cell may divide to generate two new daughter stem cells (self-renewal), or may produce a new stem cell along with a differentiated progeny cell that can further divide and differentiate into cells with specialized functions (Katsumoto, Shiraki, Miki, & Kume, 2010). Totipotent embryonic stem cells are derived from the inner cell mass during the blastocyst phase of embryonic development (Thomson et al., 1998). They are capable of producing daughter embryonic stem cells as well as progeny cells that have the potential to differentiate into precursor cells of any of the three primary germ layers endoderm, mesoderm and ectoderm (Thomson et al., 1998) and thus have the potential to initiate the development of a complete and viable organism (Evans & Kaufman, 1981). In contrast, adult (tissue) stem cells are only pluri- or multi-potent and can only differentiate along a limited number of lineages. They are present in various tissues of the body and organs, where they serve as tissue regeneration reservoirs and maintain tissue homeostasis (Verfaillie, 2002).

Adult stem cells include the hematopoietic stem cells of bone marrow, mesenchymal stem cells, neural stem cells and epidermal or melanocyte stem cells of skin (Passier & Mummery, 2003). The ability of mesenchymal stem cells to self-replicate over many passages, where they can be expanded to a sufficient number, is an important feature with regard to their clinical application in tissue and organ regeneration.

3.4 Mesenchymal stem cells (MSCs)

Friedenstein was the first in 1973 to describe MSCs as spindle-shaped, clonogenic colony-forming unit fibroblasts (CFU-Fs) cells in monolayer cultures with the potential to differentiate into osteocytes, adipocytes and chondrocytes, (Friedenstein, Chailakhyan, Latsinik, Panasyuk, & Keiliss-Borok, 1974). Starting from the observation that the stroma of the bone marrow contains supporting stem cells of non-hematopoietic origin, which were then called marrow stromal stem cells (Owen, Cave, & Joyner, 1987), Arnold Caplan finally defined the term mesenchymal stem cell in 1991 (Caplan, 1991). Subsequently Pittenger et al. were able to isolate cells with MSC properties from the BM and to stimulate them to differentiate into adipocytes, chondrocytes and osteocytes, finally proving the mesenchymal multipotency *in vitro* (Pittenger et al., 1999). These observations did not prevent MSCs from becoming the subject of considerable debate with the main critique being the lack of a clear phenotypic character defining the MSC (Horwitz & Keating, 2000). Consequently, the Mesenchymal and Tissue Stem Cell Committee of the International Society for Cellular Therapy proposed two further criteria for the definition of hMSCs. In addition to the ability to differentiate *in vitro* into adipocytes, osteoblasts and chondrocytes, MSCs under standard culture conditions they must firstly adhere to plastic and secondly express the surface antigens CD105, CD73, CD90, while CD45, CD34, CD14 or CD11b, CD79a or CD19 and HLA-DR should be absent (Dominici et al., 2006). However, these latter immunological criteria apply only to hMSCs and do not appear to define MSC-like cells of other species, such as the murine MSC (mMSC). For example, CD90 and CD105 are both strongly expressed in mMSCs (Pelekanos et al., 2012), yet they are absent in dog, goat and sheep MSCs (Rozemuller et al., 2010). In addition, mMSCs show very low expression of CD73, but strongly express CD80 that is completely absent in hMSCs (Pelekanos et al., 2012). In summary, human and mouse MSCs show differences in surface marker expression, but their plastic adherence, tissue localization and multilineage end-stage differentiation functions are conserved (Dominici et al., 2006).

In addition to adipocyte (Purpura, Aubin, & Zandstra, 2004), osteoblast (Jaiswal, Haynesworth, Caplan, & Bruder, 1997) and chondrocyte (Johnstone, Hering, Caplan, Goldberg, & Yoo, 1998) differentiation lineages MSCs have the potential to differentiate into myoblasts (Wakitani, Saito, & Caplan, 1995) and neuron-like cells (Deng, Obrocka, Fischer, & Prockop, 2001). It has been shown that under appropriate conditions they may even transdifferentiate *in vitro* towards non-mesenchymal lineages such as hepatic (Petersen et al., 1999), pancreatic (L.-B. Chen, Jiang, & Yang, 2004), cardiac (Makino et al., 1999), neural (Tropel et al., 2006), renal (Tayyeb, Shahzad, & Gibran, 2017) or epithelial-like cells such as keratinocytes. Such a wide capacity would certainly contribute to wound healing processes (Sasaki et al., 2008). Functionally defined MSCs can be isolated from various tissues and organs other than the bone marrow including the pulpa of deciduous teeth, adipose tissue, umbilical cord, Wharton's jelly and even from the monocyte fraction of peripheral blood (Squillaro, Peluso, & Galderisi, 2016). Because of the absence of cellular markers suitable for immunohistochemistry and the low abundance it has not been possible to identify the exact anatomical location of MSCs in these tissues. The only clear and specific anatomic location of MSCs is the perivascular niche surrounding the endothelial cells of sinusoids and arterioles of the blood capillaries (Oh & Nör, 2015). These MSCs are probably identical to pericytes, and might play an important role as a source of anti-inflammatory cytokines protecting the blood vessels (Caplan, 2017).

Isolation of MSCs according to ISCT criteria results in a heterogeneous population of stromal-derived cells containing a mixture of stem cells, committed progenitors and differentiated cells (Squillaro et al., 2016). It is considered that this spectrum of cell types and differentiation potential is required to allow MSCs to contribute to the regeneration of replacement tissue and wound healing, thus maintaining tissue homeostasis (Stappenbeck & Miyoshi, 2009).

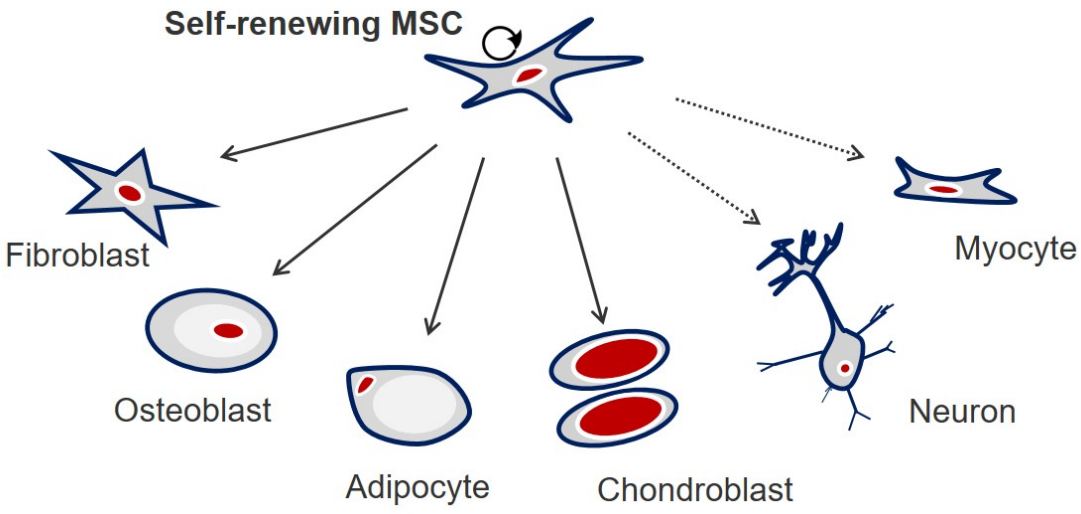

Figure 1: Differentiation potential of mesenchymal stem cells. MSCs are self-renewing, multipotent, adult stem cells that are capable of producing multiple end-stage cell lineages, especially of the skeletal type. They can differentiate into osteoblasts, adipocytes, chondroblasts, fibroblasts and myoblasts as well as lineages of non-mesenchymal origin such as neurons. (Figure is modified from an image published by Promo Cell, Heidelberg, Germany)

3.4.1 Advantageous qualities of mesenchymal stem cells in tissue regenerative cell therapy

Apart from supporting the hematopoietic stem cell niche in the BM microenvironment (Shiozawa, Havens, Pienta, & Taichman, 2008), MSCs have the potential for disease treatment and for recovery after tissue damage. Their unique multilineage differentiation potential, the relative ease of obtaining MSCs from the BM or other connective tissue, as well as their considerable *ex vivo* expandability, make MSCs attractive and suitable candidates for cell based regenerative therapeutic purposes. Positive effects have been reported in repair of bone (Quarto et al., 2001) and cartilage (Wakitani et al., 2004). In animal models it was shown that MSCs can contribute to the regeneration of damaged blood vessels and even peripheral neurons (N. F. Huang & Li, 2008; Masgutov et al., 2019).

In addition to a direct cellular repopulation MSCs are able to secret soluble factors (e.g., cytokines, chemokines and growth factors) that support cell survival and proliferation. As a consequence transplanted MSCs are able to interact with the local microenvironment or with other cells to promote the regeneration of injured tissue (Galderisi & Giordano, 2014; J. Wang, Liao, & Tan, 2011). Another important regenerative activity is the ability of MSCs to modulate the immune response (W. Jiang & Xu, 2020). Thus, *in vitro* and *in vivo* studies have reported that MSCs release soluble factors that lead to an anti-inflammatory tissue response by directly suppressing activated T-cells (Glennie, Soeiro, Dyson, Lam, & Dazzi, 2005), B cells (Corcione et al., 2006), natural killer cells (Spaggiari et al., 2008), dendritic cells (X.-X. Jiang et al., 2005) and macrophages (J. Kim & Hematti, 2009). MSCs may also act indirectly by inducing regulatory T cells (Tregs) (Di Ianni et al., 2008). It must be added that the reported immunomodulatory activity is not limited to immunosuppression in severe inflammation, but includes stimulation of the immune system through the release of proinflammatory factors (Squillaro et al., 2016). The immunomodulatory property makes MSCs attractive for a potential treatment for autoimmune diseases and graft-versus host disease (Squillaro et al., 2016). Finally, MSCs also have the ability to migrate to sites of damaged tissue and inflammation. This homing capacity is suggested to be due to a response to signalling molecules released from damaged tissue. These are suggested to bind to corresponding surface receptors on the MSCs itself, triggering migration and homing (De Becker & Van Riet, 2016). However, this mechanism is not fully understood since MSCs do not express obvious homing receptors that affect their ability to migrate (De Becker & Van Riet, 2016). However, MSCs are reported to express chemokine receptors CCR1, CCR4, CCR7, CXCR5, and CCR10 (Von Lüttichau et al., 2005). In any case, homing to sites of inflammation is a very advantageous approach to the potential of MSCs in clinical application and is often used and investigated in clinical trials.

3.4.2 Increasing use of mesenchymal stem cells in clinical trials

A number of studies have been conducted on the feasibility and effectiveness of MSC-based therapy. According to the US National Institute of Health (https://clinicaltrial.gov/), 814 clinical trials based on MSCs are currently (as of February 2020) underway, 240 of which have been completed. The number of trials has almost doubled over the last five years (Squillaro et al., 2016). Most of these studies are concerned with the regenerative therapy of damaged or otherwise degenerated connective tissue (bone, cartilage, skin, tendons), with anti-inflammatory or immunomodulating treatments (such as for reducing graft-versus-host disease) or oncological treatment (such as combating haematological malignancies and others). In trials of intra-pancreatic transplantation of autologous MSCs have also sought to halt the progression of diabetes mellitus by intervening in the chronic inflammatory processes that destroy beta cells (Scuteri & Monfrini, 2018).

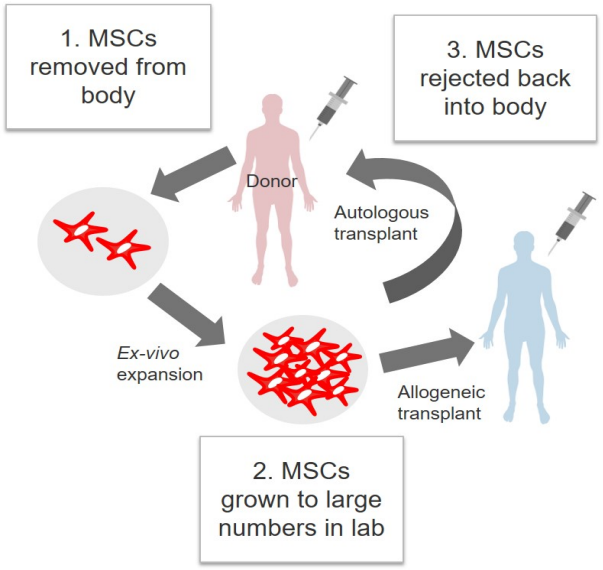

Figure 2: Autologous vs allogeneic treatment with mesenchymal stem cells. A simplified presentation of an MSC-based therapeutic approach. MSCs are isolated from BM or other connective tissue of a donor and expanded *ex vivo* in culture to a sufficient number. MSCs can then be cryopreserved until use, then thawed and reinjected into the donor (autologous) or into another patient (allogeneic). The procedure is modified according to the area of application, e.g., in tissue engineering therapy the MSCs are additionally differentiated *ex vivo* into chondrocytes and osteoblasts.

3.4.3 Risks and challenges in the clinical application of mesenchymal stem cells

3.4.3.1 Age-related changes of MSCs during ex vivo expansion

As the body ages, MSC also age and contribute to impairment of tissue maintenance and repair, which can lead to delayed or incomplete healing of fractures and other lesions and a reduced ability of MCSs to secret anti-inflammatory factors (Simona Neri & Rosa Maria Borzì, 2020; D. R. Wagner et al., 2019). In addition, MSCs are a very rare cell population in the organism, the number of which is usually not more than 0.01 % of the total cell count (Wexler et al., 2003). Due to their small cell number, the use of MSCs in clinical applications requires a massive *ex vivo* expansion in order to obtain a sufficient number of cells. However, the expansion *in vitro*, which is achieved by repeated clonal expansion, is limited. Cellular senescence often occurs during the proliferation period and is characterized by impaired stem cell multi-potency and a reduction of proliferative activity and changes in their metabolic activity (Baxter et al., 2004). This is mainly triggered by various signaling pathways, e.g. the p53/p21 and p16/RB pathways, which eventually lead to permanent cell cycle arrest in hMSCs (Yu & Kang, 2013) and the accumulation of genetic instability and DNA damage *in vitro* (Neri, 2019), in turn driving and amplifying the ageing process (Ou & Schumacher, 2018). The occurrence of accelerated cellular senescence of hMSCs (Y. Wang, Han, Song, & Han, 2012), during the required *in vitro* expansion prior to therapy, is associated with morphological changes and modifications of the secretory phenotype. These effects limit the important beneficial properties of MSCs in therapy, such as immunomodulation, differentiation potential, proliferation and homing capacity (Simona Neri & Rosa Maria Borzì, 2020).

The aim to achieve a high number of therapy-suitable MSCs from a relative low number of explanted clone-forming units is achieved by adding high concentrations of growth factors and growth-inhibiting signals to the cell culture medium. During this *in vitro* procedure, MSCs are subjected to a highly unphysiological proliferation pressure, which causes cytogenetic and

metabolic stress (Bonab et al., 2006). This could cause MSCs to undergo morphological and genetic changes (Y. Yang, Pan, Lin, & Huang, 2018) and (or) promote the accumulation of DNA damage, leading to malignant transformation (Josse et al., 2010; Miura et al., 2006). Consequently, they also could lose their tri-differentiation potential (osteogenic, adipogenic, chondrogenic) when the cultures reach the upper limit of passage (DiGirolamo et al., 1999; Y.-H. K. Yang, 2018). In addition, accelerated senescence occurs due to the high replicative stress to which MSCs are exposed as a consequence of the culture conditions and the lack of a protecting environment that creates the stem cell niche *in vivo* (Simona Neri & Rosa Maria Borzì, 2020).

Recently, our research group has observed that *in vitro* expansion under chronic oxidative stress leads to higher rate of replicative senescence and to more spontaneous and radiation-induced DNA double strand breaks (DNA-DSBs) in mouse MSCs (Höfig et al., 2016). It was also shown that mMSC gradually lose their ability to respond to radiation-induced damage with increasing time of *in vitro* expansion (D. Hladik et al., 2019)

It is important to consider and counteract these potentially adverse effects in order to improve therapies and outcomes and ultimately ensure safe treatment.

3.4.3.2 Cumulative radiation exposure can influence the fate and suitability of MSC

Previous studies suggest that MSCs are resistant to irradiation due to several mechanism, including ATM protein phosphorylation, activation of cell cycle checkpoint and efficient DSB repair (M.-F. Chen et al., 2006), which may even be beneficial in stem cell treatment and cancer therapy. However, since IR causes massive genotoxic stress by free radicals and direct hits to the DNA, MSCs are particular at risk to accumulate damages from repeated or protracted radiation exposure over longer periods of time, due to their slow cell cycle kinetics and their long residence time in the organism. If the radiation-induced genomic lesions, such as DNA-DSBs cannot be

carefully repaired, MSCs could accumulate irreversible damage leading to premature senescence (Alessio et al., 2015) to prevent transmission to their offspring cells (Watters, 1999), which could have adverse effects on regenerative stem cell therapies, or they could suffer from mutations and become prone to malignant transformation (Rando, 2006).

3.5 Non-coding RNA transcriptome

The development of new technologies for sequencing the entire genome has opened up a new perspective on the eukaryotic transcriptome and revealed a new understanding of RNA. This has challenged the notion that RNA serves only as a template for protein synthesis and is an essential bridge between DNA and protein (Kozak, 1983).

Only <2% of the human genome encodes proteins and the other 98% were considered to be transcriptionally inactive DNA (J. X. Yang, Rastetter, & Wilhelm, 2016). Today it is known that a large percentage (~70%) of the genome is actively transcribed into RNA (Birney et al., 2007; Consortium, 2007; F. F. Costa, 2010; Katayama et al., 2005). Initially it was argued that this represented transcriptional noise but recent findings have identified a rapidly growing number of functional non-coding RNAs (ncRNAs) that have been identified as regulators of biological processes including gene expression, cell cycle control, apoptosis, cell identity decisions, chromatin remodelling, and epigenetic modifications (Bartel, 2004; Tim R Mercer et al., 2011; Taft, Pheasant, & Mattick, 2007; J. X. Yang et al., 2016). These observations, when applied to the genomes or genetics of higher organism, could explain the inconsistent correlation between the number of protein coding genes and the morphological complexity of organism (Mattick, 2007).

Members of the ncRNA transcriptome referred to as housekeeping ncRNAs and studied in detail include tRNAs, rRNAs, small nucleolar (snoRNAs) and small nuclear RNA (snRNAs). These are

expressed ubiquitously and with a relatively high abundance (Fu, 2014; P. Zhang, Wu, Chen, & Chen, 2019). They each fulfil essential functions that contribute to protein synthesis (tRNAs, rRNAs) (Moldave, 1985) or are involved in RNA modifications (snoRNAs) (Matera, Terns, & Terns, 2007) and splicing (snRNAs) (Shi, 2017). This group also includes the telomere-complex associated guide RNA (TERC), which is a component of the telomerase and serves as a template for the synthesis of telomerase repeats at the end of chromosomes to extend telomeres (e.g., in germ cells) (Greider & Blackburn, 1985).

The regulatory ncRNA transcriptome has been considered to represent two sets of small ncRNAs (<200 nt) and long ncRNAs (>200 nt) (Consortium, 2012). The group of small ncRNAs includes miRNAs, piRNAs and tRNA-derived small RNAs (tsRNAs) (Fu, 2014). They are typically short (~20-30 nt), and are often processed from larger RNA precursor transcripts (M. C. Costa, Leitão, & Enguita, 2012). miRNAs can regulate biological processes by inhibiting protein factors via mRNA degradation and/or translation of target genes (gene-silencing). For this purpose miRNAs often interact with members of the Argonaut (Ago) family of proteins (Choudhuri, 2010). piRNAs instead, interact with piwi complexes to form RNA-protein complexes. Thus, they can regulate the maintenance and self-renewal of germline stem-cells (Cox et al., 1998) or silence transposons, allowing the development and maintenance of DNA integrity (Halic & Moazed, 2009). In addition, it has been discovered that piwi-piRNA complexes can epigenetically regulate gene expression at specific genomic sites (X. A. Huang et al., 2013). Similarly, tsRNAs have also been found to play various functional roles in gene expression, protein translation, epigenetic regulation, and immune processes (S. Li, Xu, & Sheng, 2018).

A group function cannot be assigned to other ncRNAs. These include the promoter associated transcripts (paRNAs), enhancer associated RNAs (eRNAs), and the most recently recognized circular RNAs (circRNAs). paRNAs are low-expressed ncRNAs of gene promoters that have been discovered in human cells and are thought to play a significant role in controlling gene expression

of downstream genes through gene silencing (Han, Kim, & Morris, 2007). In contrast, eRNAs produced by active enhancers also have been shown to possess an important functional role in regulating target gene expression, however, through activation function (W. Li et al., 2013; Melo et al., 2013; X. Wang et al., 2008). eRNAs closely resemble lncRNAs, yet are distinct due to several aspects (e.g., lower expression level, shorter, lack constant splicing and polyadenylation) (T.-K. Kim, Hemberg, & Gray, 2015). CircRNAs represent a covalently closed, continuous single stranded loop that has been found to function as miRNA (Hansen et al., 2013) and protein sponges and is also involved in the cellular radiation response (O'Leary et al., 2017).

Most attention in recent years has been paid to lncRNAs, one of the most poorly understood RNA species.

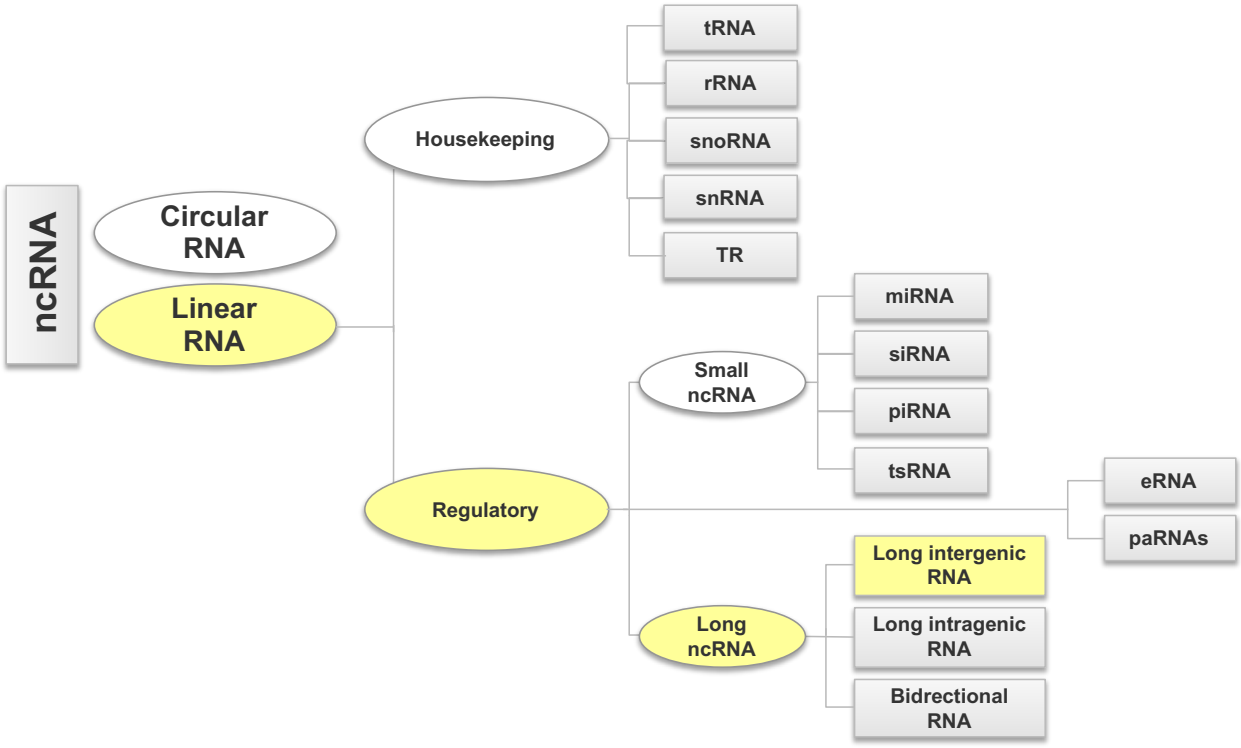

Figure 3: Classification of non-coding RNA. Schematic overview of the non-coding RNA family members (Figure is modified from an image published by La Ferlita et al., 2018 (La Ferlita et al., 2018)). The yellow parts refer to the groups to which the long-intergenic non-coding RNA Gm12606 studied in this project belongs.

3.5.1 Long non-coding RNAs (LncRNAs)

LncRNAs are RNA transcripts that are more than 200 nucleotides in length. They are observed in wide variety of organisms, including animals (Feyder & Goff, 2016), plants (Y.-C. Zhang et al., 2014), yeast (Niederer, Hass, & Zappulla, 2017), prokaryotes (Bernstein, Zopf, Freymann, & Walter, 1993) and even viruses (Reeves, Davies, McSharry, Wilkinson, & Sinclair, 2007). They may be transcribed from intergenic DNA, but some are generated from intragenic sequences where they can include both exonic and intronic sequences derived from mRNA coding genes (Moran N Cabili et al., 2011). Typically lncRNA lack long open reading frames and thus lack protein coding capacity (Marchese, Raimondi, & Huarte, 2017). However, some studies have indicated that some lncRNAs may be transcribed into very short amino acid chains (Derrien et al., 2012; Ulveling, Francastel, & Hubé, 2011). They are transcribed by RNA polymerase II and contain a 5' 7-methylguanosine cap and a 3'poly(A) tail in common with mRNA. As would be expected from the lack of constraints posed by an ORF, the sequences of lncRNAs are less conserved than those of protein coding genes (Ponjavic, Ponting, & Lunter, 2007). However, the use of chromatin-state maps to detect discrete functional sequence blocks that interfere with known protein-coding loci have identified a subset of mammalian long intergenic ncRNA (lincRNA). They are distinct from the broader lncRNA class of transcripts as many lncRNAs share sequence with coding loci, but lincRNA are located in intergenic regions (Bertone et al., 2004). They exhibit strong evolutionary conservation at the sequence level (Guttman et al., 2009) and provide an important indication, even if weak, of the functionality of lncRNAs.

LncRNA have been implicated in a variety of human disease including cancer, because they are involved in the regulation of numerous molecular pathways associated with changes in gene expression and are dysregulated in cancer cells (DiStefano, 2018; Maite Huarte, 2015; M.-C. Jiang, Ni, Cui, Wang, & Zhuo, 2019; F. Jiao et al., 2014; L. Zhang, Zhou, Pan, & Zhao, 2014). It is becoming increasingly clear that lncRNAs not only triggers for diseases, but also influence them positively (Lekka & Hall, 2018).

Thousands of potential lncRNA loci have been predicted by bioinformatic algorithms searching next-generation sequencing data sets (Fang et al., 2018), but it is not known how many of these are functional. The GENCODE consortium within the ENCODE project has been annotating and providing a comprehensive set of human lncRNAs for several years (Derrien et al., 2012). With 15,512 transcripts grouped in 9640 gene loci, the human GENCODE lncRNA catalogue is the largest manually curated catalogue of candidate human lncRNA (Harrow et al., 2012).

Thus, lncRNAs could first be classified into the following locus biotypes according to their position in relation to protein coding genes, carrying diverse functional properties (Derrien et al., 2012; Khandelwal, Bacolla, Vasquez, & Jain, 2015):

1. Long intergenic ncRNAs (lincRNA) are transcripts derived from a locus that is at least 1 kb away from the nearest protein-coding gene. They are known to modulate various biological processes, including cell cycle regulation (Nötzold et al., 2017), embryonic stem cell fate (L. Yang, Lin, & Rosenfeld, 2011) and surveillance of immune response (G. Hu et al., 2016). They often regulate nearby genes by recruiting chromatin proteins (Ahmad M Khalil et al., 2009).
2. Antisense lncRNAs are transcribed in the opposite direction relative to a protein-coding locus (Katayama et al., 2005). They are less prone to splicing and are therefore expressed at lower levels than their sense equivalent (Villegas & Zaphiropoulos, 2015). In addition, they have been reported to affect gene regulation pre-transcriptionally (e.g., via epigenetic regulation (T. R. Mercer & Mattick, 2013), by modulating the transcription process (Vance & Ponting, 2014)), and post-transcriptionally (e.g., via RNA-RNA interactions that modify mRNA structure (Batista & Chang, 2013)).
3. Sense overlapping lncRNAs, also known as exonic lncRNAs, are transcripts derived from the same genomic strand as a protein-coding gene locus (Ma, Bajic, & Zhang, 2013). This results in a lncRNA transcript that contains sequences that overlaps with those of the

mRNA exons. Their function is less well studied, but they have been shown to be unique in that they act as both an RNA and protein-coding gene (Leygue, 2007).

4. Intronic lncRNA transcripts are located within introns of a coding gene, transcribed in either the sense or antisense orientation, but do not overlap exons (Ma et al., 2013). Intronic lncRNAs may stabilize protein-coding transcripts or regulate splicing (Nakaya et al., 2007).

3.5.2 Functions of lncRNAs

Compared to protein-coding genes, lncRNAs are enriched in the nucleus relative to the cytoplasm (Derrien et al., 2012; Djebali et al., 2012), and are particularly enriched in the chromatin fraction (Tanmoy Mondal, Rasmussen, Pandey, Isaksson, & Kanduri, 2010). They are generally, but not always spliced and polyadenylated, by RNA polymerase II (Scheuermann & Boyer, 2013) and can fold into various secondary structures to interact with DNA, RNA and protein molecules (Guttman & Rinn, 2012; Marchese et al., 2017).

Attempts have been made to categorize the mechanisms of action of lncRNA. Accordingly, lncRNAs were defined by four different functionality archetypes by Wang and Chang, 2016 (Kevin C Wang & Chang, 2011):

Archetype 1 defines lncRNAs that act as signal or indicator, as their transcription is under considerable control by responding to stimuli of transcriptional activity, thus contributing to gene regulation. The lncRNAs exhibit cell type specificity as transcription occurs at very specific time and location (e.g., Xist and the role in X inactivation by silencing gene expression (Pontier & Gribnau, 2011); HOTAIR and HOTTIP and their anatomically specific expression within the HOX gene clusters (K. C. Wang, Helms, & Chang, 2009); linc-p21, that targets p53 in response to DNA damage (M. Huarte et al., 2010)).

Archetype 2 specifies lncRNAs that can bind to and titrate away other regulatory RNAs or proteins (e.g., Gas5 by competing for the binding to the DNA binding domain of the glucocorticoid receptor and acting as a decoy (Kino, Hurt, Ichijo, Nader, & Chrousos, 2010); TERRA as a natural ligand and thus inhibitor of telomerase (Redon, Reichenbach, & Lingner, 2010)).

Archetype 3 lncRNAs are guides that can bind ribonucleoproteins and direct them to their specific targets in *cis* or in *trans* (e.g., XIST by recruiting the polycomb repressor complex 2 (PRC2) to inactivate the X-chromosome in *cis* (Wutz, Rasmussen, & Jaenisch, 2002); HOTAIR by regulating epigenetic states in cells by targeting PRC2 in *trans* (Wutz et al., 2002)).

Archetype 4 defined lncRNAs serve as scaffolds for the formation of multiprotein complexes such as those required for stabilizing nuclear structures or signaling complexes (e.g., TERC and the association with catalytic protein subunit TERT to enable telomeric repeat synthesis (Lustig, 2004); ANRIL through interacting with chromatin-modifying complexes to regulate the INK4A/ARF/INK4B locus in humans (J. Gil & G. Peters, 2006)).

It becomes clear from this functional consideration that many lncRNAs are involved in regulation of gene expression and/or chromatin state. They may act at a locus distant from the site from which they are transcribed (*trans*-regulatory activity) or may act in direct proximity to their own sites of transcription (*cis*-regulatory activity) (Kopp & Mendell, 2018).

Cis regulation of lncRNAs

Typically lncRNAs are expressed at very low levels (few molecules per cell) (Hezroni et al., 2015; Ulitsky, 2016), which tends to favour a *cis* mechanism as transport to distant sites or cellular compartments would further dilute the transcripts (Gil & Ulitsky, 2019). The *cis*-acting lncRNAs act immediately adjacent to their sites of transcription to influence local chromatin structure and hence the expression of genes (Gil & Ulitsky, 2019). These changes in chromatin may be produced by epigenetic modification for example through the recruitment of chromatin-modifying complexes such as PRC2 (Davidovich & Cech, 2015). In addition to chromatin remodelling the *cis* acting lncRNAs may also regulate gene expression by recruiting transcriptional regulatory factors to the locus (Kopp & Mendell, 2018). The X-inactive specific transcript Xist is an example of this type of regulation exerted during early embryonic development in female mammals. Here one of the two X chromosomes is transcriptionally inactivated by an Xist dependent mechanism to achieve a dosage compensation between genders (Cerase, Pintacuda, Tattermusch, & Avner, 2015). Xist is transcribed from a locus on one of the X chromosomes and accumulates across the X chromosome to trigger stable silencing of the entire chromosome (Cerase et al., 2015), possibly through recruitment of PRC2 and thus initiation of H3K27me3.

Another mechanism shows that the expression level of a lncRNA does not depend on the processed transcript, but on DNA elements within the lncRNA promoter, enhancer or gene body that function independently of the transcribed RNA (e.g., Bendr) (Kopp & Mendell, 2018).

LncRNA transcripts can also recruit proteins that modulate chromatin loops and bring lncRNA enhancers near the target genes (e.g., CCAT1-L) to activate their transcription, or they recruit proteins that form chromatin loops to suppress gene expression (e.g., Morrbid) (Gil & Ulitsky, 2019). Finally, there are also lncRNAs that inhibit target gene expression by nucleosome remodelling or deposition of epigenetic modifications. These lncRNAs usually overlap the target

genes and are mostly independent of the mature lncRNA transcripts or their sequence (e.g., Air) (Gil & Ulitsky, 2019; Kopp & Mendell, 2018).

Trans-acting mechanisms of lncRNAs

Trans-acting lncRNAs by definition leave their transcription sites and fulfil their function elsewhere in the genome. Several mechanisms are attributed to them. There are *trans*-acting lncRNAs that control chromatin status or the activity of RNA polymerase II by interacting with promoters or enhancers (Kopp & Mendell, 2018). For example, the intergenic HOX antisense RNA HOTAIR (transcribed from a locus on chromosome 12) acts as an important negative regulator in *trans* of chromatin states at the HOXD locus (on chromosome 2), thereby repressing transcription. HOTAIR serves as a scaffold for assembly of the chromatin modifying PRC2, a complex that catalyses histone 3 lysine 27 trimethylation (H3K27me3) (Gupta et al., 2010).

The trans-acting lncRNAs MALAT1 and NEAT1 are components of dynamic subcellular structures (nuclear speckles or paraspeckles) and can influence the organization of nuclear architecture to regulate transcription or RNA processing (Ip & Nakagawa, 2012). Thus the metastasis-associated lung adenocarcinoma transcript MALAT1 is localized within nuclear speckles containing components of the splicing machinery, which incorporate spliceosome subunits, snRNPs, and serine/arginine-rich (SR) proteins (Hutchinson et al., 2007). It is assumed that MALAT1 regulates pre-mRNA splicing by targeting nuclear speckles to active gene loci (Hutchinson et al., 2007; V. Tripathi et al., 2010). Recent studies have also shown that MALAT1 is also involved in post-transcriptional modification of mRNA, such as N6-methyladenosine (m6A) (Liu et al., 2017) and 5-methylcytosine (m5C) that are performed by large multi-protein complexes. (Amort et al., 2017). Similarly, the nuclear-enriched abundant transcript 1 NEAT1 is recruited to paraspeckles, dynamic nuclear compartments containing proteins involved in transcription and RNA processing

(Kopp & Mendell, 2018). Paraspeckles are involved in the control of gene expression by posttranscriptional mRNA processing converting specific adenosine bases to inosine (A to I) (Bond & Fox, 2009). Trans-regulating lncRNAs are also able to bind to proteins or RNAs and modulate their activity. Prominent in this class are lncRNAs that bind to miRNAs in the cytoplasm and titrate their availability, also known as competitive endogenous RNAs (ceRNA) (Tay, Rinn, & Pandolfi, 2014).

An additional trans regulatory activity is indicated by the ability of lncRNAs to intercalate at specific sites within double stranded genomic DNA to form an RNA:DNA triple helix (Kuo et al., 2019). These regions of triple helix are achieved through the formation of Hoogsteen or reverse Hoogsteen hydrogen bonds with a purine-rich (adenine-and-guanine–rich) DNA strand either in the parallel orientation (both 5′ to 3′) or anti-parallel orientation (5′ to 3′ and 3′ to 5′). This leads to changes in the chromatin structure and the regulation of gene transcription by direct interaction in a sequence-specific manner with the DNA or through the recruitment of coactivator or corepressor proteins, as has been demonstrated for a number of lncRNAs such as MEG3 (T Mondal et al., 2015), KHPS1 (Postepska-Igielska et al., 2015), Fendrr (Grote et al., 2013), PARTICLE (O'Leary et al., 2015) and HOTAIR (Kalwa et al., 2016).

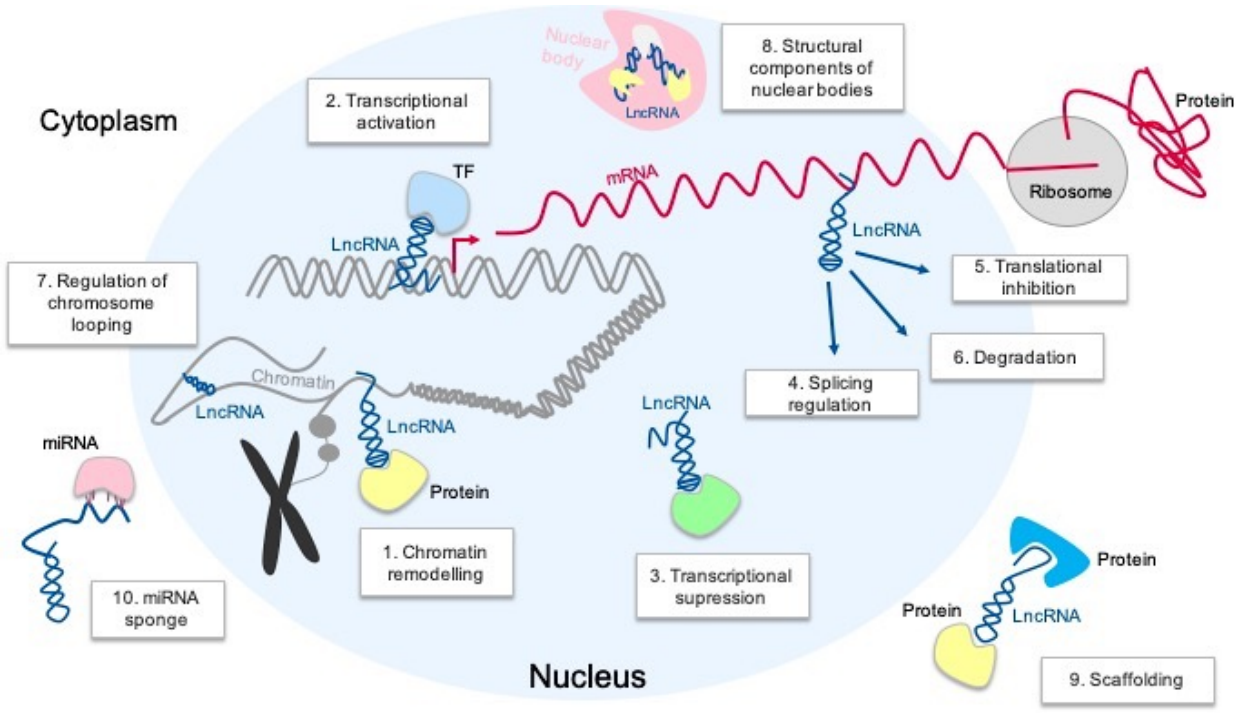

Figure 4: LncRNAs show a wide variety of functions. Simplified schematic representation of different lncRNA mechanism. LncRNAs are able to recruit different chromatin modifiers (e.g., proteins) to change the organization patterns of chromatin by promoting the deposition of activating or repressive histone marks (1). They control the recruitment of transcription factors (TF) to the promoters and thus activate the transcription of specific genes (2). LncRNAs are also able to suppress transcription by sequestering TF (3). They can bind mRNAs directly by base pairing and modulate splicing events (4), inhibit their translation (5) or trigger their degradation (6). LncRNAs are involved in the higher order organization of the nucleus by facilitating chromatin loops (7) and acting as structural components for the formation and function of nuclear bodies (8). LncRNAs can also serve as scaffolds by providing docking sites for proteins (9). They can bind miRNAs by base paring (miRNA sponges) to promote the expression of mRNAs at which the miRNA is targeted (10). (Figure is modified according to images published by Salehi et al., 2017 and Neguembor et al., 2014 (Neguembor, Jothi, & Gabellini, 2014; Salehi, Taheri, Azarpira, Zare, & Behzad-Behbahani, 2017))

3.5.3 Contribution of lncRNAs to the ageing processes

Altered expression of lncRNAs have been associated with a variety of age-related diseases, such as cancer, cardiovascular diseases (CVD), type II diabetes and Alzheimer's disease (Marttila, Chatsirisupachai, Palmer, & de Magalhães, 2020). Sequence variations in the ANRIL gene are also associated with an increased risk for CVD and periodontitis (Congrains, Kamide, Ohishi, & Rakugi, 2013). Several senescence-associated lncRNAs have been identified. A study from Abdelmohsen et al. (2013) found in a comparison of lncRNAs expressed in proliferating, early-passage, 'young' human fibroblasts with those expressed in senescent, late-passage, 'old' fibroblasts that the expression of many lncRNAs changes with senescence. This indicated a possible functional activity of these lncRNAs with ageing (Abdelmohsen, Panda, Kang, Xu, Selimyan, Yoon, Martindale, De, Wood 3rd, et al., 2013). Examples of age-related lncRNAs are Xist (in human fibroblasts (Abdelmohsen, Panda, Kang, Xu, Selimyan, Yoon, Martindale, De, Wood, et al., 2013)), MIAT (in human breast cancer cells (Alipoor, Asadi, & Torkzadeh-Mahani, 2018)), MALAT1 (in human gallbladder cancer cells (Lin et al., 2019)) which are all down-regulated in senescent cells, while HOTAIR is up-regulated (in human fibroblasts) (Marttila et al., 2020; Yoon et al., 2013). Whereas for most of them a causal relationship with cellular ageing is still unproven, recent studies have shown that lncRNAs are able to modulate specific senescence-associated pathways, such as the pRB/p16, p14/p19 (p14 in human; p19 in mice) and p53/p21 mediated pathways, acting at different stages of the cell cycle (Abdelmohsen & Gorospe, 2015). For example, overexpression of the lncRNA MIR31HG suppressed the expression of the cell cycle inhibitor p16 by interacting with the PRC2 complex (Montes et al., 2015). In addition, ANRIL, the lncRNA that is antisense to the INK4A/ARF/INK4B (p16 /p14 /p15) gene cluster in humans, inhibits the p53-p21 pathway in *trans*, resulting in reduced cell cycle arrest and inhibition of vascular smooth muscle cell senescence (Tan et al., 2019). It is also known that ANRIL inhibits the expression of P15, P16 and P14 genes in *cis* (Pasmant et al., 2007) by recruiting PRC2 (Kotake et al., 2011).

The majority of lncRNAs appear to exert their age-related actions in a tissue specific manner (Marttila et al., 2020). Another important potential influence of the ageing process trough lncRNA interaction is the maintenance and function of stem cells (Sousa-Franco, Rebelo, da Rocha, & Bernardes de Jesus, 2019).

3.5.4 Effects of ionizing radiation on lncRNA expression

A number of lncRNAs have been implicated in DNA damage response (DDR) and repair processes following exposure to ionizing radiation. The lncRNAs lincRNA-p21 and PANDA have been observed to be upregulated in the aftermath of DNA damage in response to IR, being transcriptionally regulated target genes for radiation-induced p53 (Hung et al., 2011). LincRNA-p21 may be acting as a negative feedback regulator in mouse vascular smooth muscle cells and mononuclear macrophage cells, as it is itself downregulates multiple p53 target genes, thereby inhibiting cell proliferation and inducing apoptosis (Wu et al., 2014). The LncRNA LIRR1 is reported to regulate the DDR in human bronchial epithelial BEAS-2B cell line, by increasing radiosensitivity, stopping the cell cycle in G1 phase and increasing γ-H2AX damage repair foci, (Y. Jiao et al., 2015). After high dose irradiation (5Gy), ANRIL was also reported to be upregulated in HeLa and caspase-3-deficient MCF-7 cells (Özgür et al., 2013). Due to the epigenetic regulation of the INK4A/ARF/INK4B locus by the PRC2, which is associated with growth arrest, the upregulation in radiation-induced damaged cells could be related to this.

Based on the limited evidence on the role of lncRNAs in radiation-induced DDR, Yang et al. (2019) analysed altered lncRNA expression by high-throughput RNA sequencing after high dose exposure (8Gy) in HEK293T cells and observed 49 differentially expressed lncRNAs. These are predicted to be involved in the histone mRNA metabolism process, with some genes regulating the DDR by triggering histone changes, for instance, histone degradation (Hauer et al., 2017) and Wnt signaling (M. Yang et al., 2019), as a major target of p53, which is mostly activated after

DNA damage (Watcharasit et al., 2002). Finally, it was recently found that the lncRNA PARTICLE is upregulated after low-dose radiation exposure in MDA-MB-361 breast cancer cells. Nuclear PARTICLE inhibits the transcription from the adjacent MAT2A gene through triple helix formation and interacts with PRC2 (O'Leary et al., 2015).

3.6 lncRNA regulation of mesenchymal stem cell function

LncRNAs contribute to the lineage differentiation of MSCs into osteoblasts, adipocytes, chondrocytes and muscle cells (Peng et al., 2018). In particular, they are involved in bone development and homeostasis, which is initially formed by osteoblasts developing from MSCs and the regulatory transcription factors acting on them (Katsimbri, 2017). Proteins and signaling pathways regulating osteoblast differentiation are the bone morphogenetic protein (BMP) and wingless (Wnt) signaling pathway (Cao & Chen, 2005; Day, Guo, Garrett-Beal, & Yang, 2005). The Wnt/β-catenin signaling pathways is often found to contribute to cell proliferation and differentiation and is thus influenced by the regulation of lncRNAs. For example, it has been observed that the lncRNA LET negatively affects MSC proliferation by activating Wnt/β-catenin signaling (Jin, Zhang, Lu, & Fan, 2018), while the lincRNA-p21 interacts with Wnt/β catenin and reduces cellular senescence by silencing lincRNA-p21 (Wenzheng Xia, Zhuang, Deng, & Hou, 2017). In interaction with the macrophage migration inhibitory factor and the activation of Wnt/β-catenin, lincRNA-p21 has also reduced apoptosis of MSCs (W. Xia, Zhuang, & Hou, 2018).

The canonical Wnt-signaling influences differentiation by activating β-catenin, which in turn leads to the upregulation of transcription factors that are crucial for osteoblast differentiation (Day et al., 2005). The activity is also controlled by epigenetic mechanism involving lncRNAs in which osteogenic differentiation is either promoted (e.g., H19, MALAT1) or inhibited (e.g., HOTAIR, MIR31HG) (Peng et al., 2018).

lncRNAs are also able to modulate specific signalling pathways associated with senescence in mesenchymal stem cells, such as the p16INK4A/RB signalling pathway (Yu & Kang, 2013).

3.6.1 The INK4A/ARF/INK4B locus as driver for cellular senescence and ageing

The INK4A/ARF/INK4B locus (Human Genome Organization designation **CDKN2A-CDKN2B**) on the short arm of human chromosome 9p21 and the corresponding locus on mouse chromosome 4, encodes two cyclin-dependent kinase inhibitors (p16INK4A=CDKN2A; p15INK4B=CDKN2B) and a completely unrelated gene p19/p14, which is produced from the alternative reading frame (ARF) from the INK4A gene (also known as $p19^{Arf}$ in mouse and $p14^{ARF}$ in humans) (Ouelle, Zindy, Ashmun, & Sherr, 1995). p19/p14 and p16 share their second and third exons, while p15 is translated as an independent gene located in close proximity (<8 kb) (**Figure 5**). While p16 and p19/p14 share two common exons, they are translated in different reading frames and have no amino acid homology.

Both p15 and p16 bind to CDK4 and CDK6 and block cell proliferation by preventing cyclin-dependent phosphorylation of RB (retinoblastoma), which promotes sequestration of E2F (E2 factor, transcription factor) and leads to a G1 cell cycle arrest. ARF, on the other hand, operates upstream of p53 by binding and sequestering MDM2, thereby protecting p53 from MDM2 related degradation. This in turn activates p53 resulting in either cell cycle arrest or apoptosis (Nikolay Popov & Jesús Gil, 2010; Charles J Sherr, 2001). In mouse models it was observed that engineered disruption of either the entire locus or of single genes promoted cancer development by inhibition of anti-proliferative activities, suggesting a tumor suppressor function for all three genes (W. Y. Kim & Sharpless, 2006). The locus has been found to be mutated in a wide range of human tumours, including melanoma, pancreatic adenocarcinoma, glioblastoma, leukaemia's, non-small cell lung cancer, and bladder cancer (W. Y. Kim & Sharpless, 2006).

$p16^{INK4A}$ shows an age-dependent expression pattern *in vivo.* While the expression is low or undetectable during embryonic development, it increases steadily with age. This was demonstrated in various tissues that show a more than 10-fold increase during the lifespan of humans and mice (Melk et al., 2004; Nielsen et al., 1999).

The G1-S checkpoint in the cell cycle is activated by p16 through inhibition of the cyclin-dependant kinases CDK4 (Serrano, Hannon, & Beach, 1993) and CDK6 (Parry, Bates, Mann, & Peters, 1995). This reaction is often regarded as crucial for the establishment of a senescence-like growth arrest (Mombach, Bugs, & Chaouiya, 2014). CDK4 and CDK6 in fact facilitate the phosphorylation of pRB and lead to the release of E2F (C. J. Sherr & McCormick, 2002). This mediates the transcriptional activation of proteins required for G1 to S transition and DNA replication (C. J. Sherr & McCormick, 2002).

The ectopic expression of cancer-associated cell-cycle genes (e.g., $p21^{WAF1}$, $p16^{INK4A}$, $p27^{KIP1}$, $p15^{INK4B}$, pRB, and CHK2) has been identified as a trigger for cellular senescence (Mirzayans, Andrais, Hansen, & Murray, 2012). p16,p19/p14 and p15 are even nowadays characterized as biomarkers of cellular senescence and ageing (Krishnamurthy et al., 2004; A. S. Wang & Dreesen, 2018).

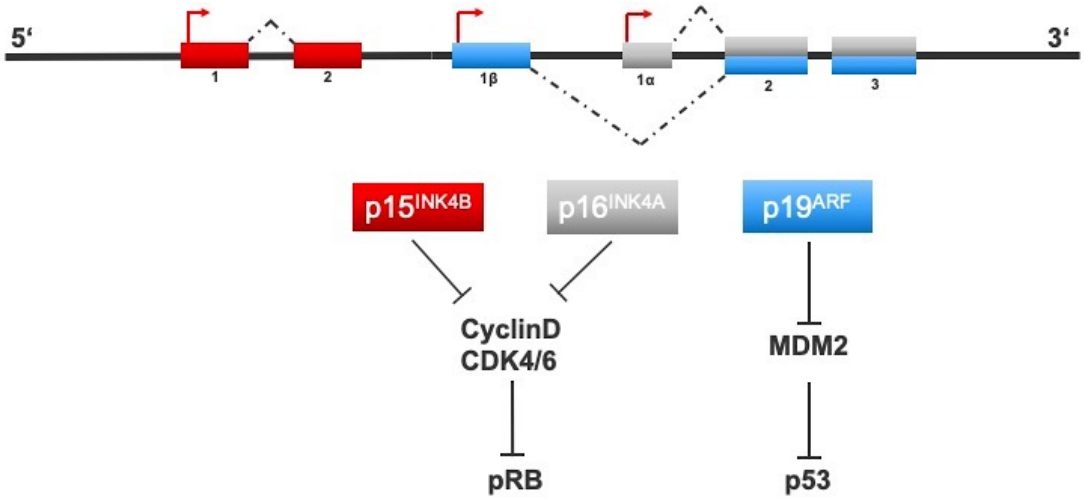

Figure 5: The and mouse Ink4a/Arf/Ink4b locus. The locus encodes three genes within 35 kilobases: p16, p19, and p15. p16 and p19 bind to cyclin-dependent kinase inhibitors and inactivate CDK4/6, which prevents the phosphorylation of pRB. p19 inhibits MDM2 and protects p53 from MDM2-mediated degradation, which leads to a stabilization of p53. (Figure is modified according to an image published by Kim et al., 2006 (W. Y. Kim & Sharpless, 2006))

In MSCs, p16-positive cells show increased activity of SA-β-galactosidase and growth retardation (Shibata et al., 2007). Furthermore, siRNA-mediated knockdown of p16 in senescent MSCs leads to a reduced number of senescent cells while maintaining proliferate capacity (Shibata et al., 2007). This suggests that p16 is an important regulator of MSC ageing (Y. Li et al., 2017; Shibata et al., 2007). Since senescence-related loss of MSC stemness leads to an impairment of tissue homeostasis and repair, it is essential to fully understand the INK4A/ARF/INK4B locus and the mechanism underlying the regulation of MSCs and cellular senescence/ageing.

The lncRNA ANRIL (CDKN2B-AS; antisense non-coding RNA in the Ink4 locus) transcribed from the $p15^{INK4B}$ locus regulates the genes of the INK4A/ARF/INK4B locus both independently and in a coordinated manner. ANRIL is transcribed in the antisense orientation relative to the cluster and regulates its neighbours in *cis* by an epigenetic mechanism (**Figure 6**). Thus, ANRIL is involved in cell proliferation, cell ageing and senescence (Gamell, Ginsberg, Haupt, & Haupt, 2017), it

interacts with the Polycomb proteins Suz12 and Cbx7, which recruit PRC1 and PRC2 at the locus, triggering histone modification and silencing of the locus (Congrains et al., 2013). Since ANRIL is only present in human cells, but the organization and structure of the INK4A/ARF/INK4B locus is conserved between human and mouse (Ouelle et al., 1995; Swafford et al., 1997), the question arose whether a similar mechanism regulating the Ink4a/Arf/Ink4b locus exists in mice.

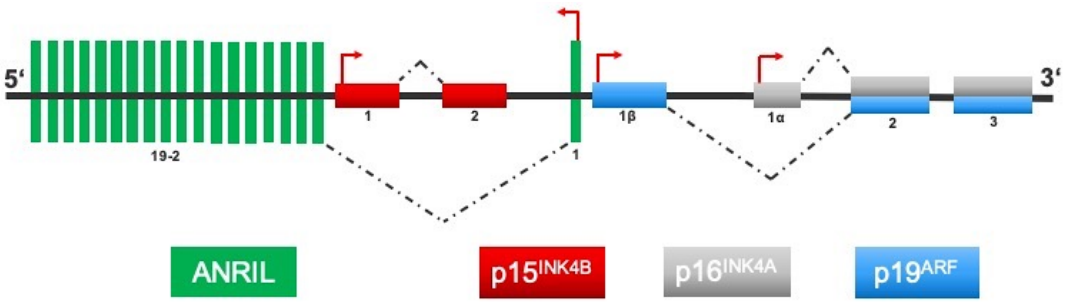

Figure 6: The human lncRNA ANRIL. ANRIL is a human long non-coding RNA encoded in the chromosome 9p21 region on the antisense strand, overlapping $p15^{INK4B}$. Therefore, ANRIL is transcribed in the opposite direction to the INK4A/ARF/INK4B locus. ANRIL has 28 splice variants and contains up to 19 exons. It silences the INK4A/ARF/INK4B locus by recruiting PRC2.

3.6.2 The novel long intergenic non-coding RNA Gm12606

The lncRNA Gm12606 (or Linc166I8) was initially identified by RNA sequencing in a murine lymphoblast library (Ensembl reference sequence ENSMUSG00000087659.7). Based on previous findings and in order to investigate the involvement of cellular ageing and radiation-induced damage response in murine mesenchymal stem cells (mMSCs), RNA sequencing was performed to compare lncRNA transcripts in young (3 weeks) unirradiated mMSCs with either aged (8 weeks old) or irradiated young (2 Gy) mMSCs. We discovered a trend towards overexpression of the lincRNA Gm12606 in both aged mMSCs and after radiation exposure compared to young mMSCs (**Figure 7**). This increase was parallel to upregulation of the nearby CDKN2A-p16 gene, suggesting a possible epigenetic interaction based on the observations of ANRIL action.

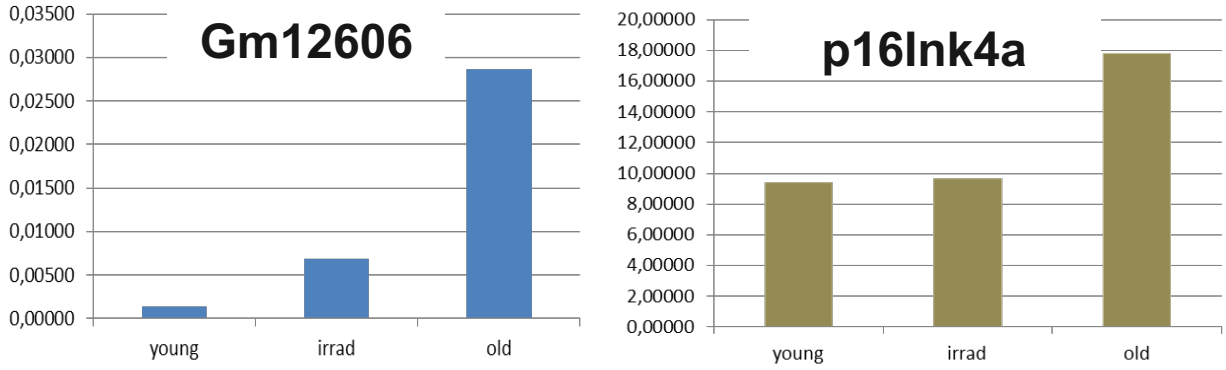

Figure 7: Identification of lincRNA Gm12606 via RNA sequencing. RNA sequencing was performed by comparing young (3 weeks), unirradiated (0Gy) mMSCs with irradiated (2Gy) and aged (8 weeks) MSCs. MSCs were isolated from FVB/N mice. Data identified a lincRNA (Gm12606) which was overexpressed in old and irradiated MSCs. This increase was parallel to the upregulation of the nearby CDKN2A/p16 gene.

Gm12606 is located on chromosome 4 (42.15 cM) in the mouse genome (**Figure 8**) in close proximity to the Ink4a/Arf/Ink4b locus in mice (**Figure 10**). The entire genomic locus of Gm12606 extends for 37705 bp and the transcript consists of two splice variants, transcript 1 (T1; 1184 bp) and transcript 2 (T2; 1055 bp), which differ in the number of exons (**Figure 9**). They share exons 2 and 4, while exon 3 is completely missing in T2. However, exon1 is present in both transcripts, but their differ in their genomic sequence. The location of exon1 of Gm12606 is very close (about 1kb) to the third common exon of the Ink4a/Arf cluster. They are both transcribed from the same strand in the same direction, but the transcripts do not overlap. Consequently, Gm12606 is characterized as a long intergenic ncRNA (lincRNA) located in the intermediate region of protein coding genes (**Figure 10**).

Figure 8: Locus of Gm12606 on chromosome 4 (42.15 cM). Gm12606 is located on chromosome 4:89,235,699-89,273,403 (reverse strand) in the mouse genome (source: http://genome.ucsc.edu).

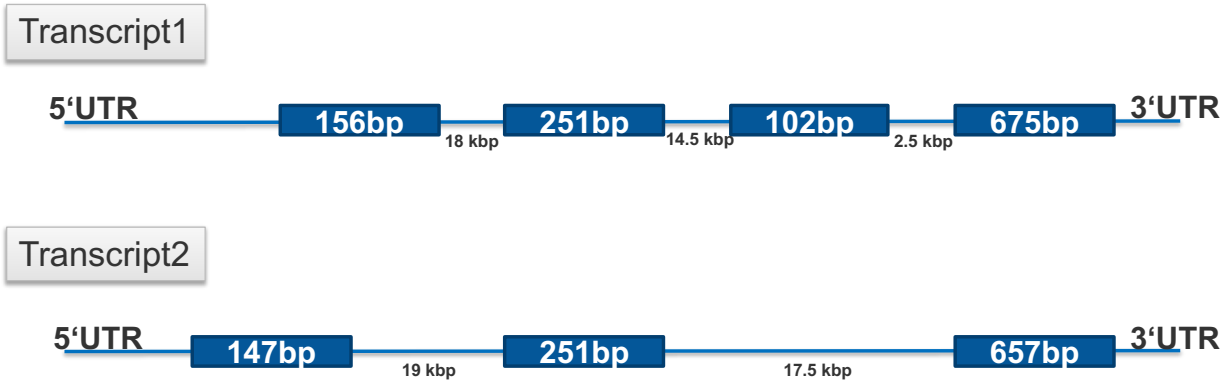

Figure 9: The two splice variants of Gm12606. T1 and T2 of Gm12606 are shown. T1 contains four exons, while T2 carries three. Both transcripts have a differing exon1 sequence but share exons 2 and 4. Exon 3 is completely missing in T2, resulting in a shorter transcript (1055 bp). T1 has a length of 1184 bp.

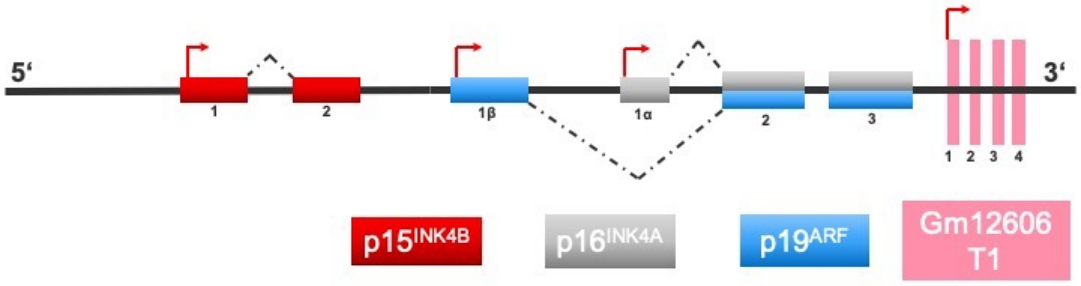

Figure 10: Gm12606 is located in close proximity to the murine Ink4a/Arf/Ink4b locus. The mouse lincRNA Gm12606 is located on chromosome 4, adjacent to the Ink4a/Arf/Ink4b locus (1kb) on the 3'UTR. The entire gene spans about 37 kb in the genome. Gm12606 and Ink4a/Arf/Ink4b are transcribed from the same strand in the same direction and each from an independent promoter.

Gm12606 has hardly been investigated so far. To date, only one publication from Mullin et al., from 2017 has been published (Mullin et al., 2017). The study indicates an interaction between the Wnt/β-catenin signaling pathway and Gm12606 after overexpression of β-catenin in neonatal primary mouse dermal fibroblasts, where the authors identified 111 lncRNAs that were differentially expressed. They focused on the most deregulated candidates and identified Gm12606 (referred as Wincr2 - Wnt-signaling induced long ncRNA), which exhibited an 8-fold difference between conditions. An increased expression of Gm12606 was determined in β-catenin overexpressed dermal fibroblast by RT-qPCR analysis (Mullin et al., 2017). For this transcript, no transgenic or knockout (KO) animal model has been reported so far. The group of Mullin et al. did not study any relation between Gm12606 and the Ink4a/Arf/Ink4b locus nearby. Due to the close proximity to the Ink4a/Arf/Ink4b locus, the parallel increase of p16 and the knowledge that lincRNAs are often involved in cell cycle regulation by targeting nearby genes (Ahmad M Khalil et al., 2009), we assume a similar interaction of Gm12606 in mice as the lncRNA ANRIL in humans. This assumption is reinforced by the finding that Gm12606 is overexpressed in ageing and irradiated mMSCs (confirmed by RNA sequencing), suggesting a role in maintaining the properties, development, and function of mMSCs.

3.7 Working Hypothesis

Functional impairments of MSC function are observed during *ex vivo* expansion and after irradiation. The expression of the lincRNA Gm12606 is altered during these processes and may be intimately connected with the functioning of the CDKN2A-p16 locus (Ink4a/Arf/Ink4b) implicated in stem cell activity. Consequently, it was **hypothesized** that the expression of p16 is regulated by the adjacent lincRNA Gm12606 during stem cell development and differentiation. As a consequence of this hypothesis, it would follow that inactivation of Gm12606 prevents age-related overexpression of p16 and thus inhibits p16-induced senescence in mMSCs (**Figure 11**). Furthermore, inactivation of Gm12606 would prevent the accumulation of DNA damage (**Figure 11**).

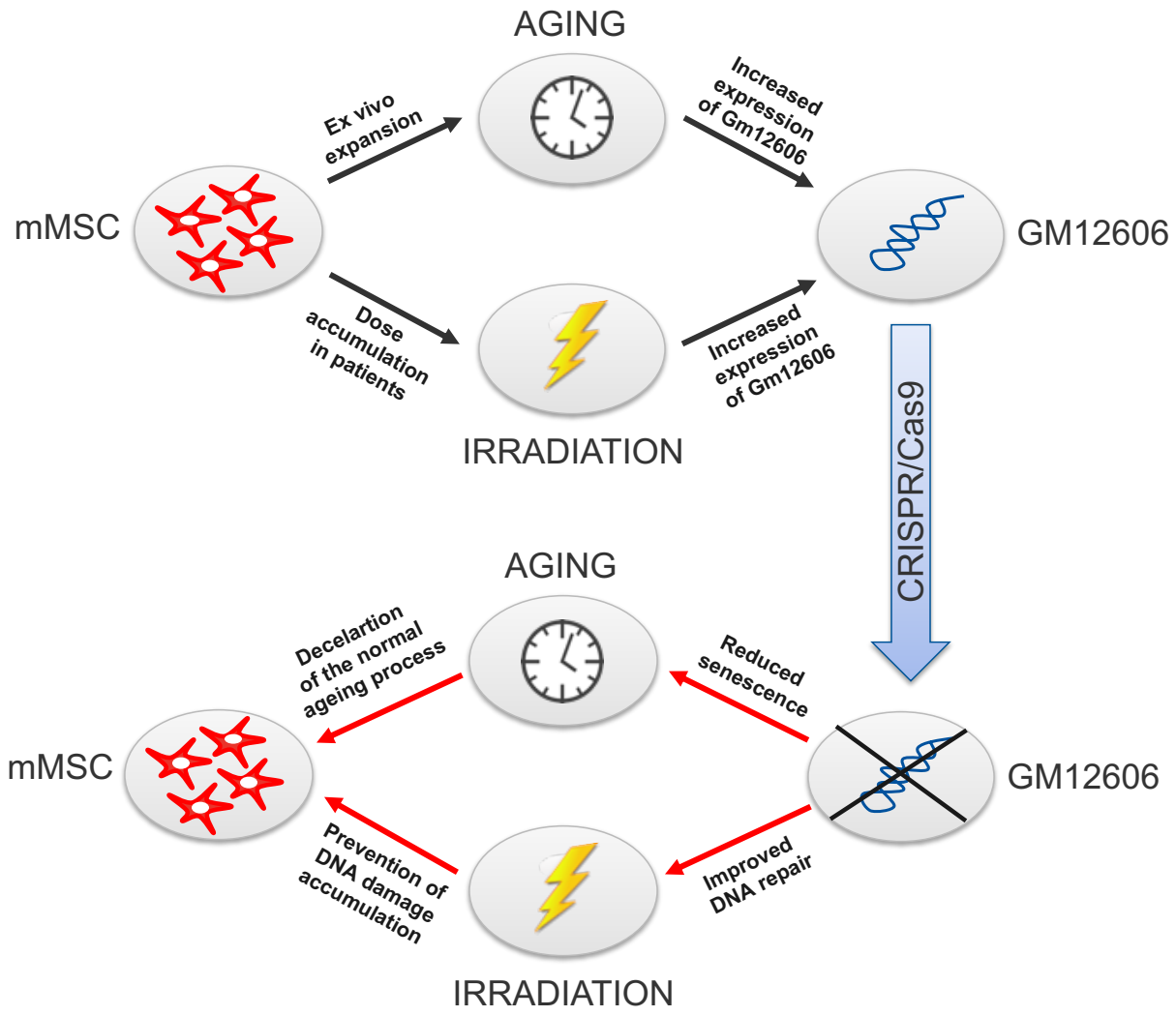

Figure 11: Graphical representation of the working hypothesis. The effect of *ex vivo* expansion and the consequence of dose accumulation by irradiation of patients, both of which result in functional impairment of MSCs, additionally leads to increased lincRNA Gm12606 expression. CRISPR/Cas9 knock out of Gm12606 is needed to improve our knowledge of the impact of Gm12606 on the properties, development, and function of mMSCs. Since Gm12606 is thought to be related to the function of the Ink4a/p16 locus, reduced senescence is hypothesized following inactivation of Gm12606, indicating that the ageing process of mMSCs would be decelerated. Furthermore, enhanced DNA repair is hypothesized as a consequence of Gm12606 inactivation, which would prevent the accumulation of DNA damage.

4. Materials

4.1 Equipment

Device	Manufacturer
^{137}Cs HWM-D 2000 (gamma source)	Hans Wälischmiller Engineering, Markdorf, Germany
Alpha Innotech ChemiImager System	Biozym, Hessisch Oldendorf, Germany
BDTM LSR II for flow cytometry analysis	BD Biosciences, Heidelberg, Germany
Centrifuge 5415C Rotor: F-45-18-11	Eppendorf, Hamburg, Germany
Centrifuge Biofuge pico Rotor: #332513	Heraeus Holding GmbH, Hanau, Germany
Centrifuge MULTIFUGE 3 S-R Rotor: 75006445	Thermo Fisher Scientific, Darmstadt, Germany
Centrifuge Rotina 420 and 420R Rotor: 4723	Andreas Hettich GmbH & Co.KG, Tuttlingen, Germany
Centrifuge SIGMA 3K15 Rotor: 11133	SIGMA Laborzentrifugen GmbH, Osterode am Harz, Germany
Electrophoresis chamber 40-1214 for horizontal midi agarose gels	PEQLAB BIOTECHNOLOGIE GmbH, Erlangen, Germany
Heating block Thermomixer compact	Eppendorf, Hamburg, Germany
Incubator 37 °C for bacterial cultures	Heraeus Holding GmbH, Hanau, Germany
Incubator 37 °C, 5% CO2 for cell culture: MCO-18AC	Panasonic Healthcare Co., Ltd., Sakata, Japan
Incubator 37 °C, 5% CO2, 2% O2 for cell culture	Sanyo, ETTEN-LEUR, The Netherlands
Incubator shaker Minitron 50	Infors HT, Einsbach, Germany
Laminar air flow work bench, UVF 6.12S	BDK Luft- u. Reinraumtechnik GmbH, Reutlingen, Germany
Laminar air flow work bench, MSC advantage	Thermo Scientific, Schwerte, Germany
Maxwell 16 DNA/RNA extraction instrument	Promega GmbH, Mannheim, Germany

Microscope Axiovert 25	Carl Zeiss, Jena, Germany
Microscope KEYENCE BZ-9000 series	KEYENCE Deutschland GmbH, Neu-Isenburg, Germany
Microwave oven TDS M1719N	Samsung, Seoul, South Korea
NanoDrop 1000 spectrophotometer.	Thermo Scientific, Schwerte, Germany
pH meter Lab850	SI Analytics GmbH, Mainz, Germany
PowerPac™ Basic Power Supply (Electrophoresis voltage and current controller)	Bio-Rad Medical Diagnostics, Dreieich, Germany
Rotations-Vakuum-Konzentratoren: RVC2-18	Martin Christ Gefriertrocknungsanlagen GmbH, Osterode am Harz, Germany
StepOnePlus Real-Time PCR System	Applied Biosystems, Darmstadt, Germany
TECAN Infinity M200 Microplate Reader	Tecan, Männedorf, Switzerland
Thermal Cycler Veriti® (PCR cycler)	Applied Biosystems, Darmstadt, Germany
Water Bath 1083 (37°C)	GFL Laborinstrumente, Burgwedel, Germany
XStrahl: RS225 X-ray source	XStrahl GmbH., Ratingen, Germany
Z Series Coulter Counter - Z1	Beckman Coulter GmbH, Krefeld, Germany

4.2 Consumables

Component	**Manufacturer**
12-well chamber slides	Ibidi, Martinsried
Cell culture flasks T25, T75 with filter-cap (CELLSTAR®)	Greiner Bio-One GmbH, Frickenhausen, Germany
Cell culture plates 6-well, 24-well, 96-well, flat bottom, transparent	Falcon™, Corning, United States
Cell scraper 25 cm	Sarstedt. Inc., Nuembrecht, Germany
Combs (16, 20, 24 teeths) for agarose ge electrophoresis	Peqlab Biotechnology GmbH, Erlangen, Germany
Cover slips (24 x 50mm)	VWR, Darmstadt, Germany
Cryo vials (1.5 ml)	VWR, Darmstadt, Germany
FACS tubes BD FalconTM 5 ml	BD Biosciences, Heidelberg, Germany

Falcon tubes (50 ml, 15 ml)	Greiner, Frickenhausen; Germany
Filter tips TipOne®	STARLAB GmbH, Hamburg, Germany
Glass microscope slides (**76 x 26mm)**	VWR, Darmstadt, Germany
MicroAmp® Optical 8-Cap Strip	Thermo Fisher Scientific, Darmstadt, Germany
MicroAmp™ Optical Tube without Cap, 0.2 ml	Thermo Fisher Scientific, Darmstadt, Germany
MILLEXGP Filter Unit 0.22 µM	Merck, Darmstadt, Germany
Petri dishes 10cm (Cell-/Tissue-cultur coated or for bacteria ?)	Nunc, Roskilde, Denmark
Serological Pipettes, sterile, 1, 5, 10, 25, 50 ml CELLSTAR®	Greiner, Frickenhausen; Germany
Reaction tubes 1.5 ml, 2 ml, (Safelock)	Eppendorf, Hamburg, Germany

4.3 Chemicals and Reagents

Chemicals	**Catalogue number**	**Manufacturer**
2-Propanol	1.09634.2500	Merck KgaA, Darmstadt, Germany
5x QPCR Mix EvaGreen® (Rox)	BS76.580.1000	Bio&SELL GmbH, Feucht / Nürnberg, Germany
10x T4 DNA Ligase Buffer	B69	Thermo Fisher Scientific, Darmstadt, Germany
10x NEB 2.1 Buffer	B72025	New England Biolabs GmbH, Frankfurt am Main, Germany
Alt-R® S.p. dCas9 Protein V3	1081066	Integrated DNA Technologies, Inc, Coralville, USA
Agarose (peqGOLD universal)	35-1020	Peqlab Biotechnologie GmbH, Erlangen, Germany
Ampicillin	A9393	Sigma-Aldrich, Taufkirchen, Germany
BactoTM Yeast extract	212750	BD Biosciences, Heidelberg, Germany
Boric acid	100165	Merk, Darmstadt, Germany
BSA (Bovine Serum Albumin)	A3059	Sigma-Aldrich, Taufkirchen, Germany

Chloroform	102445	Merck, Darmstadt, Germany
Citric acid (wieviel Hydrat ?)	X863.2	Roth, Karlsruhe
DEPC (Diethylpyrocarbonat)	A0881,0050	AppliChem, Darmstadt, Germany
Dextran sulfate	9011-18-1	USB, Buckinghamshire, England
Di-Sodiumhydrogenphosphate dihydrate	106576	Merck, Darmstadt, Germany
DMSO (Dimethylsulfoxid)	D2438	Sigma-Aldrich, Taufkirchen, Germany
DNA gel loading dye (6x)	R0611	Thermo Fisher Scientific, Darmstadt, Germany
dNTP-mix (dATP, dTTP, dGTP, dCTP) 10mM	10297-018	Thermo Fisher Scientific, Darmstadt, Germany
DPBS, no calcium, no magnesium	14190-250	Thermo Fisher Scientific, Darmstadt, Germany
DTT 0.1 M	18064-022	Thermo Fisher Scientific, Darmstadt, Germany
EDTA (Ethylenediaminetetraacetic acid, disodium salt, dihydrate)	E5314-500G	Sigma-Aldrich, Taufkirchen, Germany
Ethanol	100983	Merck, Darmstadt, Germany
Ethidium bromide (EtBr)	E1510	Sigma-Aldrich, Taufkirchen, Germany
Formamid (de-ionized)	P040.1	Roth GmbH, Karlsruhe, Germany
First strand Buffer (5x)	Y02321	Invitrogen; Carlsbad, USA
Glycerol 87%	A0970,1000	AppliChem GmbH, Darmstadt, Germany
GoTaq® Green, Master mix	M7122	Promega GmbH, Mannheim, Germany
Lipofectamine™ 2000 Transfection Reagent	11668-019	Thermo Fisher Scientific, Darmstadt, Germany
Lipofectamine™ RNAiMAX Transfection Reagent	13778030	Thermo Fisher Scientific, Darmstadt, Germany
$MgCl_2$ (Magnesiumchlorid-Hexahydrat)	A4425,0250	PanReac-AppliChem GmbH, Darmstadt, Germany

Mounting medium without DAPI (Vectashield)	4-1400	Vector, Burlingame, USA
Na acetate (CH3COONa). Trihydrat	A5268,1000	AppliChem GmbH, Darmstadt, Germany
NaCl (Sodium chloride)	A2942,5000	AppliChem GmbH, Darmstadt, Germany
Oligo(dT)12-18 primer	18418-012	Thermo Fisher Scientific, Darmstadt, Germany
One Shot® Top10 chemically competent E.Coli	C404003	Thermo Fisher Scientific, Darmstadt, Germany
Opti-MEM™	31985070	Thermo Fisher Scientific, Darmstadt, Germany
Potassium hexacyanoferrate II	P9387	Sigma-Aldrich, Taufkirchen, Germany
Potassium hexacyanoferrate III	60299-100G-F	Sigma-Aldrich, Taufkirchen, Germany
Power Up SYBR Green Mastermix	A25741	Thermo Fisher Scientific, Darmstadt, Germany
PrestoBlue® cell viability reagent	A-13262	Thermo Fisher Scientific, Darmstadt, Germany
Propidium iodide	P3566	Thermo Fisher Scientific, Darmstadt, Germany
Random hexamer DNA primers	48190011	Thermo Fisher Scientific, Darmstadt, Germany
RNaseOUT Ribonuclease Inhibitor	10777019	Thermo Fisher Scientific, Darmstadt, Germany
Roti®-Histofix 4 %	P087.6	Roth, Karlsruhe
SDS (Sodium Dodecyl Sulphate)	17-1313-01	GE Healthcare Biosciences AB, Uppsala, Sweden
STEM-CELLBANKER®	11890	AMS Biotechnology (Europe) Limited, Oxfordshire, UK
Triton X-100	9002931	Sigma-Aldrich, Taufkirchen, Germany
tRNA from E. coliMRE600	10109541001	Roche Diagnostics GmbH, Mannheim, Germany
TWEEN® 20	P9416	Sigma-Aldrich, Taufkirchen, Germany

Vanadyl-Ribonucleoside complex (NEB)	94740-250MG	Sigma-Aldrich, Taufkirchen, Germany
X-gal (5-Bromo-4-chloro-3-indolyl β-galactopyranosite)	R0401	Thermo Fisher Scientific, Darmstadt, Germany

4.4 Molecular weight and length standards

Marker	**Catalogue number**	**Producer**
GeneRulerTM 100bp DNA ladder	SM0241	Thermo Fisher Scientific, Darmstadt, Germany
M1 lambda Hind III and 174 Hae III		Provided by M.Rosemann

4.5 Solutions and Buffers

Solution or Buffer	**Reagents**
LB agar (pH 7.0)	1 l LB media (pH 7.5), 20 g Agar
LB media (pH 7.5)	10 g BactoTM Tryptone, 5 g BactoTM Yeast extract, 10 g NaCl, 1 l Water
Microinjection buffer (pH 7.2)	5 mM Tris, 0.1 mM EDTA
Senescence staining solution (pH 6.0)	1.42 g di-Sodium hydrogen phosphate dehydrate (40 mM), 200 ml Distilled water, 1.75 g NaCl (150 mM), 81.32 mg MgCl2 (2 mM), 400 mg Hexacyanoferrat II (5 mM), 320 mg Hexacyanoferrat III (5 mM), 100 µL X-gal (50 mg/ml) to 5ml of Buffer
Stellaris pre-hybridization solution	10 % Formamide (deionized), 2x SSC
Stellaris hybridization solution (50 µL)	2x SSC, 10 % Formamide, 50 µg competitor E. coli tRNA, 10 % Dextrane sulfate, 2 mg/ml BSA, 10 mM Vanadyl-ribonucleoside complex, 1 ng/ µl Gm12606 probe

TBE buffer 5x (pH 8.3)	1.1 M Tris, 900 mM Boric acid, 25 mM EDTA
TE-Buffer (pH 7.0)	10 mM Tris-HCl, 1 mM EDTA
Tissue (tail-tip) lysis buffer	50 mM Tris pH 8, 100 mM EDTA, 100 mM NaCl, 1% SDS, 0.5 mg/ml Proteinase K

4.6 Commercial kits

Kit name	**Catalogue number**	**Producer**
BigDye® Terminator v3.1 Cycle Sequencing Kit	4337454	Thermo Fisher Scientific, Darmstadt, Germany
EnGen® sgRNA Synthesis Kit, S. pyogenes	E3322S	New England Biolabs, Ipswich, USA
Maxwell® 16 miRNA Tissue Kit	AS1470	Promega Corporation; Madison, USA
pGEM®-T PCR cloning	A3600	Promega Corporation; Madison, USA
PureYield Plasmid Midiprep System	A2492	Promega Corporation; Madison, USA
QIAamp DNA Mini Kit	51304	Qiagen, Hilden, Germany
QIAprep Spin Miniprep Kit	27106	Qiagen, Hilden, Germany
QIAquick Gel Extraction Kit	28704	Qiagen, Hilden, Germany
QIAquick PCR Purification Kit	28104	Qiagen, Hilden, Germany
TOPO® TA Cloning Kit	K4595-40	Thermo Fisher Scientific, Darmstadt, Germany
Wizard® Genomic DNA Purification Kit	A1120	Promega Corporation; Madison, USA

4.7 Vectors

Vectors	Catalogue number	Producer
Bluescript plasmid containing a U6 promoter (pBS-U6-Cas9)		Addgene, Watertown, USA (obtained from Institute of Developmental Genetics (O.Ortiz), Helmholtz Centre Munich)

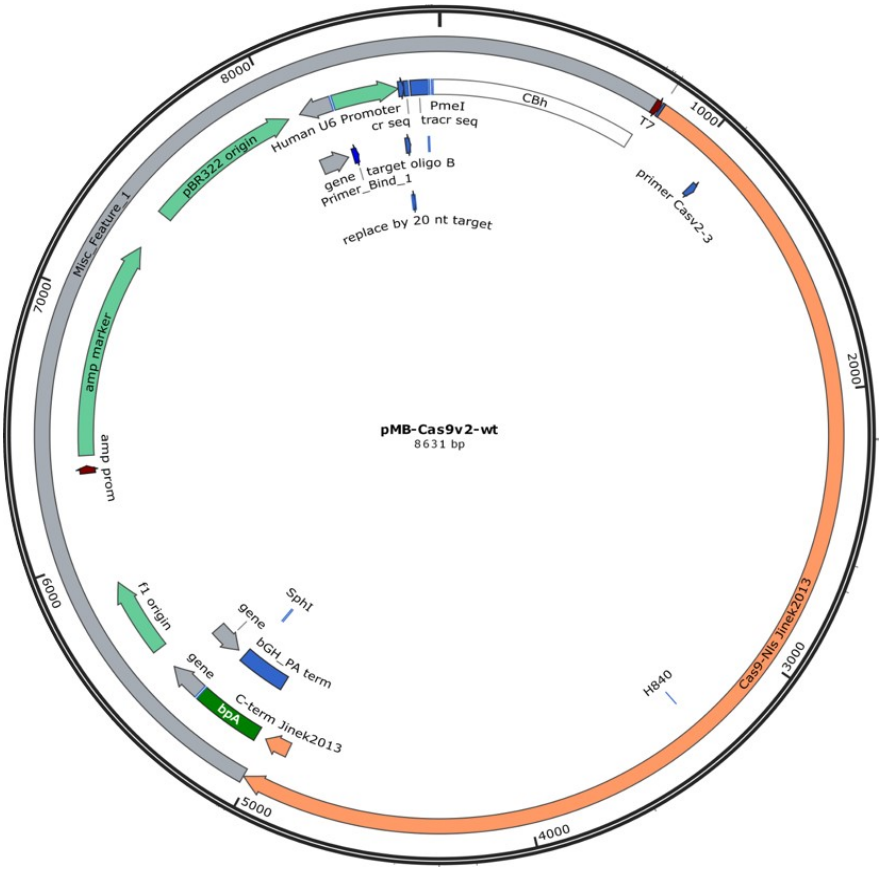

Figure 12: CRISPR/Cas9 vector (obtained from Institute of Developmental Genetics (O.Ortiz), Helmholtz Centre Munich). Plasmid containing a U6 promoter driving transcription of the inserted gRNA sequence and expression of the Cas9 enzyme (pBS-U6-Cas9) for CRISPR/Cas9- mediated KO of the lincRNA Gm12606 *in vitro*.

4.8 Antibodies

Primary Antibodies	Catalogue number	Producer
Anti-γH2AX, monoclonal, mouse	05636	Millipore; Schwalbach, Germany
Anti-53BP1, polyclonal, rabbit	NB100-305	Novus Biological; Littleton, USA
Secondary antibodies:		
Cy3-conjugated anti-mouse, sheep	515-165-003	Jackson Immunoresearch; West Grove, USA
Alexa 488-conjugated anti-rabbit, goat	Lot. 659082	Invitrogen; Oregon, USA

4.9 Enzymes

Enzyme	Catalogue number	Producer
BbsI	R05395	New England Biolabs GmbH, Frankfurt am Main, Germany
Proteinase K, recombinant	03115879001	Roche Diagnostics, Basel, Switzerland
StemPro® Accutase	A1110501	Gibco™ Thermo Fisher Scientific, Darmstadt, Germany
SuperScript® II Reverse Transcriptase	18064-022	Thermo Fisher Scientific, Darmstadt, Germany
T4 DNA Ligase	E10011	Thermo Fisher Scientific, Darmstadt, Germany
Trypsin-EDTA 0.05%	25300-054	Gibco™ Thermo Fisher Scientific, Darmstadt, Germany

4.10 Single guide RNAs (sgRNAs)

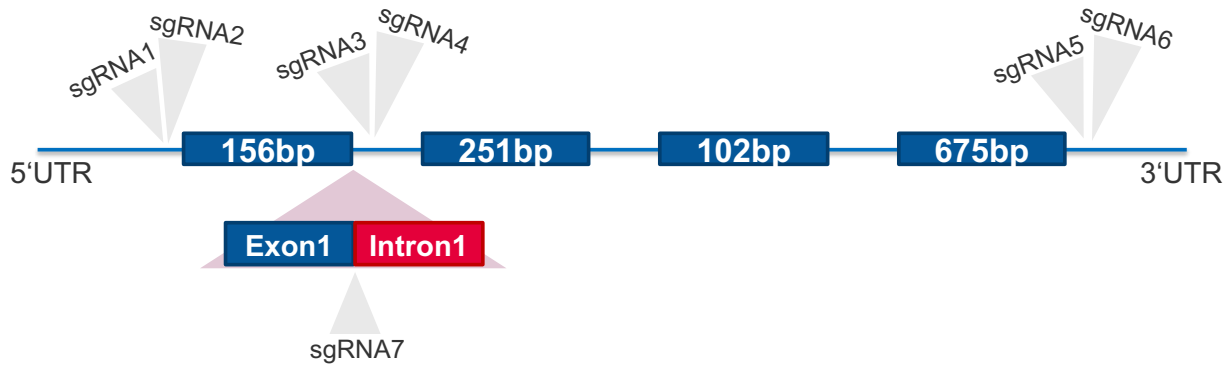

Figure 13: Target sites in the DNA of Gm12606 T1 of all sgRNAs used in this project. DNA oligonucleotides were generated and designed with the help of the CRISPR design tool CRISPOR (Haeussler et al., 2016) produced by Eurofins Genomics GmbH. Sequences are listed in the following table.

Region	sgRNA	Quality score	Guide sequence 5'-3'	On-target locus	Number of predicted off-target sites
5'UTR	sgRNA 1	84	TTGGTTTGGTTTAAACGGTT TGG	chr4: +88918547	182 (20 are in genes)
5'UTR	sgRNA 2	79	GGGGGTCCCCACCCGCTCAG AGG	chr4: -88918674	120 (27 are in genes)
In1	sgRNA 3	96	CTCGCACAGAAAGCCGCGTC AGG	chr4: +88918227	36 (6 are in genes)
In1	sgRNA 4	92	TGGAGTTCCTATCCCCGTTG GGG	chr4: +88918117	68 (4 are in genes)
3'UTR	sgRNA 5	56	AGGAAGATTCTTGACTCTTG AGG	chr4: -+88881529	338 (13 are in genes)
3'UTR	sgRNA 6	91	GTGATTCATATACGATGCCT AGG	chr4: +88881215	68 (4 are in genes)
Ex1/In1	sgRNA 7	76	CTCTTAGAGCCCCATGGGTTC AGG	chr4:	153 (11 are in genes)

4.11 PCR Primers

4.11.1 Genotyping

All primers were designed with the help of the website http://genscript.com/tools/pcr-primers-designer. The annealing temperature for the primers has been set at approximately 59 °C. The oligonucleotides were provided by the manufacturer in lyophilized form of 40 nmol and were dissolved in RNase-free water to working concentrations of 10 pmol/µl.

	Gene	Forward primer 5'-3'	Reverse primer 5'-3'
P1	**Gm12606 (5'UTR-3'UTR) Flanking whole gene**	TGTACCTCAAATAGCAAACAGTTAC	GAAAACACGGGGAAAGCAAGTC
P2	**Gm12606 (5'UTR-In1) Flanking sgRNA 1&2 binding site**	TGTACCTCAAATAGCAAACAGTTAC	GTTAATAAGCAGTGCTCCAATG
P3	**Gm12606 (5'UTR-In1) Flanking sgRNA 3&4 binding site**	GTGGTTCAGACTCTTAGAGC	AAAAAAAACTTAACAGTGTTTACCAAATC
P4	**Gm12606 (Ex4-3'UTR) Flanking sgRNA 5&6 binding site**	AATTTATGACAAAAGATGCCATGAG	GAAAACACGGGGAAAGCAAGTC

P5	**Gm12606 (Exon1-In1) Flanking Ex1/In1 junction**	GCCGGACAGAGCAGACCCCA	GTCCGAGCTATACAGAAGAATC AAGCG
P6	**Gm12606 (5'UTR-In1) Flanking Ex1/In1 junction**	ACCCTAGAGGGGGTTCCATC	CAATGTTCAATGGAGGGCCG

4.11.2 Real-time PCR

All primers were designed with the help of the website http://genscript.com/tools/pcr-primers-designer. The annealing temperature for the primers has been set at 60 °C. The oligonucleotides were provided by the manufacturer in lyophilized form of 40 nmol and were dissolved in RNase-free water to working concentrations of 5 pmol/µl.

Gene	**Forward primer 5'-3'**	**Reverse primer 5'-3'**
14-3-3b	TAAACAAACCACGGTGTCCA	GCTGCATTTCTTTCTTGCTG
Bmi1	GTCAGCTGATGCTGCCAAT	CCTCTTCTCCTCATCTGCAA
Dkk2	TAGGAAGGCCACACTCCAAG	CCTGATGGAGCACTGGTTTG
Gm12606_T1 (Exon2-4)	GGCCTGGATAGAGGTCTCC	TAGTTCTCTCCATCGGTTTCC
Gm12606_T2 (Exon1-2)	ACTGGAGCTCAGGGTTCAGC	GGCTCTTCGGGAGAGATC
Gm12606_T1/T2 (Exon2-3/4)	GGTACCTAGGCCCACATCTC	TGTAGATGGATTCGCTGGGT
Klf4	GAACTCACACAGGCGAGAAA	AAAGGCCCTGTCACACTTCT
Nestin	GAACTGGCACACCTCAAGAT	GTGTCTGCAAGCGAGAGTTC
P15 (Ink4b)	CTCCAGCTCGACAAG	CAATTCATCACTGGGCTTTG
P16 (Ink4a)	GAACTCGAGGAGAGCCATCT	GGGTACGACCGAAAGAGTTC
P19 (Arf)	GGTCACTGTGAGGATTCAGC	ACATGTTCACGAAAGCCAGA

P21	ACCATGTCCAATCCTGGTG	AGAGACAACGGCACACTTTG
P27	TCTCAGGCAAACTCTGAGG	CTTCTGTTCTGTTGGCCCTT
Rb1	CTTGCATGGCTTTCAGATTC	TGCAGTATGGTTACCCTGGA
Rbbp1	CGAGAGTGAGACTCTGGATCA	TCCTCCCTCTGTTGGTCTTC
Rbl1	GTCAAGGAAGTTCGCACTGA	GTAGCGCTCATGGACAGAAA
Tbp (Housekeeping gene)	ACTTCGTGCAAGAAATGCTG	CTTCACTCTTGGCTCCTGTG

4.12 Gm12606 oligonucleotides for knockdown

Antisense LNA GapmeR in vitro standard oligos from Exiqon; Vedbaek, Denmark

Product name	Product number	Product Sequence 5'-3'	Concentration (pmol)
LincR166/8_1 (Gm12606)	300600	GTAGATGGATTCGCTG	100
LincR166/8_2 (Gm12606)	300600	AGCGAGGGAAGTGAGT	100

4.13 Mice

FVB/N mice – bred and maintained at the central animal facility of the Helmholtz Centre Munich, Germany

C3H/H-Nhg mice – bred and maintained at the central animal facility of the Helmholtz Centre Munich, Germany

C57BL/6N mice – Charles River Laboratories, Sulzfeld, Germany

4.14 Cell culture

4.14.1 Standard tissue culture media and supplements for MSC culturing and differentiation

Basal medium + Serum	Company
DMEM (1x) + GlutaMAX + 10% HyClone Fetal Bovine Serum (FBS)	Gibco Thermo Fisher Scientific, Darmstadt, Germany
DMEM/F-12, GlutaMAX + 10% MSC Qualified Fetal Bovine Serum (FBS)	Gibco Thermo Fisher Scientific, Darmstadt, Germany
Stem Pro Osteoblast Differentiation Basal Medium + 10% Stem Pro Osteogenesis Supplement	Gibco Thermo Fisher Scientific, Darmstadt, Germany
Stem Pro Adipocyte Differentiation Basal Medium + 10% Stem Pro Adipogenesis Supplement	Gibco Thermo Fisher Scientific, Darmstadt, Germany
Stem Pro Chondrocyte Differentiation Basal Medium + 10% Stem Pro Chondrogenesis Supplement	Gibco Thermo Fisher Scientific, Darmstadt, Germany

4.14.2 Cell lines

Mouse osteosarcoma (MOS) and primary mouse osteoblasts (mOB) cell line (kindly generated and provided by Dr. Michael Rosemann)

4.15 Software

Software	Version	Application	Provider
AxioVisionAC 4.2		Micro-Image processing	Carl Zeiss, Oberkochen, Germany
BZ-II Analyzer		Micro-Image processing and analysis	KEYENCE Germany GmbH, Neu-Isenburg, Germany
GraphPad Prism 5.04		Statistical Analysis and graphical presentation	GraphPad Software, USA
ImageJ - Fiji		Image processing and analysis	Open Source
SnapGene Viewer		Vector and sequence design and visualization	Open Source
StepOne software v2.3		Quantitative Real-Time PCR Data analysis	Applied Biosystems, Darmstadt, Germany

5. Methods

5.1 Cell culture

5.1.1 Cultivation of primary murine MSCs

Primary mMSCs were isolated from the bone marrow plugs released from the femurs and tibias of C3H/H-Nhg, FVB/N or C57BL/6N mice. Prior to extraction, mice were sacrificed by CO_2 asphyxiation. Limbs were cleaned from adherent tissue and the marrow expressed into a 15 ml Falcon tube using ice cold PBS passed through a 27G injection needle. The resulting marrow was suspended as single cells by gentle vortexing. The cells were centrifuged at 1300 rpm for 5 min and the supernatant discarded. Finally, the cells were resuspended in 12 mL of DMEM/F12 media containing 10 % mesenchymal stem cell qualified FBS. For adhesion, cultures were seeded in T25 cell culture flasks because MSCs have the ability to bind to plastic substrates, and maintained under hypoxic conditions (2% O_2, 5% CO_2) at 37°C in a humidified atmosphere. The medium was exchanged with fresh media after 4h and then after a further 16-20h. The exhausted medium containing non-adherent cells was collected aseptically and transferred to a new flask to increase the maximum yield of mMSCs by allowing late attaching cells to adhere. Twice a day during the following 3 days the non-adherent cells were eliminated by media exchange (protocol modified from Soleimani and Nadri (Soleimani & Nadri, 2009)). After 7 days and reaching 80 % confluency, the adherent cells were passaged by flooding the plastic surfaces with StemPro Accutase Reagent. Recovered cells were counted using a Cell Counter Analyzer and subsequently passaged once a week by splitting in a 1:3 ratio. After each passage the rock-inhibitor Y-27632 (an inhibitor of non-canonical Wnt-signalling) was added to a final concentration of 10 nM. Rock-inhibitor was found to prevent detachment of hMSCs and promote their proliferation and differentiation (Nakamura, Yoshimura, Kaneko, Sato, & Hara, 2014). After 3, 5 or 7 passages,

primary mouse MSCs were resuspended in stem cell banker medium, frozen at -80 °C, and stored in liquid nitrogen the next day for use in subsequent experiments.

5.1.2 Cultivation of mouse osteoblast and mouse osteosarcoma cells

Mouse osteosarcoma (MOS) and primary mouse osteoblast (mOB) cells (kindly generated and provided by Dr. Michael Rosemann) were cultured in DMEM (1x) + GlutaMAX media containing 10% HyClone Fetal Bovine Serum (FBS) under normoxic conditions (20-21% O_2, 5% CO_2) at 37 °C in a humidified atmosphere. At 80 % confluency, cells were detached by using 0.05% trypsin-EDTA and passaged in a 1:5 ratio.

5.2 Irradiation

During the first year of this project, *in-vitro* γ-irradiation of cells was performed using an HWM-D-2000 (Siemens, Germany) Cs137 γ-source providing a dose rate of 0.5 Gy/ min. Cells were kept at room temperature during irradiation and control cells were sham-irradiated by carrying the controls to the radiation facility without exposing them to irradiation. During subsequent years the HWM-D-2000 radiation facility was replaced by an X-ray cabinet RS225 (XStrahl GmbH Germany). Here the dose rate was calibrated at 0.82 Gy/min with 10 mA and 195 kV X-ray radiation. A 3 mm-thick aluminium filter was used for beam hardening at a 60 cm distance. Sham-irradiated controls were treated according to the same protocol, but without switching on the X-ray-beam.

5.3 Molecular biological techniques

5.3.1 DNA isolation

DNA isolation from mouse tail tips and ear biopsies

Analysis of the success of gene editing was performed by PCR of genomic DNA isolated from tail or ear biopsies of F1 and F2 progeny animals. 2 mm long tail tip or ear tissue was cut off from each mouse by Dr. Michael Rosemann. Tail or ear tissue samples were removed, and the tissue digested with 750 µL tail tip lysis buffer at 55 °C in a thermomixer heating block at 800 rpm overnight. 250 µL 6M NaCl was added, and the lysates mixed by vortexing then centrifuged for 20 min at 4 °C and 10000 rpm. To precipitate the DNA, 400µL of clear suspension was carefully removed and mixed in a 1.5 ml Eppendorf tube with 1 ml of 95% ethanol, shaken by hand and centrifuged at 13000 rpm for 10 min. The precipitated DNA pellet was washed with 500 µL 75% ethanol. The ethanol was removed and the pellet air dried and resuspended in 200 µL nuclease-free water by mixing in a thermomixer at 50 °C for 30 min. The DNA concentration was measured with a NanoDrop 1000 spectrophotometer. An OD 260/280 ratio of ~1.8 was accepted as an indicator of DNA purity.

DNA isolation from cultured cells

DNA was isolated from cells using the QIAamp DNA Mini Kit according to manufacturer's procedure. Prior to extraction the cells were released from the cell culture dishes with Accutase or Trypsin/EDTA specify and 1x PBS washes. After centrifugation the cell pellets were stored at -80 °C or used directly for DNA extraction. The pellets were lysed with 200 µL PBS and 20 µL proteinase K and 200 µL buffer AL, mixed thoroughly by vortexing for 15 sec and incubated at 56 °C for 10 min in a thermomixer heating block. After the addition of 200 µL 100% ethanol the pellet was mixed one again by vortexing for 15 sec. The pellet was transferred to a QIAamp spin column and centrifuged at 8000 rpm for 1 min. The filtrate was discarded, and the column washed with

500 µL Buffer AW1 and AW2 followed by centrifugation (8000 rpm for 1 min) after each wash. Finally, the DNA was eluted from the column by pipetting 50-100 µL nuclease-free water and collected by centrifugation for 1 min and 8000 rpm. The DNA concentration was measured with a NanoDrop 1000 spectrophotometer. An OD 260/280 ratio of ~1.8 was accepted as an indicator of DNA purity.

5.3.2 RNA isolation

Total RNA was isolated from cells using the Maxwell® 16 miRNA Tissue Kit according to manufacturer's procedure. Cells were recovered from the cell culture dishes with Accutase or Trypsin/EDTA and 1x PBS washes. After centrifugation the cell pellet was treated with 200 µL of cooled homogenization solution that contains thioglycerol provided by the company. After the addition of 200 µL lysis buffer and 15 µL proteinase K, the solution was mixed by vortexing and incubated for 10 min at RT. The resultant cell lysate was transferred to the Maxwell device and miRNA extraction settings selected. After recovery the total RNA content was measured using a NanoDrop 1000 spectrophotometer. An OD 260/280 ratio of ~2.0 was accepted as an indicator of RNA purity.

5.3.3 Polymerase chain reaction (PCR)

DNA amplification was performed by PCR using 2x GoTaq® Green PCR Master mix that contains $MgCl_2$, dNTPs, reaction buffers and Taq DNA polymerase. For mouse genotyping, the concentration of the PCR master mix was increased as needed to ensure successful DNA amplification. A no template control (NTC) was performed as the negative control to detect primer dimer formation and contamination.

Table 1: PCR reaction mixture

Component	Quantity (µL)
Master mix (GoTaq® Green) 2x	10
Forward primer (10 pmol)	1
Reverse primer (10 pmol)	1
Nuclease free water	7
Template DNA (30 ng/µl)	1
Total volume	20

Primer sequences used for DNA amplification are listed in chapter 4.11.1. PCR reactions were performed using the Veriti® thermal cycler with the parameters listed below.

Table 2: PCR reaction program

Step	Time (sec)	Temperature (°C)	Cycles
Initialization	60	96	1x
Denaturation	10	94	35x
Annealing	15	55-60	
Elongation	120	72	
Final hold	∞	4	

5.3.4 Agarose gel-electrophoresis

PCR products were analysed on 1.5 - 2.5% TBE agarose gels, depending on the expected amplicon length. The required amount of agarose was dissolved in 100 ml 1x TBE electrophoresis buffer and boiled in a microwave oven followed by cooling to about 50°C with stirring. 5 µL EtBr (10 mg/ml) was added and the mixture was poured into gel casts with the appropriate combs inserted. After the gel solidified the combs were removed and the gels placed in an electrophoresis chamber filled with 1x TBE buffer. For analysis of amplification of DNA templates, samples were prepared by adding 2 µL loading dye to 10 µL of PCR product, and for cDNA templates analysis, 4 µL loading dye was mixed to 20 µL of qPCR product. For size analysis 7 µL of a 100 bp molecular weight ladder were loaded to the first well of the gel. Electrophoresis was done at 90V with run times of between 1 and 2 hours (depending on amplicon size). The PCR products were visualized using the Alpha Innotec ChemiImager Transilluminator System at 312nm. Images were captured by the CCD camera through an orange band-pass filter and stored as 16bit tiff graphic files.

5.3.5 Reverse transcription

Total RNA was used for the synthesis of complementary DNA (cDNA) using random hexamers and (or) oligo (dT) primers. 200 ng of RNA was dried in a vacuum concentrator for 20 min by 30 °C. 10µl nuclease free water plus the diluted primers and dNTPs were added directly to the dried RNA and incubated for 5 min at 65 °C in a thermomixer. The primers were allowed to anneal to the RNA by incubation on ice for at least 5 min.

Table 3: Reverse transcription reaction mixture

Component	Quantity (µL)
Template RNA (200 ng/µL)	
dNTP mix (10 mM)	1
Random hexamers (50 µM)	0.5
Oligo dT (0.5 µg/µL)	0.5
Nuclease free water	10
Total volume	12

5x First stranded buffer, DTT and Rnase inhibitor were added to the RNA/primer mixture, mixed carefully and placed for 2 min at RT (for random hexamers hybridization) with subsequent 2 min incubation at 42 °C (for oligo dT hybridization).

Table 4: Reverse transcription reaction program

Component	Quantity (µL)
First stranded (5x)	4
DTT (0.1 M)	2
Rnase Out (40 U/µL) not same name as in text	1
Total volume	7

Synthesis of the single stranded cDNA was initiated by adding 1 µL 200 U/µL Superscript II reverse transcriptase. The reaction tube was kept for 10 min at RT (for random hexamers hybridization) followed by incubation for 50 min at 42 °C (for oligo dT hybridization). Inactivation of the enzyme was achieved by heating at 70 °C for 15 min. The synthesized cDNA was diluted in a ration of 1:5 with nuclease free water stored at -20 °C till further use.

5.3.6 Real time polymerase chain reaction (RT-qPCR)

RT-qPCR is a precise method for the quantitative assessment of gene expression. It was performed with 2x Power Up SYBR Green (ROX) Master Mix using the StepOne Plus Real time PCR machine. Power Up SYBR Green provides additional features, including the incorporation of UDG to prevent carry-over contamination and a dual hot-start mechanism to improve reaction specificity by preventing an early start of Taq polymerase activity at low temperatures.

The relative transcript level of the lncRNA or mRNA template in a sample was determined using the comparative 2-ΔΔCt method with Ct values automatically generated by the StepOne Plus software. This method compares the relative changes in gene expression of a gene of interest compared to a control. Baseline and threshold were adjusted separately for each gene. Ct values of genes of interest were normalized in relation to the endogenous control (The TATA binding protein (TBP)). Ct values for calibrators (e.g., sham irradiated or not-treated samples) were also determined in relation to endogenous control. These values were subtracted from each other and used for calculation. The lncRNA or mRNA expression was measured using divergent primers manufactured by Eurofins Genomics GmbH, Ebersberg. A list of primer sequences is available in section 4.11.2. An NTC was performed as a negative control to monitor primer dimer formation as well as contamination and to avoid false positive results. Setup for RT-qPCR reaction and program are shown in the following tables.

For this project the SYBR Green reporter was used in the amplification reactions performed with the StepOne Plus Real time PCR device. SYBR Green has the advantage to examine the quality of the RT-qPCR reaction by melting curve analysis. Single melting curve peaks indicate good quality by pure amplification products. If multiple peaks are present, the reaction contains either unspecific products, multiple mRNA isoforms, primer dimers or PCR heteroduplexes.

Table 5: RT-qPCR reaction mixture

Component	**Quantity (µL)**
Master mix (2x Power Up SYBR Green)	10
Forward primer (5 pmol)	1
Reverse primer (5 pmol)	1
Nuclease free water	6
Template cDNA (200 ng/µl) or DNA	2
Total volume	20

Table 6: RT-qPCR reaction program

Step	Time (sec)	Temperature (°C)	Cycles
UDG activation	120	50	
Dual-Lock DNA polymerase	2	95	
Denaturation	15	95	40x
Annealing/ Elongation	60	60	
Melt Curve Stage I	15	95	
Melt Curve Stage II	60	60	
Melt Curve Stage III	95	95	
Final hold	∞	4	

5.3.7 Sequencing

The precise location of a genomic deletion in lncRNA as well as the correct amplification of PCR products was determined by sequencing of the PCR products using flanking primers. For this purpose, the PCR products were purified using a QIA quick PCR amplification kit according to the manufacturer's protocol. Subsequent sequencing reactions were performed using the BigDye® Terminator v3.1 Cycle Sequencing Kit. The reaction mixture was prepared using 150-300 ng template DNA. Two separate reactions, one with the forward and one with the reverse primer, were performed for each sample to guarantee accurate sequencing reads.

Table 7: Sequencing reaction mixture

Component	Quantity (µL)
BigDye® Terminator v3.1 reaction mix	8
Forward primer (5 pmol) or reverse primer (5 pmol)	1
Nuclease free water	to make up the volume to 20 µl
Template DNA (purified product)	required for 150-300 ng of DNA
Total volume	20

Primer sequences used for sequencing are listed in chapter 4.11.1. Sequencing reaction was performed with the Veriti® thermal cycler under the following reaction conditions.

Table 8: Sequencing reaction program

Step	Time (sec)	Temperature (°C)	Cycles
Initialization	60	96	1x
Denaturation	10	96	25x
Annealing	5	50	
Elongation	240	60	
Final hold	∞	4	

The amplified dye-terminator DNA fragments were precipitated from the reaction mixture by adding 70 µL 70% ethanol and the solution transferred to the wells of barcode labelled 96-well plates provided by the sequencing facility of Helmholtz Centre Munich. Plates were centrifuged at 4500 rpm for 30 min, followed by a brief upside-down centrifugation to remove the supernatant. 100 µL 70% ethanol was added to the wells and the plates kept at RT for 15 min before the centrifugation was repeated as before. Pellets were air dried for 30 min and 50 µL of HPLC grade or nuclease-free water were added to each well. The plates were covered with silicone sealing membrane and sequencing was performed. Snap Gene Viewer was used to analyse the sequencing results.

5.3.8 Stellaris® RNA Fluorescence in situ hybridization (RNA-FISH)

Stellaris RNA FISH is an RNA imaging technique that enables the combined detection, localization and quantification of intracellular RNA molecules using fluorescence microscopy. The procedure was performed according to the manufacturer's protocol for adherent cells. Probes complementary to the target RNA were designed using the online probe designer tool (https://biosearchtech.com/Account/Login?return=/stellaris-designer) with 25 specific probes selected using the Gm12606 input sequence. Custom oligonucleotide probe was commercially synthesized, and dual end labelled with Quasar®570 (Ex: 552 nm; Em: 570 nm).

MOS, mMSCs and mOB were grown on 12-well chamber slides for two days before cells were fixed with Roth HistoFix for 30 min, followed by two washes with 1x PBS. For permeabilization 250 µL ethanol were added to the cells for at least 1h or stored up to one week at 4 °C in 1x PBS. Pre-hybridization buffer and hybridization buffer were prepared as described in section 4.5. All solutions (except the probe) were autoclaved before use and sterile deionized water was treated with DEPC (Diethylpyrocarbonat) to remove RNAse contamination. Prior to treatment, 1 µL of probe again was mixed with 100 µL hybridization buffer. Ethanol was aspirated from the cells and

they were washed with 1x PBS. 250 µL pre-hybridization buffer was added and cells incubated for 5 min at RT. Pre-hybridization buffer was discarded and cells subsequently covered with 100 µL hybridization buffer containing the probe. Cells were incubated overnight (~16h) in the dark at 37 °C in a humidified chamber, followed by two washing steps with an incubation in pre-hybridization buffer for 15 min at 37 °C. The pre-hybridization buffer was removed, and cells washed additionally with 1x PBS. In order to make the nuclei visible, cells were counterstained with Hoechst 33342 in PBS (1:2000) by covering cells for 10 min, followed by three washing steps carried out three times with 1x PBS. Cells were mounted with Vectashield and cover slipped. Fluorescence images were acquired with the Keyence microscope and associated BZ II viewer software.

5.3.9 Differentiation assay

Alterations in the mesenchymal lineage multipotency of mMSCs was investigated by treating cells with mixtures of growth factors and cytokines e.g., dexamethasone, glycerophosphate and ascorbic acid to provoke either osteogenic, adipogenic or chondrogenic differentiation (induced differentiation). Cells were seeded in 6-well plates and cultured in appropriate amounts of cell culture medium up to 80 % confluency. To induce adipogenic differentiation the MSC growth medium was replaced by an adipogenic differentiation medium consisting of the Stem Pro Adipocyte differentiation basal medium and Stem Pro Adipogenesis supplement (containing insulin) in a ration of 1:10 ratio. For osteogenic differentiation, cells were treated with Stem Pro Osteoblast Differentiation Basal Medium and Stem Pro Osteogenesis Supplement (containing dexamethasone, glycerol-phosphate, and ascorbic acid) at the ratio of 1:10. To stimulate mMSC chondrogenic differentiation very dense cultures of MSCs were required. Therefore, mMSCs were seeded in a single drop in 500 µL medium and allowed to adhere to the surface for 2 hours. After adhesion the medium was supplemented with Stem Pro Chondrocyte Differentiation Basal

Medium and Stem Pro Chondrogenesis Supplement (containing TGF-beta, insulin, dexamethasone, and sodium pyruvate) in a ratio of 1:10.

Cells were cultivated for four days in the appropriate differentiation medium and harvested by scraping with a sterile cell scraper. Pellets were washed with 1x PBS and stored in -80°C. RNA was isolated using the Maxwell® 16 miRNA Tissue Kit. cDNA synthesis and RT-qPCR were performed according to standard procedure.

5.3.10 Antisense oligonucleotide-mediated knockdown of Gm12606 *in vitro (*LNA GapmeR transfection)

Antisense oligonucleotide (ASO)-mediated knockdown was achieved and used to examine the involvement of Gm12606 in the regulation of nearby genes. In contrast to siRNA knockdown, ASO can also downregulate RNA that is exclusively in the nucleus and activate Rnase H mediated target degradation. mMSCs were cultured under normal conditions (chapter 5.2). 250000 cells were seeded in 6-well cell culture plates and cells transiently transfected the next day with lipofectamine RNAiMAX transfection reagent and Antisense LNA longRNA GapmeR in vitro standard oligonucleotides. The sequences of the oligonucleotides were designed using Exiqon's GapmeR Design Algorithm (chapter 4.12) and two different oligonucleotides were provided by the company that were co-transfected. 5 µL lipofectamine had been diluted in 120 µL Opti-MEM medium. Similarly, 123 µL Opti-MEM medium was added to different volumes of LNA oligonucleotides (100/150/200 pmol/µL) (2 µl; 3 µl, 4 µl). The diluted lipofectamine was combined with the diluted LNA oligonucleotides, incubated for 15 min at RT and transferred to 1750 µL culture medium that was added to the cell cultures. Cells were incubated for either 24h or 48h before harvesting. To exclude off-target effects caused by the oligonucleotides control cells were exposed to a negative control scrambled 17 nt LNAs oligonucleotides (scr) produced by the company Sigma-Aldrich Chemie GmbH. In addition, lipofectamine only transfected cells were

used for an initial comparative analysis. After incubation the transfected cells were removed from the dishes with 0.05 % Trypsin/EDTA or Accutase, 1 x PBS washes and stored in -80 °C for further gene expression analysis.

5.4 CRISPR/Cas9

The original aim of the study was to generate a Gm12606 knock-out mouse by either deleting exon1 of Gm12606 located next to the p16 gene of interest or by eliminating the entire 37 kb Gm12606 fragment. Due to the inability of lncRNAs to produce proteins, one guide RNA is not sufficient to delete the entire gene. Therefore, two guide RNAs are required to flank the lncRNA in order to achieve efficient deletion (KO) of the targeted gene. Since T1 in mMSCs increased with age, as shown in preliminary RNA sequencing data, and the goal was to reverse ageing in mMSCs, it was decided to conduct further investigations exclusively with Gm12606 T1.

5.4.1 Identification and testing of CRISPR/Cas9 sgRNAs *in vitro*

Different sgRNA oligonucleotides (“single guide RNAs”) were first tested *in vitro* by cloning strategy using a CRISPR/Cas9 vector (**Figure 12**, provided by IDG). The vector contained a Cas9 expression cassette and a multiple cloning site for sgRNA sequences driven by the U6 promoter. sgRNAs for cloning experiments were generated from DNA oligonucleotides and designed with the help of the CRISPR design tool CRISPOR (Haeussler et al., 2016) and produced by Eurofins Genomics GmbH (Ebersberg, Germany). The oligonucleotides were provided by the manufacturer in lyophilized form of 40 nmol and were dissolved in RNase-free water to working concentrations of 1 pmol/µl. Because mMSCs appeared refractory to plasmid transfection and single cell cloning, the MOS immortalized murine osteosarcoma cell line was used to establish the knockout *in vitro*.

Cloning sgRNA oligonucleotides into pBS-U6-Cas9 vector

In order to introduce sgRNA 1, 2, 3, 4, 5, 6 sequences into the U6 promoter vector (pMB-U6-Cas9), a BbsI restriction digestion of the vector was performed using 1 µg of the plasmid according to manufacturer's instructions. To form double stranded DNA molecules homologous to the target sequence, reverse and complement DNA oligonucleotides with a concentration of 1 pmol/µL were mixed in a ratio of 1:1 in 50 µL TE-buffer. Oligonucleotides were then incubated at 98°C for 10 min and cooled down slowly to 40 °C in 25x 2 °C steps, thereby annealing and generating Bbs1 compatible insert. To ligate the inserts into the Bbs1-digested pU6-Cas9 vectors, 50 ng of the linear plasmids were incubated overnight at 16 °C with the double-stranded sgRNA DNA oligonucleotides (4 µL), T4 DNA ligase buffer (1.5 µL), T4 ligase (1.5 µL) and water (5 µL). As the insertion destroys Bbs1 sites the vector without inserts could be removed by incubating the ligated plasmids (15 µL) with BbsI for 30 min at 37 °C (water (30 µL), 10x NEB 2.1 Buffer (5 µL) and 1 µL of the enzyme) and following 30 min at 65 °C. For the transformation of the ligated vector into chemically competent cells, 1 µL plasmid was added to a 50 µL suspension of DH5α chemically competent E. coli. In a heat shock reaction, cells were incubated for 30 sec at 42 °C and put on ice for 10 min. Cells were mixed with 1 ml of SOC medium containing 50 µg/ml ampicillin and incubated for 1h in 37 °C with gentle agitation. After an hour, 500 µL of the suspension was spread on a 50 µg/ml ampicillin containing LB agar plate and incubated overnight in 37 °C. The next day clones were picked and further expanded in 100ml LB suspension culture with 50 µg/ml ampicillin incubated overnight at 37 °C in a shaker incubator (180 rpm). Midi plasmid preparation was performed using the PureYield Plasmid Midiprep System following the manufacturer's instructions.

Co-Transfection of sgRNA plasmid DNA

MOS cells were lipofected with paired sgRNAs that flanked the target region to be deleted. One day before transfection, 2.5 x 10^5 MOS cells were seeded with 2 ml of growth medium in 6-well plates. Liposomal-DNA complexes were prepared by dilution of 2,5 µg plasmid DNA in 105 µL Gibco Opti-MEM and dilution of 5 µL Lipofectamin 2000 in 120 µL Opti-MEM. After 5 min incubation at room temperature, both solutions were combined to a final volume of 250 µL, mixed gently by 3 times inverting the tube and incubated for 20 min at RT. Aliquots were added to individual wells containing the cells and 1750 µL medium by moving the plate back and forward. Cells were incubated overnight at 37 °C and DNA was extracted 24h and 48h later using the QIAamp DNA Mini Kit to screen for deleted regions.

Screening of deleted regions

Screening by standard genomic PCR followed by gel electrophoresis was performed to determine the size and length of the resulting Gm12606 deletions obtained from the *in-vitro* CRISPR/Cas9 experiment. This was established using different primer combinations flanking the sgRNA target positions in the genome. Finally, to identify the exact position of a potential deletion, PCR products were cloned into the pGEM-T vector using the pGEM®-T PCR cloning kit from Promega according to manufacturer's instructions and subjected to standard dye-terminator DNA sequencing.

5.4.2 Generation of *Gm12606* KO and KI mice via microinjection of single-cell embryos (performed by the Institute of Developmental Genetics (IDG; F. Giesert), Helmholtz Zentrum München)

Although there are several functional experiments to investigate the role of lncRNAs *in vitro* (siRNA and antisense oligonucleotides (ASO)), CRISPR/Cas9 system allows the generation of conditional knock-out (KO) or knock-in (KI) mice that precisely inhibit the target lncRNA to examine whether there is a potential epigenetic interaction between Gm12606 and p16 in mMSCs.

sgRNA for the animal experiments were generated from DNA oligonucleotides (Metabion, Planegg/Steinkirchen, Germany) by *in vitro* transcription utilizing the EnGen® sgRNA Synthesis Kit, S. pyogenes following the manufacturer's instructions (Institute of Developmental Genetics (F. Giesert), Helmholtz Centre Munich).

For the generation of the Gm12606 **KO** mouse line, gene specific single guide RNAs (sgRNA1, sgRNA2, sgRNA5, gRNA6) (Chapter 4.10) were used (in various combinations). sgRNAs were generated from DNA oligonucleotides by *in vitro* transcription using the EnGen® sgRNA Synthesis Kit, S. pyogenes according to the manufacturer's instructions.

For the generation of a Gm12606 **KI** mouse line, sgRNA7 (Chapter 4.10) and a donor, consisting of a specific targeting oligo harbouring the Gm12606 poly-A site and a 5' and 3' homology region targeting vector has been utilized (Integrated DNA Technologies Inc. /IDT, Coralville, IA, USA) (**Figure 14**). The goal here was to either obtain a truncated Gm12606 T1 transcript or to generate a splice site deletion.

Prior to pronuclear injection in single cell embryos, sgRNA was diluted together with recombinant Cas9 protein and the targeting oligo in microinjection buffer to a working concentration of 50 ng/µL (sgRNA), 50 ng/µL (Cas9) and 50 ng/µL (targeting oligo). Single-cell embryos were obtained by

mating C57BL/6N males with C57BL/6N females superovulated with 7.5 units of PMSG (Pregnant Mare`s Serum Gonadotropin) and 7.5 units of HCG (Human Chorionic Gonadotropin). To target the Gm12606 in single-cell embryos, injections were done into the larger pronucleus. After injection, zygotes were transferred into pseudopregnant CD1 female mice to obtain live pups. All mice showed normal development and appeared healthy. The animals were handled according to institutional guidelines and were approved by the Animal Welfare Committee of the Government of Upper Bavaria (AZ 55.2-2532.Vet_02-14-205). The mice were housed in standard cages in a specifically pathogen-free facility in a 12 h light/dark cycle with ad libitum access to food and water. Analysis of gene editing events were performed on genomic DNA isolated from tail or ear biopsies using the Wizard Genomic DNA Purification Kit (Promega, Mannheim, Germany) following the manufacturer's instructions.

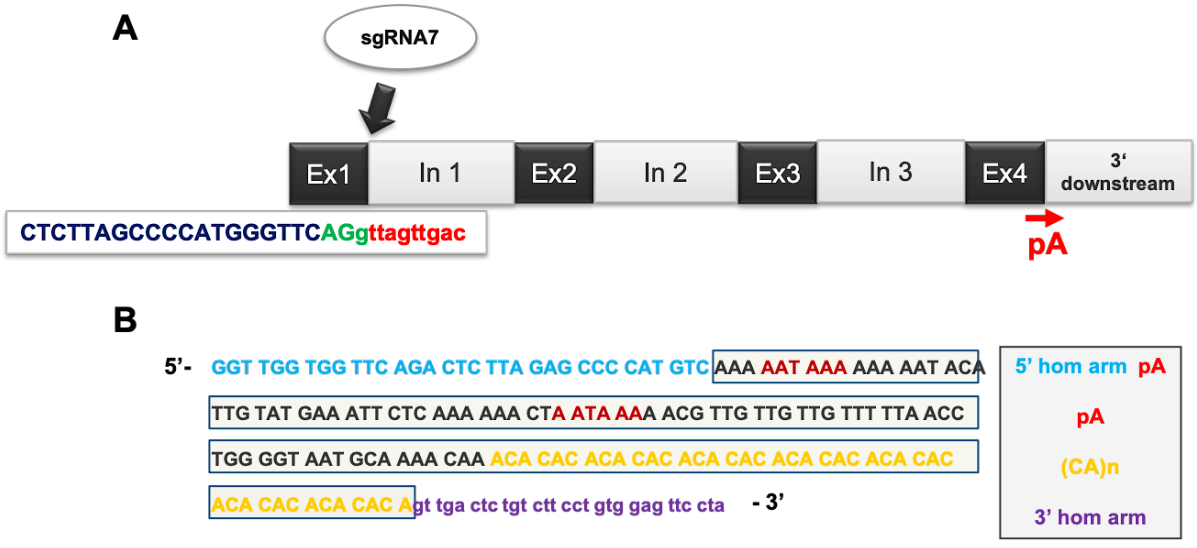

Figure 14: CRISPR/Cas9 exon1/intron1 splice site deletion and poly-A signal knock-in. (A) Schematic overview of sgRNA 7 targeting the exon1/intron1 splice site of the Gm12606 gene. Target sequence is highlighted in blue, the PAM site in green and the intron sequence in red. The poly-A site (pA) is located within exon 4 of Gm12606 and is highlighted in red. (**B**) The homologous repair template containing the poly-A sequence (framed) of Gm12606 and flanked by the 5' (blue) and 3' (purple) homology arm.

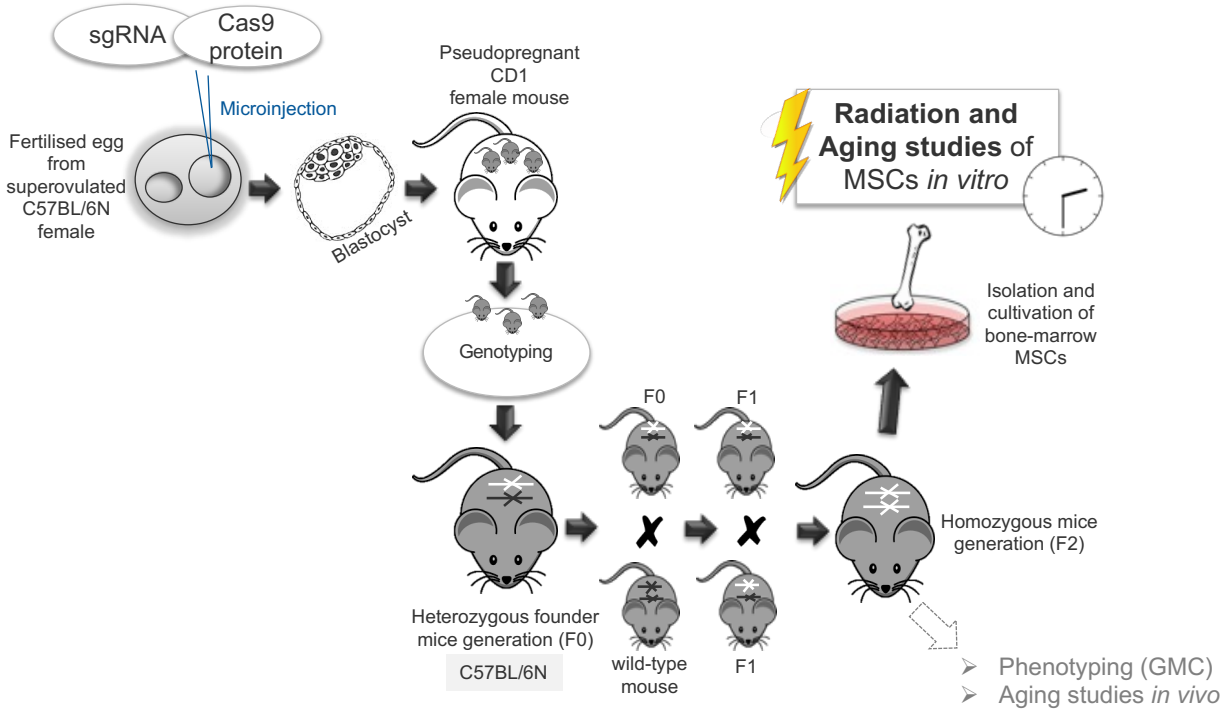

Figure 15: Workflow and breeding strategy (in collaboration with the IDG, F. Giesert Lab). Graphical representation of the workflow for CRISPR/Cas9-mediated depletion of the lincRNA Gm12606 in vivo. sgRNAs and the Cas9 proteins were microinjected into the larger pronucleus of a fertilized oocyte from superovulated C57BL/6N female mouse. After several cell divisions *in vitro*, zygotes were transferred to pseudopregnant CD1 females to obtain live pups. Genomic DNA was extracted from tail or ear biopsies of pups and genotyped. Mice showing a deletion event in the target locus (heterozygous FO founder mice) were mated with wt littermates, as soon as they reached sexual maturity (6-8 weeks), to obtain F1 heterozygous offspring. After genotyping, heterozygous F1 offspring were paired to generate F2 generation mice with a homozygous KO mouse of Gm12606. Breeding was continued to obtain a sufficient number of homozygous mice.

5.4.3 In-vitro fertilization (IVF)

IVF using frozen sperm from mouse 72 was performed by the Department of Comparative Medicine of the Helmholtz Centre Munich. In case of one founder mouse (72, harbouring deletion of the entire exon1 of Gm12606), sperms were frozen after autopsy, which became necessary because of developmental genito-urinary problems. Using this sperm an *in vitro* fertilization with wild-type (wt) oocytes was done with following embryo transfer. Ear biopsies were taken from the mice and DNA extracted according to standard procedure described in chapter 5.3.1.

5.4.4 Mouse genotyping

The genomic DNA obtained from CRISPR/Cas9 gene edited C57BL/6N mice was genotyped to determine the presence of gene deletions. The Gm12606 locus was analysed by a series of locus specific PCR amplifications and the products resolved by agarose gel-electrophoresis. Length of the DNA fragments was measured by comparison with DNA molecular weight markers.

5.5 Presto Blue cell viability assay

To study cell proliferation the Presto Blue cell viability assay was performed. mMSCs were isolated as described above and passaged after one week of cultivation (p1). 4000 cells were transferred into 96-well culture plates and continued to grow for 3 days. Cell medium was replaced with Presto Blue cell viability reagent (1:10) mixed with mMSC culture medium and incubated for 30 min at 37 °C. Fluorescence of the Presto Blue reagent was measured with the Tecan Infinite M200 microplate reader at 560 nm excitation and 590 nm emission wavelength. A blank well filled with culture medium and Presto Blue was used to investigate background florescence. After completion of the assay the residual Presto Blue reagent was removed from the wells by replacing the medium with fresh mMSC medium and the cells were allowed to grow further. The

measurements were repeated every three days. Cells in culture media without Presto Blue reagent were used as internal controls. Results of the blanks were subtracted from the fluorescence values. Data were collected over two weeks and results plotted (days vs. relative fluorescence units).

5.6 Senescence associated β-galactosidase staining

Senescent cells have increased lysosomal activity due to the activation of ß-galactosidase. This can be detected by the formation of an insoluble blue coloration (indigo) released by the cleavage of the chromogenic ß-galactosidase substrate X-Gal and the resultant intracellular dimerization of the indole moieties. To measure senescence in murine MSCs, 20000 cells were cultured in each well of 24 well plates. At different time points after starting the culture (6, 9 and 12 days after seeding), the adherent cells were washed two times with PBS and fixed with Roth HistoFix (4 % PFA) for 10 min, followed by additional washing steps. Senescence staining solution containing X-gal was applied as described in chapter 4.5 and added to completely cover the cells. Cells were incubated overnight at 37 °C in a humidified atmosphere (**Figure 16**). Thereafter the staining solution was replaced by PBS and blue-stained senescent cells were visualized and quantified under brightfield microscopy. Three images were generated from each of two technical replicates and the experiment was repeated with four biological replicates. Senescent cells were counted in relation to the total cell number. In case of very high confluency, propidium iodide was added to the cells to identify nuclei. This enabled the number of total cells to be determined more accurately (**Figure 17**).

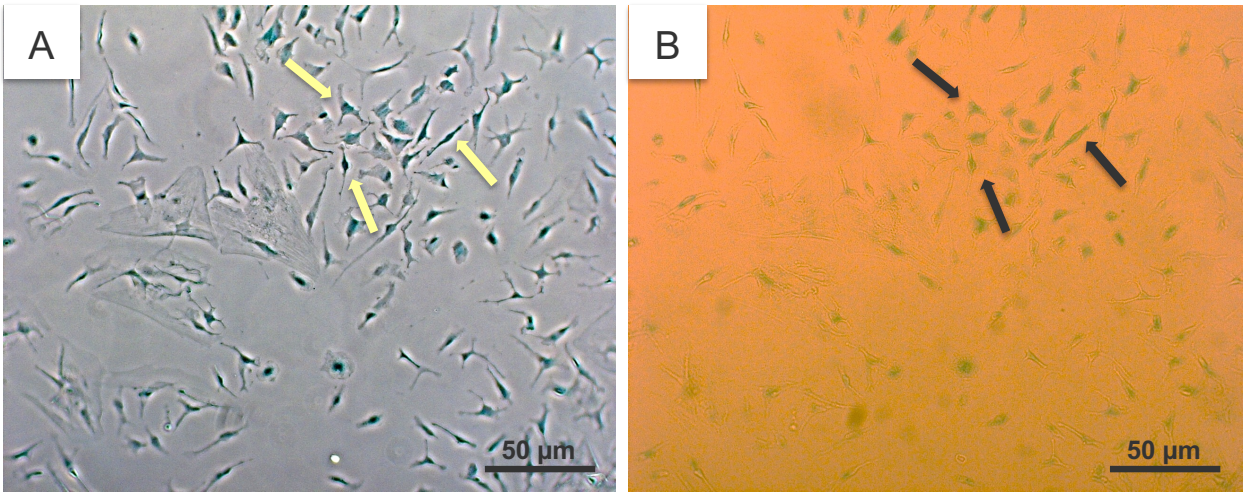

Figure 16: Representative image of SA-β-gal-positive cells for the detection of senescence induction using Zeiss Axiovert 25 microscope. (A) Images were first acquired with phase contrast to determine the total cell number. (B) Light intensity was increased to improve the visibility of SA-β-gal-positive cells (blue).

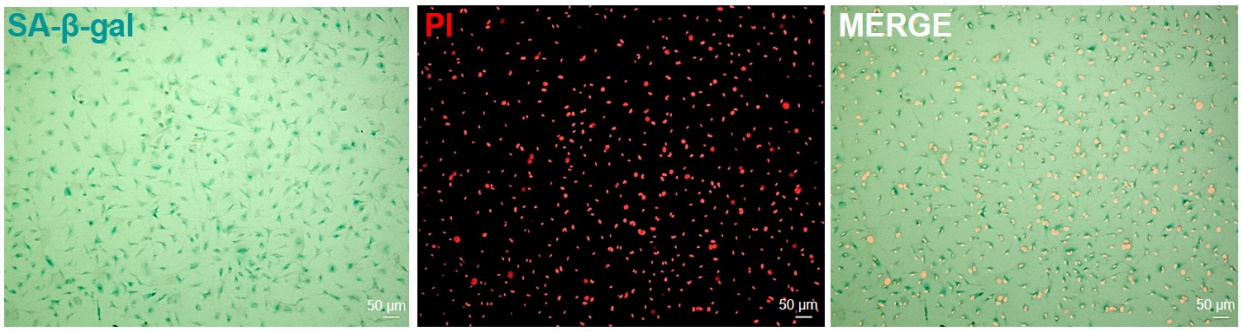

Figure 17: Representative image of SA-β-gal-positive cells (blue) for the detection of senescence induction using KEYENCE BZ-9000 microscope. In case of very high confluency, propidium iodide was added to the cells to allow visualization of the cell nuclei (red) for precise counting of the total cell number.

5.7 Immunofluorescence staining of DNA damage repair foci

To Investigate DSB repair and repair kinetics after irradiation the presence of co-localized γH2AX and 53BP1 labelled repair foci was analysed. 60000 cells per well of wild-type or homozygous Gm12606-1$^{-/-}$ mMSCs were cultured on sterile glass microscope slides and irradiated after two days with X-ray doses of 0, 1, 2 and 4 Gy. After 90, 180, 360 and 1440 min after irradiation the cells were fixed with Roth HistoFix for 10 min, followed by two washes with 1x PBS. Cells were permeablized with 0.2% Triton X100 in PBS for 5 min and washed twice with 1x PBS for 5 min at RT. Non-specific antibody binding was blocked by incubating the permeabilized cells for 1h in 1% BSA, 0.15% glycine in PBS (PBS^{+}) for 1h in humidified atmosphere at RT. Primary antibodies (mouse monoclonal anti-γH2AX antibody (1:500) and rabbit polyclonal anti-53BP1 antibody (1:500)) directed against the repair foci markers were combined and diluted in PBS^{+} then applied to the cells overnight in a humidified chamber at 4 °C. After extensive washing (3 x 15 min in 1xPBS) the appropriate secondary antibodies (1:500 Cy3-conjugated sheep anti-mouse IgG and 1:200 Alexa 488-conjugated goat anti-rabbit IgG) were combined and diluted in PBS+ then added to the cells for 1h at RT. Further washing steps as described above were carried out. The cells were counterstained with Hoechst 33342 solution and stored in PBS at 4 °C and mounted directly before microscopy with PBS and covered with glass coverslips.

Images of co-localized foci from γH2AX and 53BP1 were acquired using the Keyence fluorescence microscope and the associated BZ II viewer software. γH2AX and 53BP1 were detected by excitation of the Cy3 and Alexa488 lasers with an exposure time of 1/3 sec for the green and red channel and 1/25 sec for the blue channel (DAPI detection). At least 50 nuclei were analysed and visualized with the 100× oil immersion lens. Images were processed with the BZ-II Analyzer software for haze reduction and black balance to minimize background signals (**Figure 18**). For analysis with the Keyence counting software, only foci with co-localized γH2AX and 53BP1 signals were automatically evaluated with a threshold value of 70 threshold, which

correlated with the size of the foci. To obtain the dose-response of radiation-induced DNA-DSBs, the mean number of foci and the standard error of mean of counted foci were plotted linear to the *in vitro* radiation dose exposure.

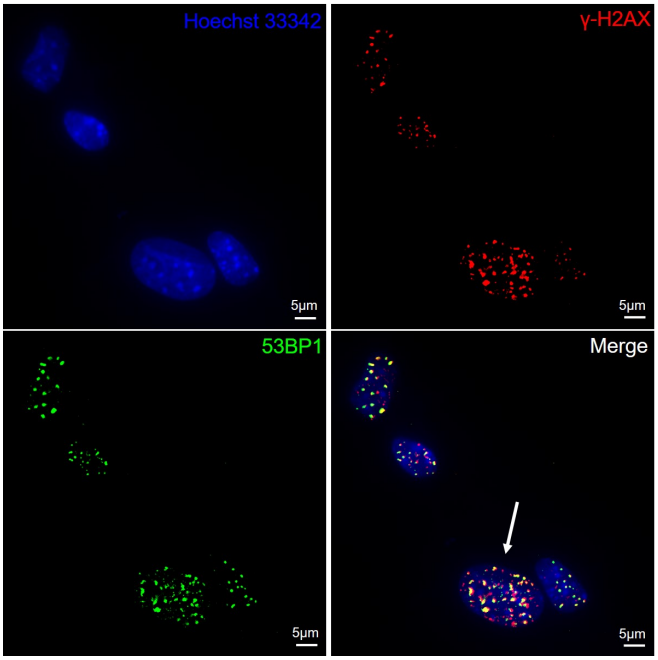

Figure 18: Representative image of the induction of γH2AX and 53BP1 DNA repair foci in mMSCs. Immunofluorescence staining of co-localized (yellow) γH2AX (red) and 53BP1 (green) foci indicating DNA damage repair. The images were taken with the KEYENCE BZ-9000 microscope and a 100x immersion objective. Keyence analyser software was used to reduce hazard and balance black backgrounds and to count co-localized signals. The red and green signals are the artificial colouring generated by the software. Enlarged cell nuclei (white arrow) were classified as differentiated mMSCs and were excluded from measurements.

5.8 Statistical analysis

Statistical analysis of the data was performed using GraphPad Prism 5.04 & 8.4.0 software. Experiments were conducted using two technical and at least three biological replicates. Statistical analyses were applied using the two-sided student T-test. The effect of two independent variables was analysed using two-way ANOVA with significance determined * for p-value <0.05, ** for p-value <0.01, *** for p-value <0.001, and **** for p-value <0.0001. Data was presented as mean ± SEM.

.

6. Results

6.1 Confirmation of the splice variants (T1 & T2) of Gm12606

The lincRNA Gm12606 was recently recognized as a potentially functional lncRNA by Mullin et al. in 2017 (Mullin et al., 2017). Full length sequences of both possible transcripts (T1&T2) were downloaded from the Ensembl Genome Browser and are provided in **Appendix A**. Closer examination of the Gm12606 locus using the Repeat Masker tool provided by the UCSC Genome Browse identified multiple repeat elements (**Figure 19**).

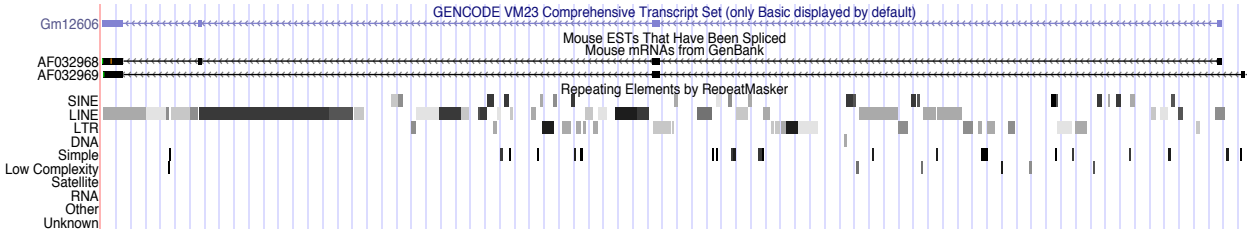

Figure 19: Repetitive elements within the Gm12606 locus. This image was created using the Arian Smit's Repeat Masker tool, which scans the DNA sequence for repetitive elements. The degree of colour shading reflects the degree of mismatch, base deletion, and base insertion. The higher the combined number of these, the lighter the shading. (http://genome.ucsc.edu)

Repetitive sequences, especially LINE, were discovered within the introns of Gm12606. Shorter sequence stretches with a partial homology to repeat elements also map to the four exons of Gm12606. Consequently, care was taken to design PCR and RT-qPCR primers only from regions that lack such repetitive elements. Suitable primers (chapter 4.11.2) were found confirming the presence and expression of two splice variants of Gm12606 by RT-qPCR and sequencing (**Figure 20,21**). Sequencing of the PCR amplified cDNA products confirmed the splice junctions connecting the exons as listed in the sequences provided by Ensemble database (**Appendix A**).

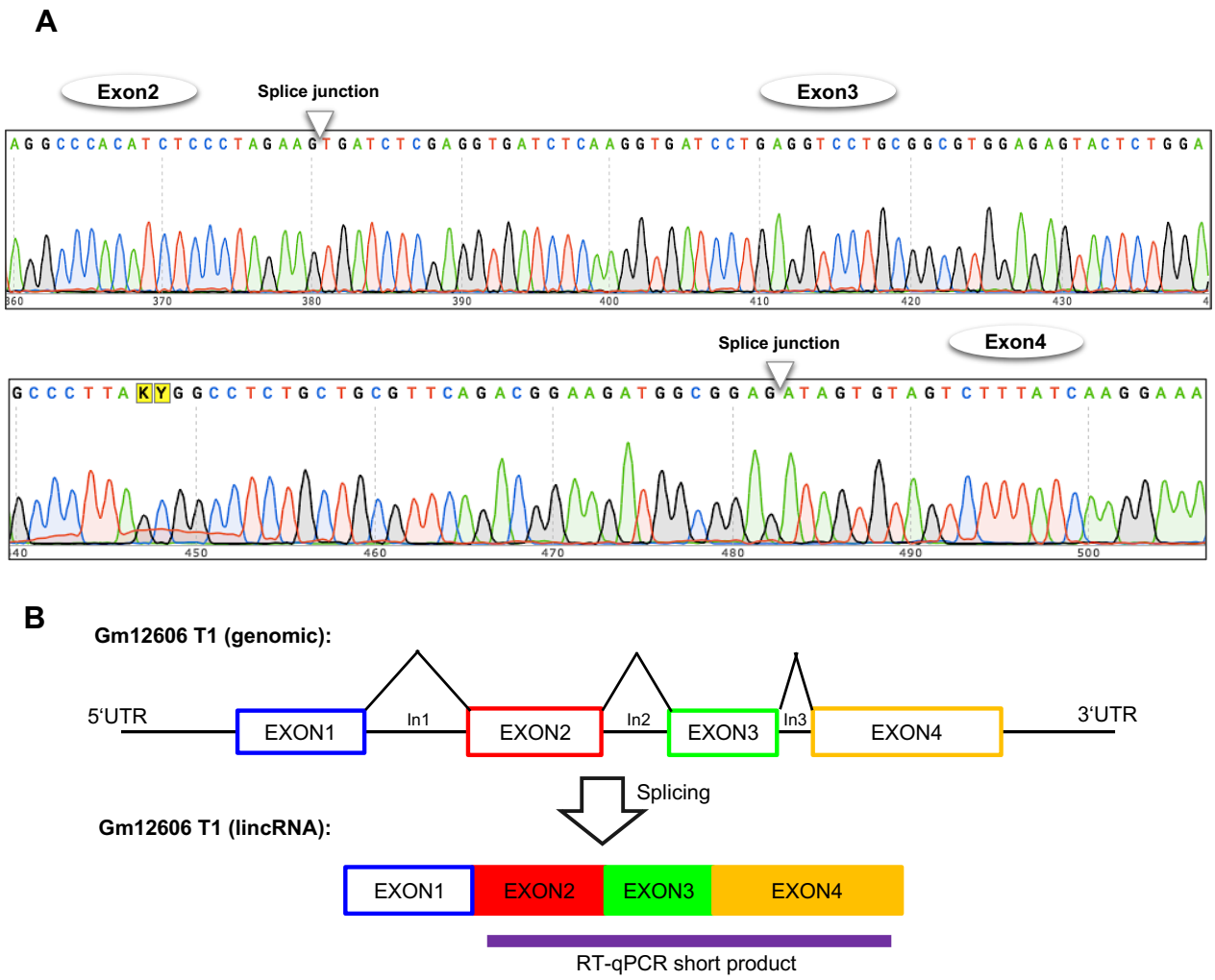

Figure 20: Sequence alignment of spliced Gm12606 T1. (**A**) Chromatogram of spliced T1. Sequencing of a RT-qPCR product confirmed the presence of the spliced lincRNA Gm12606 T1. The white arrow indicates the splice junctions connecting exons 2 and 3, as well as exon 3 and 4. (**B**) Simplified representation of the lincRNA Gm12606 T1 with its 4 exons before and after splicing. RT-qPCR short product spans exon 2 (red), exon 3 (green), and exon 4 (orange).

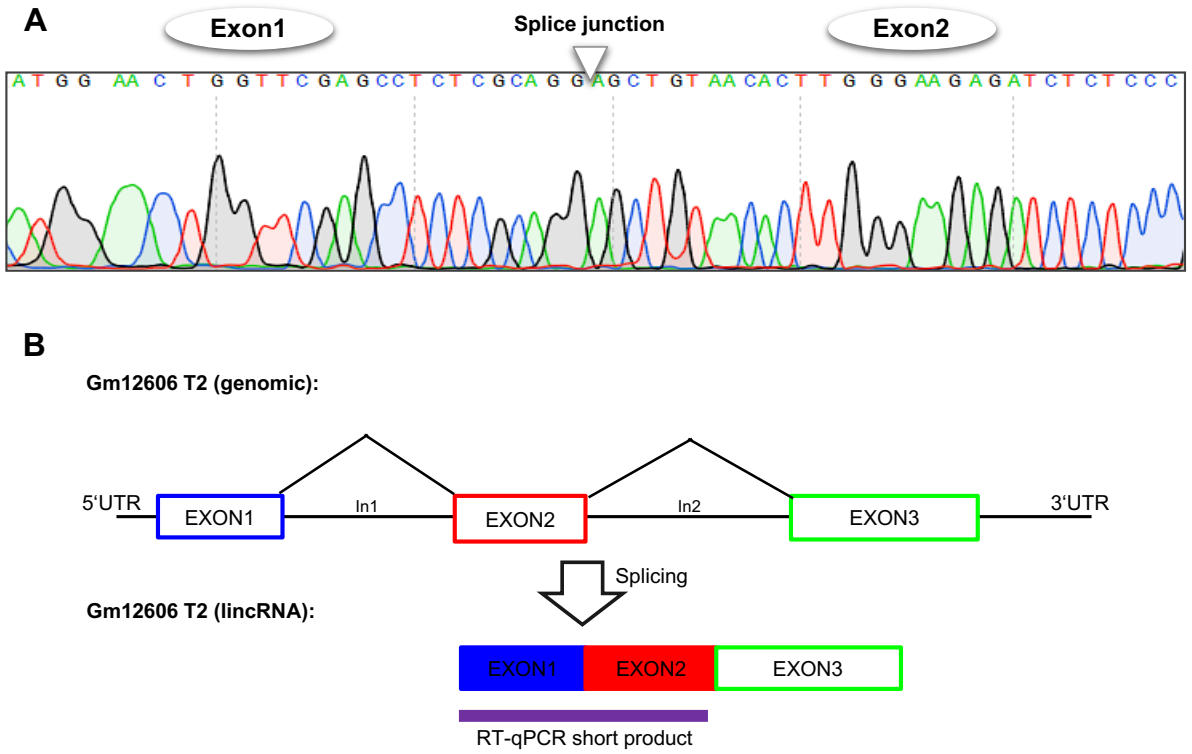

Figure 21: Sequence alignment of spliced Gm12606 T2. (**A**) Chromatogram of spliced T2. Sequencing of a RT-qPCR product confirmed the presence of the spliced lincRNA Gm12606 T2. The white arrow indicates the splice junctions connecting exons 1 and 2. (**B**) Simplified representation of the lincRNA Gm12606 T2 with its 3 exons before and after splicing. RT-qPCR short product spans exon1 (blue) and exon 2 (red).

6.2 Age and radiation-related changes of Gm12606 in mMSCs

To confirm the presence of T1 and T2 in mMSCs and to study whether ageing and exposure to ionizing radiation affects the expression of Gm12606 T1 and T2, fold differences of RT-qPCR amplified lincRNA were compared in mMSCs after *in vitro* ageing. Additionally, aliquots of cells were irradiated with 0 or 2 Gy γ-exposure 24h before harvesting the RNA for gene expression analysis by RT-qPCR.

6.2.1 The cell morphology of bone-marrow mMSCs changed with increasing age

Primary mMSCs were isolated from the bone marrow of FVB/N mice and were cultured up to 7 weeks, passaging once a week. They are characterized by their adhesion to cell plastic surface. The cellular morphology of mMSCs consisted of a heterogenous cell population at each time point was examined (**Figure 22**). At 3 and 5 weeks, cells with flattened spindle-shaped morphology, typical of mMSCs, predominated. As the passaging number increased, the proportion of larger cells with a trapezoidal shape grew as mMSCs began to differentiate. The more the mMSCs aged (i.e., with each week and passage), the more differentiated cells emerged in the cell culture flasks and the higher the cell heterogeneity.

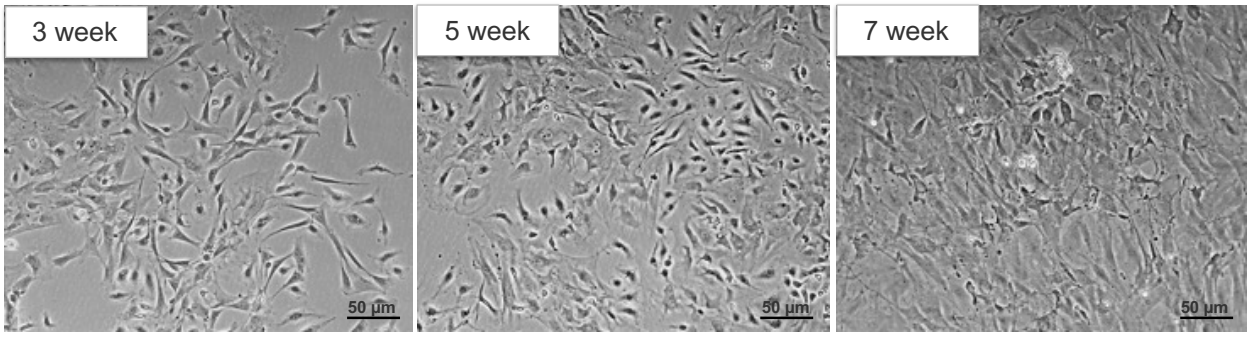

Figure 22: Morphology of BM-derived mMSCs isolated from FVB/N mice strain. Three representative images of primary mMSCs after cells were cultured for 3 weeks, 5 weeks, and 7 weeks *in vitro* under hypoxic conditions and passaged once per week. Scale bars are 50 µm.

6.2.2 Gm12606 T1 and T2 are increased during *in vitro* ageing of mMSCs

Comparing the relative expression of Gm12606 transcription in 3-week-young mMSCs with that of 5- and 7-week-old mMSCs, T1 was significantly upregulated 4.3 ± 1.4-fold (*p=0.0102) after 5 weeks and a dramatical elevation of T1 levels were determined after 7 weeks (71,7 ± 20,1-fold, *p=0.0116) (**Figure 23**). After 7 weeks in culture, no significant changes in the expression of T2 was found. T2 transcription was also different (3.8 ± 1,8-fold, *p=0.0330) in the 5-week-old mMSCs (**Figure 23B**). A strong dependence of Gm12606 expression with the degree of differentiation of mMSCs and increase of heterogeneity (**Figure 22**) becomes obvious.

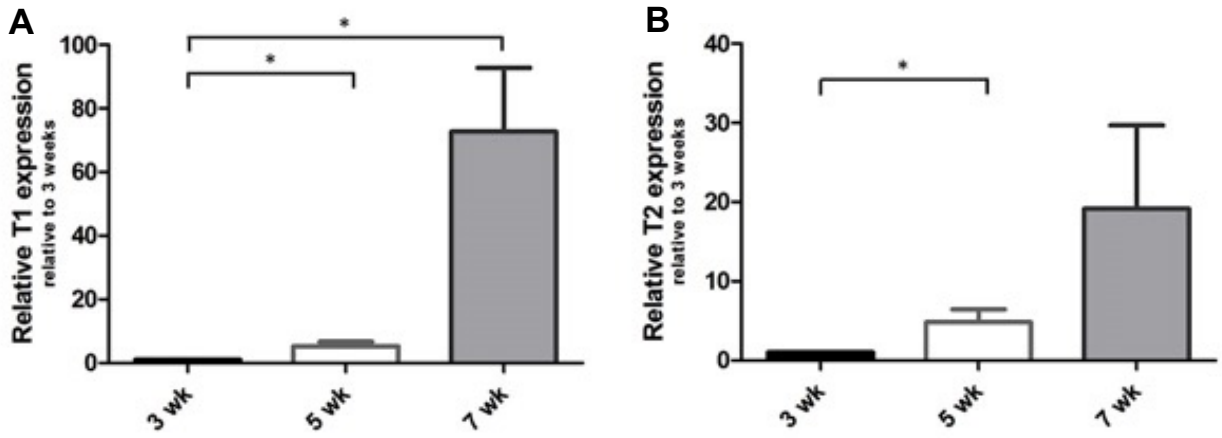

Figure 23: Expression of Gm12606 transcripts in in vitro aged mMSCs. Histograms show the relative expression values of T1 and T2 in mMSCs from C3H mice obtained by RT-qPCR at week (wk) 3,5 and 7. 3 wk represents the young control and was normalized to 1 for comparison purposes. TBP was used as a housekeeping gene. Data are represented as mean ± SEM (3 wk =n=6, 5 wk=n=6, 7 wk=n=3, two-sided t-test, *p < 0.05, **p < 0.01, ***p < 0,001) with values presented in the text. (**A**) Expression of T1 in young vs old mMSCs. (**B**) Expression of T2 in young vs old mMSCs.

6.2.3 Elevated Gm12606 expression after exposure to ionizing radiation

6.2.3.1 The transcription of T1 and T2 in 5-week-old mMSCs is upregulated following irradiation

RT-qPCR analysis of Gm12606 transcription was performed at 3, 5, and 7 weeks 24h after an acute exposure to 2 Gy in mMSCs and compared to sham-irradiated controls. Results showed a slight difference of T1 expression (1.05 ± 0.3-fold greater than sham-irradiated controls; **p=0.0053) in 5-week-old mMSCs (**Figure 24A**). Following 2 Gy exposure, transcript levels of T2 were increased in the 5 (2.8 ± 0.5-fold, **p=0.008), and 7-week-old cells, reaching a 2.0 ± 0.6-fold upregulation by the latest time point (*p=0.02) (**Figure 24B**).

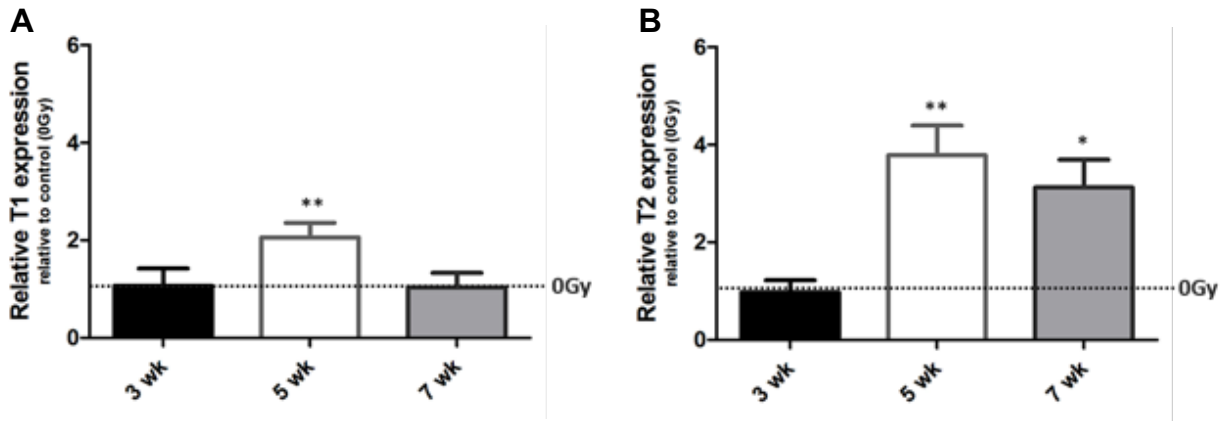

Figure 24: Expression of Gm12606 transcripts in young and ageing mMSCs post 2 Gy irradiation exposure. Histograms show the relative expression values of T1 and T2 obtained by RT-qPCR at week 3,5 and 7, 24h post 2 Gy γ-radiation exposure from mMSCs of C3H mice compared to sham irradiated. 0 Gy represents the sham-irradiated control and was normalized to 1 (dashed line) for comparison purposes. TBP was used as a housekeeping gene. Data are represented as mean ± SEM (T1=n=6, T2=n=3, two-sided t-test, *p < 0.05, **p < 0.01) with values presented in the text. Expression of T1 (**A**) and T2 (**B**) in irradiated mMSCs compared to sham-irradiated controls.

6.2.3.2 Radiation enhances the expression of Gm12606 T1 at later time points

To study the change in expression of Gm12606 T1 over a constant time period, 3-week-old mMSCs were first exposed to 0 or 1 Gy γ-irradiation and cultivated for 24 days. Every second day

the cells were harvested and analysed by RT-qPCR. Two factor analysis (days post exposure and radiation exposure) was performed using 2-way ANOVA, the results of which are presented in **Appendix B**. It was found that the expression of Gm12606 was influenced by both days and radiation exposure. There was a significant increase of the transcription level of Gm12606 by days (****p=0.0001), although the expression pattern oscillated strongly in either irradiated or sham-irradiated cells. A significant difference was also noted when comparing mMSCs exposed to 1 Gy irradiation with sham-irradiated controls (**p=0.0067), indicating an elevated expression of Gm12606 following irradiation (**Figure 25**). The difference in Gm12606 expression between irradiated and control mMSCs was most obvious at later time points, starting from day 20 post irradiation. This could indicate that increased Gm12606 expression is related to accelerated senescence in irradiated mMSCs.

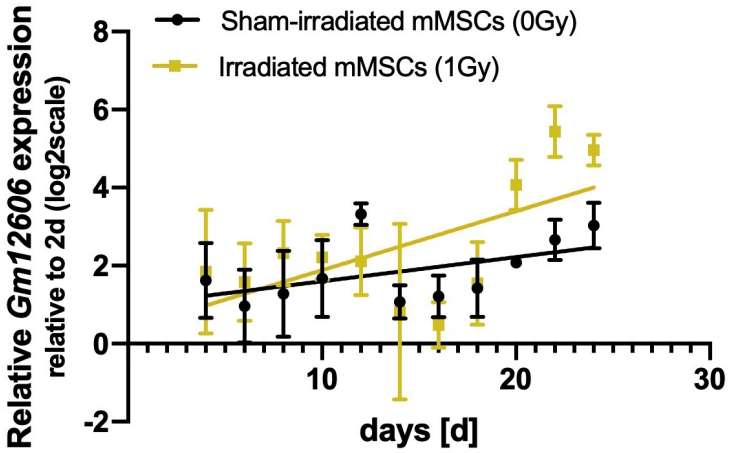

Figure 25: Expression of Gm12606 (T1) in irradiated and sham-irradiated mMSCs over a constant time period. Plot shows the relative expression values of Gm12606 (T1) in 0 or 1 Gy γ- irradiated 3-week-old mMSCs (shown on the log2 scale) from C3H mice obtained by RT-qPCR over a 4-24-days' time period. Fold changes were calculated by normalizing the day 2 controls to 1. TBP was used as a housekeeping gene. Data are represented as mean ± SEM (n=3, 2wANOVA, radiation **p < 0.01, days, ****p < 0.0001) with values presented in the text.

6.2.3.3 *The increased transcription of Gm12606 T1 in irradiated mMSCs is dependent on the radiation dose*

The expression of Gm12606 T1 and T2 in mMSCs was measured after 1.5h and 72h following 0, 0.25, 0.5, 1,0 and 2.0 Gy X-irradiation. According to previous results (**Figure 23**), indicating that the radiation effect is most prominent in mMSCs after 5-weeks in culture, this timepoint was used for the study. Two factor analysis (dose and hours) was performed using 2-way ANOVA. The results of which are presented in **Appendix B**. It was found that the expression of T1 and T2 was influenced significantly by dose alone (2-way ANOVA, T1=**p=0.0027, T2=*p=0.0161). The peak expression of T1 and T2 (3.5 ± 0.17-fold) was detected 1.5h following 1 Gy X-radiation exposure. 2.7 ± 0.5-fold increase of T2 was also measured 72h following 0.25 Gy radiation compared to sham-irradiated controls. No significant change could be examined comparing the expression of T1 and T2 1.5h or 72h after radiation exposure, whereas a time-dependent reduction of Gm12606 expression after 1 and 2 Gy exposure was obvious (**Figure 26**).

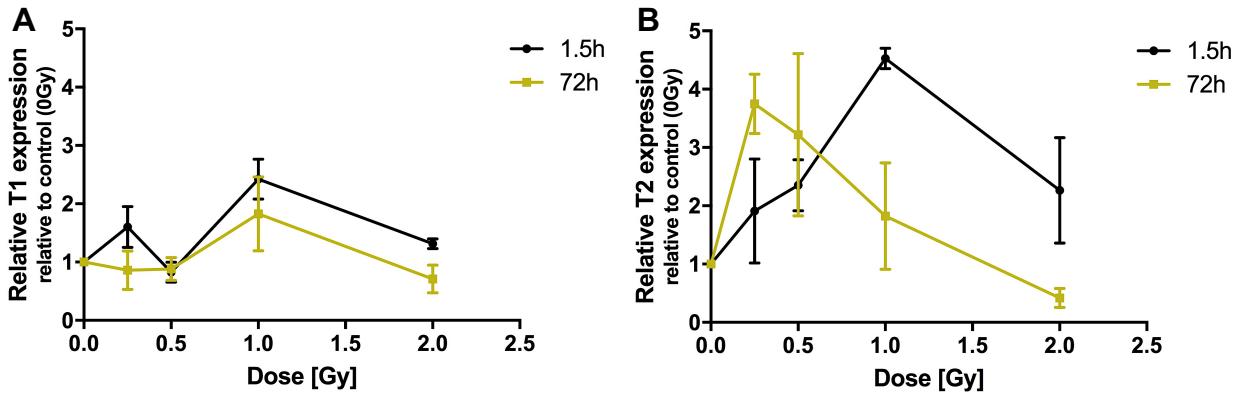

Figure 26: Time and dose dependency of Gm12606 in X-irradiated mMSCs. Plots show the relative expression values of Gm12606 T1 and T2 cDNA in 5-week-old mMSCs, measured 1.5 h or 72 h after X-irradiation. 0 Gy represents the sham-irradiated control and was normalized to 1 for comparison purposes. TBP was used as a housekeeping gene. Data are represented as mean ± SEM (n=3, 2wANOVA, dose *p < 0.05, **p < 0.01; two-sided, paired t-test; *p <0.05, **p <0.01) with values presented in the text. Expression of T1 (**A**) and T2 (**B**) in irradiated mMSCs compared to sham-irradiated controls.

6.3 Gm12606 expression is cell type specific

Following the discovery that lncRNAs have multiple functions and the expression can vary across cell types expression of Gm12606 was compared in three different cell lines of mesenchymal origin. mMSCs were compared with murine osteoblasts (mOB), precursor cells of the bone-forming osteocyte, and an osteosarcoma cell line (MOS). To investigate whether Gm12606 levels are also present in the very early development of the mouse, murine embryonic stem cells (mESCs) were also included for RT-qPCR analysis.

6.3.1 Differential gene expression of Gm12606 across different cell lines of mesenchymal origin

RT-qPCR analysis of Gm12606 transcription was performed with cDNA obtained from mOB, mMSC, MOS, and mESC, as well as pooled embryo (embryonic) cDNA from BALB/c mice, which served as a calibrator. Results obtained revealed that the highest expression of Gm12606 was present in mOB (2.28 ± 0.27-fold), followed by mMSCs (0.78 ± 0.04-fold) and MOS (0.03 ± 0.02-fold). No transcription could be detected in mESC that are pluripotent (**Figure 27**).

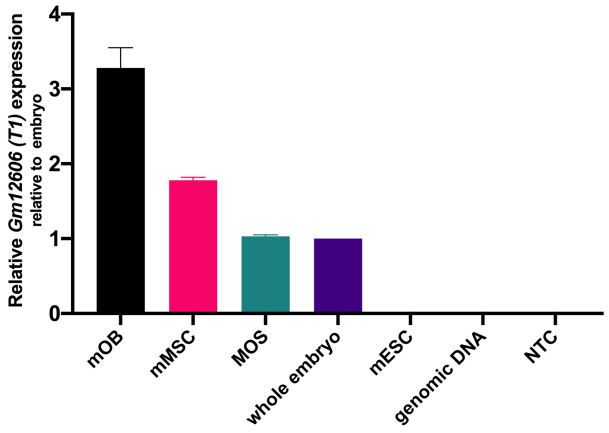

Figure 27: Relative expression of Gm12606 in several cell lines. Histogram shows the expression of Gm12606 (T1) in mOB, mMSCs, MOS, and mESC. Pooled whole embryonic cDNA was used as a calibrator and was normalized to 1 for comparison purposes. TBP was used as a housekeeping gene. NTC and genomic DNA were used as general controls for nucleic acid contamination. Data are represented as mean ± SEM (n=2) with values presented in the text.

6.3.2 The intracellular location of Gm12606 differs with cell types

The subcellular location of Gm12606 transcripts was visualized by Stellaris *in-situ* hybridization (Stellaris-FISH) in mMSCs, MOS and mOB (**Figure 28,29,30**). Due to limitations in probe design due to the presence of repetitive elements in transcript-specific target exons, the probe set consisting of 25 individual oligonucleotides was not able to differentiate between T1 and T2 transcripts. Therefore, the Stellaris FISH signals could indicate expression of either transcripts or a mixture of both. Gm12606 was detected by the FISH methodology in all three cell types examined, in agreement with the RT-qPCR data (**Table 9**).

In the murine osteosarcoma cell line (MOS) the occurrence of Gm12606 fluorescence signals was very heterogeneous with a large fraction of cells showing low to undetectable expression. In positive cells the Gm12606 transcript was located predominantly in the cytoplasm but with some signal within the nucleus (**Figure 28**).

In contrast, the level of Gm12606 signals in mOB nuclei was rather high compared with MOS cells and mMSCs, but still with a considerable degree of cell-to-cell heterogeneity (**Figure 29**). The presence of Gm12606 was found exclusively within the nucleus, with many strong signals, but strikingly absent in the nucleoli (the location of ribosome synthesis and assembly). The staining pattern appeared highly non-uniform with each nucleus, with some areas showing bright aggregates of signal and other areas showing less signal. No Gm12606 RNA could be detected in the cytoplasm.

However, in 5-week-old, and 7-week-old mMSCs, Gm12606 transcripts were found exclusively in the cytoplasm (**Figure 30**), and no difference was detected between these two age groups. The signals here appeared more diffusely distributed than the nuclear signals in mOB cells. In 3-week-old cells, the presence of Gm12606 could not be detected via Stellaris probes.

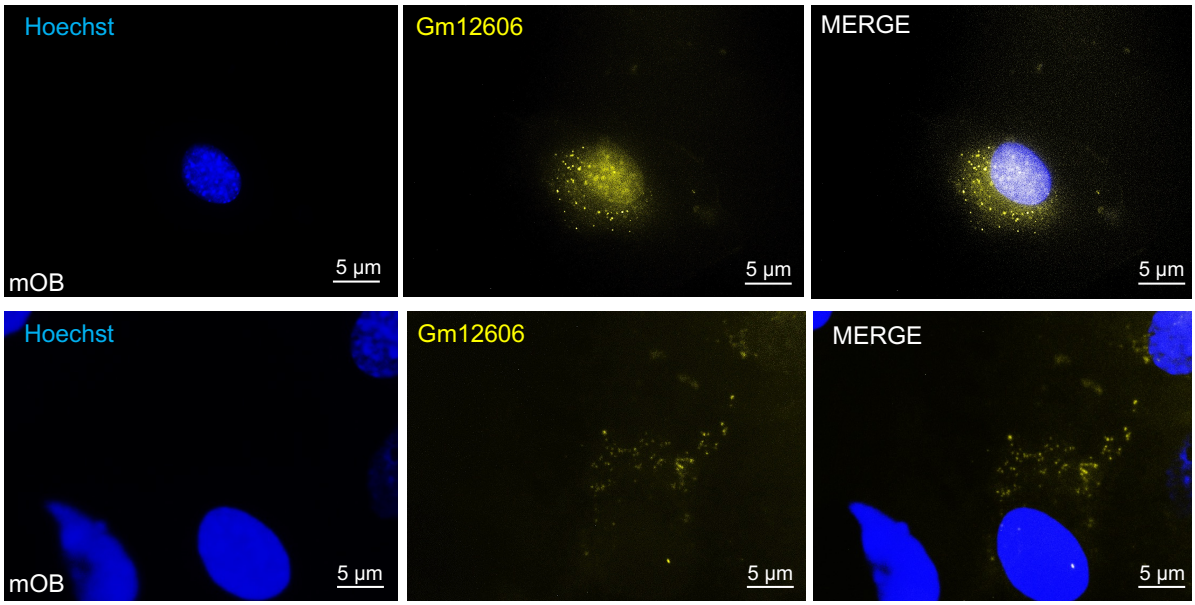

Figure 28: Detection and localization of Gm12606 by Stellaris-FISH in MOS cells. Two representative fluorescence images of Gm12606 signals (yellow, middle) in MOS cells hybridized with Quasar 570-labeled Stellaris probes. Cells were counter-stained with Hoechst 33342 (left). Merged images are shown in the right panel. Scale bars are 5 µm.

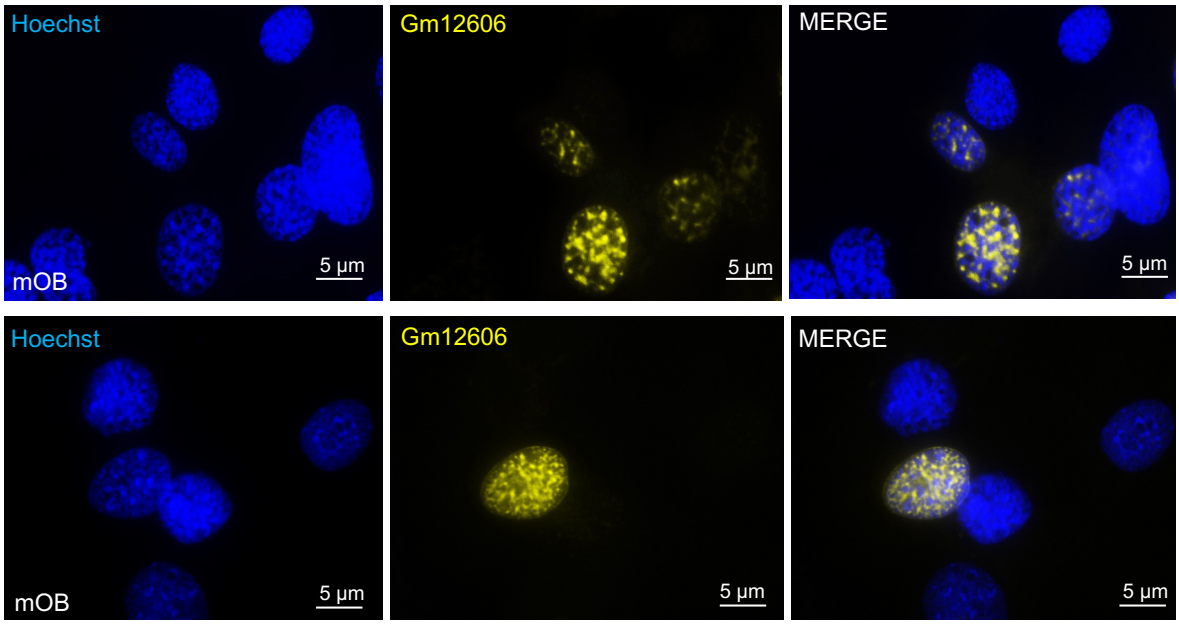

Figure 29: Detection and localization of Gm12606 by Stellaris-FISH in mOB cells. Two representative fluorescence images of Gm12606 signals (yellow, middle) in mOB hybridized with Quasar 570-labeled Stellaris probes. Cells were counter-stained with Hoechst 33342 (left). Merged images are shown in the right panel. Scale bars are 5 µm.

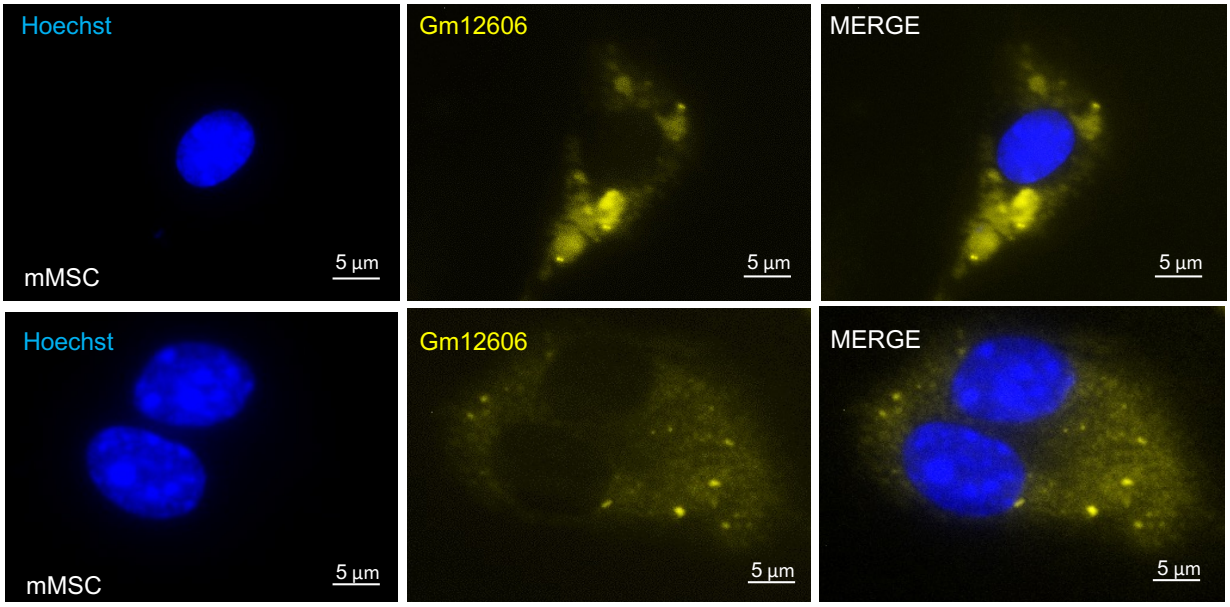

Figure 30: Detection and localization of Gm12606 by Stellaris-FISH in mMSCs. Two representative fluorescence images of Gm12606 signals (yellow, middle) in mMSCs hybridized with Quasar 570-labeled Stellaris probes. Cells were counter-stained with Hoechst 33342 (left). Merged images are shown in the right panel. 5-week-old mMSCs are shown in the upper image, while 7-week-olds are shown in the lower image. Scale bars are 5 µm.

Table 9: Summary of Stellaris-FISH Gm12606 abundancy in relation to RT-qPCR result

	Nuclear	Cytoplasmic	Expression levels (RT-qPCR)
MOS	-/+	+	+
mOB	+++	-	+++
mMSC	--	++	++

6.3.3 Gm12606 expression is increased in pre-osteoblasts during induced osteogenic differentiation

The main feature of MSCs is their potential to differentiate into cells of the mesenchymal lineage, including osteoblasts, adipocytes, and chondrocytes. During the induced differentiation process of mMSCs *in vitro,* the expression of Gm12606 and p16 mRNA was analysed by RT-qPCR after 14 days in culture.

Both transcripts of Gm12606 exhibit a strong and significant increase following induced osteoblast differentiation, with T1 going up 3.64 ± 0.6-fold (*p=0.0254) and T2 going up 3.20 ± 0.5-fold (*p=0.0193). In contrast, Gm12606 levels were not altered during adipogenic or chondrogenic differentiation (**Figure 31A-B**).

The proximity to the p16 locus suggests that p16 is regulated by Gm12606, implying a parallel increase of both genes. Regarding p16 levels in adipocytes, osteoblasts, and chondrocytes, a significant 2.25 ± 0.5-fold (*p=0.0440) increase was also observed in osteogenic differentiated cells compared to undifferentiated mMSC controls (**Figure 31C**). While transcription of p16 was unchanged in chondrocytes, levels were significantly downregulated in adipocytes (0.36 ± 0.04-fold, *p=0.0306).

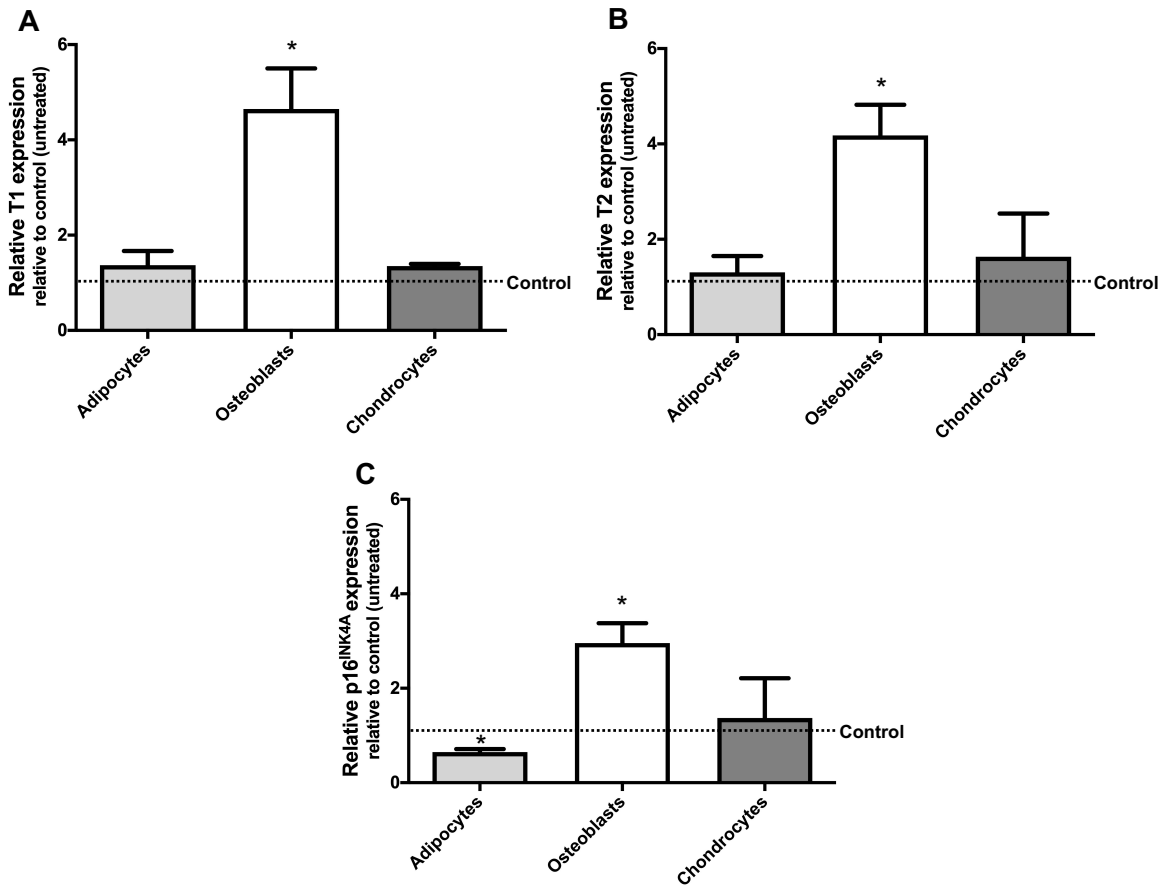

Figure 31: Expression of Gm12606 and p16 following induced adipogenic, osteogenic and chondrogenic differentiation. Histograms show the levels of T1, T2 and p16 transcription in adipocytes, osteoblast and chondrocytes compared to the levels in undifferentiated control (mMSCs). Control represents the undifferentiated mMSCs and was normalized to 1 (dashed line) for comparison purposes. TBP was used as a housekeeping gene. Data are represented as mean ± SEM (n=3, two-sided t-test, *$p < 0.05$). Expression of Gm12606 T1 (**A**), Gm12606 T2 (**B**) and p16 (**C**) RNA.

6.4 Antisense oligonucleotide-mediated knockdown of Gm12606

Downregulation of Gm12606 in mMSCs was achieved by using antisense oligonucleotides (ASO). Design of the ASO probes was again restricted to these exons common to both transcripts due to presence of repetitive elements elsewhere in the Gm12606 transcripts. Two commercially produced ASO designed to bind to exons 2 and 4 of Gm12606 respectively were therefore selected that target both transcripts. Successful of Gm12606 after 24h and 48h was achieved in mMSCs, as shown by the very significant decrease of up to 90% in expression after transfection (**Figure 32**). The expression levels of untreated mMSCs were comparable to lipofectamine controls indicating the specificity of knockdown rather than the effect of transfection agent, but at this point an effect of RNA transfection may still be possible.

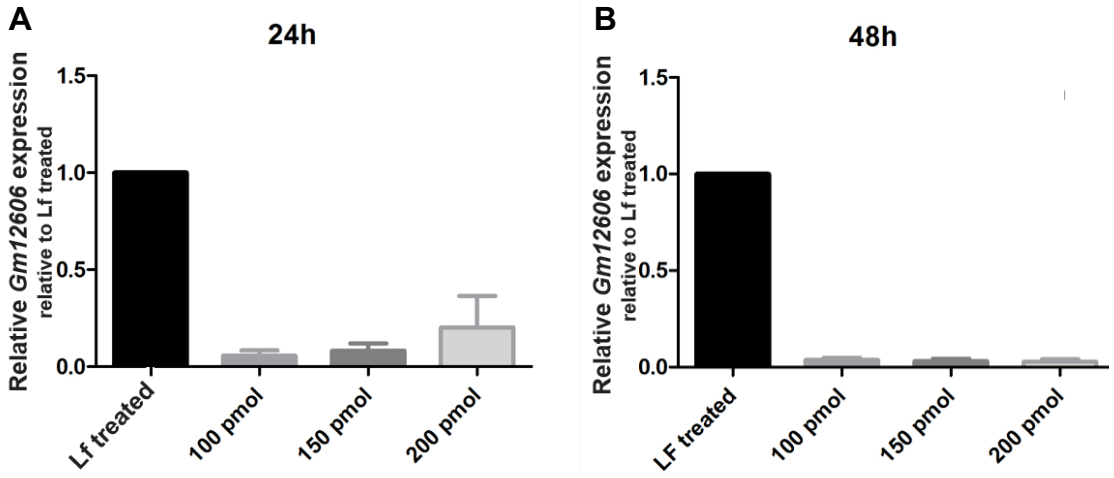

Figure 32: Efficient downregulation of Gm12606 T1 after 24h and 48h by antisense oligonucleotides. The lincRNA Gm12606 was successfully downregulated in ASO transfected cells using different concentrations (100, 150, 200 pmol) compared to lipofectamine controls. Lipofectamin treated mMSCs were normalized to 1 for comparison purposes. TBP was used as a housekeeping gene. Expression of Gm12606 after 24h (**A)** and 48h (**B**) following ASO treatment. (n=1).

6.4.1 Gm12606 silencing decreased transcription from the nearby Ink4a/Arf/Ink4b locus in *cis*

The lowest concentration of 100 pmol of ASO for transfection was used for studying a possible cis regulation of the nearby Ink4a/Arf/Ink4b locus. A structurally similar sequence scrambled (scr) control ASO, that does not target any known mouse gene, was used as a control, and ruled out the possibility that the effect of Gm12606 downregulation was promoted by the transfection itself.

A 75% (+/- 2%) decrease of Gm12606 was already achieved 24h after transfection (**p=0.0079) (**Figure 33A)** and was kept at this level or went down even further after 48h (89% ± 1%-downregulation, ***p=0.0001) (**Figure 33B**).

Changes of p16 (0.78 ± 0.2-fold, *p=0.0187), p19 (0.73 ± 0.2-fold, **p=0.0014) and p15 (0.66 ± 0.1-fold, **p=0.0060) transcript levels were significantly decreased 48h after ASO transfection. This indicates that there is a delayed downregulation of the p16 locus following the reduced levels of Gm12606.

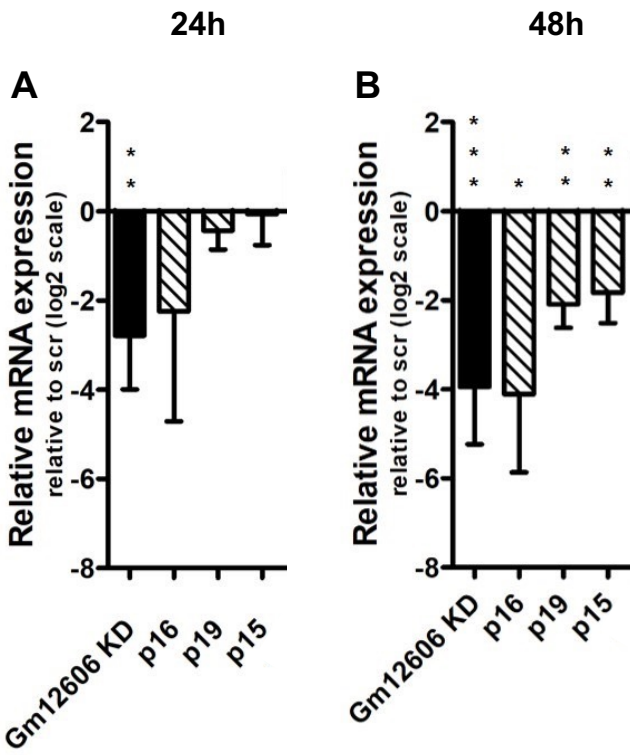

Figure 33: Effect of Gm12606 silencing on Ink4a/Arf/Ink4b locus transcription. Histograms show the expression of Gm12606, p16, p19, and p15 (shown on the log2 scale) after ASO-mediated Gm12606 knockdown in mMSCs compared to scr controls. The expression in scr control-mMSCs was normalized to 1 for comparison purposes. TBP was used as a housekeeping gene. Data are represented as mean ± SEM (n=3, two-sided t-test, *p < 0.05, **p < 0.01, ***p < 0.001). Expression of Gm12606, p16, p19, and p15 was measured 24h (**A**) and 48h (**B**) after ASO mediated knockdown of Gm12606.

6.4.2 Specificity of the altered transcription of the p16 locus in Gm12606 downregulated mMSCs

To exclude the possibility that the decline in p16, p19 and p15 transcripts were due to a general, genome-wide transcriptional downregulation after Gm12606 knockdown, the expression from several loci on different chromosomes (chr.) was examined by RT-qPCR. The genes were either located on the same chromosome or were distributed within other chromosomes of the genome. Selected genes and chromosomes were Klf4 (Krueppel-like factor 4, chr.4), p21 (Cyclin Dependent Kinase Inhibitor 1A, chr.17), Hmga1 (High Mobility Group AT-Hook 1, chr.17), p27 (Cyclin Dependent Kinase Inhibitor 1B, chr.6), Rb1 (RB Transcriptional Corepressor 1, chr.6), Rbl1 (RB Transcriptional Corepressor Like 1, chr.12), Rbbp1 (AT-Rich Interaction Domain 4A, chr.12), Dkk2 (Dickkopf WNT Signaling Pathway Inhibitor 2, chr.3), Nes (Nestin, chr.3), 14-3-3β (Protein Kinase C Inhibitor Protein 1, chr.2), and Bmi1 (BMI1 Proto-Oncogene, Polycomb Ring Finger, chr.2).

No significant change was found in gene expression of p21, Hmga1, Rbl1, Rbpp1, Nestin, 14-3-3β, and Bmi1, suggesting that these results are not a general effect of downregulation by itself.

There was a significant upregulation of Klf4 after 24h (0.80 ± 1.2-fold, *p=0.0153) as well as 48h (1.24 ± 1.3-fold, *p=0.0166) (**Figure 34A-B**) of ASO transfection. Dkk2 levels were significantly reduced up to 65% (0.65 ± 0.1-fold, **p=0.0011) after 24h of ASO transfection. Transcript levels later increased again to 57% towards control cells (0.57 ± 0.1-fold, *p=0.0117) in the later time point (48h) (**Figure 34A-B**). In addition, impaired Rb1 transcription (0.54 ± 0.1-fold, *p=0.0119) was observed 24h (**Figure 34A**) after switching off Gm12606.

Several effects on remote genes could be identified, suggesting either a regulation of the lincRNA Gm12606 in *trans* or a secondary effect emanating from the downregulated Ink4a/Arf/Ink4b locus.

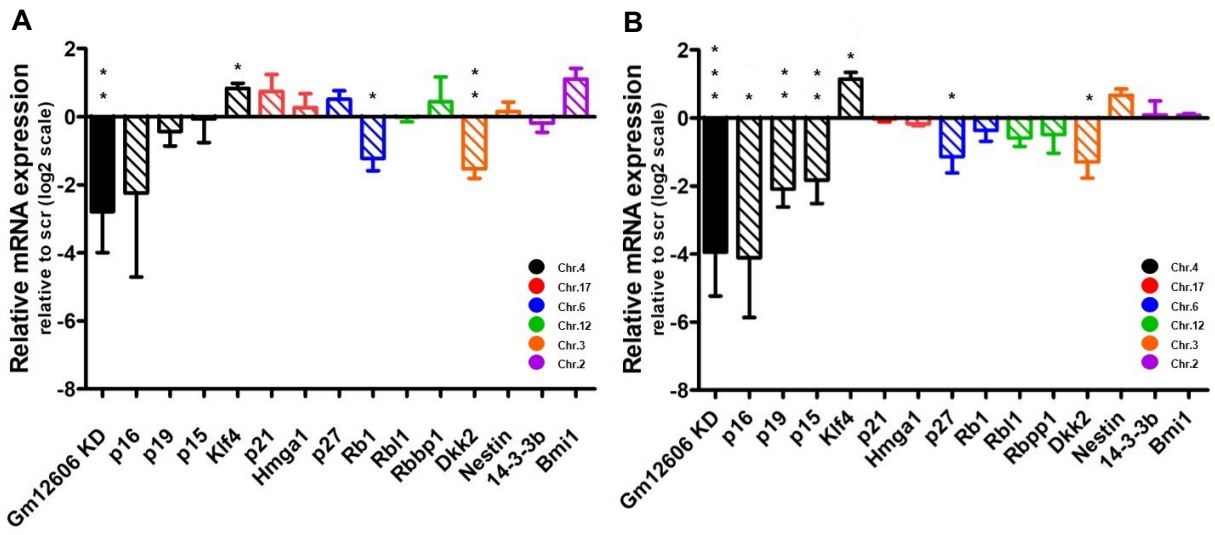

Figure 34: Effect of Gm12606 knockdown on the transcription of distant genes. Histograms show the expression of several genes after ASO-mediated Gm12606 knockdown (shown on the log2 scale) in mMSCs compared to scr controls. The expression in scr control mMSCs was normalized to 1 for comparison purposes. TBP was used as a housekeeping gene. Data are represented as mean ± SEM (n=3, two-sided t-test, *p < 0.05, **p < 0.01, ***p < 0.001). Expression levels of all genes was determined 24h (**A**) and 48h (**B**) after ASO mediated knockdown of Gm12606.

6.5 Establishment of a CRISPR/Cas9 knockout strategy for Gm12606 T1

6.5.1 Validation of sgRNA activity *in vitro*

Applying sgRNA 1, 2, 5, and 6 (**Figure 35A**) to delete a large fragment, double transfections with two plasmids containing pairs of sgRNAs were done to flank the entire Gm12606 locus. PCR results showed that each product generated by combining dual sgRNA harboured the desired large fragment deletion (**Figure 35B**). Sequencing indicated precise Cas9 activity at the target site by inducing DSBs exactly three nucleotides away from the PAM sequence, thereby producing a 37513 bp deletion (**Figure 36**). Due to the efficient deletion of the large fragment *in vitro*, this method was further used to generate a knockout mouse *in vivo*.

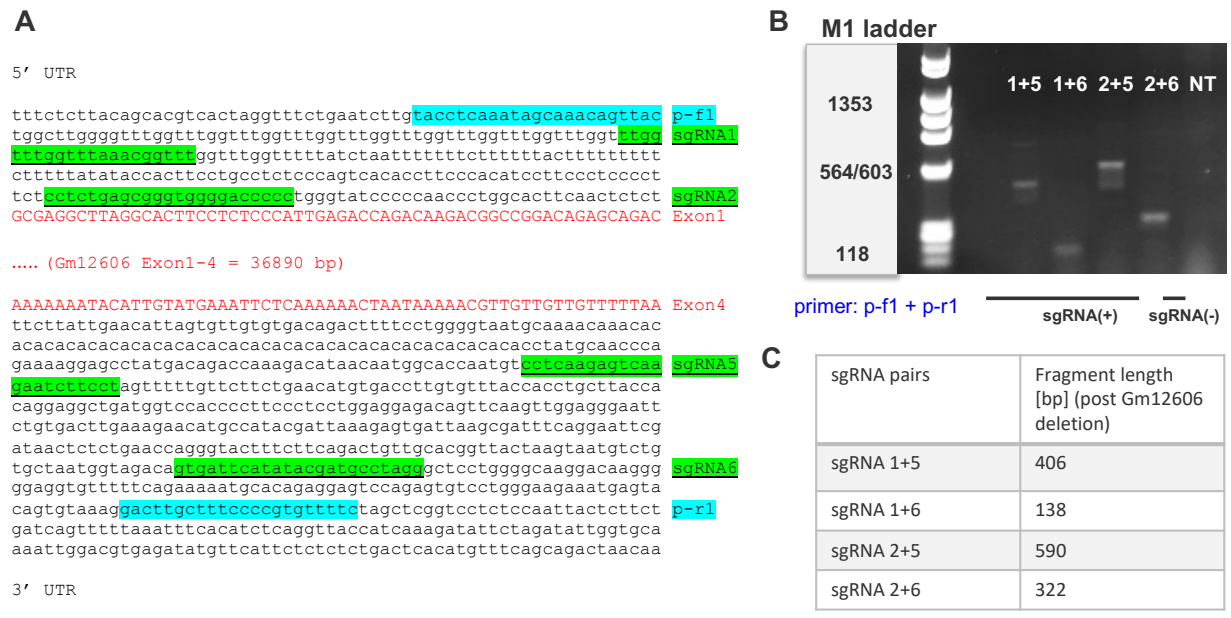

sgRNA pairs	Fragment length [bp] (post Gm12606 deletion)
sgRNA 1+5	406
sgRNA 1+6	138
sgRNA 2+5	590
sgRNA 2+6	322

Figure 35: *In vitro* CRISPR/Cas9-mediated large fragment deletion of Gm12606 in MOS cells. (**A**) Sequence of the PCR amplified region surrounding Gm12606 exon1-4 (red). The PCR primers (blue) are flanking the CRISPR/Cas9 target sites (green). (**B**) PCR detection of chromosomal fragments deletion between sgRNA1 + sgRNA5, sgRNA1 + sgRNA6, sgRNA2 + sgRNA5, and sgRNA2 + sgRNA6. Non-transfected cells (NT) were used as a negative control. Genomic DNA was extracted from treated and non-treated MOS cells, and PCR product loaded onto a 1.5 % agarose gel. (**C**) Table of expected amplicon size for co-transfected samples. Screening confirmed expected mut status shown in (**B**).

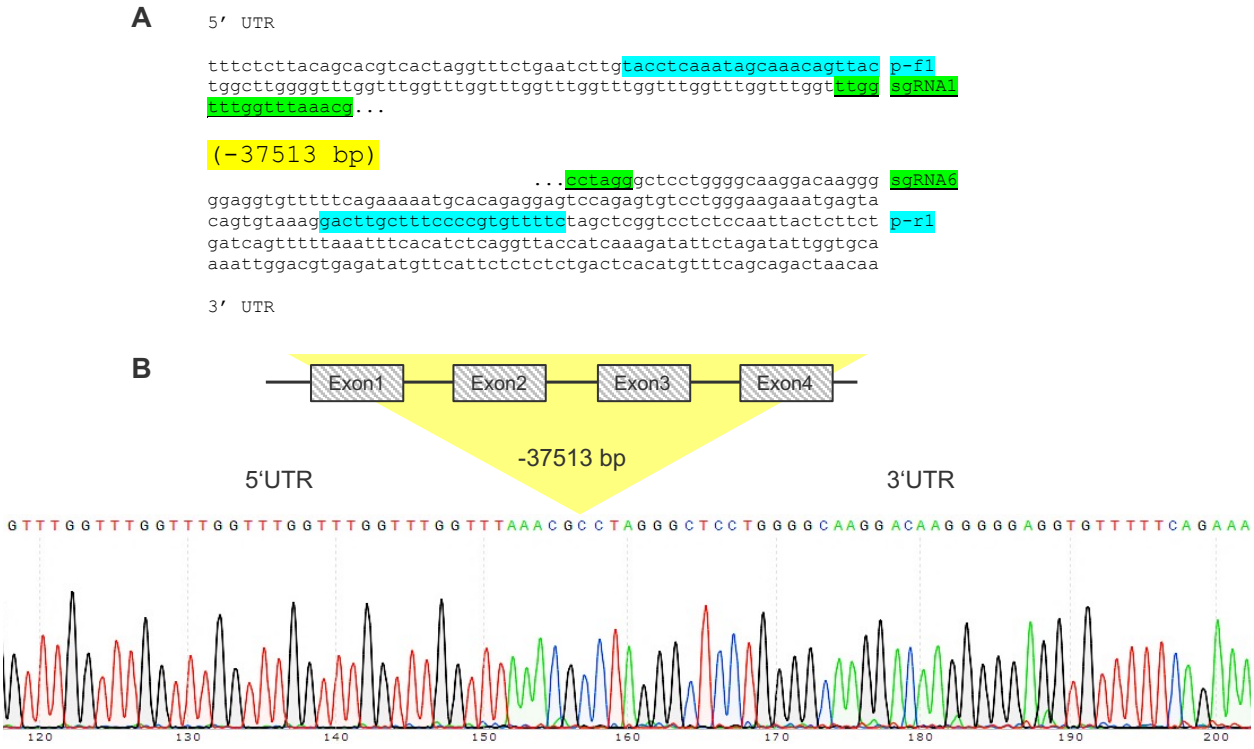

Figure 36: Sequence of Gm12606 gene with the CRISPR/Cas9-mediated Gm12606 deletion in MOS cells. (**A**) Sequence of the PCR amplified region lacking the CRISPR/Cas9-deleted fragment. Precise Cas9 activity at the target sits (green) is shown. In total 36890 bp of Gm12606, 171 bp of the 5'UTR and 452 bp of the 3'UTR were depleted (in total -37513 bp). (**B**) Chromatogram shows the sequence of mut Gm12606 gene following complete fragment deletion (-37513 bp) *in vitro*.

6.5.2 In vivo deletion of a large genomic fragment in mice using multiple sgRNAs

Prior to pronuclear microinjection into mouse zygotes, sgRNAs (sgRNA 1, 2, 5, 6) were pooled and mixed with a recombinant Cas9 protein (performed by IDG, F. Giesert). The aim was to generate a large fragment deletion of the Gm12606 locus in mice (same as in MOS cells). Primers (sequences provided in section 4.11.1) surrounding the entire region were designed to validate the predicted large fragment deletions. In total, 71 pups were obtained from pseudopregnant CD1 mice into which microinjected mouse zygotes were transferred. PCR results showed that 0 of 71 (0%) contained the desired Gm12606 deletion (**Figure 37B**). Some animals had small deletions

or insertions at or around single sgRNA target sites (e.g., mouse nr. 4) (**Figure 38B, lower image**), others had larger deletions between the nearest sgRNA target sites, such as mouse nr. 2, and 8 (**Figure 38B, upper image**). The latter mutant (mut) mice with potential promoter deletions have died before they could be mated.

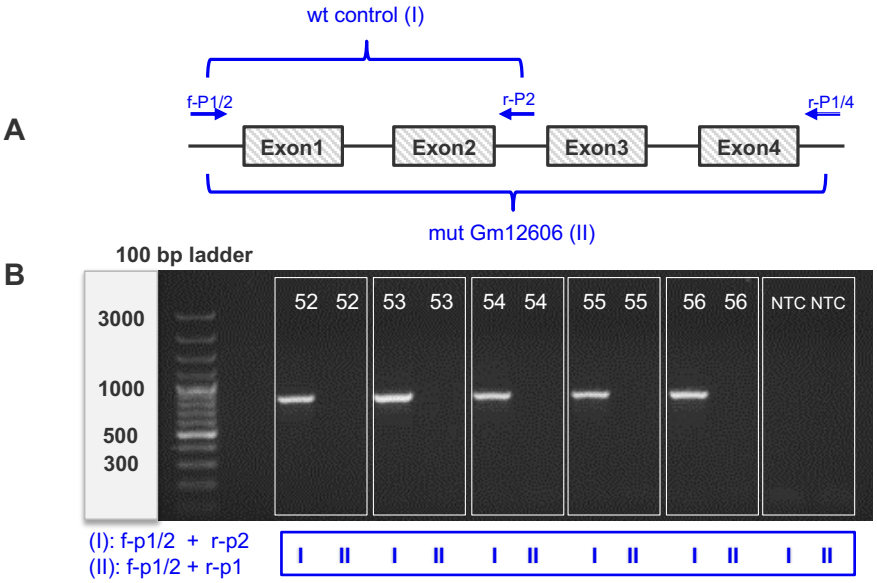

Figure 37: Genotyping of mice after CRISPR/Cas9 Gm12606 large fragment deletion. (**A**) The CRISPR targeted Gm12606 T1 locus was PCR amplified from pup genomic DNA using primer pair f-P1/2 + r-P2 and primer pair f-P1/2 + r-P1/4. Position of Gm12606 specific primer is shown in blue. Smaller fragment was amplified (primer pair I) and used as a wt control. For the detection of the large fragment deletion (mut Gm12606) primer pair II was used. (**B**) PCR detection of genomic DNA fragments of CRISPR/Cas9 mediated mouse 52-56. PCR products were separated on a 1.5 % agarose gel. As an example, the results of 5 out of 71 pups are shown. Expected band size for wt was 778 bp and for the mut alleles was 402 bp. All mice were wt. No specific product was detected for the mutants.

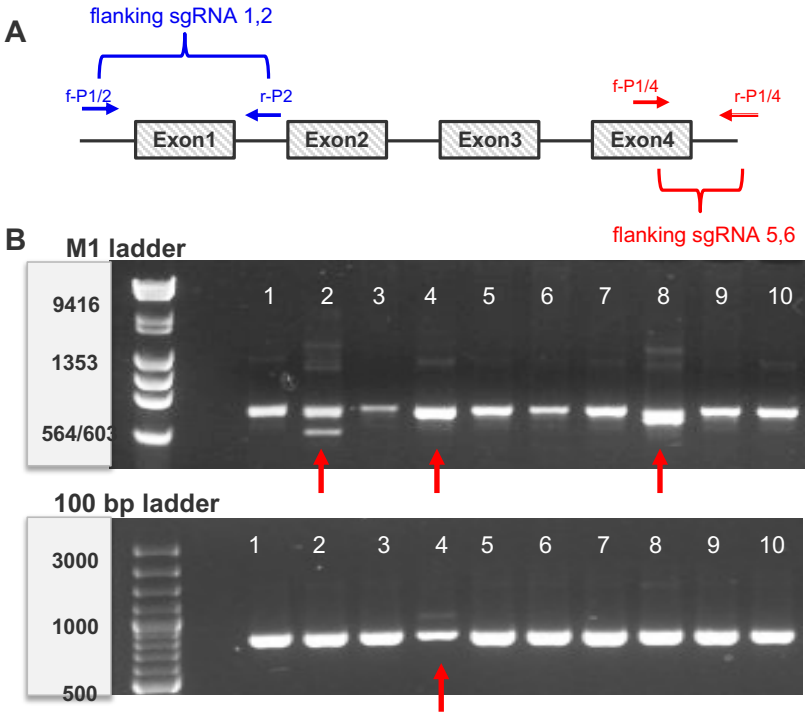

Figure 38: CRISPR/Cas9-mediated deletion of potential promoter in mice. (**A**) The CRISPR targeted *Gm12606 T1* locus was PCR amplified from pup genomic DNA using primer pair f-P1/2 + r-P2 (flanking sgRNA 1,2) and primer pair f-P1/4 + r-P1/4 (flanking sgRNA 5,6). Position of Gm12606 specific primer is shown in blue (for sgRNA 1,2) and red (for sgRNA 5,6). (**B**) Image of PCR results. PCR products were separated on a 1.5 % agarose gel. Pooled sgRNA microinjection into mice zygotes produced founder that harbour deletions between the nearest sgRNA target sites (Lanes 2,8, upper image) and small deletions or insertions at or around single sgRNA target sites (Lane 4, upper and lower image).

6.6 CRISPR/Cas9 exon1/intron1 splice site deletion and poly-A signal knock-in

In addition to the initially planned large deletion it is also possible to constitutively eliminate transcription by insertion of a poly-A signal (KI) into the genome. For this purpose, a new sgRNA was designed (sgRNA7) targeting the exon1/intron1 splice site of Gm12606 (**Figure 14**). Generation of the Gm12606 KO mouse from one-cell embryos was performed via microinjection of sgRNA7, recombinant Cas9 protein and a non-homologous end joining inhibitor (i53) to increase the efficiency of homologous recombination (performed by IDG, F. Giesert).

6.6.1 One sgRNA leads to a series of mutations with splice site deletions and a partial knock-in

In total 23 viable pups were obtained. Primers (sequences provided in section 4.11.1) located in exon1 and intron1 (**Figure 39A**) were designed to validate the predicted mutations to the splice site. PCR results revealed that 10 of 23 (43%) founder exhibited sequence alterations (**Figure 39B**). Some animals had small deletions and/or insertions (InDel) within exon1 (mice 74, 80, 82, 83, 88, 94), others had larger InDel containing splice site deletions (mice 73, 76 and 79) (**Appendix C)**. Wild-type mice generated single bands. PCR amplicons from heterozygous mice yielded two distinct bands, a lower one for homoduplexes and an upper one for heteroduplexes. In addition, three bands were detected in three samples 73, 76, 79, indicating a biallelic or mosaic status (**Figure 39B**), which results from editing the cells at different stages of embryonic development (Mehravar, Shirazi, Nazari, & Banan, 2019). Sequencing confirmed that two animals (74, 80) had a heterozygous mutation affecting only one allele and two compound heterozygous mice, each with two differently mutated alleles (76 and 79, biallelic). A more detailed examination of mouse 79 showed a partial knock-in of the homologous repair template, starting with several CA-repeats (**Appendix C**), but with an interruption after 43 bp. The whole donor construct was

not integrated into the DNA within this study. Mice showing a deletion event in the target locus (heterozygous FO founder mice) were mated with wild-type littermates, to obtain F1 heterozygous offspring. Genotyping of F1 offspring confirmed germline transmission of the CRISPR/Cas9 induced mutations (**Figure 40**). Furthermore, genotyping of F1 offspring confirmed the biallelic edit of mice 76 and 79 by yielding two distinct mutants and no wild-type animals, whereas pups from mouse 73 remained with only one mutant, besides having many wild-type littermates (**Figure 40**).

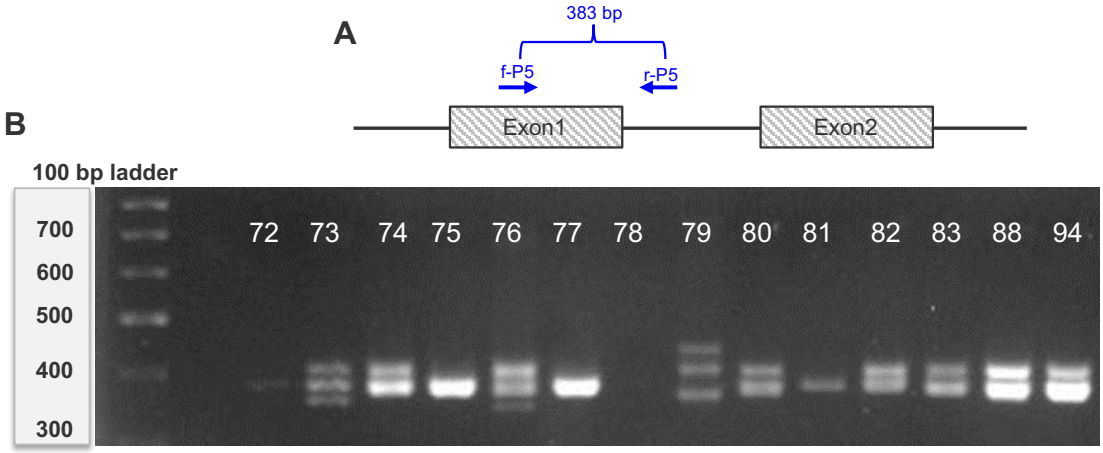

Figure 39: Variety of sgRNA 7-indueced mutations in mice. (**A**) The CRISPR targeted Gm12606 exon1/intron1 splice site region was PCR amplified from pup genomic DNA using primer pair f-P5 (located within exon1) + r-P5 (blue) resulting in a 383 bp product (**B**) Image of a selection of PCR results from founder mice harbouring different sequence alterations. PCR products were separated on a 2.5 % agarose gel. Mice 74, 80, 82, 83, 88, 94 had small deletions and/or insertions (InDel) within exon1, while mice 73, 76 and 79 had larger InDel containing splice site deletions. Sequencing of samples confirmed wt or mut status (**Appendix C**). All mut yielded heteroduplex bands. PCR amplicons of mice 72 and 78 were not detected.

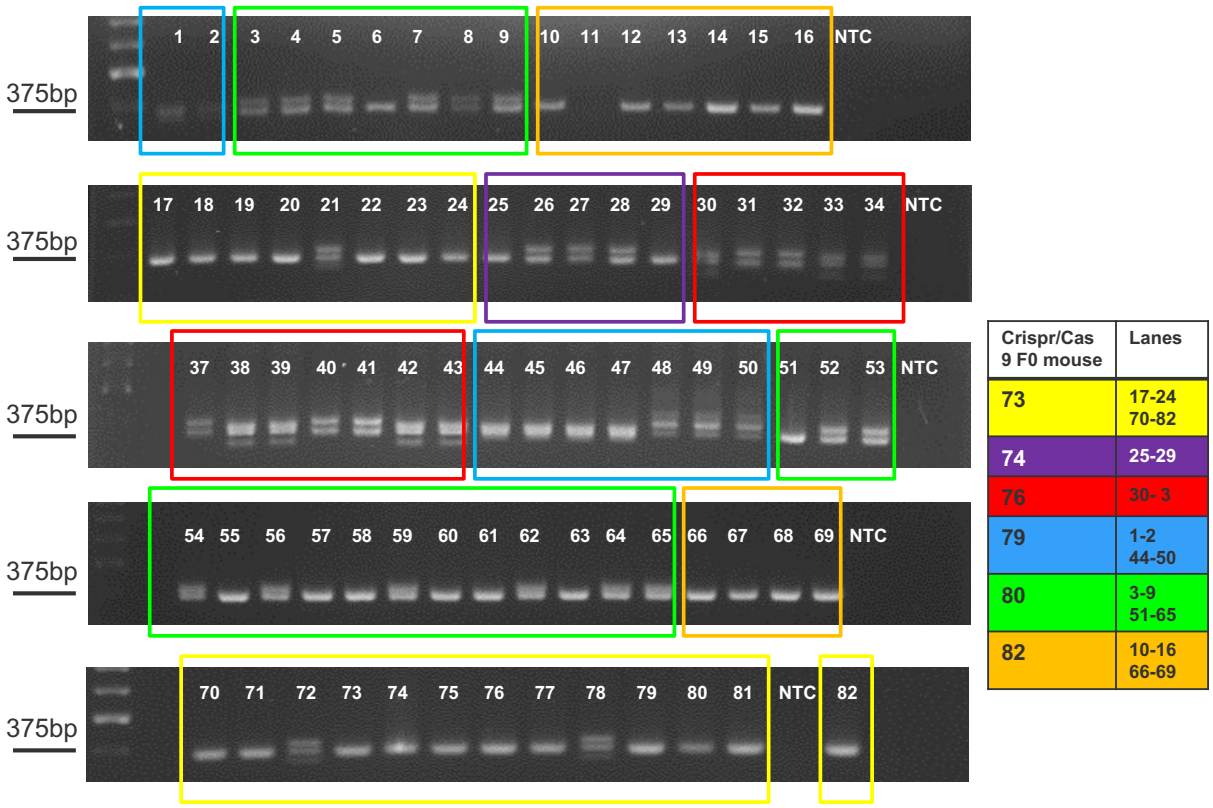

Figure 40: Genotyping of F1 offspring. Selected PCR images of F1 mice showing deletion events. F0 mice 73, 74, 76, 79, 80, 82 with sequence alterations (**Figure 39**) were mated with wt littermates to obtain F1 heterozygous offspring. Offspring were genotyped to validate germline transmission of CRISPR/Cas9 mutations. All F1 mice exhibited mutation events except mouse 82 (orange). Offspring from mice 76 (red) and 79 (blue) yielded two distinct mut and no wt animals. PCR products were separated on a 2.5 % agarose gel.

It is well known that CRISPR/Cas9 processing can cause imprecise, complex mutations with an increased rate of larger deletions (Shin et al., 2017), which are frequently not directly detectable. New primer has been designed that surround a larger region beyond exon1 (**Figure 41A**). Results showed that founder mouse 72 harboured a large fragment deletion, while mouse 78 was still undetectable (**Figure 41B**). Sequencing of the edited locus of mouse 72 indicated that a total of 256 bp had been removed, including the entire exon1 sequence (-156 bp) of Gm12606 and another 92 bp within the 5'UTR site and intron1 (-8 bp) (**Figure 42**). This male was used as a

founder (72) as the region features an exon1 and splice site deletion and a potential promoter area erasure that may cause the desired reduction of Gm12606 transcription. Before mouse was sacrificed due to developmental genito-urinary problems, the sperm was stored, and IVF performed.

A total of 3 of 4 females became pregnant following IVF with frozen sperm from mouse 72 and delivered 18 offspring (**Appendix C**). From these animals' two female and three male heterozygous mutants (F1) (**Figure 43**) were crossed to generate homozygous mice (F2). Four male wild-type littermates were kept until sexual maturity, sacrificed and mMSCs isolated from the bone-marrow for further ageing and radiation studies *in vitro*.

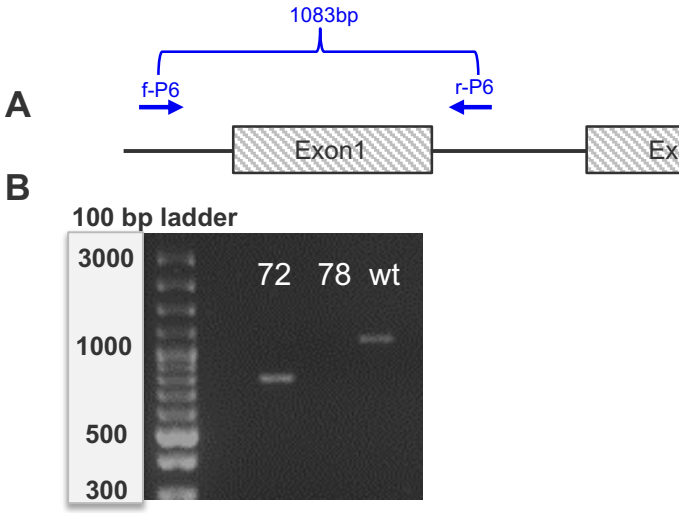

Figure 41: Large fragment mutation of founder mouse 72. (**A**) The CRISPR targeted Gm12606 exon1/intron1 splice site region was PCR amplified from pup genomic DNA using primer pair f-P6 (located within 5'UTR, blue) + r-P6 (located within intron1, blue) resulting in a 1083 bp product. (**B**) Image of PCR result demonstrating a deletion of -253 bp in mouse 72 compared to the wt control. Genomic DNA of mouse 78 could not amplify the Gm12606 sequence. PCR products were separated on a 2.5 % agarose gel.

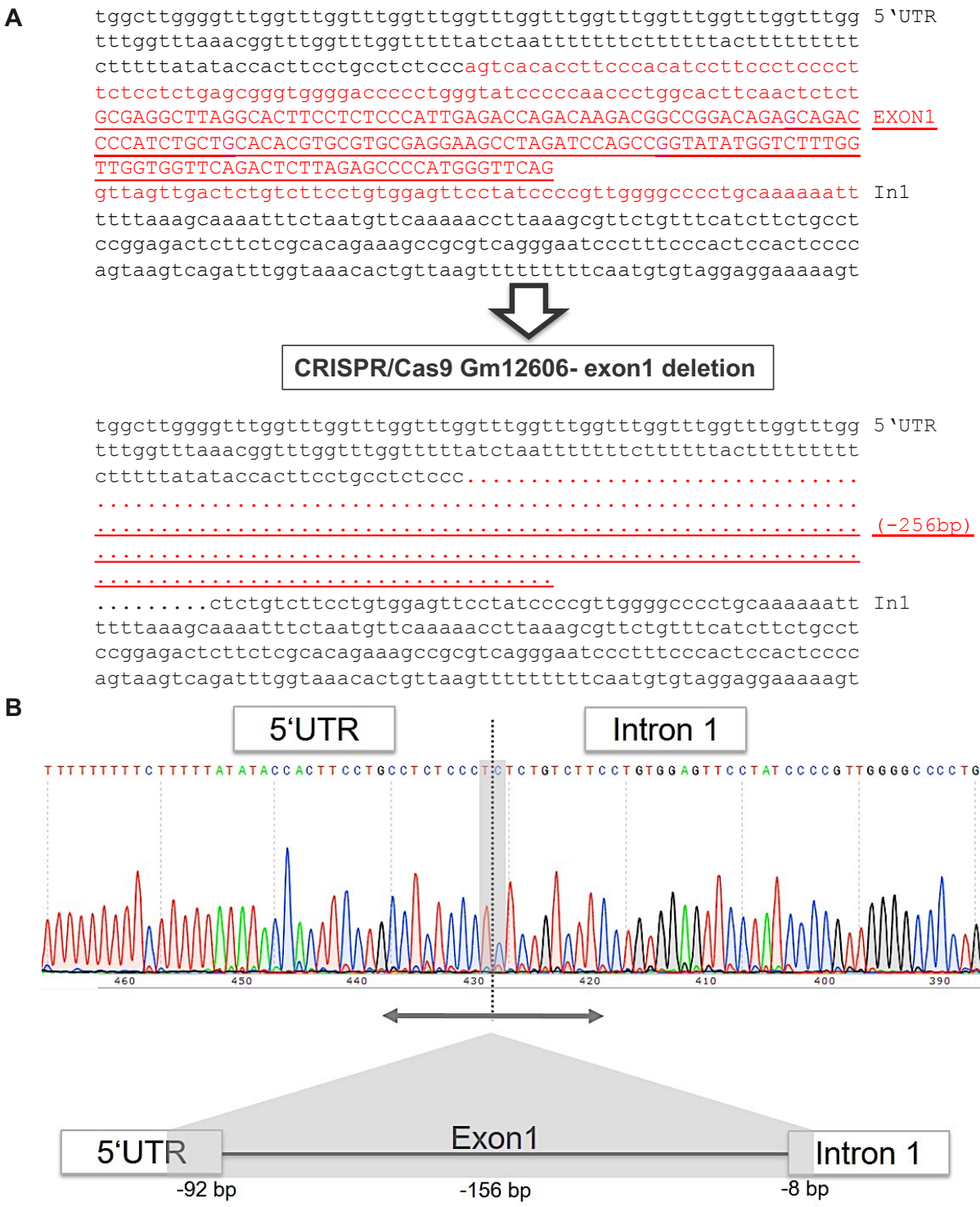

Figure 42: Sequence of mutated Gm12606 T1 gene in founder mouse 72. (**A**) Sequence of the PCR amplified region before and after the CRISPR/Cas9 exon1-fragment deletion. 256 bp were missing, including exon1 (-156 bp) + intron1 (-8 bp) + 5'UTR (-92 bp) (red) (**B**) Chromatogram confirmed the -256 bp fragment deletion in mouse 72.

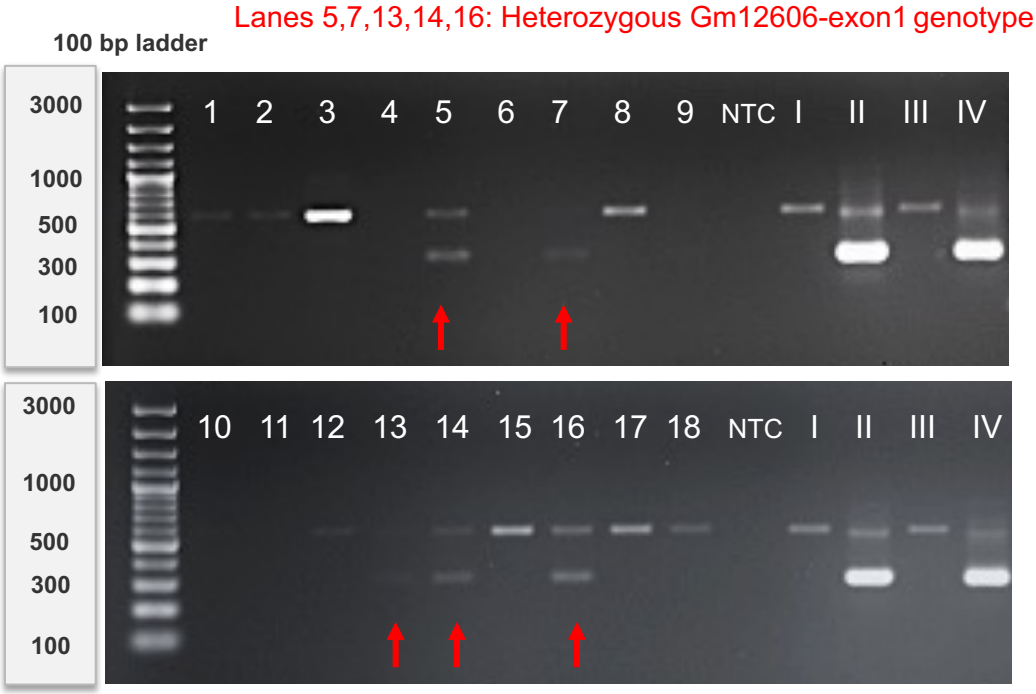

Figure 43: Heterozygous mutants after IVF. PCR detection of heterozygous mutants after IVF from frozen sperm of mouse 72. In total 18 pups were born. Two female (5,16) and three male (7,13,14) mice exhibited a heterozygous Gm12606-1$^{-/+}$ mutation (red arrow), lacking 256 bp. These animals were paired to generate F2 generation mice. PCR products were separated on a 2.5 % agarose gel. Different controls were used (Lane I-IV), which also contained a positive control from gDNA of the FO mouse 72 (Lane II), and a negative control (NTC) to exclude contamination and false positive amplifications.

6.7 Effects of Gm12606 T1 exon1 deletion on mMSCs *in vitro*

6.7.1 No detectable expression of Gm12606 T1 using RT-qPCR

mMSCs from homozygous exon1-deficient (Gm12606-1$^{-/-}$) C57BL/6 male mice were isolated from bone marrow, expanded for three weeks *in vitro,* and compared with mMSCs from wild-type littermates (Gm12606-1$^{+/+}$)**.** The loss of expression of Gm12606 T1 transcripts in Gm12606-1$^{-/-}$ mMSCs was confirmed by RT-qPCR, which did not produce an amplified signal even after 40 cycles (Ct-values > 40). T2, which contains a different exon 1 that was unaffected by the CRISPR/Cas9 deletion, was slightly, but not significantly, increased (1.6 ± 0.5-fold increase p=0.1640 compared to wild-type cells) (**Figure 44**).

Figure 44: Expression of T2 in mMSCs from Gm12606 T1 depleted mice. Histogram shows the relative expression of T2 in mMSCs of C57BL/6 mice lacking T1 exon 1 (hom (Gm12606-1$^{-/-}$)) compared to wt controls. Wt represents the control littermates and was normalized to 1 for comparison purposes. TBP was used as a housekeeping gene. Data are represented as mean ± SEM (n=4, two-sided, paired t-test).

6.7.2 Reduced cell growth of Gm12606 T1 exon1-deficient mMSCs

To investigate the effect of Gm12606 mutation *in vivo* on mMSC cell growth, Presto Blue Cell Viability Assay was performed on mMSCs of passage 3 (p3) by measuring relative fluorescence units every third day. The Presto Blue signal representing cell viability of mMSCs from wild-type (Gm12606-1$^{+/+}$) and hom (Gm12606-1$^{-/-}$) mice on day 3 after plating did not differ significantly (2way ANOVA, p=0.7386). However, the subsequent growth kinetics of Gm12606-1$^{-/-}$mMSCs was reduced (2way ANOVA, ***p=0.0007). The number of proliferating cells accumulated in cells of both genotypes plateaued at different times; day 10 for wild-type and day 12 for mutant Gm12606-1$^{-/-}$, but then declined, with Gm12606 mutant cells slightly more abundant after 15 days of passaging (**Figure 45**).

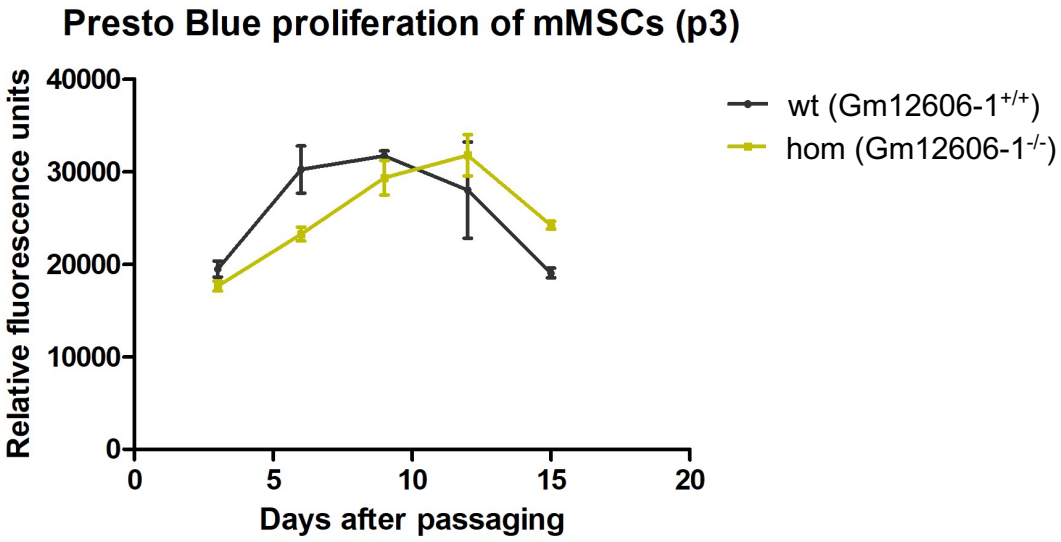

Figure 45: Effect of Gm12606 on long-term growth of mMSCs (p3). Plot shows the numbers of viable mMSCs (p3) from wt and mut Gm12606-1$^{-/-}$ cells presented as relative fluorescence units, obtained over a 15-days' time period. Data are represented as mean ± SEM (n=3, 2wANOVA, days ***p < 0,001) with values presented in the text.

6.7.3 The transcription of the nearby Ink4a/Arf/Ink4b locus is reduced after deletion of Gm12606 T1 exon1 in mMSCs

The transient knockdown of Gm12606 was shown before to cause a downregulation of the adjacent Ink4a/Arf/Ink4b cluster (**Figure 33**) in mMSCs. To examine whether the expression of p16, p19 and p15 also changed in the Gm12606 exon1 deleted mMSCs, RT-qPCR of mMSCs from three mice (n=3) was performed in both early passage 3 and aged passage 7 mMSCs. In mMSCs (p3) isolated from hom (Gm12606-1$^{-/-}$) mice, a substantial downregulation of p19^{Arf} (48%, p=0.1749) and p15^{Ink5b} (42%, p=0.1301) expression was noted compared to wild-type (Gm12606-1$^{+/+}$) controls, but no significance was achieved (**Figure 46A**). p16 levels were reduced by 19% (p=0.7078) (**Figure 46A**), while in the aged mMSCs (p7) the p16 expression was significantly downregulated by 0.68 ± 0.1-fold (**p=0.0099) (**Figure 46B**). Likewise, p19 and p15 mRNA was significantly reduced in aged mMSCs from passage 7, ranging from 0.77 ± 0.04 (p19 **p=0.0023) to 0.65 ± 0.1 -fold (p15 **p=0.0093) over controls (**Figure 46B**).

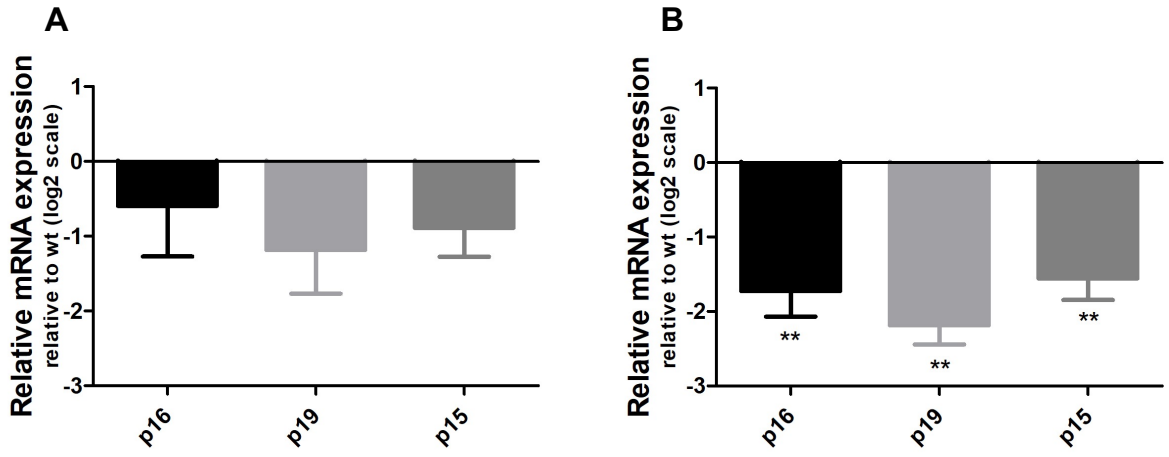

Figure 46: Effect of Gm12606 exon1 deletion on Ink4a/Arf/Ink4b locus in mMSC. Histograms show the expression of p16, p19, and p15 (shown on the log2 scale) in mMSCs after exon1 Gm12606 exhaustion in mice in vivo compared to wt controls. The expression in wt (Gm12606-1$^{+/+}$) mMSCs was normalized to 1 for comparison purposes. TBP was used as a housekeeping gene. Data are represented as mean ± SEM (n=3, two-sided, paired, t-test, **p < 0.01) with values presented in the text. Expression of Gm12606, p16, p19, and p15 in early passage 3 mMSCs (**A**) and aged passage 7 mMSCs (**B**) following Gm12606 exon1 depletion.

6.7.4 Gm12606 T1 disruption leads to a reduction of senescence in ageing mMSCs

As previous results indicated an upregulation of Gm12606 T1 levels in ageing mMSCs (**Figure 23A**), it was investigated if Gm12606-exon1 deletion *in vivo* would have an effect on ageing mMSCs *in vitro*. The percentage of SA-β-gal-positive cells in passage 3 and passage 7 mMSCs was determined over a period of 12 days. For two factor analysis (wt vs hom and days after seeding) 2-way ANOVA was performed, the results of which are presented in **Appendix B.**

The influence of Gm12606 knockout on cellular senescence *in vitro* was dependent on the passage number when the experiment started. At passage 3, the level of senescence 6, 9 and 12 days after cell seeding (**Figure 47**) was lower in mMSCs from hom (Gm12606-1$^{-/-}$) compared to wt mice (day6 = - 8%, day9 = - 9% and day12 = - 14%), and this change was highly significant (2way ANOVA, wt vs hom ***p=0.0004) (**Figure 48**).

Investigating the occurrence of senescence in aged mMSCs from passage 7 revealed a rapid increase of senescent cells in wt (Gm12606-1$^{+/+}$) (**Figure 49**) with more than 60% of the cells from passage 7 being positive (day6 = 64% ± 5%, day9 = 66% ± 2% and day12 = 62% ± 7% SA-β-gal-positive cells). However, in mMSCs of Gm12606-exon1 deleted mice the frequency of senescent cells during the same time course was much lower, with 12% ± 1% of senescent cells seen on day 6, 15% ± 1% at day 9 and 31% ± 2% at day 12. The difference between wild-type and hom Gm12606-exon1 mMSCs was very high (2way ANOVA, wt vs hom *****p<0.0001) (**Figure 50**). This suggests inactivation of Gm12606 has a direct influence on the development of cellular senescence in mMSCs.

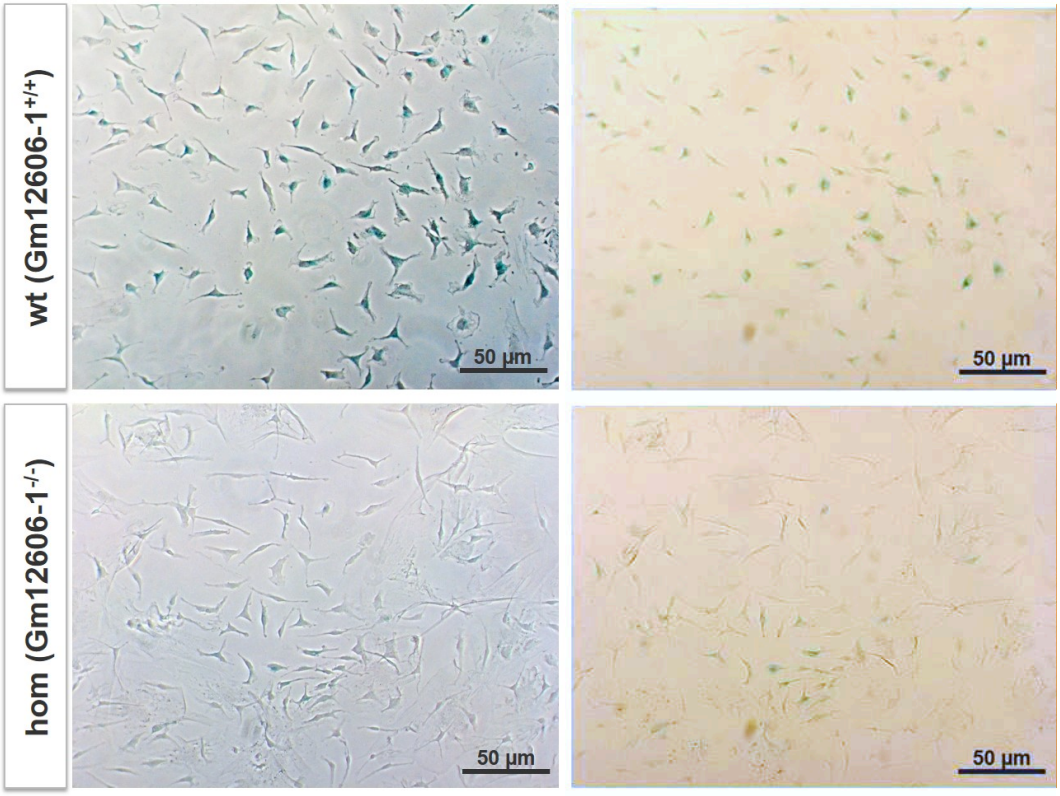

Figure 47: Representative images of mMSCs passage 3 from homozygous Gm12606-1$^{-/-}$ mutant mice compared to wild-type Gm12606-1$^{+/+}$ controls after SA-β-gal staining. Images were taken 12 days after seeding with phase contrast (left) for cell counting and with bright field illumination (right) for the detection of SA-β-gal positive cells (blue) using the Zeiss Axiovert 25 microscope. Hom Gm12606-1$^{-/-}$ mutated mMSCs are shown in the upper pictures, while wt Gm12606-1$^{+/+}$ are shown in the lower pictures. Scale bars are 50 µm.

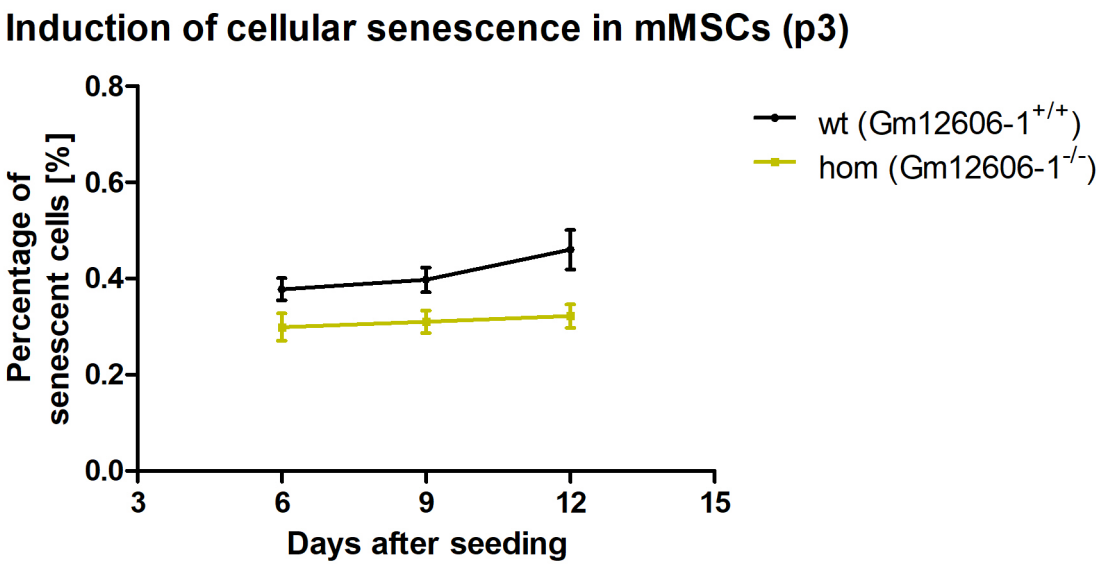

Figure 48: Induction of cellular senescence in mMSCs from passage 3 of homozygous Gm12606-1$^{-/-}$ mutant mice compared to wild-type Gm12606-1$^{+/+}$ controls. Plot shows the percentage of senescent cells 6, 9 and 12 days after cell seeding in mMSCs from wt Gm12606-1$^{+/+}$ (black) and hom Gm12606-1$^{-/-}$ (yellow) mice. Four biological and 2 technical replicates were used. Data are represented as mean ± SEM (n=4, 2wANOVA, wt vs hom ***p < 0.001) with values presented in the text.

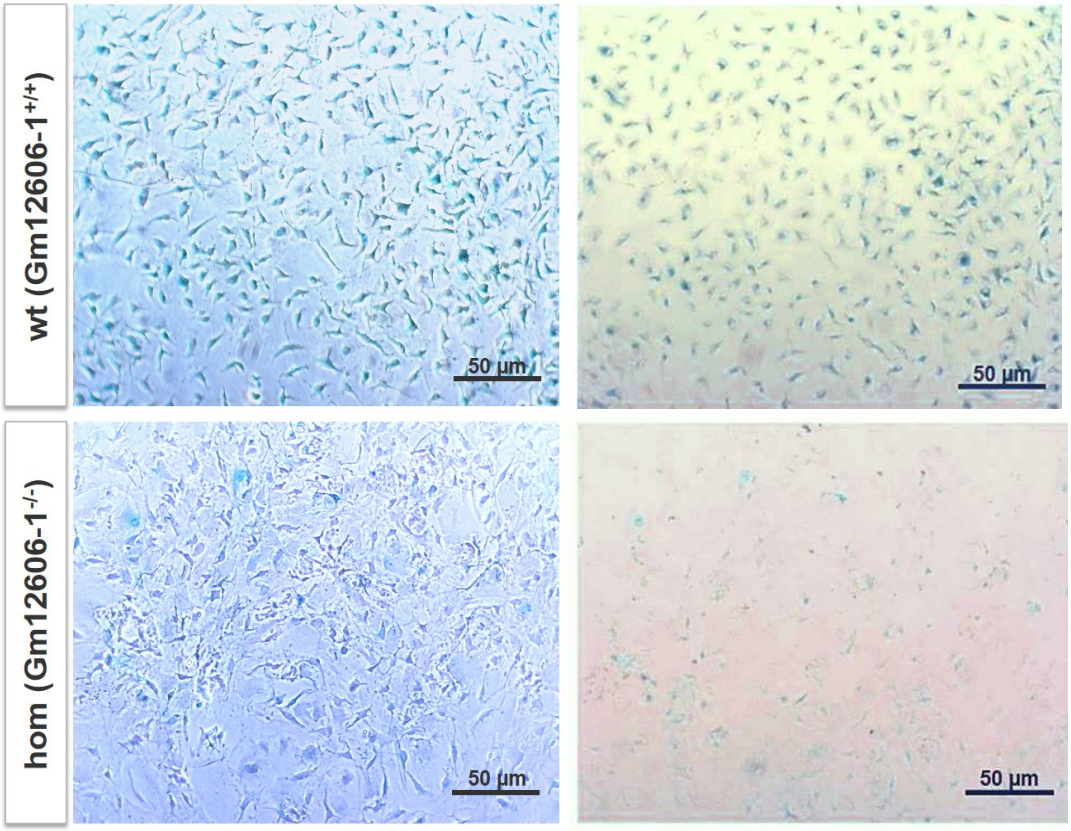

Figure 49: Representative images of mMSCs passage 7 from homozygous Gm12606-1$^{-/-}$ mutant mice compared to wild-type Gm12606-1$^{+/+}$ controls after SA-β-gal staining. Images were taken 12 days after seeding with phase contrast (left) and with increased light intensity (right) for the detection of SA-β-gal positive cells (blue) (method as in **Figure 17)**. Hom Gm12606-1$^{-/-}$ mutated mMSCs are shown in the upper picture, while wt Gm12606-1$^{+/+}$ are shown in the lower picture. Scale bars are 50 µm.

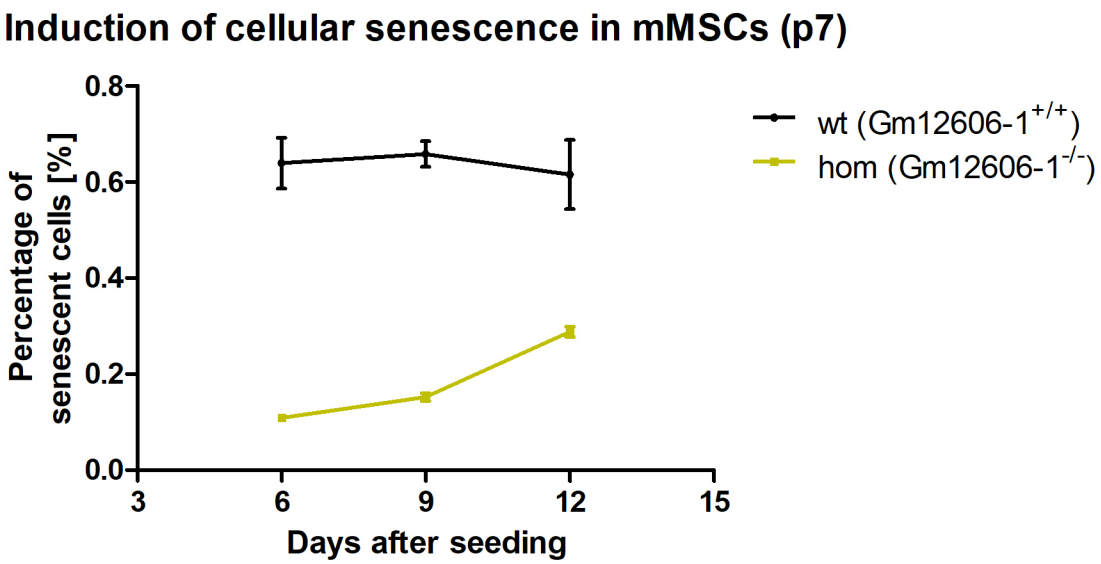

Figure 50: Induction of cellular senescence in mMSCs from passage 7 from homozygous Gm12606-1$^{-/-}$ mutant mice compared to wild-type Gm12606-1$^{+/+}$ controls. Plot shows the percentage of senescent cells 6, 9 and 12 days after cell seeding in mMSCs from wt Gm12606-1$^{+/+}$ (black) and hom Gm12606-1$^{-/-}$ (yellow) mice. Three biological and 2 technical replicates were used. Data are represented as mean ± SEM (n=3, 2wANOVA, wt vs hom *****p < 0.00001) with values presented in the text.

6.7.5 Increased repair γH2AX and 53BP1 foci formation after γ-irradiation of mMSCs following Gm12606 T1 exon1 deletion *in vivo*

To study whether the deletion of exon1 of Gm12606, and the resultant changes in phenotype, affects the DNA damage repair the mMSCs (p3) from four hom Gm12606-1$^{-/-}$ mice were compared with those from four wild-type controls (Gm12606-1$^{+/+}$). The occurrence of γH2AX and 53BP1 DNA damage repair foci was measured by immunofluorescence staining 90 min after X-irradiation, when the maximum number of foci is reached, with doses of 0 Gy, 1 Gy, 2 Gy, 4 Gy (**Figure 51**).

The number of co-localized γH2AX/53BP1 foci, indicating ongoing repair of damage continuing after 90min increased continuously and significantly with dose (2wANOVA, dose ****p<0.0001). Comparing the numbers of foci in wild-type and Gm12606-exon1 mutant mMSCs, initial induction of repair foci was similar in cells of both genotypes after 0, 1 and 2 Gy X-ray exposure, while the foci formation was altered after 4 Gy exposure (**Figure 52**). Foci formation after 4Gy was higher in Gm12606-exon1 mutant mMSCs (mean value 17.3 ± 0.8 foci per nucleus) as compared with wild-type mMSCs (13.5 ± 0.3 foci per nucleus), with the difference reaching significance (2wANOVA, wt vs hom **p=0.0032) (**Figure 52**).

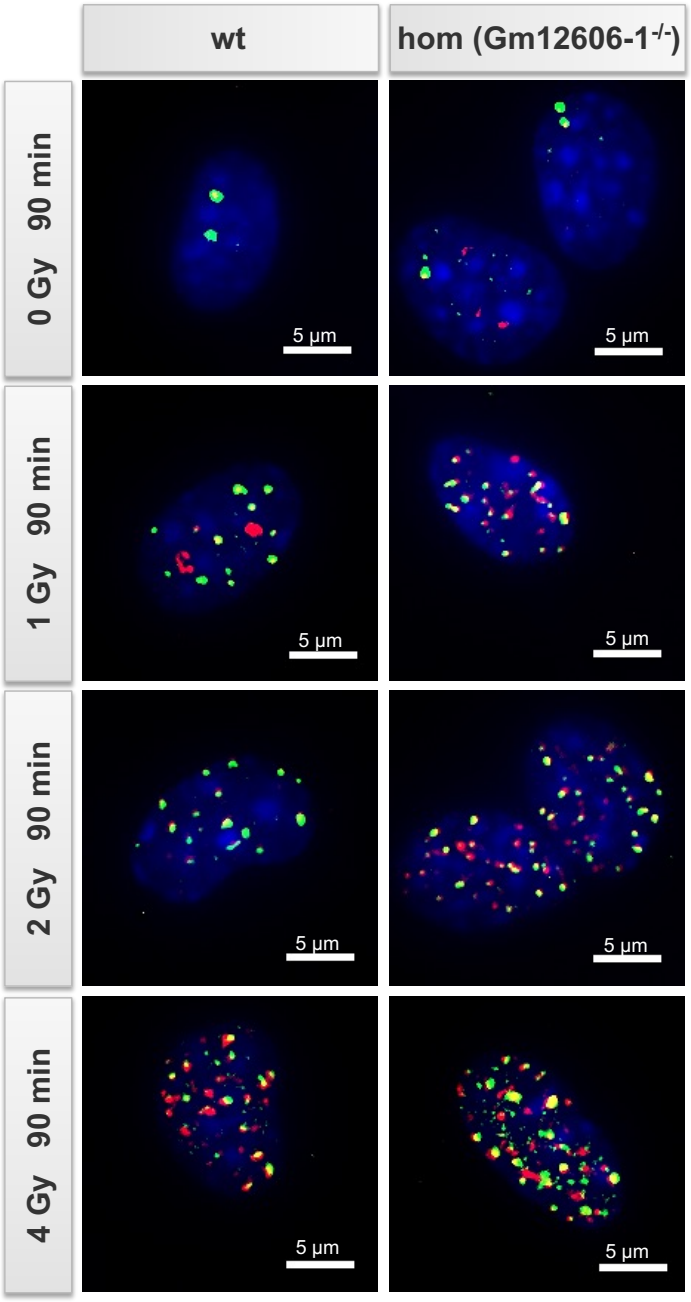

Figure 51: Representative images of γH2AX and 53BP1 foci formation in mMSCs passage 3 from homozygous Gm12606-1$^{-/-}$ mutant mice compared to wild-type Gm12606-1$^{+/+}$ controls. Immunofluorescence-stained images were acquired 90 min after acute exposure to different doses of X-rays (0 Gy, 1 Gy, 2 Gy, 4 Gy) using the KEYENCE BZ-9000 fluorescence microscope showing localised (yellow) γH2AX (red) and 53BP1 (green) foci and indicating DNA damage repair. Co-localized foci (yellow) were counted for the detection of radiation-induced DSBs of hom Gm12606-1$^{-/-}$ mut (right) and wt Gm12606-1$^{+/+}$ (left) mMSCs. The red and green signals are the artificial colouring generated by the software. Scale bars are 5 µm.

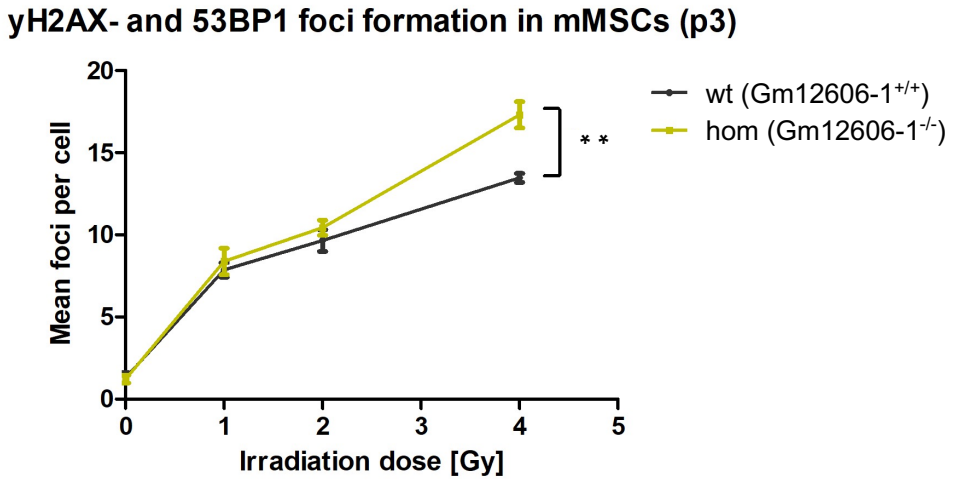

Figure 52: Induction of γH2AX and 53BP1 foci formation in mMSCs passage 3 from homozygous Gm12606-1$^{-/-}$ mutant mice compared to wild-type Gm12606-1$^{+/+}$ controls. Plot shows the mean foci per cell 90 min after acute exposure to X-irradiation of 0, 1 2 and 4 Gy in mMSCs from wt Gm12606-1$^{+/+}$ (black) and hom Gm12606-1$^{-/-}$ (yellow) mice. Data are represented as mean ± SEM (n=4, 2wANOVA, wt vs hom **p < 0.01, 2wANOVA, dose ****p<0.0001) with values presented in the text.

6.7.6 DNA repair kinetics is altered in *Gm12606* T1 exon1 deleted mMSCs

To analyse the kinetic of DNA DSB repair in mMSCs (p3) of four hom Gm12606-1$^{-/-}$ and wild-type controls (Gm12606-1$^{+/+}$), γH2AX and 53BP1 foci were analysed at different time points (90, 180, 360, 1440 min) post 2 Gy irradiation (**Figure 53**) and data obtained are shown as the resulting mean and standard error. In previous experiment, no significant difference was observed after 2 Gy exposure at 90 min (**Figure 52**). The mean foci number was plotted on a logarithmic scale (**Figure 54**). mMSC conditions initially showed a similar pattern of DSB repair in the first three time points. At each subsequent time point the remaining foci were reduced (2wANOVA, time after radiation ****p<0.0001). However, the remaining foci after 24h (1440 min) were 3.0 ± 0.1-times higher in the mMSCs of wild-type Gm12606-1$^{+/+}$ controls than in the Gm12606-1$^{-/-}$ mutants (1.8 ± 0.2), demonstrating that significantly less breaks remain unrepaired after 24h in mMSCs harbouring the Gm12606-exon1 deletion (2wANOVA, wt vs hom **p=0.0022) (**Figure 54**).

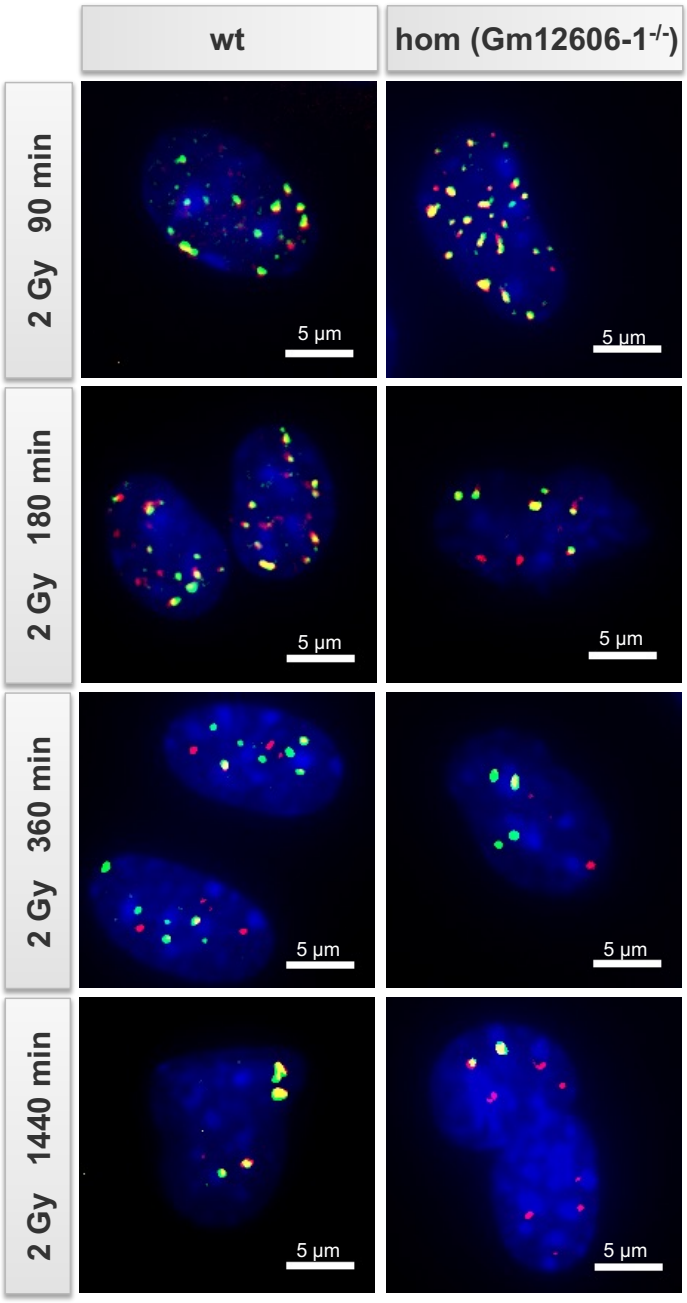

Figure 53: Representative images of DNA repair kinetics of radiation-induced DNA double strand breaks in mMSCs passage 3 from homozygous Gm12606-1$^{-/-}$ mutant mice compared to wild-type Gm12606-1$^{+/+}$ controls. Images were acquired 90, 180, 360 and 1440 min after acute exposure to 2 Gy X-irradiation using the KEYENCE BZ-9000 fluorescence microscope showing localized (yellow) γH2AX (red) and 53BP1 (green) foci and indicating DNA damage repair. Co-localized foci (yellow) were counted for the detection of DNA damage response of hom Gm12606-1$^{-/-}$ mut (right) and wt Gm12606-1$^{+/+}$ (left) mMSCs. The red and green signals are the artificial colouring generated by the software. Scale bars are 5 µm.

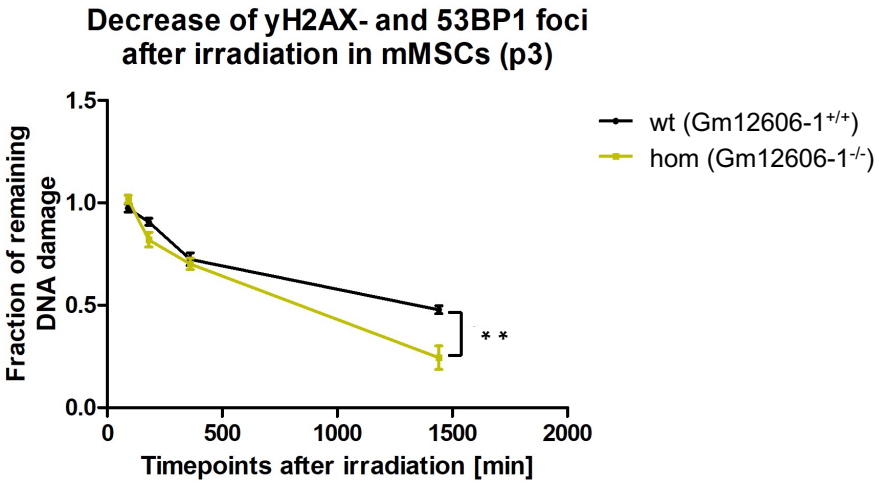

Figure 54: DNA repair kinetics of radiation-induced DNA double strand breaks in mMSCs passage 3 from homozygous Gm12606-1$^{-/-}$ mutant mice compared to wild-type Gm12606-1$^{+/+}$ controls Plot shows the fraction of repaired foci 90, 180, 360 and 1440 min after acute exposure to 2 Gy X-irradiation in mMSCs from wt Gm12606-1$^{+/+}$ (black) and hom Gm12606-1$^{-/-}$ (yellow) mice. Data are represented as mean ± SEM (n=4, 2wANOVA, wt vs hom **p < 0.01, 2wANOVA, dose ****p<0.0001) with values presented in the text.

6.8 Summary of results

The results in this study showed an increase in expression of T1 of the lincRNA Gm12606 during *in vitro* ageing of mMSCs from wild-type FVB/N mice between week 3 and 7 (**Figure 23**). An overexpression of Gm12606 was also observed 24h after γ-irradiation in 5- and 7-week-old mMSCs (**Figure 24**). This radiation response was more pronounced in T2. Three days later, the radiation-induced upregulation of T1 has completely vanished, before it went up again 20 days later (**Figure 25**). The radiation-response of T2 (in 5-week-old mMSCs) was dose-dependent and biphasic and initially increased to a maximum at 1 Gy (1.5h post irradiation) or even after 0.25 Gy (72h post irradiation) and returned to control levels at 2 Gy (**Figure 26**).

Beyond that, Gm12606 RNA expression showed a strong dependence on cell type and intracellular localization. Overall, expression was highest in the committed osteoblast precursor cells *in vitro*, reduced by about 50 % in mMSCs (from the same donor mice), and reduced to 32 % in an osteosarcoma cell line (MOS) from the same mouse strain (**Figure 27**). In mouse embryonic stem cells, Gm12606 T1 expression was undetectable (**Figure 27**). When osteogenic differentiation was induced in mMSCs by growth factor stimulation, Gm12606 expression resulted in a 3.64-fold upregulation (**Figure 31**). The significant differences in the overall T1 expression between mMSCs, mOB and MOS (same mouse strain) were contrasted by a very strong specificity of the intracellular localization of Gm12606 RNA. mMSCs exhibited a diffuse, weak signal only in the cytoplasm (**Figure 30**), while mOB showed a pronounced cell-to-cell heterogeneity, with about 20-30% of all cells exhibiting a strong, spotted nuclear signal (**Figure 29**). Cells of the MOS cell line had a weak cytoplasmic staining pattern (**Figure 28**), which in contrast to mMSCs was not diffuse but focal like the nuclear signal in mOB.

Antisense oligo-mediated knockdown of Gm12606 strongly influenced the transcription of the nearby Ink4a/Arf/Ink4b locus. 48h after Gm12606 antisense transfection, both the target transcript and the transcript of CDKN2A-Ink4a (p16) were downregulated by log2FD of -4 (or 16-fold

reduction) (**Figure 33**). Transcription of the alternative CDKN2A-transcript Arf (p19) and of the distal gene CDKN2B-Ink4b (p15) was also downregulated following Gm12606 knockdown, suggesting a *cis*-action (**Figure 33**). Out of 11 other randomly selected genes on other chromosomes, only Dkk2 (part of the Wnt signaling pathway), RB1 (involved in p16 signaling) and CDKN1B-Kip1 (p27), another CDK inhibitor involved in regulation of cell growth, quiescence and apoptosis, showed a slight downregulation (**Figure 34**).

CRISPR/Cas9-mediated knockout resulted in a homozygous mouse line with complete exon1 deletion of Gm12606, including 92bp of the 5'UTR (**Figure 41, 42**). This led to a complete absence of T1, suggesting that essential promotor or regulatory elements were destroyed. Expression of T2, which uses an alternative exon1 (and hence another 5'UTR), was still present, but a gradual up-or downregulation was not significant (**Figure 44**).

Bone-marrow derived mMSCs from mutant Gm12606-exon1$^{-/-}$ mice showed prolonged proliferation *in vitro* (**Figure 45**). With increasing passage numbers, mMSCs from Gm12606-exon1$^{-/-}$ mice retained a significantly lower percentage of cellular senescence (28%) than cells from wild-type littermates (> 60%), as measured in passage 7 for 12 days after plating (**Figure 50**).

Furthermore, early passage mMSCs from mutant Gm12606-exon1$^{-/-}$ mice exhibited a higher initial foci formation after 4 Gy compared to cells from wild-type littermates (**Figure 52**). At the same time, these cells repair more DNA double strand breaks (especially with the slow component), so that fewer DNA breaks were not repaired (**Figure 54**).

7. Discussion

This study aims to provide an insight into the underlying mechanism of ageing of mMSCs using an *ex vivo* model system. The goal was to study the role of long non-coding RNA Gm12606 in the replicative lifespan of mMSCs in order to better understand the ageing process. Our initial RNA-Seq transcriptome profiling identified a lincRNA, Gm12606, whose expression was dramatically increased both in ageing mMSCs and after ionizing radiation. Gm12606 is located on chromosome 4 (42.15 cM) in the mouse genome in close proximity to the Ink4a/Arf/Ink4b locus in mice. Since CDKN2A/p16, one of the proteins encoded at this locus, is known to be upregulated during cellular senescence, the hypothesis was proposed that Gm12606 might be involved in regulation of Ink4a/Arf/Ink4b. It is becoming increasingly clear that some lncRNAs are able to regulate the transcriptional activity of neighbouring genes in *cis*, probably by affecting the chromatin-DNA interaction via DNA-lncRNA binding (Michael S Werner & Alexander J Ruthenburg, 2015). Following the discovery of the proximity of the Gm12606 locus to the Ink4a/Arf/Ink4b locus, which in addition to CDKN2A/p16 (Ink4a) also codes for the cell cycle regulators p19 (Arf) and p15 (Ink4b), the focus was placed on understanding the relationship between the lncRNA Gm12606 and this locus critical to the regulation of cell proliferation and senescence.

7.1 Identification and detection of the long intergenic non-coding RNA Gm12606

This study identified Gm12606, a mouse lincRNA that is expressed and regulated in mesenchymal stem cells in dependence on their age *in vitro*. The lincRNA was originally identified in a cDNA library of LPS responding macrophages (GenBank Acc. No. AF032969) and later was

found upregulated in cells after transgenic activation of the Wnt pathway (Mullin et al., 2017). The molecular function of Gm12606 lncRNA, in particular actions on possible downstream effector genes or proteins were unknown and formed the basis for much of the experimental work described here. Two splice variants, which share two exons but differ in their first exon, were originally identified from the Gm12606 gene. The locus was mapped to an intergenic location between known protein-coding genes and is located in close proximity (1kB) to the Ink4a/Arf/Ink4b cluster (p16/p19/p15). Thus, Gm12606 is one of many intergenic transcripts produced by the mammalian genome that could have a variety of functional roles, from processing embryonic stem cell pluripotency to cell proliferation and the suppression of malignant progression (Guttman et al., 2009).

Moreover, it is known that lincRNAs are expressed at low levels and are more tissue- and developmental specific than protein-coding genes (Moran N Cabili et al., 2011; Derrien et al., 2012). In this study, Gm12606 was found to be expressed at low levels (in early passage mMSCs) and very low levels (in pluripotent stem cells like ES and iPS). If one assumes a role of this lncRNA *in cis* for the folding of a single locus, a few transcripts would indeed be sufficient to trigger such a mechanism. Sequencing results generated by RT-qPCR short products also proved that exons of the two transcripts were precisely linked, excluding the intronic regions (**Figure 20,21**). The sequences of the spliced transcript are almost consistent with those provided in the databases (**Appendix A**).

7.1.1 The expression of Gm12606 is elevated in murine osteoblasts

The expression of Gm12606 was not limited to mMSCs but was also found in other cells of the mesenchymal lineage, namely mOB cells and MOS cells, whereas no transcription was detected in early embryonic stem cells (**Figure 27**). Mullin et al., found Gm12606 overexpressed in dermal fibroblasts (Mullin et al., 2017). Fibroblasts are morphologically indistinguishable from MSCs and

are also described as plastic-adherent mesenchymal cells (Flavell et al., 2008). There is also evidence that MSCs can differentiate into fibroblast *in vitro* by promoting differentiation with growth factors (Hankemeier et al., 2005; Moreau et al., 2005). The mesenchymal origin of fibroblasts and the assumption that Gm12606 has only been detected in these cells so far suggests that Gm12606 may be more specific for cells of mesenchymal origin, but further studies in different tissues/cells are lacking to make an accurate conclusion.

Interestingly, the level of Gm12606 (T1) was most abundant in mOB, i.e., in cells of the highest degree of differentiation of all studied cells. Also, upon the induced osteogenic differentiation of mMSCs the expression of both Gm12606 transcripts was strongly, while the expression did not increase during induced adipogenesis or chondrogenesis (**Figure 31**). In parallel, p16 was also increased in the osteogenic differentiated cells (**Figure 31**). This suggests that Gm12606 may play a developmental and tissue specific role in accordance with the expression of p16. This is consistent with evidence pointing to a group of other lncRNAs as key regulators of cell differentiation, especially during osteogenesis of hMSCs (e.g., MALAT, H19, HOTAIR, MEG3, DANCR), which usually operate through regulation of osteogenic markers or key regulators of the Wnt-signaling pathway (Carrion et al., 2014; Liang et al., 2016; J. Zhang, Hao, Yin, Xu, & Guo, 2019; Zhu & Xu, 2013; Zuo et al., 2013).

7.1.2 LncRNAs and the Wnt-pathway in mesenchymal stem cell differentiation

lncRNA H19, can promote osteogenesis in rat ectomesenchymal stem cells by activating Wnt/β-catenin signaling (Gong, Peng, Yin, & Yang, 2018). A link was also observed between lncRNAs and miRNAs, in particular in the regulation of osteogenesis (Wei, Wei, Zhao, Guo, & Liu, 2017; J. Wu et al., 2018). LincRNA-POIR, for instance, was found to positively regulate osteogenic differentiation of human periodontal mesenchymal stem cells *in vitro* and *in vivo* by acting as a competing endogenous RNA for miR-182, and whose target gene inhibits the canonical Wnt

signaling pathway (L. Wang et al., 2016). Previous reports have also shown that Wnt/β-catenin signaling is regulated during ageing of hMSCs, wherein it is activated through the DNA damage response and p53/p21 pathways (D.-y. Zhang, Wang, & Tan, 2011). In addition, loss of Wnt was found to cause bone-marrow adiposity in pre-osteoblasts by producing more fat cells than osteoblasts (Song et al., 2012), indicating increased expression of Wnt/β-catenin is required for moving the MSC differentiation towards the osteoblast lineage. All these findings further provide support that a combination of Wnt signaling and lncRNA regulation is involved in osteoblast differentiation of mesenchymal stem cells. The only existing publication concerning Gm12606 identified the lncRNA as a downstream target of Wnt/β-catenin signaling in primary dermal fibroblasts (Mullin et al., 2017), but in their study no molecular mechanism was proposed for the possible transcriptional regulation of Gm12606 by direct binding of transcription factors (such as β-catenin) to a lncRNA promotor.

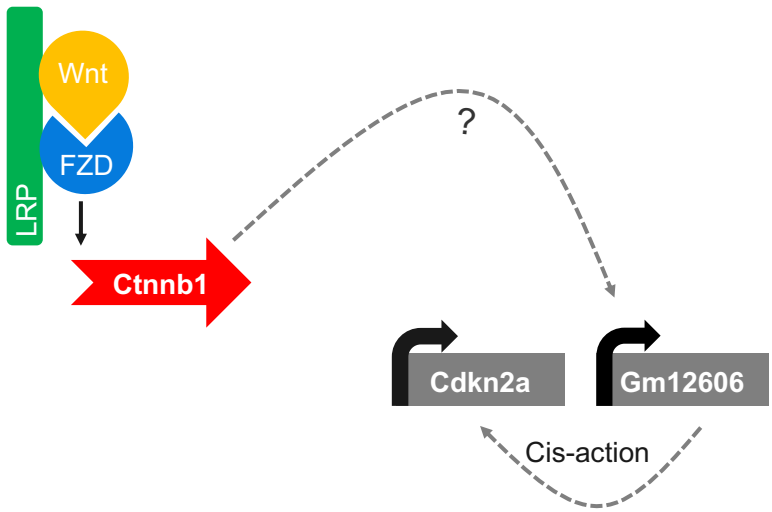

Figure 55: Wnt/β-catenin signaling pathway involving Gm12606. Canonical Wnt/β-catenin signaling is activated in the presence of the ligand Wnt by binding to the receptor frizzled (FZD) and the co-receptor LRP (LDL receptor related protein). This causes Ctnnb1 (encoding β-catenin) to release from its inhibitory complex and localizes to the nucleus, where it may ultimately bind to the promoter of the lincRNA Gm12606 to trigger its transcription. However, the actual regulatory mechanism is currently unknown. Consequently, Gm12606 is able to initiate p16 transcription by *cis*-mediated action.

7.1.3 Gm12606 exhibit different subcellular localization in different mouse cell types

Knowledge of subcellular localization patterns of lncRNAs can provide fundamental insights into potential functions of lncRNA in different cellular compartments. Apart from the strong dependence of Gm12606 expression on the degree of differentiation (**Figure 22**), it was also obvious that in dependence on cell type and cell status, Gm12606 can occupy different subcellular localisations. RNA FISH revealed differences in Gm12606 localization between murine osteosarcoma cells (MOS), pre-osteoblasts (mOB), and mMSC. Interestingly, the intensity of fluorescence signals within the three cell lines and the intracellular localization of Gm12606 also differed. In pre-osteoblasts, fluorescence signals were detected only within the cell nucleus, with apparent cell-to-cell heterogeneity (**Figure 29**). The signals were distributed within the nucleus, exclude the nucleoli and showing 'clumping' that may indicate association with specific nuclear structures such as chromatin attachment domains or nuclear speckles (Moran N. Cabili et al., 2015; Vidisha Tripathi et al., 2010). The patterns we observed were reminiscent of MALAT1 and the localization within specific subnuclear compartments called nuclear speckles, of which there are ~20–30 per nucleus found in HeLa cells (Vidisha Tripathi et al., 2010). MALAT1 interacts with splicing factors within nuclear speckles to regulate the alternative splicing of pre-mRNAs (Vidisha Tripathi et al., 2010), a mechanism that also may fit the function of Gm12606 in mOB, but which remains to be explored. Cabili et al. (2015) characterized the localization of 34 lncRNAs in human cells using the RNA-FISH method and demonstrated that lncRNAs are mostly found simultaneously in the nucleus as well as in the cytoplasm, but remarkably, a large number of lncRNAs are predominantly nuclear and show uniform patterns. This suggest that these localizations correspond to functional categories (Moran N. Cabili et al., 2015), such as epigenetic regulation of transcription of a proximal gene (A. M. Khalil et al., 2009). The frequently observed common patterns for chromatin regulation, as shown for XIST, AIR or ANRIL, are less but bright and tightly localized nuclear foci (Vidisha Tripathi et al., 2010). These were localized to the transcription site itself. However, since the Gm12606 signals in mOB cells are spread rather

diffusely distributed throughout the nucleus, this is inconsistent with the notion that chromatin regulation is present in pre-osteoblasts.

In this study, it was observed that the Gm12606 transcript in mMSCs was apparently restricted to the cytoplasm (**Figure 30**). Moreover, no difference was found in different age groups of 5- and 7-week-old mMSC, but in 3-week-old cells signals were absent altogether. This is well in line with the observation of increased Gm12606 transcript expression in mMSCs with increased passage numbers (**Figure 23**). Cytoplasmic localization of lncRNAs has a major impact on protein production, including protein sequestration (Kino et al., 2010), miRNA activity (J. Wu et al., 2018), and mRNA translation (Carrieri et al., 2012). Previous reports have shown that a number of miRNAs can regulate p16 translation by directly binding p16 mRNA. miRNA-24, for example, inhibits cellular senescence in human diploid fibroblasts by supressing p16 translation (Lal et al., 2008). This demonstrates a possible regulation of p16 by miRNAs, but no such effect has yet been described for lncRNA. In contrast, β-catenin and the transcription factor JUNB are part of a cytoplasmic regulation process involving lincRNA-p21, that also accumulates in the cytoplasm and forms hybrids through complimentary base-paring with CTNNB1 (encoding β-catenin) mRNA and JUNB mRNA, resulting in decreased translation of β-catenin and JUNB (Noh, Kim, McClusky, Abdelmohsen, & Gorospe, 2018; Yoon et al., 2012).

Alternatively, Gm12606 signals in the cytoplasm could indicate an inactive form of lncRNA or molecules that are waiting there for degradation (Carlevaro-Fita, Rahim, Guigó, Vardy, & Johnson, 2016). Another hypothesis could be that Gm12606 transcript is exported to the cytoplasm during stem cell stage, but nuclear Gm12606 levels increase during cell differentiation and/or senescence, positively regulating p16 levels (Shibata et al., 2007). A reverse effect has been observed with the lncRNA MIR31HG, where MIR31HG is exported to the cytoplasm during senescence (Montes et al., 2015), shifting from nuclear localization to the cytoplasm. Detailed investigation on such a mechanism, however, would require the identification of nuclear import or

export signals in the transcript of Gm12606. But it is known that epigenetic modifications of RNA molecules, in particular at their 3'UTR (Meyer et al., 2012), can have an influence on their nuclear, cytoplasmic or ribosomal localization (Frye et al., 2016).

There is also evidence that *cis*-regulatory activity of lncRNA depends on DNA elements within the locus and is independent of the presence of transcribed RNA (Kopp & Mendell, 2018). Nuclear lincRNA-p21, for example, carries novel DNA enhancer elements within the gene body and regulates Cdkn1a/p21 in *cis* even in tissues in which lincRNA-p21 is not expressed (Groff et al., 2016; Kopp & Mendell, 2018). In addition, a recent study by Engreitz et al. (2016) identified five out of 12 (e.g., Bendr, Blustr) lncRNAs in mouse embryonic stem cells which affect the expression of neighbouring genes without requiring the specific lncRNA transcript (Engreitz et al., 2016). Regulation apparently occurred via enhancer-like activity of gene promoters, the process of transcription, or splicing of the transcript itself (Engreitz et al., 2016). With respect to lincRNA-p21 this effect was supported by the short half-life and low copy number of lincRNA-p21 (Dimitrova et al., 2014), which would fit the low expression levels of Gm12606 in this study and argues against a role as a trans-acting lncRNA. However, Dimitrova et al. also showed that knockdown of lincRNA-p21 with ASOs was sufficient to downregulate Cdkn1a in murine fibroblasts, indicating that the transcript is nevertheless required for loco regulatory activity in some context (Kopp & Mendell, 2018).

Stellaris-FISH further revealed that in MOS and mMSCs, transcript abundance was very low in individual cells, with high levels of cell-to-cell heterogeneity. One theory suggests that a small number of cells in the population can express high numbers of lncRNAs (Moran N. Cabili et al., 2015). In this study, this would explain the presence of strong signals in a few cells, while others showed no signals at all. It is also interesting to relate this cell-to-cell heterogeneity with our observations of radiation-induced premature differentiation or replicative senescence (Daniela

Hladik et al., 2019) in mMSCs, both mechanisms also show a non-uniformity among cells of equal passage number and chronologic age.

As reported by a previous study, the two transcripts of the lncRNA CCAT1 have different localizations, with the longer transcript being nuclear while the shorter form is cytoplasmic (Xiang et al., 2014). Since it was not possible to distinguish between Gm12606 T1 and T2 by Stellaris-FISH in this study, it is not certain which of the two transcripts or both were detected. A precise distinction remains open, but the RT-qPCR assays suggest that the foci in mMSCs and mOB represent distinct transcripts.

7.2 Gm12606 expression is elevated during ageing and after irradiation in mouse mesenchymal stem cells

7.2.1 Ageing affects the expression of T1 in mesenchymal stem cells

In concordance with accumulating evidence showing that a variety of lncRNAs are involved in ageing and ageing-related disease (He, Tu, & Liu, 2018), *in vitro* growth of several passages of wild-type mMSCs established that T1 of Gm12606 experienced a ~70-fold upregulation in 7-week-old, compared to 3-week-old MSCs (**Figure 23**). No significant changes were observed in the expression of T2 after 7 weeks, suggesting that both transcripts differ not only in their first exon, but also in their transcriptional activation. Based on the concomitant morphological changes in *in-vitro* aged mMSCs (levels of cell heterogeneity and increased fraction of differentiated cells) (**Figure 22**) during this period, there may be additionally a causal relationship between the level of Gm12606 T1 transcription and the degree of differentiation. It should be noted that premature differentiation is a part of the ageing process of MSCs *in vitro* (Cicero et al., 2016), as cells develop too early into a specialized cell type or move more toward a specific cell type. This is often evidenced by preferential adipogenic rather than osteogenic differentiation in ageing MSCs in

previous reports (Justesen et al., 2001; Moerman, Teng, Lipschitz, & Lecka-Czernik, 2004) and vice versa is also observed in the premature-ageing disease Hutchinson-Gilford Progeria Syndrome (Blondel et al., 2014; Scaffidi & Misteli, 2008). As mentioned earlier, T1 and T2 were upregulated in cells in which osteogenic differentiation of mMSCs was induced, strengthening the differentiation theory but weakening the aspect that T1 is predominantly affected by ageing, whereas T2 might have a different function.

7.2.2 γ-irradiation causes a more pronounced change in T2

Cellular ageing is also known to exert a detrimental effect on the DNA damage response following exposure to ionizing radiation (Sperka, Wang, & Rudolph, 2012). To investigate the acute radiation effect of Gm12606, T1 and T2 expression was examined in mMSCs irradiated with 2 Gy 24h after exposure to γ-irradiation in comparison to sham-irradiated controls. When examining the acute effect of γ-irradiation, a more pronounced change in transcript T2 than in T1 was found (**Figure 24**), confirming different functionalities with respect to both transcripts. Three days later, the radiation-induced upregulation of T1 has completely vanished, before it goes up again 20 days later (**Figure 25**). 4-24-days' time period analysis of Gm12606 (**Figure 25**) has further revealed that irradiation has a potentiating effect on Gm12606 T1 expression in mMSCs and therefore may lead to premature ageing and cellular senescence. This is in agreement with a number of previous findings (Richardson, 2009; Walburg Jr, 1975) and knowledge that γ-and X-irradiation of moderate doses can contribute to cellular and organismal ageing (Aliper, Bozdaganyan, Orekhov, Zhavoronkov, & Osipov, 2019; Alwood et al., 2012; Candéias et al., 2017). It is thus clear that a single exposure to ionizing irradiation, including stem cells, lead to premature ageing, with potential implications for the long-term side effects of a radiotherapy in cancer patients.

In addition, low-dose γ-irradiation has been found to cause spontaneous adipogenic differentiation of primary mMSCs (Yu Wang, Zhu, Wang, & Chen, 2016). Based on the increased expression of Gm12606 in mMSCs after irradiation, this effect may provide further evidence that Gm12606 T2 expression may also be linked to cell differentiation.

7.3 Gm12606 is implicated in the regulation of the Ink4a/Arf/Ink4b locus

To date, the only publication that dealt with expression of the lincRNA Gm12606 has mapped it as a downstream Wnt-effector, but any association with cellular phenotypes were not investigated (Mullin et al., 2017). Since many lincRNA have been found to be *cis*-acting epigenetic regulators of their neighbouring genes (Ulitsky & Bartel, 2013), such as ANRIL, which mediates recruitment of the polycomb repressor complex to the promoters of the neighbouring genes CDKN2B (p15-INK4B) and CDKN2A (p14-ARF, p16-INK4A), thereby regulating cell proliferation and senescence in humans (Yap et al., 2010), the principal *cis*-regulatory pathway has attracted attention in this study. Starting from the proximity (1kb) of p16 to Gm12606, the goal was to investigate a possible regulatory interaction targeting this cell-cycle inhibitor. p16 was frequently found to be increased in mammalian ageing (Melk et al., 2004) and especially during senescence of murine and human cell types (Mirzayans et al., 2012), e.g., fibroblasts (Alcorta et al., 1996), islets (Halvorsen, Beattie, Lopez, Hayek, & Levine, 2000), keratinocytes (Kiyono et al., 1998), endothelial cells (J. Chen et al., 2006), macrophages (Randle, Zindy, Sherr, & Roussel, 2001), and even hMSCs (Feng et al., 2014). Using an antisense oligonucleotide-mediated silencing of Gm12606 in mMSCs, a significant reduction of p16 transcription was shown (**Figure 33**), which is in line with the hypothesis of the Ink4a gene being a target of Gm12606 regulation. This implies that the knockdown effect of Gm12606 on p16 is most likely triggered by the downregulation of

Gm12606 levels and not by the application and its chemicals themselves, as such an effect would occur earlier. Moreover, the finding showed that not only p16, but the entire Ink4a/Arf/Ink4b locus was affected by Gm12606 knockdown (**Figure 33**). This is akin to the effects attributed to the lncRNA ANRIL, located at a position in the human INK4A/ARF/INK4B complex (Nikolay Popov & Jesús Gil, 2010), however ANRIL represses the expression of INK4A, ARF, and INK4B genes (N. Popov & J. Gil, 2010).

In general, Gm12606 is expressed at very low levels as measured by RT-qPCR, which tends to favour a *cis* mechanism. This conclusion is further supported by the finding that many lncRNA in the nucleus, especially in the chromatin fraction, are localized at their transcriptional sites, with low expression levels, but where they play regulatory roles in *cis*, specifically widespread roles in chromatin regulation (Gil & Ulitsky, 2019). Their enrichment in chromatin correlates with the transcriptional activity of neighbouring genes (M. S. Werner & A. J. Ruthenburg, 2015), as shown in particular for XIST, GAS5, MIAT, MEG3, which are enriched in in the nucleus, consistent with a role in transcription or chromatin regulation (Derrien et al., 2012). Transport of low-level transcripts to other nuclear compartments may dilute the transcripts too much to mediate plausible function in *trans* (Gil & Ulitsky, 2019). Furthermore, it should be considered that the probability of a transcript present in only a few copies in the nucleus could find a matching DNA target sequence anywhere in the genome, is extremely low.

However, genes on distal loci, namely Klf4, Rb1, p27 and Dkk2 were also affected by Gm12606 knockdown, but at a much low level than the genes in direct vicinity (**Figure 34**). Impaired Rb1 transcription was observed 24h following ASO transfection, while p27 was downregulated at the later time point (48h). It is possible to speculate that this might be an indirect effect that is mediated by the Ink4/Rb1/E2F pathway, for example, as p16 and even p15 are involved in Rb1 targeting via CDK4/6 and cyclinD (Serrano et al., 1993). However, the delayed (after 48h) reduced expression of the Ink4a/Arf/Ink4b cluster, in correlation with decreased Rb1 expression only after

24h, suggest an alternative regulation involving Gm12606 leading to Rb1 suppression. Although inactivation of p16 is the most effective mechanism found to block the cyclinD-Rb1 pathway during invasive cancer progression (Nuovo, Plaia, Belinsky, Baylin, & Herman, 1999), evidence suggests that 10% of small cell lung cancers retain wildtype RB function while p16 is inactivated (Kaye, 2002), further raising the possibility for alternative Ink4-dependant pathways that bypass Rb1. Another would be the CDK2/cyclinE/p27 pathway, which also involves a cell proliferation suppressor function by inducing a G1 arrest. The resulting suppression of CDK4/6 and cyclinD, mediated by the induction of p16, simultaneously releases p27, leading to suppressed CDK2/cyclinE complex activity (H. Jiang, Chou, & Zhu, 1998). More precisely, reduced p16 transcription is then closely related to functional inactivation of p27, which may have been shown here at 48h after ASO transfection, since a similar mechanism has already been confirmed by others (Matsuda et al., 2003). At 24h and 48h after downregulation of Gm12606, the transcription factor Klf4 was significantly upregulated, while Dkk2 expression was reduced. Klf4 induces growth arrest in several cell types, especially following DNA damage (X. Chen et al., 2001) by increasing expression of cell cycle genes, e.g., p21, cyclinD (Ghaleb & Yang, 2017), as well as p16 and p27 (Tiwari et al., 2019). Thus, overexpression of Klf4 was found to be related to cell senescence in human epithelial cells, via a p21 mediated mechanism (Xu et al., 2016). This effect argues here against the p16 theory but strengthens the hypothesis of premature cell senescence after loss of Gm12606 in mMSCs, which could be induced by accumulation of several factors, including *trans*-regulation by Gm12606. In addition, the strong significant decrease of DKK2 (a negative regulator of the Wnt/β-catenin signalling pathway) already 24h after Gm12606 knockdown considered a regulatory effect linked to Gm12606 in *trans*. As Wnt/β-catenin keeps hMSCs in a self-renewing and undifferentiated state (Etheridge, Spencer, Heath, & Genever, 2004), DKK2 reverses this effect by inhibiting the Wnt coreceptors Lrp5 and 6 (Niehrs, 2006). Like any other knockdown technology, the Gm12606 GapmeR ASO method is also limited in its transient effects. Whereas

direct effects onto gene-expression could be nicely demonstrated, long-term consequences for the stem cell function requires a permanent reduction of the lincRNA Gm12606 expression.

Therefore, a source of Gm12606-1$^{-/-}$ mMSCs was generated by CRISPR/Cas9-mediated gene editing in a C57/BL6 mouse line. This line was used as a source of BM mMSCs with a homozygous Gm12606-exon1 deletion. In comparison with Gm12606 wild-type littermates from heterozygote intercross, the mRNA levels of p16, p19, and p15 were strongly reduced in ageing mutated mMSCs (p7) by 68 % (p16), 77% (p19) and 65% (p15) (**Figure 46**). While expression from the Ink4a/Arf/Ink4b locus was indeed slightly diminished in the mutant-mMSCs from passage 3, the effect was only significant in the ageing mMSCs from passage 7, which also agrees with the findings that Gm12606 is dramatically increased in ageing mMSCs (**Figure 23**). Interestingly, CDKN2A-Arf (p19) transcription compared to CDKN2A-Ink4a (p16) and CDKN2B-Ink4b (p15) levels, were most strongly reduced in the mMSCs from Gm12606-exon1 depleted mice (**Figure 46**), suggesting that the three transcripts at the Ink4a/Arf/Ink4b locus are differentially affected by Gm12606. Previous studies have already noted that there is an inconsistency between Ink4a and Arf of cell ageing among mice and humans. The general impression is that p16 is the main initiator of senescence and tumour suppression in human cells, while p19 is more prominent in mouse cells (Jesús Gil & Gordon Peters, 2006). This may explain the slightly more reduced expression of p19 expression compared to transcription levels of p16. Assuming that the Gm12606 transcript indeed causes a specific loop folding of the adjacent chromatin, it is reasonable to imagine that this folding changes the proximity of the three Ink4a/Arf/Ink4b promoters to enhancer elements in a different manner.

These results suggest that Gm12606 controls a locus, containing three closely related tumour suppressor genes that trigger antiproliferative activities of pRB and p53 (C. J. Sherr, 2001). Accordingly, downregulation of the genes would initiate the activation of pRB and p53 and provide mMSCs with an increased proliferative potential. In summary, the two different methods used to

suppress Gm12606 transcription (GapmeR ASO knockdown and CRISPR/Cas9 deletion) confirm that the main regulatory effect onto the nearby Ink4a/Arf/Ink4b locus is exerted by the transcript and does not require changes in the DNA.

7.4 Loss of Gm12606 prevents the progression of cellular senescence in ageing mMSCs

Ageing influences the behaviour of MSCs in different ways, depending on several factors, but senescence is the most common physiological status associated with accelerated ageing. MSCs enter senescence *in vitro* earlier than *in vivo* because high *ex vivo* expansion requires the production of a suitable number of MSCs (Bernardo et al., 2011). However, this reduces the DNA synthesis and repair efficiency of MSCs, leading to accumulation of DNA damage (Bonab et al., 2006; Cai et al., 2014; Neri, 2019) and is a major drawback in terms of clinical application. Therefore, MSCs are confronted with radical changes in their physiological and chemical milieu (Stenderup, Justesen, Clausen, & Kassem, 2003), resulting in loss of stem cell properties, senescence and even malignant transformation (Røsland et al., 2009; W. Wagner, Ho, & Zenke, 2010). Previous studies already have questioned the ability to decelerate the ageing effect during *ex vivo* expansion of MSCs to improve therapeutic efficacy and ensure safe treatment (Y. Li et al., 2017). One strategy might be to prevent senescence by interfering in senescence-associated regulatory mechanism. Since p16, p19 and p15 play critical roles in cellular senescence and ageing (Krishnamurthy et al., 2004; Kuilman, Michaloglou, Mooi, & Peeper, 2010; A. S. Wang & Dreesen, 2018), downregulation of the genes may stop accelerated ageing and senescence in mMSCs. However, all three genes/proteins also have tumor suppressor functions. They are frequently found mutated (with deletions or silenced) in a variety of tumor (Charles J. Sherr, 2000), including leukaemia (Eischen, Weber, Roussel, Sherr, & Cleveland, 1999), lymphoma (Schmitt,

McCurrach, de Stanchina, Wallace-Brodeur, & Lowe, 1999), or melanoma (Kamb et al., 1994). Therefore, it is not advised to intervene in the genome of cells that are to be used therapeutically. If instead a regulatory mechanism involving a lncRNA (Gm12606 in mouse or ANRIL in human) could transiently downregulate INK4A/ARF/INK4B (e.g., by ASO) to slow MSC ageing *ex vivo* prior therapy, this would be relatively risk-free.

In line with the hypothesis, there was a highly significant decrease of homozygous Gm12606-exon1 mutant mMSCs undergoing senescence. The results are in agreement with the downregulation of the Ink4a/Arf/Ink4b locus as a consequence of the Gm12606 deletion (**Figure 50**). Consequently, this suggests that Gm12606 (T1) is involved in the regulation of the Ink4a/Arf/Ink4b locus, which in turn affects the ageing process by slowing down the induction of senescence in ageing mMSCs.

7.5 Loss of Gm12606 renders mMSCs more efficient for the repair of IR induced DNA double strand breaks

The ability of MSCs to regenerate tissue diminishes with age and leads to cellular senescence, resulting in permanent cell cycle arrest and accumulation of DNA damage (Yu & Kang, 2013). In addition, the trigger of DNA damage is the formation of free radical (ROS) and the consequent oxidative stress induced by IR, and on the other hand DNA-DSBs, which occur due to radiation exposure (W. Kim et al., 2019). All these effects are the basis of senescence. Considering the above aspects in accordance to p16 (Ink4a) that increases with age and is associated with senescence in MSCs (Cheng et al., 2011), a strategy that improves the DNA damage response by enhancing the DNA repair capacity, could be an efficient strategy to counteract the ageing effect. Just like other identified lncRNAs involved in the DDR after exposure to IR (Hung et al.,

2011; O'Leary et al., 2015; Özgür et al., 2013; Wu et al., 2014), in this study as already described, Gm12606 has been shown to be affected by radiation exposure (**Figure 24)**.

Then, the effect of reduced Gm12606 expression was analysed as the level of DNA damage recognition in Gm12606-exon1 mutant and wild-type mMSCs treated with IR. This demonstrated that the loss of Gm12606-exon1 contributed to an increased γH2AX and 53BP1 repair foci formation, especially after high doses (4Gy) in mMSCs (**Figure 52**), indicating a more efficient recognition of DNA-DSBs. For further evaluation of the findings and validation, repair kinetic analysis was performed. Clearly, it could be shown that after 24h following radiation exposure significant fewer foci remain unrepaired in mMSCs of Gm12606-exon1 deficient mice (**Figure 54**). The exact reason for the reduced number of remaining DNA-foci may have arisen from two possibilities regarding fast and slow repair kinetics. Previous studies described a biphasic progression of DNA damage repair kinetics dominated by an initial fast component and later gradual (slow) repair of DNA-DSBs (Iliakis et al., 2004). Here, it is quite obvious that the first phase of fast repair occurs initially between 0-6h removing DNA-DSBs, followed by the second phase of slow repair which occurs between 6-24h (**Figure 56**). With this interpretation, it can be concluded either that the kinetics of the fast components are the same for homozygous mMSCs from Gm12606-exon1 mutant and wild-type mice, while Gm12606-exon1 mutant mMSCs showed improved repair of DNA-DSBs in the second phase since more foci disappeared (**Figure 56A**) or indicate that Gm12606-exon1 KO mMSCs have an increased repair rate in the first phase since the fast component lasts longer (**Figure 56B**). The latter is more likely as cell heterogeneity changes after Gm12606/Ink4a/Arf/Ink4b decrease, consequently more or less cells are in different cell cycle phases (G0, G1, G2), and thus the use of the different repair pathways (non-homologous end-joining (NHEJ)/ homology directed repair (HR)) also shifts. In terms of kinetics, with only four time points, it is not possible to distinguish whether the slow component has altered or whether the relative proportions of the fast/slow component have changed.

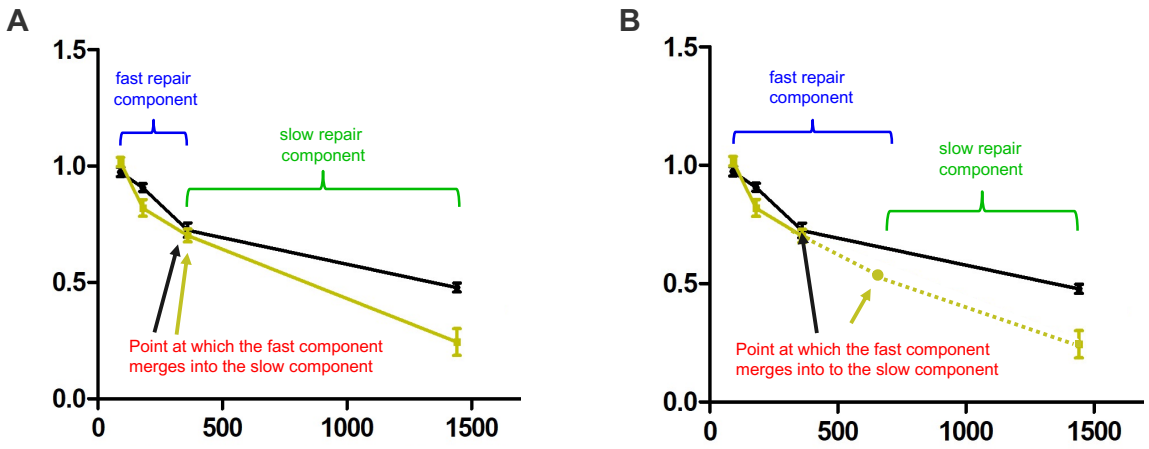

Figure 56: Theories of increased repair kinetics in mMSCs after KO of Gm12606 T1. Representation of two possibilities regarding biphasic repair progression of DNA-DSBs by fast (blue) and slow (green) repair kinetics. The first phase of fast repair is shown between 0-6h, followed by the second phase of slow repair which occurs between 6-24h. (**A**) Proportions of DNA breaks repaired by the fast component are the same for homozygous mMSCs from Gm12606-exon1 mut (yellow) and wt (black) mice, while Gm12606-1 mutant mMSCs showed an improved repair in the second phase (slow component). (**B**) Proportion of DNA breaks repaired by the fast component of Gm12606-exon1 mut mMSCs (yellow) is higher than in mMSCs from wt littermates (black), since the fast component lasts longer.

Moreover, it has been previously shown by others that mice lacking p16 exhibit increased regeneration and repair potential in ageing mice associated with a reduced decline of bone-marrow stem cells, herby mitigating the physiological effects of ageing on stem cells by enhancing injury repair in aged tissue (Janzen et al., 2006). Taken together, this underpins that better and more complete removal of DNA-DSBs has been demonstrated in mutant Gm12606-exon1$^{-/-}$ mMSCs.

A previous study of our group showed an age-related decline in the recognition of radiation induced DSBs and a retarded DNA damage repair, indicating possible accumulating errors in the damage response machinery with cumulative ageing in mMSCs (D. Hladik et al., 2019). The loss of Gm12606 functionality and consequent stagnation of the ageing process may counteract this effect, preventing the accumulation of DNA damage, leading to malignant transformation.

It is most likely that the positive effect of Gm12606 knockout on DNA-DSB repair is indirectly mediated by the reduced level of cellular senescence, rather than by a direct link between this lncRNA and the activity of DNA repair enzymes as senescent cells may lose their DNA repair capacity (Collin, Huna, Warnier, Flaman, & Bernard, 2018; d'Adda di Fagagna, 2008; S. Maynard, E. F. Fang, M. Scheibye-Knudsen, D. L. Croteau, & V. A. Bohr, 2015). However, the effect of Gm12606 knockout on senescence was not as advanced in the younger cells from passage 3.

7.6 Conclusion

Numerous concerns arise with advancing age of MSCs as their long-lasting expandability is indispensable for their therapeutic application. Irradiation and ageing of the cells may accelerate the decay of stem cell potentials and properties, leading to premature differentiation and reduced DNA repair capacities, which eventually induces cellular senescence.

Thus, in this project we compiled the current knowledge about the potential role of the lincRNA Gm12606 in age-related mMSCs. It was demonstrated that bone-marrow derived mMSCs from wild-type mice showed a dramatic increase in the expression of T1 of the lincRNA Gm12606 during *in vitro* ageing of the cells, whereas transient overexpression of T2 was observed after γ-irradiation. This indicates different functionalities with respect to both transcripts. Beyond that, Gm12606 RNA expression exhibited a strong dependence on cell type and intracellular localization. Overall, expression was highest in committed osteoblast precursor cells *in vitro*, whereas expression was reduced in mMSCs, MOS and undetectable in embryonic stem cells. This suggests that there is a general trend towards higher expression of Gm12606 T1 in cells that have a more limited lifespan *in vitro* or are already closer to the end of their normal lifespan. The significant differences in the overall expression between mMSCs, mOB and MOS were counterbalanced by a very strong specificity of intracellular localization of Gm12606 RNA.

Whether the different staining pattern of Gm12606 RNA (nuclear vs. cytoplasmic, diffuse vs. focal spotted) reflects differences in function remains an open hypothesis. Both, Gm12606 knockdown *in vitro* and CRISPR/Cas9-mediated Gm12606 (T1) knockout *in vivo* strongly affected transcription of the nearby Ink4a/Arf/Ink4b locus, suggesting a *cis* action. Consequently, bone-marrow derived mMSCs from Gm12606-exon1-deficient mutant mice retained a significantly lower percentage of cellular senescence with increasing passage number than cells from wild-type littermates, indicating a downstream effect of Gm12606 T1 inactivation on CDKN2A-Ink4a (p16), CDKN2B-Ink4b (p15), and CDKN2A-Arf (p19) transcription. In early passages of mMSCs, the loss of Gm12606-exon1 also contributed a more efficient recognition of DNA-double strand breaks and a better and more complete removal of the latter. Taken together, these data suggest that the functional impairments in mMSCs observed during *ex vivo* expansion and after irradiation are closely related to the function of Gm12606, which epigenetically regulates the adjacent Ink4a/Arf/Ink4b locus during stem cell development and differentiation.

Illustrating the role of Gm12606, a lincRNA was found in mouse that slows down or even reverses the ageing effect of mMSCs *in vitro* and that could have direct relevance for human cells and open up new possibilities for effective and safe patient treatment. Finally, it should be noted that a closer look at the genome reveals that many biological important genes are accompanied by proximal lncRNAs whose function is not yet clarified. While their crucial existence is now undisputed, it is apparent that they will continue to surprise and reveal many kinds of complex mechanisms in the future.

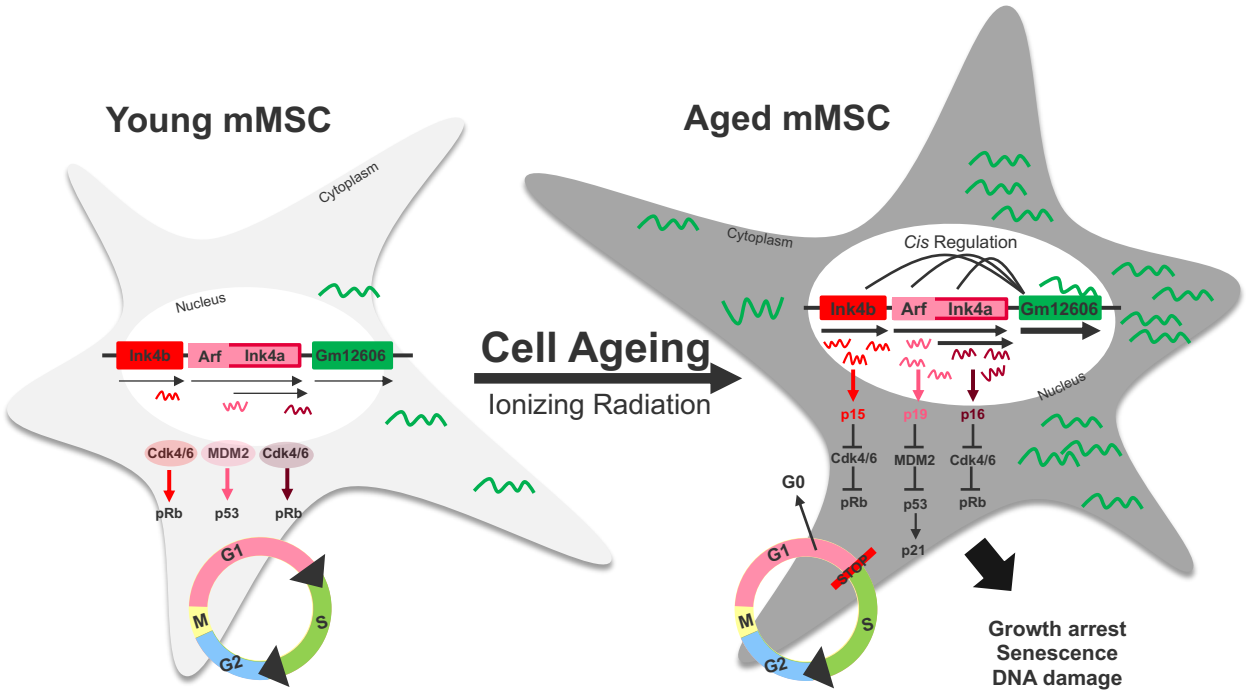

Figure 57: Simplified representation of young and aged murine mesenchymal stem cells and Gm12606 functionality following cell ageing and/or ionizing radiation. The signaling pathways p16-pRb, p19-p53 and p15-pRb mediate the stress response (ageing & IR) in mMSCs through the epigenetic regulation of Gm12606. Increased expression of Gm12606 in aged mMSCs and/or IR leads to epigenetic cis regulation of the Ink4a/Arf/Ink4b locus, resulting in enhanced levels of p16, p19 and p15 mRNA and proteins. p16 and p15 inhibit Cdk4/6 activity and induce Rb phosphorylation, causing cell cycle arrest. p19 prevents MDM2-mediated degradation of p53, activating p21, a Cdk inhibitor. In summary, this stops the cell cycle by blocking the G1 to S transition, which in turn triggers growth arrest, senescence, and DNA damage.

II. References

Abdelmohsen, K., & Gorospe, M. (2015). Noncoding RNA control of cellular senescence. *Wiley Interdisciplinary Reviews: RNA, 6*(6), 615-629.

Abdelmohsen, K., Panda, A., Kang, M.-J., Xu, J., Selimyan, R., Yoon, J.-H., . . . Gorospe, M. (2013). Senescence-associated lncRNAs: senescence-associated long noncoding RNAs. *Aging Cell, 12*(5), 890-900. doi:10.1111/acel.12115

Abdelmohsen, K., Panda, A., Kang, M. J., Xu, J., Selimyan, R., Yoon, J. H., . . . Becker, K. G. (2013). Senescence‐associated l nc RNA s: senescence‐associated long noncoding RNA s. *Aging Cell, 12*(5), 890-900.

Alcorta, D. A., Xiong, Y., Phelps, D., Hannon, G., Beach, D., & Barrett, J. C. (1996). Involvement of the cyclin-dependent kinase inhibitor p16 (INK4a) in replicative senescence of normal human fibroblasts. *Proceedings of the National Academy of Sciences, 93*(24), 13742-13747.

Alessio, N., Del Gaudio, S., Capasso, S., Di Bernardo, G., Cappabianca, S., Cipollaro, M., . . . Galderisi, U. (2015). Low dose radiation induced senescence of human mesenchymal stromal cells and impaired the autophagy process. *Oncotarget, 6*(10), 8155.

Aliper, A. M., Bozdaganyan, M. E., Orekhov, P. S., Zhavoronkov, A., & Osipov, A. N. (2019). Replicative and radiation-induced aging: a comparison of gene expression profiles. *Aging (Albany NY), 11*(8), 2378-2387. doi:10.18632/aging.101921

Alipoor, F. J., Asadi, M. H., & Torkzadeh-Mahani, M. (2018). MIAT lncRNA is overexpressed in breast cancer and its inhibition triggers senescence and G1 arrest in MCF7 cell line. *J Cell Biochem, 119*(8), 6470-6481. doi:10.1002/jcb.26678

Alwood, J. S., Kumar, A., Tran, L. H., Wang, A., Limoli, C. L., & Globus, R. K. (2012). Low-dose, ionizing radiation and age-related changes in skeletal microarchitecture. *J Aging Res, 2012*, 481983. doi:10.1155/2012/481983

Amort, T., Rieder, D., Wille, A., Khokhlova-Cubberley, D., Riml, C., Trixl, L., . . . Lusser, A. (2017). Distinct 5-methylcytosine profiles in poly(A) RNA from mouse embryonic stem cells and brain. *Genome Biol, 18*(1), 1. doi:10.1186/s13059-016-1139-1

Baker, D. J., Wijshake, T., Tchkonia, T., LeBrasseur, N. K., Childs, B. G., van de Sluis, B., . . . van Deursen, J. M. (2011). Clearance of p16Ink4a-positive senescent cells delays ageing-associated disorders. *Nature, 479*(7372), 232-236. doi:10.1038/nature10600

Barcellos-Hoff, M. H., Park, C., & Wright, E. G. (2005). Radiation and the microenvironment–tumorigenesis and therapy. *Nature Reviews Cancer, 5*(11), 867-875.

Barja, G. (2003). Mammalian and bird aging, oxygen radicals, and restricted feeding (Vol. 3, pp. 173-189).

Bartel, D. P. (2004). MicroRNAs: genomics, biogenesis, mechanism, and function. *Cell, 116*(2), 281-297.

Batista, P. J., & Chang, H. Y. (2013). Long noncoding RNAs: cellular address codes in development and disease. *Cell, 152*(6), 1298-1307. doi:10.1016/j.cell.2013.02.012

Baxter, M. A., Wynn, R. F., Jowitt, S. N., Wraith, J. E., Fairbairn, L. J., & Bellantuono, I. (2004). Study of telomere length reveals rapid aging of human marrow stromal cells following in vitro expansion. *Stem Cells, 22*(5), 675-682. doi:10.1634/stemcells.22-5-675

Bellantuono, I., Sanguinetti, G., & Keith, W. N. (2012). Progeroid syndromes: models for stem cell aging? *Biogerontology, 13*(1), 63-75. doi:10.1007/s10522-011-9347-2

Bernardo, M. E., Cometa, A. M., Pagliara, D., Vinti, L., Rossi, F., Cristantielli, R., . . . Locatelli, F. (2011). Ex vivo expansion of mesenchymal stromal cells. *Best Practice & Research Clinical Haematology, 24*(1), 73-81.

Bernstein, H. D., Zopf, D., Freymann, D. M., & Walter, P. (1993). Functional substitution of the signal recognition particle 54-kDa subunit by its Escherichia coli homolog. *Proc Natl Acad Sci U S A, 90*(11), 5229-5233. doi:10.1073/pnas.90.11.5229

Bertone, P., Stolc, V., Royce, T. E., Rozowsky, J. S., Urban, A. E., Zhu, X., . . . Snyder, M. (2004). Global Identification of Human Transcribed Sequences with Genome Tiling Arrays. *Science, 306*(5705), 2242-2246. doi:10.1126/science.1103388

Birney, E., Stamatoyannopoulos, J. A., Dutta, A., Guigo, R., Gingeras, T. R., Margulies, E. H., . . . de Jong, P. J. (2007). Identification and analysis of functional elements in 1% of the human genome by the ENCODE pilot project. *Nature, 447*(7146), 799-816. doi:10.1038/nature05874

Blondel, S., Jaskowiak, A. L., Egesipe, A. L., Le Corf, A., Navarro, C., Cordette, V., . . . Nissan, X. (2014). Induced pluripotent stem cells reveal functional differences between drugs currently investigated in patients with hutchinson-gilford progeria syndrome. *Stem Cells Transl Med, 3*(4), 510-519. doi:10.5966/sctm.2013-0168

Bonab, M. M., Alimoghaddam, K., Talebian, F., Ghaffari, S. H., Ghavamzadeh, A., & Nikbin, B. (2006). Aging of mesenchymal stem cell in vitro. *BMC cell biology, 7*(1), 14. doi:10.1186/1471-2121-7-14

Bond, C. S., & Fox, A. H. (2009). Paraspeckles: nuclear bodies built on long noncoding RNA. *The Journal of cell biology, 186*(5), 637-644. doi:10.1083/jcb.200906113

Brenner, D. J., & Hall, E. J. (2007). Computed tomography—an increasing source of radiation exposure. *New England Journal of Medicine, 357*(22), 2277-2284.

Cabili, M. N., Dunagin, M. C., McClanahan, P. D., Biaesch, A., Padovan-Merhar, O., Regev, A., . . . Raj, A. (2015). Localization and abundance analysis of human lncRNAs at single-cell and single-molecule resolution. *Genome Biol, 16*(1), 20-20. doi:10.1186/s13059-015-0586-4

Cabili, M. N., Trapnell, C., Goff, L., Koziol, M., Tazon-Vega, B., Regev, A., & Rinn, J. L. (2011). Integrative annotation of human large intergenic noncoding RNAs reveals global properties and specific subclasses. *Genes Dev, 25*(18), 1915-1927.

Cai, J., Miao, X., Li, Y., Smith, C., Tsang, K., Cheng, L., & Wang, Q. F. (2014). Whole-genome sequencing identifies genetic variances in culture-expanded human mesenchymal stem cells. *Stem Cell Reports, 3*(2), 227-233. doi:10.1016/j.stemcr.2014.05.019

Campisi, J., & Di Fagagna, F. D. A. (2007). Cellular senescence: when bad things happen to good cells. *Nature reviews Molecular cell biology, 8*(9), 729-740.

Candéias, S. M., Mika, J., Finnon, P., Verbiest, T., Finnon, R., Brown, N., . . . Badie, C. (2017). Low-dose radiation accelerates aging of the T-cell receptor repertoire in CBA/Ca mice. *Cell Mol Life Sci, 74*(23), 4339-4351. doi:10.1007/s00018-017-2581-2

Cao, X., & Chen, D. (2005). The BMP signaling and in vivo bone formation. *Gene, 357*(1), 1-8.

Caplan, A. I. (1991). Mesenchymal stem cells. *J Orthop Res, 9*(5), 641-650. doi:10.1002/jor.1100090504

Caplan, A. I. (2017). New MSC: MSCs as pericytes are Sentinels and gatekeepers. *J Orthop Res, 35*(6), 1151-1159. doi:10.1002/jor.23560

Carlevaro-Fita, J., Rahim, A., Guigó, R., Vardy, L. A., & Johnson, R. (2016). Cytoplasmic long noncoding RNAs are frequently bound to and degraded at ribosomes in human cells. *RNA (New York, N.Y.), 22*(6), 867-882. doi:10.1261/rna.053561.115

Carrieri, C., Cimatti, L., Biagioli, M., Beugnet, A., Zucchelli, S., Fedele, S., . . . Gustincich, S. (2012). Long non-coding antisense RNA controls Uchl1 translation through an embedded SINEB2 repeat. *Nature, 491*(7424), 454-457. doi:10.1038/nature11508

Carrion, K., Dyo, J., Patel, V., Sasik, R., Mohamed, S. A., Hardiman, G., & Nigam, V. (2014). The long non-coding HOTAIR is modulated by cyclic stretch and WNT/β-CATENIN in human aortic valve cells and is a novel repressor of calcification genes. *PLoS One, 9*(5), e96577.

Cerase, A., Pintacuda, G., Tattermusch, A., & Avner, P. (2015). Xist localization and function: new insights from multiple levels. *Genome Biol, 16*(1), 166.

Chen, J., Huang, X., Halicka, D., Brodsky, S., Avram, A., Eskander, J., . . . Goligorsky, M. S. (2006). Contribution of p16INK4a and p21CIP1 pathways to induction of premature senescence of human endothelial cells: permissive role of p53. *Am J Physiol Heart Circ Physiol, 290*(4), H1575-1586. doi:10.1152/ajpheart.00364.2005

Chen, L.-B., Jiang, X.-B., & Yang, L. (2004). Differentiation of rat marrow mesenchymal stem cells into pancreatic islet beta-cells. *World journal of gastroenterology: WJG, 10*(20), 3016.

Chen, M.-F., Lin, C.-T., Chen, W.-C., Yang, C.-T., Chen, C.-C., Liao, S.-K., . . . Lee, K.-D. (2006). The sensitivity of human mesenchymal stem cells to ionizing radiation. *International Journal of Radiation Oncology* Biology* Physics, 66*(1), 244-253.

Chen, X., Johns, D. C., Geiman, D. E., Marban, E., Dang, D. T., Hamlin, G., . . . Yang, V. W. (2001). Krüppel-like factor 4 (gut-enriched Krüppel-like factor) inhibits cell proliferation by blocking G1/S progression of the cell cycle. *Journal of Biological Chemistry, 276*(32), 30423-30428.

Cheng, H., Qiu, L., Ma, J., Zhang, H., Cheng, M., Li, W., . . . Liu, K. (2011). Replicative senescence of human bone marrow and umbilical cord derived mesenchymal stem cells and their differentiation to adipocytes and osteoblasts. *Mol Biol Rep, 38*(8), 5161-5168. doi:10.1007/s11033-010-0665-2

Choudhuri, S. (2010). Small noncoding RNAs: biogenesis, function, and emerging significance in toxicology. *Journal of biochemical and molecular toxicology, 24*(3), 195-216.

Cicero, A. L., Jaskowiak, A.-L., Egesipe, A.-L., Tournois, J., Brinon, B., Pitrez, P. R., . . . Nissan, X. (2016). A High Throughput Phenotypic Screening reveals compounds that counteract premature osteogenic differentiation of HGPS iPS-derived mesenchymal stem cells. *Sci Rep, 6*(1), 1-11.

Collin, G., Huna, A., Warnier, M., Flaman, J.-M., & Bernard, D. (2018). Transcriptional repression of DNA repair genes is a hallmark and a cause of cellular senescence. *Cell death & disease, 9*(3), 1-14.

Congrains, A., Kamide, K., Ohishi, M., & Rakugi, H. (2013). ANRIL: molecular mechanisms and implications in human health. *Int J Mol Sci, 14*(1), 1278-1292. doi:10.3390/ijms14011278

Consortium, E. P. (2007). Identification and analysis of functional elements in 1% of the human genome by the ENCODE pilot project. *Nature, 447*(7146), 799.

Consortium, E. P. (2012). An integrated encyclopedia of DNA elements in the human genome. *Nature, 489*(7414), 57-74.

Corcione, A., Benvenuto, F., Ferretti, E., Giunti, D., Cappiello, V., Cazzanti, F., . . . Pistoia, V. (2006). Human mesenchymal stem cells modulate B-cell functions. *Blood, 107*(1), 367-372.

Costa, F. F. (2010). Non-coding RNAs: Meet thy masters. *Bioessays, 32*(7), 599-608. doi:10.1002/bies.200900112

Costa, M. C., Leitão, A. L., & Enguita, F. J. (2012). Biogenesis and mechanism of action of small non-coding RNAs: insights from the point of view of structural biology. *Int J Mol Sci, 13*(8), 10268-10295.

Cox, D. N., Chao, A., Baker, J., Chang, L., Qiao, D., & Lin, H. (1998). A novel class of evolutionarily conserved genes defined by piwi are essential for stem cell self-renewal. *Genes Dev, 12*(23), 3715-3727.

d'Adda di Fagagna, F. (2008). Living on a break: cellular senescence as a DNA-damage response. *Nat Rev Cancer, 8*(7), 512-522. doi:10.1038/nrc2440

Davidovich, C., & Cech, T. R. (2015). The recruitment of chromatin modifiers by long noncoding RNAs: lessons from PRC2. *RNA (New York, N.Y.), 21*(12), 2007-2022. doi:10.1261/rna.053918.115

Day, T. F., Guo, X., Garrett-Beal, L., & Yang, Y. (2005). Wnt/β-catenin signaling in mesenchymal progenitors controls osteoblast and chondrocyte differentiation during vertebrate skeletogenesis. *Developmental cell, 8*(5), 739-750.

De Becker, A., & Van Riet, I. (2016). Homing and migration of mesenchymal stromal cells: how to improve the efficacy of cell therapy? *World journal of stem cells, 8*(3), 73.

de Lange, T. (2005). Shelterin: the protein complex that shapes and safeguards human telomeres. *Genes Dev, 19*(18), 2100-2110. doi:10.1101/gad.1346005

Deng, W., Obrocka, M., Fischer, I., & Prockop, D. J. (2001). In vitro differentiation of human marrow stromal cells into early progenitors of neural cells by conditions that increase intracellular cyclic AMP. *Biochemical and biophysical research communications, 282*(1), 148-152.

Derrien, T., Johnson, R., Bussotti, G., Tanzer, A., Djebali, S., Tilgner, H., . . . Knowles, D. G. (2012). The GENCODE v7 catalog of human long noncoding RNAs: analysis of their gene structure, evolution, and expression. *Genome research, 22*(9), 1775-1789.

Desouky, O., Ding, N., & Zhou, G. (2015). Targeted and non-targeted effects of ionizing radiation. *Journal of Radiation Research and Applied Sciences, 8*(2), 247-254.

Di Ianni, M., Del Papa, B., De Ioanni, M., Moretti, L., Bonifacio, E., Cecchini, D., . . . Tabilio, A. (2008). Mesenchymal cells recruit and regulate T regulatory cells. *Experimental hematology, 36*(3), 309-318.

DiGirolamo, C. M., Stokes, D., Colter, D., Phinney, D. G., Class, R., & Prockop, D. J. (1999). Propagation and senescence of human marrow stromal cells in culture: a simple colony‐forming assay identifies samples with the greatest potential to propagate and differentiate. *British journal of haematology, 107*(2), 275-281.

Dikomey, E., Brammer, I., Johansen, J., Bentzen, S. M., & Overgaard, J. (2000). Relationship between DNA double-strand breaks, cell killing, and fibrosis studied in confluent skin fibroblasts derived from breast cancer patients. *Int J Radiat Oncol Biol Phys, 46*(2), 481-490. doi:10.1016/s0360-3016(99)00335-1

Dikomey, E., Dahm-Daphi, J., Brammer, I., Martensen, R., & Kaina, B. (1998). Correlation between cellular radiosensitivity and non-repaired double-strand breaks studied in nine mammalian cell lines. *Int J Radiat Biol, 73*(3), 269-278. doi:10.1080/095530098142365

Dimitrova, N., Zamudio, J. R., Jong, R. M., Soukup, D., Resnick, R., Sarma, K., . . . Sharp, P. A. (2014). LincRNA-p21 activates p21 in cis to promote Polycomb target gene expression and to enforce the G1/S checkpoint. *Mol Cell, 54*(5), 777-790.

Dimov, I., & Maduro, M. F. (2019). The C. elegans intestine: organogenesis, digestion, and physiology. *Cell and Tissue Research, 377*(3), 383-396. doi:10.1007/s00441-019-03036-4

DiStefano, J. K. (2018). The emerging role of long noncoding RNAs in human disease *Disease Gene Identification* (pp. 91-110): Springer.

Djebali, S., Davis, C. A., Merkel, A., Dobin, A., Lassmann, T., Mortazavi, A., . . . Schlesinger, F. (2012). Landscape of transcription in human cells. *Nature, 489*(7414), 101-108.

Doksani, Y., Wu, J. Y., de Lange, T., & Zhuang, X. (2013). Super-resolution fluorescence imaging of telomeres reveals TRF2-dependent T-loop formation. *Cell, 155*(2), 345-356. doi:10.1016/j.cell.2013.09.048

Dominici, M., Le Blanc, K., Mueller, I., Slaper-Cortenbach, I., Marini, F., Krause, D., . . . Horwitz, E. (2006). Minimal criteria for defining multipotent mesenchymal stromal cells. The International Society for Cellular Therapy position statement. *Cytotherapy, 8*(4), 315-317. doi:10.1080/14653240600855905

Dunne, A. L., Price, M. E., Mothersill, C., McKeown, S. R., Robson, T., & Hirst, D. G. (2003). Relationship between clonogenic radiosensitivity, radiation-induced apoptosis and DNA damage/repair in human colon cancer cells. *British Journal of Cancer, 89*(12), 2277-2283. doi:10.1038/sj.bjc.6601427

Eischen, C. M., Weber, J. D., Roussel, M. F., Sherr, C. J., & Cleveland, J. L. (1999). Disruption of the ARF-Mdm2-p53 tumor suppressor pathway in Myc-induced lymphomagenesis. *Genes Dev, 13*(20), 2658-2669. doi:10.1101/gad.13.20.2658

Engreitz, J. M., Haines, J. E., Perez, E. M., Munson, G., Chen, J., Kane, M., . . . Lander, E. S. (2016). Local regulation of gene expression by lncRNA promoters, transcription and splicing. *Nature, 539*(7629), 452-455. doi:10.1038/nature20149

Etheridge, S. L., Spencer, G. J., Heath, D. J., & Genever, P. G. (2004). Expression profiling and functional analysis of wnt signaling mechanisms in mesenchymal stem cells. *Stem Cells, 22*(5), 849-860. doi:10.1634/stemcells.22-5-849

Evans, M. J., & Kaufman, M. H. (1981). Establishment in culture of pluripotential cells from mouse embryos. *Nature, 292*(5819), 154-156.

Fang, S., Zhang, L., Guo, J., Niu, Y., Wu, Y., Li, H., . . . Sun, X. (2018). NONCODEV5: a comprehensive annotation database for long non-coding RNAs. *Nucleic Acids Res, 46*(D1), D308-D314.

Feng, X., Xing, J., Feng, G., Huang, D., Lu, X., Liu, S., . . . Gu, Z. (2014). p16(INK4A) mediates age-related changes in mesenchymal stem cells derived from human dental pulp through the DNA damage and stress response. *Mech Ageing Dev, 141-142*, 46-55. doi:10.1016/j.mad.2014.09.004

Feyder, M., & Goff, L. A. (2016). Investigating long noncoding RNAs using animal models. *The Journal of clinical investigation, 126*(8), 2783-2791. doi:10.1172/JCI84422

Flavell, S. J., Hou, T. Z., Lax, S., Filer, A. D., Salmon, M., & Buckley, C. D. (2008). Fibroblasts as novel therapeutic targets in chronic inflammation. *British journal of pharmacology, 153 Suppl 1*(Suppl 1), S241-S246. doi:10.1038/sj.bjp.0707487

Fontana, L., Partridge, L., & Longo, V. D. (2010). Extending healthy life span--from yeast to humans. *Science, 328*(5976), 321-326. doi:10.1126/science.1172539

Friedenstein, A. J., Chailakhyan, R. K., Latsinik, N. V., Panasyuk, A. F., & Keiliss-Borok, I. V. (1974). Stromal cells responsible for transferring the microenvironment of the hemopoietic tissues. Cloning in vitro and retransplantation in vivo. *Transplantation, 17*(4), 331-340. doi:10.1097/00007890-197404000-00001

Frye, M., Jaffrey, S. R., Pan, T., Rechavi, G., & Suzuki, T. (2016). RNA modifications: what have we learned and where are we headed? *Nature Reviews Genetics, 17*(6), 365-372. doi:10.1038/nrg.2016.47

Fu, X.-D. (2014). Non-coding RNA: a new frontier in regulatory biology. *National science review, 1*(2), 190-204.

Fumagalli, M., Rossiello, F., Clerici, M., Barozzi, S., Cittaro, D., Kaplunov, J. M., . . . Beausejour, C. M. (2012). Telomeric DNA damage is irreparable and causes persistent DNA-damage-response activation. *Nature cell biology, 14*(4), 355-365.

Galderisi, U., & Giordano, A. (2014). The gap between the physiological and therapeutic roles of mesenchymal stem cells. *Medicinal research reviews, 34*(5), 1100-1126.

Gamell, C., Ginsberg, D., Haupt, S., & Haupt, Y. (2017). New insights on the regulation of INK4/ARF locus expression. *Oncotarget, 8*(63), 106147-106148. doi:10.18632/oncotarget.22258

Gems, D., & Partridge, L. (2013). Genetics of longevity in model organisms: debates and paradigm shifts. *Annual review of physiology, 75*, 621-644.

Ghaleb, A. M., & Yang, V. W. (2017). Krüppel-like factor 4 (KLF4): What we currently know. *Gene, 611*, 27-37. doi:10.1016/j.gene.2017.02.025

Gil, J., & Peters, G. (2006). Regulation of the INK4b-ARF-INK4a tumour suppressor locus: all for one or one for all. *Nature reviews. Molecular cell biology, 7*(9), 667-677. doi:10.1038/nrm1987

Gil, J., & Peters, G. (2006). Regulation of the INK4b–ARF–INK4a tumour suppressor locus: all for one or one for all. *Nature reviews Molecular cell biology, 7*(9), 667-677.

Gil, N., & Ulitsky, I. (2019). Regulation of gene expression by cis-acting long non-coding RNAs. *Nature Reviews Genetics*, 1-16.

Glennie, S., Soeiro, I., Dyson, P. J., Lam, E. W.-F., & Dazzi, F. (2005). Bone marrow mesenchymal stem cells induce division arrest anergy of activated T cells. *Blood, 105*(7), 2821-2827.

Gong, Y. Y., Peng, M. Y., Yin, D. Q., & Yang, Y. F. (2018). Long non-coding RNA H19 promotes the osteogenic differentiation of rat ectomesenchymal stem cells via Wnt/β-catenin signaling pathway. *Eur Rev Med Pharmacol Sci, 22*(24), 8805-8813. doi:10.26355/eurrev_201812_16648

Gordon, L. B., Cao, K., & Collins, F. S. (2012). Progeria: translational insights from cell biology. *The Journal of cell biology, 199*(1), 9-13. doi:10.1083/jcb.201207072

Gorgoulis, V. G., & Halazonetis, T. D. (2010). Oncogene-induced senescence: the bright and dark side of the response. *Curr Opin Cell Biol, 22*(6), 816-827. doi:10.1016/j.ceb.2010.07.013

Green, D. R., Galluzzi, L., & Kroemer, G. (2011). Mitochondria and the autophagy-inflammation-cell death axis in organismal aging. *Science, 333*(6046), 1109-1112. doi:10.1126/science.1201940

Greider, C. W., & Blackburn, E. H. (1985). Identification of a specific telomere terminal transferase activity in Tetrahymena extracts. *Cell, 43*(2 Pt 1), 405-413. doi:10.1016/0092-8674(85)90170-9

Groff, A. F., Sanchez-Gomez, D. B., Soruco, M. M., Gerhardinger, C., Barutcu, A. R., Li, E., . . . Lee, J. C. (2016). In vivo characterization of Linc-p21 reveals functional cis-regulatory DNA elements. *Cell Rep, 16*(8), 2178-2186.

Grote, P., Wittler, L., Hendrix, D., Koch, F., Währisch, S., Beisaw, A., . . . Herrmann, B. G. (2013). The tissue-specific lncRNA Fendrr is an essential regulator of heart and body wall development in the mouse. *Dev Cell, 24*(2), 206-214. doi:10.1016/j.devcel.2012.12.012

Gupta, R. A., Shah, N., Wang, K. C., Kim, J., Horlings, H. M., Wong, D. J., . . . Rinn, J. L. (2010). Long non-coding RNA HOTAIR reprograms chromatin state to promote cancer metastasis. *Nature, 464*(7291), 1071-1076.

Guttman, M., Amit, I., Garber, M., French, C., Lin, M. F., Feldser, D., . . . Lander, E. S. (2009). Chromatin signature reveals over a thousand highly conserved large non-coding RNAs in mammals. *Nature, 458*(7235), 223-227. doi:10.1038/nature07672

Guttman, M., & Rinn, J. L. (2012). Modular regulatory principles of large non-coding RNAs. *Nature, 482*(7385), 339-346.

Haeussler, M., Schönig, K., Eckert, H., Eschstruth, A., Mianné, J., Renaud, J.-B., . . . Concordet, J.-P. (2016). Evaluation of off-target and on-target scoring algorithms and integration into the guide RNA selection tool CRISPOR. *Genome Biol, 17*(1), 148. doi:10.1186/s13059-016-1012-2

Halic, M., & Moazed, D. (2009). Transposon silencing by piRNAs. *Cell, 138*(6), 1058-1060. doi:10.1016/j.cell.2009.08.030

Hall, E. J. (1989). Radiation and life. *Bulletin of the New York Academy of Medicine, 65*(4), 430.

Halvorsen, T. L., Beattie, G. M., Lopez, A. D., Hayek, A., & Levine, F. (2000). Accelerated telomere shortening and senescence in human pancreatic islet cells stimulated to divide in vitro. *J Endocrinol, 166*(1), 103-109. doi:10.1677/joe.0.1660103

Han, J., Kim, D., & Morris, K. V. (2007). Promoter-associated RNA is required for RNA-directed transcriptional gene silencing in human cells. *Proc Natl Acad Sci U S A, 104*(30), 12422-12427. doi:10.1073/pnas.0701635104

Hankemeier, S., Keus, M., Zeichen, J., Jagodzinski, M., Barkhausen, T., Bosch, U., . . . Griensven, M. V. (2005). Modulation of proliferation and differentiation of human bone marrow stromal cells by fibroblast growth factor 2: potential implications for tissue engineering of tendons and ligaments. *Tissue engineering, 11*(1-2), 41-49.

Hansen, T. B., Jensen, T. I., Clausen, B. H., Bramsen, J. B., Finsen, B., Damgaard, C. K., & Kjems, J. (2013). Natural RNA circles function as efficient microRNA sponges. *Nature, 495*(7441), 384-388. doi:10.1038/nature11993

Harrow, J., Frankish, A., Gonzalez, J. M., Tapanari, E., Diekhans, M., Kokocinski, F., . . . Searle, S. (2012). GENCODE: the reference human genome annotation for The ENCODE Project. *Genome research, 22*(9), 1760-1774.

Hauer, M. H., Seeber, A., Singh, V., Thierry, R., Sack, R., Amitai, A., . . . Gasser, S. M. (2017). Histone degradation in response to DNA damage enhances chromatin dynamics and recombination rates. *Nat Struct Mol Biol, 24*(2), 99-107. doi:10.1038/nsmb.3347

Hayflick, L. (2000). The future of ageing. *Nature, 408*(6809), 267-269.

Hayflick, L., & Moorhead, P. S. (1961). The serial cultivation of human diploid cell strains. *Experimental cell research, 25*(3), 585-621.

He, J., Tu, C., & Liu, Y. (2018). Role of lncRNAs in aging and age‐related diseases. *Aging Medicine, 1*(2), 158-175.

Hezroni, H., Koppstein, D., Schwartz, M. G., Avrutin, A., Bartel, D. P., & Ulitsky, I. (2015). Principles of long noncoding RNA evolution derived from direct comparison of transcriptomes in 17 species. *Cell Rep, 11*(7), 1110-1122.

Hladik, D., Hofig, I., Oestreicher, U., Beckers, J., Matjanovski, M., Bao, X., . . . Rosemann, M. (2019). Long-term culture of mesenchymal stem cells impairs ATM-dependent recognition of DNA breaks and increases genetic instability. *Stem Cell Res Ther, 10*(1), 218. doi:10.1186/s13287-019-1334-6

Hladik, D., Höfig, I., Oestreicher, U., Beckers, J., Matjanovski, M., Bao, X., . . . Rosemann, M. (2019). Long-term culture of mesenchymal stem cells impairs ATM-dependent recognition of DNA breaks and increases genetic instability. *Stem Cell Research & Therapy, 10*(1), 218.

Höfig, I., Ingawale, Y., Atkinson, M. J., Hertlein, H., Nelson, P. J., & Rosemann, M. (2016). p53-dependent senescence in mesenchymal stem cells under chronic normoxia is potentiated by low-dose γ-irradiation. *Stem cells international, 2016*.

Horwitz, E. M., & Keating, A. (2000). Nonhematopoietic mesenchymal stem cells: what are they? *Cytotherapy, 2*(5), 387-388. doi:10.1080/146532400539305

Hu, G., Gong, A.-Y., Wang, Y., Ma, S., Chen, X., Chen, J., . . . Drescher, K. M. (2016). LincRNA-Cox2 promotes late inflammatory gene transcription in macrophages through modulating SWI/SNF-mediated chromatin remodeling. *the Journal of immunology, 196*(6), 2799-2808.

Hu, H. Y., He, L., & Khaitovich, P. (2014). Deep sequencing reveals a novel class of bidirectional promoters associated with neuronal genes. *BMC genomics, 15*(1), 457.

Huang, N. F., & Li, S. (2008). Mesenchymal stem cells for vascular regeneration. *Regenerative medicine, 3*(6), 877-892. doi:10.2217/17460751.3.6.877

Huang, X. A., Yin, H., Sweeney, S., Raha, D., Snyder, M., & Lin, H. (2013). A major epigenetic programming mechanism guided by piRNAs. *Dev Cell, 24*(5), 502-516. doi:10.1016/j.devcel.2013.01.023

Huarte, M. (2015). The emerging role of lncRNAs in cancer. *Nature medicine, 21*(11), 1253.

Huarte, M., Guttman, M., Feldser, D., Garber, M., Koziol, M. J., Kenzelmann-Broz, D., . . . Rinn, J. L. (2010). A large intergenic noncoding RNA induced by p53 mediates global gene repression in the p53 response. *Cell, 142*(3), 409-419. doi:10.1016/j.cell.2010.06.040

Hung, T., Wang, Y., Lin, M. F., Koegel, A. K., Kotake, Y., Grant, G. D., . . . Wang, P. (2011). Extensive and coordinated transcription of noncoding RNAs within cell-cycle promoters. *Nature genetics, 43*(7), 621.

Hutchinson, J. N., Ensminger, A. W., Clemson, C. M., Lynch, C. R., Lawrence, J. B., & Chess, A. (2007). A screen for nuclear transcripts identifies two linked noncoding RNAs associated with SC35 splicing domains. *BMC genomics, 8*, 39. doi:10.1186/1471-2164-8-39

Iliakis, G., Wang, H., Perrault, A. R., Boecker, W., Rosidi, B., Windhofer, F., . . . Pantelias, G. (2004). Mechanisms of DNA double strand break repair and chromosome aberration formation. *Cytogenet Genome Res, 104*(1-4), 14-20. doi:10.1159/000077461

Ip, J. Y., & Nakagawa, S. (2012). Long non-coding RNAs in nuclear bodies. *Dev Growth Differ, 54*(1), 44-54. doi:10.1111/j.1440-169X.2011.01303.x

Itahana, K., Zou, Y., Itahana, Y., Martinez, J. L., Beausejour, C., Jacobs, J. J., . . . Dimri, G. P. (2003). Control of the replicative life span of human fibroblasts by p16 and the polycomb protein Bmi-1. *Mol Cell Biol, 23*(1), 389-401. doi:10.1128/mcb.23.1.389-401.2003

Jaiswal, N., Haynesworth, S. E., Caplan, A. I., & Bruder, S. P. (1997). Osteogenic differentiation of purified, culture‐expanded human mesenchymal stem cells in vitro. *Journal of cellular biochemistry, 64*(2), 295-312.

Janzen, V., Forkert, R., Fleming, H. E., Saito, Y., Waring, M. T., Dombkowski, D. M., . . . Scadden, D. T. (2006). Stem-cell ageing modified by the cyclin-dependent kinase inhibitor p16INK4a. *Nature, 443*(7110), 421-426. doi:10.1038/nature05159

Jiang, H., Chou, H. S., & Zhu, L. (1998). Requirement of cyclin E-Cdk2 inhibition in p16(INK4a)-mediated growth suppression. *Mol Cell Biol, 18*(9), 5284-5290. doi:10.1128/mcb.18.9.5284

Jiang, M.-C., Ni, J.-J., Cui, W.-Y., Wang, B.-Y., & Zhuo, W. (2019). Emerging roles of lncRNA in cancer and therapeutic opportunities. *Am J Cancer Res, 9*(7), 1354.

Jiang, W., & Xu, J. (2020). Immune modulation by mesenchymal stem cells. *Cell proliferation, 53*(1), e12712-e12712. doi:10.1111/cpr.12712

Jiang, X.-X., Zhang, Y., Liu, B., Zhang, S.-X., Wu, Y., Yu, X.-D., & Mao, N. (2005). Human mesenchymal stem cells inhibit differentiation and function of monocyte-derived dendritic cells. *Blood, 105*(10), 4120-4126.

Jiao, F., Hu, H., Yuan, C., Wang, L., Jiang, W., Jin, Z., . . . Wang, L. (2014). Elevated expression level of long noncoding RNA MALAT-1 facilitates cell growth, migration and invasion in pancreatic cancer. *Oncol Rep, 32*(6), 2485-2492.

Jiao, Y., Liu, C., Cui, F. M., Xu, J. Y., Tong, J., Qi, X. F., . . . Zhu, W. (2015). Long intergenic non-coding RNA induced by X-ray irradiation regulates DNA damage response signaling in the human bronchial epithelial BEAS-2B cell line. *Oncology letters, 9*(1), 169-176.

Jin, X., Zhang, Z., Lu, Y., & Fan, Z. (2018). Suppression of long non‐coding RNA LET potentiates bone marrow‐derived mesenchymal stem cells (BMSCs) proliferation by up‐regulating TGF‐β1. *Journal of cellular biochemistry, 119*(3), 2843-2850.

Johnstone, B., Hering, T. M., Caplan, A. I., Goldberg, V. M., & Yoo, J. U. (1998). In vitrochondrogenesis of bone marrow-derived mesenchymal progenitor cells. *Experimental cell research, 238*(1), 265-272.

Josse, C., Schoemans, R., Niessen, N.-A., Delgaudine, M., Hellin, A.-C., Herens, C., . . . Bours, V. (2010). Systematic chromosomal aberrations found in murine bone marrow-derived mesenchymal stem cells. *Stem cells and development, 19*(8), 1167-1173.

Justesen, J., Stenderup, K., Ebbesen, E., Mosekilde, L., Steiniche, T., & Kassem, M. (2001). Adipocyte tissue volume in bone marrow is increased with aging and in patients with osteoporosis. *Biogerontology, 2*(3), 165-171.

Kalwa, M., Hänzelmann, S., Otto, S., Kuo, C. C., Franzen, J., Joussen, S., . . . Wagner, W. (2016). The lncRNA HOTAIR impacts on mesenchymal stem cells via triple helix formation. *Nucleic Acids Res, 44*(22), 10631-10643. doi:10.1093/nar/gkw802

Kamb, A., Gruis, N. A., Weaver-Feldhaus, J., Liu, Q., Harshman, K., Tavtigian, S. V., . . . Skolnick, M. H. (1994). A cell cycle regulator potentially involved in genesis of many tumor types. *Science, 264*(5157), 436-440. doi:10.1126/science.8153634

Katayama, S., Tomaru, Y., Kasukawa, T., Waki, K., Nakanishi, M., Nakamura, M., . . . Kawai, J. (2005). Antisense transcription in the mammalian transcriptome. *Science, 309*(5740), 1564-1566.

Katsimbri, P. (2017). The biology of normal bone remodelling. *European journal of cancer care, 26*(6), e12740.

Katsumoto, K., Shiraki, N., Miki, R., & Kume, S. (2010). Embryonic and adult stem cell systems in mammals: ontology and regulation. *Dev Growth Differ, 52*(1), 115-129. doi:10.1111/j.1440-169X.2009.01160.x

Kaye, F. J. (2002). RB and cyclin dependent kinase pathways: defining a distinction between RB and p16 loss in lung cancer. *Oncogene, 21*(45), 6908-6914. doi:10.1038/sj.onc.1205834

Khalil, A. M., Guttman, M., Huarte, M., Garber, M., Raj, A., Morales, D. R., . . . van Oudenaarden, A. (2009). Many human large intergenic noncoding RNAs associate with chromatin-modifying complexes and affect gene expression. *Proceedings of the National Academy of Sciences, 106*(28), 11667-11672.

Khalil, A. M., Guttman, M., Huarte, M., Garber, M., Raj, A., Rivea Morales, D., . . . Rinn, J. L. (2009). Many human large intergenic noncoding RNAs associate with chromatin-modifying complexes and affect gene expression. *Proc Natl Acad Sci U S A, 106*(28), 11667-11672. doi:10.1073/pnas.0904715106

Khandelwal, A., Bacolla, A., Vasquez, K. M., & Jain, A. (2015). Long non‐coding RNA: A new paradigm for lung cancer. *Molecular carcinogenesis, 54*(11), 1235-1251.

Kim, J., & Hematti, P. (2009). Mesenchymal stem cell–educated macrophages: A novel type of alternatively activated macrophages. *Experimental hematology, 37*(12), 1445-1453.

Kim, T.-K., Hemberg, M., & Gray, J. M. (2015). Enhancer RNAs: a class of long noncoding RNAs synthesized at enhancers. *Cold Spring Harbor perspectives in biology, 7*(1), a018622-a018622. doi:10.1101/cshperspect.a018622

Kim, W., Lee, S., Seo, D., Kim, D., Kim, K., Kim, E., . . . Youn, B. (2019). Cellular Stress Responses in Radiotherapy. *Cells, 8*(9), 1105. doi:10.3390/cells8091105

Kim, W. Y., & Sharpless, N. E. (2006). The regulation of INK4/ARF in cancer and aging. *Cell, 127*(2), 265-275.

Kino, T., Hurt, D. E., Ichijo, T., Nader, N., & Chrousos, G. P. (2010). Noncoding RNA gas5 is a growth arrest- and starvation-associated repressor of the glucocorticoid receptor. *Sci Signal, 3*(107), ra8. doi:10.1126/scisignal.2000568

Kirkwood, T. B. (2005). Understanding the odd science of aging. *Cell, 120*(4), 437-447.

Kiyono, T., Foster, S. A., Koop, J. I., McDougall, J. K., Galloway, D. A., & Klingelhutz, A. J. (1998). Both Rb/p16INK4a inactivation and telomerase activity are required to immortalize human epithelial cells. *Nature, 396*(6706), 84-88. doi:10.1038/23962

Kopp, F., & Mendell, J. T. (2018). Functional Classification and Experimental Dissection of Long Noncoding RNAs. *Cell, 172*(3), 393-407. doi:10.1016/j.cell.2018.01.011

Kotake, Y., Nakagawa, T., Kitagawa, K., Suzuki, S., Liu, N., Kitagawa, M., & Xiong, Y. (2011). Long non-coding RNA ANRIL is required for the PRC2 recruitment to and silencing of p15 INK4B tumor suppressor gene. *Oncogene, 30*(16), 1956-1962.

Kozak, M. (1983). Comparison of initiation of protein synthesis in procaryotes, eucaryotes, and organelles. *Microbiological reviews, 47*(1), 1.

Krishnamurthy, J., Torrice, C., Ramsey, M. R., Kovalev, G. I., Al-Regaiey, K., Su, L., & Sharpless, N. E. (2004). Ink4a/Arf expression is a biomarker of aging. *J Clin Invest, 114*(9), 1299-1307. doi:10.1172/jci22475

Kuilman, T., Michaloglou, C., Mooi, W. J., & Peeper, D. S. (2010). The essence of senescence. *Genes Dev, 24*(22), 2463-2479.

Kuo, C.-C., Hänzelmann, S., Sentürk Cetin, N., Frank, S., Zajzon, B., Derks, J.-P., . . . Costa, I. G. (2019). Detection of RNA-DNA binding sites in long noncoding RNAs. *Nucleic Acids Res, 47*(6), e32-e32. doi:10.1093/nar/gkz037

La Ferlita, A., Battaglia, R., Andronico, F., Caruso, S., Cianci, A., Purrello, M., & Di Pietro, C. (2018). Non-coding RNAs in endometrial physiopathology. *International journal of molecular sciences, 19*(7), 2120.

Lal, A., Kim, H. H., Abdelmohsen, K., Kuwano, Y., Pullmann, R., Jr., Srikantan, S., . . . Gorospe, M. (2008). p16(INK4a) translation suppressed by miR-24. *PLoS One, 3*(3), e1864-e1864. doi:10.1371/journal.pone.0001864

Lekka, E., & Hall, J. (2018). Noncoding RNAs in disease. *FEBS letters, 592*(17), 2884-2900. doi:10.1002/1873-3468.13182

Lessard, J., & Sauvageau, G. (2003). Bmi-1 determines the proliferative capacity of normal and leukaemic stem cells. *Nature, 423*(6937), 255-260. doi:10.1038/nature01572

Lessard, J., & Sauvageau, G. (2003). Bmi-1 determines the proliferative capacity of normal and leukaemic stem cells. *Nature, 423*(6937), 255-260. doi:10.1038/nature01572

Lewis, K. N., Mele, J., Hayes, J. D., & Buffenstein, R. (2010). Nrf2, a guardian of healthspan and gatekeeper of species longevity. *Integrative and comparative biology, 50*(5), 829-843.

Leygue, E. (2007). Steroid receptor RNA activator (SRA1): unusual bifaceted gene products with suspected relevance to breast cancer. *Nuclear receptor signaling, 5*, e006-e006. doi:10.1621/nrs.05006

Li, S., Xu, Z., & Sheng, J. (2018). tRNA-Derived Small RNA: A Novel Regulatory Small Non-Coding RNA. *Genes, 9*(5), 246.

Li, W., Notani, D., Ma, Q., Tanasa, B., Nunez, E., Chen, A. Y., . . . Rosenfeld, M. G. (2013). Functional roles of enhancer RNAs for oestrogen-dependent transcriptional activation. *Nature, 498*(7455), 516-520. doi:10.1038/nature12210

Li, Y., Wu, Q., Wang, Y., Li, L., Bu, H., & Bao, J. (2017). Senescence of mesenchymal stem cells. *Int J Mol Med, 39*(4), 775-782.

Liang, W.-C., Fu, W.-M., Wang, Y.-B., Sun, Y.-X., Xu, L.-L., Wong, C.-W., . . . Zhang, J.-F. (2016). H19 activates Wnt signaling and promotes osteoblast differentiation by functioning as a competing endogenous RNA. *Sci Rep, 6*(1), 1-11.

Lin, N., Yao, Z., Xu, M., Chen, J., Lu, Y., Yuan, L., . . . Xu, R. (2019). Long noncoding RNA MALAT1 potentiates growth and inhibits senescence by antagonizing ABI3BP in gallbladder cancer cells. *Journal of experimental & clinical cancer research : CR, 38*(1), 244-244. doi:10.1186/s13046-019-1237-5

Liu, N., Zhou, K. I., Parisien, M., Dai, Q., Diatchenko, L., & Pan, T. (2017). N6-methyladenosine alters RNA structure to regulate binding of a low-complexity protein. *Nucleic Acids Res, 45*(10), 6051-6063. doi:10.1093/nar/gkx141

López-Otín, C., Blasco, M. A., Partridge, L., Serrano, M., & Kroemer, G. (2013). The hallmarks of aging. *Cell, 153*(6), 1194-1217.

Lustig, A. J. (2004). Telomerase RNA: a flexible RNA scaffold for telomerase biosynthesis. *Curr Biol, 14*(14), R565-567. doi:10.1016/j.cub.2004.07.013

Ma, L., Bajic, V. B., & Zhang, Z. (2013). On the classification of long non-coding RNAs. *RNA Biol, 10*(6), 925-933. doi:10.4161/rna.24604

Makino, S., Fukuda, K., Miyoshi, S., Konishi, F., Kodama, H., Pan, J., . . . Abe, H. (1999). Cardiomyocytes can be generated from marrow stromal cells in vitro. *The Journal of clinical investigation, 103*(5), 697-705.

Marchese, F. P., Raimondi, I., & Huarte, M. (2017). The multidimensional mechanisms of long noncoding RNA function. *Genome Biol, 18*(1), 206.

Marttila, S., Chatsirisupachai, K., Palmer, D., & de Magalhães, J. P. (2020). Ageing-associated changes in the expression of lncRNAs in human tissues reflect a transcriptional modulation in ageing pathways. *Mechanisms of Ageing and Development, 185*, 111177. doi:https://doi.org/10.1016/j.mad.2019.111177

Masgutov, R., Masgutova, G., Mullakhmetova, A., Zhuravleva, M., Shulman, A., Rogozhin, A., . . . Rizvanov, A. (2019). Adipose-Derived Mesenchymal Stem Cells Applied in Fibrin Glue

Stimulate Peripheral Nerve Regeneration. *Frontiers in Medicine, 6*(68). doi:10.3389/fmed.2019.00068

Matera, A. G., Terns, R. M., & Terns, M. P. (2007). Non-coding RNAs: lessons from the small nuclear and small nucleolar RNAs. *Nature reviews Molecular cell biology, 8*(3), 209-220.

Matsuda, Y., Ichida, T., Genda, T., Yamagiwa, S., Aoyagi, Y., & Asakura, H. (2003). Loss of p16 Contributes to p27 Sequestration by Cyclin D₁-Cyclin-dependent Kinase 4 Complexes and Poor Prognosis in Hepatocellular Carcinoma. *Clinical cancer research, 9*(9), 3389-3396.

Mattick, J. S. (2007). A new paradigm for developmental biology. *Journal of Experimental Biology, 210*(9), 1526-1547.

Maynard, S., Fang, E. F., Scheibye-Knudsen, M., Croteau, D. L., & Bohr, V. A. (2015). DNA Damage, DNA Repair, Aging, and Neurodegeneration. *Cold Spring Harbor perspectives in medicine, 5*(10). doi:10.1101/cshperspect.a025130

Maynard, S., Fang, E. F., Scheibye-Knudsen, M., Croteau, D. L., & Bohr, V. A. (2015). DNA Damage, DNA Repair, Aging, and Neurodegeneration. *Cold Spring Harbor perspectives in medicine, 5*(10), a025130. doi:10.1101/cshperspect.a025130

McMillan, T. J., Cassoni, A. M., Edwards, S., Holmes, A., & Peacock, J. H. (1990). The relationship of DNA double-strand break induction to radiosensitivity in human tumour cell lines. *Int J Radiat Biol, 58*(3), 427-438. doi:10.1080/09553009014551781

Mehravar, M., Shirazi, A., Nazari, M., & Banan, M. (2019). Mosaicism in CRISPR/Cas9-mediated genome editing. *Developmental Biology, 445*(2), 156-162. doi:https://doi.org/10.1016/j.ydbio.2018.10.008

Melk, A., Schmidt, B. M., Takeuchi, O., Sawitzki, B., Rayner, D. C., & Halloran, P. F. (2004). Expression of p16INK4a and other cell cycle regulator and senescence associated genes in aging human kidney. *Kidney international, 65*(2), 510-520.

Melo, C. A., Drost, J., Wijchers, P. J., van de Werken, H., de Wit, E., Oude Vrielink, J. A., . . . Agami, R. (2013). eRNAs are required for p53-dependent enhancer activity and gene transcription. *Mol Cell, 49*(3), 524-535. doi:10.1016/j.molcel.2012.11.021

Mercer, T. R., & Mattick, J. S. (2013). Structure and function of long noncoding RNAs in epigenetic regulation. *Nat Struct Mol Biol, 20*(3), 300-307. doi:10.1038/nsmb.2480

Mercer, T. R., Wilhelm, D., Dinger, M. E., Solda, G., Korbie, D. J., Glazov, E. A., . . . Matthaei, K. I. (2011). Expression of distinct RNAs from 3′ untranslated regions. *Nucleic Acids Res, 39*(6), 2393-2403.

Meyer, Kate D., Saletore, Y., Zumbo, P., Elemento, O., Mason, Christopher E., & Jaffrey, Samie R. (2012). Comprehensive Analysis of mRNA Methylation Reveals Enrichment in 3′ UTRs and near Stop Codons. *Cell, 149*(7), 1635-1646. doi:https://doi.org/10.1016/j.cell.2012.05.003

Miquel, J., Economos, A. C., Fleming, J., & Johnson, J. E., Jr. (1980). Mitochondrial role in cell aging. *Exp Gerontol, 15*(6), 575-591. doi:10.1016/0531-5565(80)90010-8

Mirzayans, R., Andrais, B., Hansen, G., & Murray, D. (2012). Role of p 1 6 I N K 4 A in Replicative Senescence and DNA Damage-Induced Premature Senescence in p53-Deficient Human Cells. *Biochemistry research international, 2012*.

Miura, M., Miura, Y., Padilla‐Nash, H. M., Molinolo, A. A., Fu, B., Patel, V., . . . Baker, C. C. (2006). Accumulated chromosomal instability in murine bone marrow mesenchymal stem cells leads to malignant transformation. *Stem Cells, 24*(4), 1095-1103.

Moerman, E. J., Teng, K., Lipschitz, D. A., & Lecka‐Czernik, B. (2004). Aging activates adipogenic and suppresses osteogenic programs in mesenchymal marrow stroma/stem cells: the role of PPAR‐γ2 transcription factor and TGF‐β/BMP signaling pathways. *Aging Cell, 3*(6), 379-389.

Moldave, K. (1985). Eukaryotic protein synthesis. *Annu Rev Biochem, 54*, 1109-1149. doi:10.1146/annurev.bi.54.070185.005333

Mombach, J. C. M., Bugs, C. A., & Chaouiya, C. (2014). Modelling the onset of senescence at the G1/S cell cycle checkpoint. *BMC genomics, 15 Suppl 7*(Suppl 7), S7-S7. doi:10.1186/1471-2164-15-S7-S7

Mondal, T., Rasmussen, M., Pandey, G. K., Isaksson, A., & Kanduri, C. (2010). Characterization of the RNA content of chromatin. *Genome research, 20*(7), 899-907.

Mondal, T., Subhash, S., Vaid, R., Enroth, S., Uday, S., Reinius, B., . . . Hoberg, E. (2015). MEG3 long noncoding RNA regulates the TGF-beta pathway genes through formation of RNA-DNA triplex structures. Nat Commun 6: 7743.

Montes, M., Nielsen, M. M., Maglieri, G., Jacobsen, A., Højfeldt, J., Agrawal-Singh, S., . . . Pedersen, J. S. (2015). The lncRNA MIR31HG regulates p16 INK4A expression to modulate senescence. *Nature communications, 6*(1), 1-15.

Moreau, J. E., Chen, J., Bramono, D. S., Volloch, V., Chernoff, H., Vunjak-Novakovic, G., . . . Altman, G. H. (2005). Growth factor induced fibroblast differentiation from human bone marrow stromal cells in vitro. *J Orthop Res, 23*(1), 164-174. doi:10.1016/j.orthres.2004.05.004

Morris, B. J., Willcox, D. C., Donlon, T. A., & Willcox, B. J. (2015). FOXO3: a major gene for human longevity-a mini-review. *Gerontology, 61*(6), 515-525.

Moskalev, A. A., Smit-McBride, Z., Shaposhnikov, M. V., Plyusnina, E. N., Zhavoronkov, A., Budovsky, A., . . . Fraifeld, V. E. (2012). Gadd45 proteins: relevance to aging, longevity and age-related pathologies. *Ageing research reviews, 11*(1), 51-66.

Mullin, N. K., Mallipeddi, N. V., Hamburg-Shields, E., Ibarra, B., Khalil, A. M., & Atit, R. P. (2017). Wnt/β-catenin Signaling Pathway Regulates Specific lncRNAs That Impact Dermal Fibroblasts and Skin Fibrosis. *Frontiers in genetics, 8*(183). doi:10.3389/fgene.2017.00183

Nakamura, K., Yoshimura, A., Kaneko, T., Sato, K., & Hara, Y. (2014). ROCK inhibitor Y-27632 maintains the proliferation of confluent human mesenchymal stem cells. *J Periodontal Res, 49*(3), 363-370. doi:10.1111/jre.12114

Nakaya, H. I., Amaral, P. P., Louro, R., Lopes, A., Fachel, A. A., Moreira, Y. B., . . . Verjovski-Almeida, S. (2007). Genome mapping and expression analyses of human intronic noncoding RNAs reveal tissue-specific patterns and enrichment in genes related to regulation of transcription. *Genome Biol, 8*(3), R43.

Neguembor, M., Jothi, M., & Gabellini, D. (2014). Long noncoding RNAs, emerging players in muscle differentiation and disease. *Skeletal muscle, 4*, 8. doi:10.1186/2044-5040-4-8

Neri, S. (2019). Genetic Stability of Mesenchymal Stromal Cells for Regenerative Medicine Applications: A Fundamental Biosafety Aspect. *Int J Mol Sci, 20*(10). doi:10.3390/ijms20102406

Neri, S., & Borzì, R. M. (2020). Molecular Mechanisms Contributing to Mesenchymal Stromal Cell Aging. *Biomolecules, 10*(2), 340.

Neri, S., & Borzì, R. M. (2020). Molecular Mechanisms Contributing to Mesenchymal Stromal Cell Aging. *Biomolecules, 10*(2). doi:10.3390/biom10020340

Niederer, R. O., Hass, E. P., & Zappulla, D. C. (2017). Long Noncoding RNAs in the Yeast S. cerevisiae. *Adv Exp Med Biol, 1008*, 119-132. doi:10.1007/978-981-10-5203-3_4

Niehrs, C. (2006). Function and biological roles of the Dickkopf family of Wnt modulators. *Oncogene, 25*(57), 7469-7481. doi:10.1038/sj.onc.1210054

Nielsen, G. P., Stemmer-Rachamimov, A. O., Shaw, J., Roy, J. E., Koh, J., & Louis, D. N. (1999). Immunohistochemical survey of p16INK4A expression in normal human adult and infant tissues. *Laboratory investigation; a journal of technical methods and pathology, 79*(9), 1137-1143.

Noh, J. H., Kim, K. M., McClusky, W. G., Abdelmohsen, K., & Gorospe, M. (2018). Cytoplasmic functions of long noncoding RNAs. *Wiley Interdiscip Rev RNA, 9*(3), e1471-e1471. doi:10.1002/wrna.1471

Nötzold, L., Frank, L., Gandhi, M., Polycarpou-Schwarz, M., Groß, M., Gunkel, M., . . . Diederichs, S. (2017). The long non-coding RNA LINC00152 is essential for cell cycle progression through mitosis in HeLa cells. *Sci Rep, 7*(1), 2265. doi:10.1038/s41598-017-02357-0

Nuovo, G. J., Plaia, T. W., Belinsky, S. A., Baylin, S. B., & Herman, J. G. (1999). In situ detection of the hypermethylation-induced inactivation of the p16 gene as an early event in oncogenesis. *Proc Natl Acad Sci U S A, 96*(22), 12754-12759. doi:10.1073/pnas.96.22.12754

O'Leary, V. B., Smida, J., Matjanovski, M., Brockhaus, C., Winkler, K., Moertl, S., . . . Atkinson, M. J. (2017). The circRNA interactome-innovative hallmarks of the intra- and extracellular radiation response. *Oncotarget, 8*(45), 78397-78409. doi:10.18632/oncotarget.19228

O'Sullivan, R. J., & Karlseder, J. (2010). Telomeres: protecting chromosomes against genome instability. *Nature reviews. Molecular cell biology, 11*(3), 171-181. doi:10.1038/nrm2848

O'Leary, V. B., Ovsepian, S. V., Carrascosa, L. G., Buske, F. A., Radulovic, V., Niyazi, M., . . . Anastasov, N. (2015). PARTICLE, a triplex-forming long ncRNA, regulates locus-specific methylation in response to low-dose irradiation. *Cell Rep, 11*(3), 474-485.

Oh, M., & Nör, J. E. (2015). The Perivascular Niche and Self-Renewal of Stem Cells. *Frontiers in physiology, 6*, 367-367. doi:10.3389/fphys.2015.00367

Ou, H.-L., & Schumacher, B. (2018). DNA damage responses and p53 in the aging process. *Blood, 131*(5), 488-495.

Ouelle, D. E., Zindy, F., Ashmun, R. A., & Sherr, C. J. (1995). Alternative reading frames of the INK4a tumor suppressor gene encode two unrelated proteins capable of inducing cell cycle arrest. *Cell, 83*(6), 993-1000.

Owen, M. E., Cave, J., & Joyner, C. J. (1987). Clonal analysis in vitro of osteogenic differentiation of marrow CFU-F. *J Cell Sci, 87 (Pt 5)*, 731-738.

Özgür, E., Mert, U., Isin, M., Okutan, M., Dalay, N., & Gezer, U. (2013). Differential expression of long non-coding RNAs during genotoxic stress-induced apoptosis in HeLa and MCF-7 cells. *Clinical and Experimental Medicine, 13*(2), 119-126. doi:10.1007/s10238-012-0181-x

Palm, W., & Lange, T. d. (2008). How Shelterin Protects Mammalian Telomeres. *Annual review of genetics, 42*(1), 301-334. doi:10.1146/annurev.genet.41.110306.130350

Parry, D., Bates, S., Mann, D. J., & Peters, G. (1995). Lack of cyclin D-Cdk complexes in Rb-negative cells correlates with high levels of p16INK4/MTS1 tumour suppressor gene product. *Embo j, 14*(3), 503-511.

Pasmant, E., Laurendeau, I., Héron, D., Vidaud, M., Vidaud, D., & Bieche, I. (2007). Characterization of a germ-line deletion, including the entire INK4/ARF locus, in a melanoma-neural system tumor family: identification of ANRIL, an antisense noncoding RNA whose expression coclusters with ARF. *Cancer Res, 67*(8), 3963-3969.

Passier, R., & Mummery, C. (2003). Origin and use of embryonic and adult stem cells in differentiation and tissue repair. *Cardiovascular research, 58*(2), 324-335.

Pegoraro, G., Kubben, N., Wickert, U., Göhler, H., Hoffmann, K., & Misteli, T. (2009). Ageing-related chromatin defects through loss of the NURD complex. *Nat Cell Biol, 11*(10), 1261-1267. doi:10.1038/ncb1971

Pelekanos, R. A., Li, J., Gongora, M., Chandrakanthan, V., Scown, J., Suhaimi, N., . . . Little, M. H. (2012). Comprehensive transcriptome and immunophenotype analysis of renal and cardiac MSC-like populations supports strong congruence with bone marrow MSC despite maintenance of distinct identities. *Stem Cell Res, 8*(1), 58-73. doi:10.1016/j.scr.2011.08.003

Peng, S., Cao, L., He, S., Zhong, Y., Ma, H., Zhang, Y., & Shuai, C. (2018). An Overview of Long Noncoding RNAs Involved in Bone Regeneration from Mesenchymal Stem Cells. *Stem Cells Int, 2018*, 8273648. doi:10.1155/2018/8273648

Petersen, B., Bowen, W., Patrene, K., Mars, W., Sullivan, A., Murase, N. a., . . . Goff, J. (1999). Bone marrow as a potential source of hepatic oval cells. *Science, 284*(5417), 1168-1170.

Pittenger, M. F., Mackay, A. M., Beck, S. C., Jaiswal, R. K., Douglas, R., Mosca, J. D., . . . Marshak, D. R. (1999). Multilineage potential of adult human mesenchymal stem cells. *Science, 284*(5411), 143-147. doi:10.1126/science.284.5411.143

Ponjavic, J., Ponting, C. P., & Lunter, G. (2007). Functionality or transcriptional noise? Evidence for selection within long noncoding RNAs. *Genome research, 17*(5), 556-565.

Pontier, D. B., & Gribnau, J. (2011). Xist regulation and function explored. *Hum Genet, 130*(2), 223-236. doi:10.1007/s00439-011-1008-7

Popov, N., & Gil, J. (2010). Epigenetic regulation of the INK4b-ARF-INK4a locus: in sickness and in health. *Epigenetics, 5*(8), 685-690. doi:10.4161/epi.5.8.12996

Popov, N., & Gil, J. (2010). Epigenetic regulation of the INK4b-ARF-INK4a locus: in sickness and in health. *Epigenetics, 5*(8), 685-690.

Postepska-Igielska, A., Giwojna, A., Gasri-Plotnitsky, L., Schmitt, N., Dold, A., Ginsberg, D., & Grummt, I. (2015). LncRNA Khps1 Regulates Expression of the Proto-oncogene SPHK1 via Triplex-Mediated Changes in Chromatin Structure. *Mol Cell, 60*(4), 626-636. doi:10.1016/j.molcel.2015.10.001

Powers, E. T., Morimoto, R. I., Dillin, A., Kelly, J. W., & Balch, W. E. (2009). Biological and chemical approaches to diseases of proteostasis deficiency. *Annu Rev Biochem, 78*, 959-991. doi:10.1146/annurev.biochem.052308.114844

Purpura, K. A., Aubin, J. E., & Zandstra, P. W. (2004). Sustained in vitro expansion of bone progenitors is cell density dependent. *Stem Cells, 22*(1), 39-50.

Quarto, R., Mastrogiacomo, M., Cancedda, R., Kutepov, S. M., Mukhachev, V., Lavroukov, A., . . . Marcacci, M. (2001). Repair of large bone defects with the use of autologous bone marrow stromal cells. *New England Journal of Medicine, 344*(5), 385-386.

Randle, D. H., Zindy, F., Sherr, C. J., & Roussel, M. F. (2001). Differential effects of p19(Arf) and p16(Ink4a) loss on senescence of murine bone marrow-derived preB cells and macrophages. *Proc Natl Acad Sci U S A, 98*(17), 9654-9659. doi:10.1073/pnas.171217498

Rando, T. A. (2006). Stem cells, ageing and the quest for immortality. *Nature, 441*(7097), 1080-1086.

Reddy, S. S. K., & Chaiban, J. T. (2017). THE ENDOCRINOLOGY OF AGING: A KEY TO LONGEVITY "GREAT EXPECTATIONS". *Endocr Pract, 23*(9), 1107-1116. doi:10.4158/ep171793.Ra

Redon, S., Reichenbach, P., & Lingner, J. (2010). The non-coding RNA TERRA is a natural ligand and direct inhibitor of human telomerase. *Nucleic Acids Res, 38*(17), 5797-5806. doi:10.1093/nar/gkq296

Reeves, M. B., Davies, A. A., McSharry, B. P., Wilkinson, G. W., & Sinclair, J. H. (2007). Complex I binding by a virally encoded RNA regulates mitochondria-induced cell death. *Science, 316*(5829), 1345-1348. doi:10.1126/science.1142984

Ren, R., Ocampo, A., Liu, G. H., & Izpisua Belmonte, J. C. (2017). Regulation of Stem Cell Aging by Metabolism and Epigenetics. *Cell Metab, 26*(3), 460-474. doi:10.1016/j.cmet.2017.07.019

Richardson, R. B. (2009). Ionizing radiation and aging: rejuvenating an old idea. *Aging, 1*(11), 887-902. doi:10.18632/aging.100081

Røsland, G. V., Svendsen, A., Torsvik, A., Sobala, E., McCormack, E., Immervoll, H., . . . Lønning, P. E. (2009). Long-term cultures of bone marrow–derived human mesenchymal stem cells

frequently undergo spontaneous malignant transformation. *Cancer Res, 69*(13), 5331-5339.

Rozemuller, H., Prins, H.-J., Naaijkens, B., Staal, J., Bühring, H.-J., & Martens, A. C. (2010). Prospective isolation of mesenchymal stem cells from multiple mammalian species using cross-reacting anti-human monoclonal antibodies. *Stem cells and development, 19*(12), 1911-1921.

Salama, R., Sadaie, M., Hoare, M., & Narita, M. (2014). Cellular senescence and its effector programs. *Genes Dev, 28*(2), 99-114.

Salehi, S., Taheri, M. N., Azarpira, N., Zare, A., & Behzad‐Behbahani, A. (2017). State of the art technologies to explore long non‐coding RNAs in cancer. *Journal of cellular and molecular medicine, 21*(12), 3120-3140.

Sasaki, M., Abe, R., Fujita, Y., Ando, S., Inokuma, D., & Shimizu, H. (2008). Mesenchymal stem cells are recruited into wounded skin and contribute to wound repair by transdifferentiation into multiple skin cell type. *the Journal of immunology, 180*(4), 2581-2587.

Satijn, D. P., Gunster, M. J., van der Vlag, J., Hamer, K. M., Schul, W., Alkema, M. J., . . . Otte, A. P. (1997). RING1 is associated with the polycomb group protein complex and acts as a transcriptional repressor. *Mol Cell Biol, 17*(7), 4105-4113. doi:10.1128/mcb.17.7.4105

Scaffidi, P., & Misteli, T. (2008). Lamin A-dependent misregulation of adult stem cells associated with accelerated ageing. *Nat Cell Biol, 10*(4), 452-459. doi:10.1038/ncb1708

Scheuermann, J. C., & Boyer, L. A. (2013). Getting to the heart of the matter: long non‐coding RNAs in cardiac development and disease. *The EMBO journal, 32*(13), 1805-1816.

Schmitt, C. A., McCurrach, M. E., de Stanchina, E., Wallace-Brodeur, R. R., & Lowe, S. W. (1999). INK4a/ARF mutations accelerate lymphomagenesis and promote chemoresistance by disabling p53. *Genes Dev, 13*(20), 2670-2677. doi:10.1101/gad.13.20.2670

Scuteri, A., & Monfrini, M. (2018). Mesenchymal Stem Cells as New Therapeutic Approach for Diabetes and Pancreatic Disorders. *Int J Mol Sci, 19*(9), 2783. doi:10.3390/ijms19092783

Serrano, M., Hannon, G. J., & Beach, D. (1993). A new regulatory motif in cell-cycle control causing specific inhibition of cyclin D/CDK4. *Nature, 366*(6456), 704-707. doi:10.1038/366704a0

Sherr, C. J. (2000). The Pezcoller Lecture: Cancer Cell Cycles Revisited. *Cancer Res, 60*(14), 3689-3695.

Sherr, C. J. (2001). The INK4a/ARF network in tumour suppression. *Nature reviews. Molecular cell biology, 2*(10), 731-737. doi:10.1038/35096061

Sherr, C. J. (2001). The INK4a/ARF network in tumour suppression. *Nature reviews Molecular cell biology, 2*(10), 731-737.

Sherr, C. J., & McCormick, F. (2002). The RB and p53 pathways in cancer. *Cancer Cell, 2*(2), 103-112. doi:10.1016/s1535-6108(02)00102-2

Shi, Y. (2017). Mechanistic insights into precursor messenger RNA splicing by the spliceosome. *Nature reviews Molecular cell biology, 18*(11), 655-670. doi:10.1038/nrm.2017.86

Shibata, K. R., Aoyama, T., Shima, Y., Fukiage, K., Otsuka, S., Furu, M., . . . Neo, M. (2007). Expression of the p16INK4A gene is associated closely with senescence of human mesenchymal stem cells and is potentially silenced by DNA methylation during in vitro expansion. *Stem Cells, 25*(9), 2371-2382.

Shin, H. Y., Wang, C., Lee, H. K., Yoo, K. H., Zeng, X., Kuhns, T., . . . Hennighausen, L. (2017). CRISPR/Cas9 targeting events cause complex deletions and insertions at 17 sites in the mouse genome. *Nature communications, 8*(1), 15464. doi:10.1038/ncomms15464

Shiozawa, Y., Havens, A. M., Pienta, K. J., & Taichman, R. S. (2008). The bone marrow niche: habitat to hematopoietic and mesenchymal stem cells, and unwitting host to molecular parasites. *Leukemia, 22*(5), 941-950. doi:10.1038/leu.2008.48

Sia, J., Szmyd, R., Hau, E., & Gee, H. E. (2020). Molecular Mechanisms of Radiation-Induced Cancer Cell Death: A Primer. *Frontiers in Cell and Developmental Biology, 8*(41). doi:10.3389/fcell.2020.00041

Soleimani, M., & Nadri, S. (2009). A protocol for isolation and culture of mesenchymal stem cells from mouse bone marrow. *Nat Protoc, 4*(1), 102-106. doi:10.1038/nprot.2008.221

Song, L., Liu, M., Ono, N., Bringhurst, F. R., Kronenberg, H. M., & Guo, J. (2012). Loss of wnt/ β ‐ catenin signaling causes cell fate shift of preosteoblasts from osteoblasts to adipocytes. *Journal of Bone and Mineral Research, 27*(11), 2344-2358.

Sousa-Franco, A., Rebelo, K., da Rocha, S. T., & Bernardes de Jesus, B. (2019). LncRNAs regulating stemness in aging. *Aging Cell, 18*(1), e12870-e12870. doi:10.1111/acel.12870

Spaggiari, G. M., Capobianco, A., Abdelrazik, H., Becchetti, F., Mingari, M. C., & Moretta, L. (2008). Mesenchymal stem cells inhibit natural killer–cell proliferation, cytotoxicity, and cytokine production: role of indoleamine 2, 3-dioxygenase and prostaglandin E2. *Blood, The Journal of the American Society of Hematology, 111*(3), 1327-1333.

Sperka, T., Wang, J., & Rudolph, K. L. (2012). DNA damage checkpoints in stem cells, ageing and cancer. *Nature reviews. Molecular cell biology, 13*(9), 579-590. doi:10.1038/nrm3420

Squillaro, T., Peluso, G., & Galderisi, U. (2016). Clinical trials with mesenchymal stem cells: an update. *Cell transplantation, 25*(5), 829-848.

Stappenbeck, T. S., & Miyoshi, H. (2009). The role of stromal stem cells in tissue regeneration and wound repair. *Science, 324*(5935), 1666-1669.

Stenderup, K., Justesen, J., Clausen, C., & Kassem, M. (2003). Aging is associated with decreased maximal life span and accelerated senescence of bone marrow stromal cells. *Bone, 33*(6), 919-926.

Sugrue, T., Brown, J. A., Lowndes, N. F., & Ceredig, R. (2013). Multiple facets of the DNA damage response contribute to the radioresistance of mouse mesenchymal stromal cell lines. *Stem Cells, 31*(1), 137-145.

Swafford, D. S., Middleton, S. K., Palmisano, W. A., Nikula, K. J., Tesfaigzi, J., Baylin, S. B., . . . Belinsky, S. A. (1997). Frequent aberrant methylation of p16INK4a in primary rat lung tumors. *Molecular and cellular biology, 17*(3), 1366-1374.

Taft, R. J., Pheasant, M., & Mattick, J. S. (2007). The relationship between non ‐ protein ‐ coding DNA and eukaryotic complexity. *Bioessays, 29*(3), 288-299.

Tan, P., Guo, Y.-H., Zhan, J.-K., Long, L.-M., Xu, M.-L., Ye, L., . . . Wang, H.-Q. (2019). LncRNA-ANRIL inhibits cell senescence of vascular smooth muscle cells by regulating miR-181a/Sirt1. *Biochemistry and Cell Biology, 97*(5), 571-580.

Tay, Y., Rinn, J., & Pandolfi, P. P. (2014). The multilayered complexity of ceRNA crosstalk and competition. *Nature, 505*(7483), 344-352. doi:10.1038/nature12986

Tayyeb, A., Shahzad, N., & Gibran, A. (2017). Differentiation of mesenchymal stem cells towards nephrogenic lineage and their enhanced resistance to oxygen peroxide-induced oxidative stress. *Iranian journal of kidney diseases, 11*(4), 271.

Thomson, J. A., Itskovitz-Eldor, J., Shapiro, S. S., Waknitz, M. A., Swiergiel, J. J., Marshall, V. S., & Jones, J. M. (1998). Embryonic Stem Cell Lines Derived from Human Blastocysts. *Science, 282*(5391), 1145-1147. doi:10.1126/science.282.5391.1145

Tiwari, A., Swamynathan, S., Alexander, N., Gnalian, J., Tian, S., Kinchington, P. R., & Swamynathan, S. K. (2019). KLF4 Regulates Corneal Epithelial Cell Cycle Progression by Suppressing Canonical TGF-β Signaling and Upregulating CDK Inhibitors P16 and P27. *Invest Ophthalmol Vis Sci, 60*(2), 731-740. doi:10.1167/iovs.18-26423

Tripathi, V., Ellis, J. D., Shen, Z., Song, D. Y., Pan, Q., Watt, A. T., . . . Prasanth, K. V. (2010). The nuclear-retained noncoding RNA MALAT1 regulates alternative splicing by modulating SR splicing factor phosphorylation. *Mol Cell, 39*(6), 925-938. doi:10.1016/j.molcel.2010.08.011

Tripathi, V., Ellis, J. D., Shen, Z., Song, D. Y., Pan, Q., Watt, A. T., . . . Prasanth, K. V. (2010). The nuclear-retained noncoding RNA MALAT1 regulates alternative splicing by modulating SR splicing factor phosphorylation. *Mol Cell, 39*(6), 925-938. doi:10.1016/j.molcel.2010.08.011

Tropel, P., Platet, N., Platel, J. C., Noël, D., Albrieux, M., Benabid, A. L., & Berger, F. (2006). Functional neuronal differentiation of bone marrow‐derived mesenchymal stem cells. *Stem Cells, 24*(12), 2868-2876.

Ulitsky, I. (2016). Evolution to the rescue: using comparative genomics to understand long non-coding RNAs. *Nature Reviews Genetics, 17*(10), 601.

Ulitsky, I., & Bartel, D. P. (2013). lincRNAs: genomics, evolution, and mechanisms. *Cell, 154*(1), 26-46. doi:10.1016/j.cell.2013.06.020

Ulveling, D., Francastel, C., & Hubé, F. (2011). When one is better than two: RNA with dual functions. *Biochimie, 93*(4), 633-644.

Vance, K. W., & Ponting, C. P. (2014). Transcriptional regulatory functions of nuclear long noncoding RNAs. *Trends Genet, 30*(8), 348-355. doi:10.1016/j.tig.2014.06.001

Verfaillie, C. M. (2002). Adult stem cells: assessing the case for pluripotency. *Trends in cell biology, 12*(11), 502-508.

Vijg, J., & Montagna, C. (2017). Genome instability and aging: Cause or effect? *Translational Medicine of Aging, 1*, 5-11.

Villasante, A., Strati, K., Ortega, S., Cañamero, M., Blasco, M., & Serrano, M. (2009). The Ink4/Arf locus is a barrier for iPS cell reprogramming. *Nature, 460*, 1136-1139. doi:10.1038/nature08290

Villegas, V. E., & Zaphiropoulos, P. G. (2015). Neighboring gene regulation by antisense long non-coding RNAs. *Int J Mol Sci, 16*(2), 3251-3266. doi:10.3390/ijms16023251

Von Lüttichau, I., Notohamiprodjo, M., Wechselberger, A., Peters, C., Henger, A., Seliger, C., . . . Nelson, P. J. (2005). Human adult CD34- progenitor cells functionally express the chemokine receptors CCR1, CCR4, CCR7, CXCR5, and CCR10 but not CXCR4. *Stem Cells Dev, 14*(3), 329-336. doi:10.1089/scd.2005.14.329

Wagner, D. R., Karnik, S., Gunderson, Z. J., Nielsen, J. J., Fennimore, A., Promer, H. J., . . . McKinley, T. O. (2019). Dysfunctional stem and progenitor cells impair fracture healing with age. *World journal of stem cells, 11*(6), 281.

Wagner, W., Ho, A. D., & Zenke, M. (2010). Different facets of aging in human mesenchymal stem cells. *Tissue Engineering Part B: Reviews, 16*(4), 445-453.

Wakitani, S., Mitsuoka, T., Nakamura, N., Toritsuka, Y., Nakamura, Y., & Horibe, S. (2004). Autologous bone marrow stromal cell transplantation for repair of full-thickness articular cartilage defects in human patellae: two case reports. *Cell transplantation, 13*(5), 595-600.

Wakitani, S., Saito, T., & Caplan, A. I. (1995). Myogenic cells derived from rat bone marrow mesenchymal stem cells exposed to 5‐azacytidine. *Muscle & Nerve: Official Journal of the American Association of Electrodiagnostic Medicine, 18*(12), 1417-1426.

Walburg Jr, H. (1975). Radiation-induced life-shortening and premature aging *Advances in radiation biology* (Vol. 5, pp. 145-179): Elsevier.

Wang, A. S., & Dreesen, O. (2018). Biomarkers of Cellular Senescence and Skin Aging. *Frontiers in genetics, 9*, 247-247. doi:10.3389/fgene.2018.00247

Wang, C., Jurk, D., Maddick, M., Nelson, G., Martin‐Ruiz, C., & Von Zglinicki, T. (2009). DNA damage response and cellular senescence in tissues of aging mice. *Aging Cell, 8*(3), 311-323.

Wang, H., Wang, L., Erdjument-Bromage, H., Vidal, M., Tempst, P., Jones, R. S., & Zhang, Y. (2004). Role of histone H2A ubiquitination in Polycomb silencing. *Nature, 431*(7010), 873-878. doi:10.1038/nature02985

Wang, J., Liao, L., & Tan, J. (2011). Mesenchymal-stem-cell-based experimental and clinical trials: current status and open questions. *Expert opinion on biological therapy, 11*(7), 893-909.

Wang, K. C., & Chang, H. Y. (2011). Molecular mechanisms of long noncoding RNAs. *Mol Cell, 43*(6), 904-914.

Wang, K. C., Helms, J. A., & Chang, H. Y. (2009). Regeneration, repair and remembering identity: the three Rs of Hox gene expression. *Trends Cell Biol, 19*(6), 268-275. doi:10.1016/j.tcb.2009.03.007

Wang, L., Wu, F., Song, Y., Li, X., Wu, Q., Duan, Y., & Jin, Z. (2016). Long noncoding RNA related to periodontitis interacts with miR-182 to upregulate osteogenic differentiation in periodontal mesenchymal stem cells of periodontitis patients. *Cell death & disease, 7*(8), e2327-e2327. doi:10.1038/cddis.2016.125

Wang, X., Arai, S., Song, X., Reichart, D., Du, K., Pascual, G., . . . Kurokawa, R. (2008). Induced ncRNAs allosterically modify RNA-binding proteins in cis to inhibit transcription. *Nature, 454*(7200), 126-130. doi:10.1038/nature06992

Wang, Y., Han, Z. B., Song, Y. P., & Han, Z. C. (2012). Safety of mesenchymal stem cells for clinical application. *Stem Cells Int, 2012*, 652034. doi:10.1155/2012/652034

Wang, Y., Zhu, G., Wang, J., & Chen, J. (2016). Irradiation alters the differentiation potential of bone marrow mesenchymal stem cells. *Molecular medicine reports, 13*(1), 213-223.

Watcharasit, P., Bijur, G. N., Zmijewski, J. W., Song, L., Zmijewska, A., Chen, X., . . . Jope, R. S. (2002). Direct, activating interaction between glycogen synthase kinase-3beta and p53 after DNA damage. *Proc Natl Acad Sci U S A, 99*(12), 7951-7955. doi:10.1073/pnas.122062299

Watters, D. (1999). Molecular mechanisms of ionizing radiation‐induced apoptosis. *Immunology and cell biology, 77*(3), 263-271.

Wei, B., Wei, W., Zhao, B., Guo, X., & Liu, S. (2017). Long non-coding RNA HOTAIR inhibits miR-17-5p to regulate osteogenic differentiation and proliferation in non-traumatic osteonecrosis of femoral head. *PLoS One, 12*(2), e0169097. doi:10.1371/journal.pone.0169097

Werner, M. S., & Ruthenburg, A. J. (2015). Nuclear fractionation reveals thousands of chromatin-tethered noncoding RNAs adjacent to active genes. *Cell Rep, 12*(7), 1089-1098.

Werner, M. S., & Ruthenburg, A. J. (2015). Nuclear Fractionation Reveals Thousands of Chromatin-Tethered Noncoding RNAs Adjacent to Active Genes. *Cell Rep, 12*(7), 1089-1098. doi:10.1016/j.celrep.2015.07.033

Wexler, S. A., Donaldson, C., Denning‐Kendall, P., Rice, C., Bradley, B., & Hows, J. M. (2003). Adult bone marrow is a rich source of human mesenchymal 'stem'cells but umbilical cord and mobilized adult blood are not. *British journal of haematology, 121*(2), 368-374.

Wiese, D. M., Ruttan, C. C., Wood, C. A., Ford, B. N., & Braid, L. R. (2019). Accumulating Transcriptome Drift Precedes Cell Aging in Human Umbilical Cord-Derived Mesenchymal Stromal Cells Serially Cultured to Replicative Senescence. *STEM CELLS Translational Medicine, 8*(9), 945-958. doi:10.1002/sctm.18-0246

Wu, G., Cai, J., Han, Y., Chen, J., Huang, Z.-P., Chen, C., . . . Liu, Y. (2014). LincRNA-p21 regulates neointima formation, vascular smooth muscle cell proliferation, apoptosis, and atherosclerosis by enhancing p53 activity. *Circulation, 130*(17), 1452-1465.

Wu, J., Zhao, J., Sun, L., Pan, Y., Wang, H., & Zhang, W. B. (2018). Long non-coding RNA H19 mediates mechanical tension-induced osteogenesis of bone marrow mesenchymal stem cells via FAK by sponging miR-138. *Bone, 108*, 62-70. doi:10.1016/j.bone.2017.12.013

Wu, Z., Zhang, W., Song, M., Wang, W., Wei, G., Li, W., . . . Liu, G. H. (2018). Differential stem cell aging kinetics in Hutchinson-Gilford progeria syndrome and Werner syndrome. *Protein Cell, 9*(4), 333-350. doi:10.1007/s13238-018-0517-8

Wutz, A., Rasmussen, T. P., & Jaenisch, R. (2002). Chromosomal silencing and localization are mediated by different domains of Xist RNA. *Nat Genet, 30*(2), 167-174. doi:10.1038/ng820

Xia, W., Zhuang, L., Deng, X., & Hou, M. (2017). Long noncoding RNA-p21 modulates cellular senescence via the Wnt/β-catenin signaling pathway in mesenchymal stem cells. *Molecular medicine reports, 16*(5), 7039-7047.

Xia, W., Zhuang, L., & Hou, M. (2018). Role of lincRNAp21 in the protective effect of macrophage inhibition factor against hypoxia/serum deprivationinduced apoptosis in mesenchymal stem cells. *Int J Mol Med, 42*(4), 2175-2184. doi:10.3892/ijmm.2018.3767

Xiang, J.-F., Yin, Q.-F., Chen, T., Zhang, Y., Zhang, X.-O., Wu, Z., . . . Lu, X. (2014). Human colorectal cancer-specific CCAT1-L lncRNA regulates long-range chromatin interactions at the MYC locus. *Cell Research, 24*(5), 513-531.

Xu, Q., Liu, M., Zhang, J., Xue, L., Zhang, G., Hu, C., . . . Xu, N. (2016). Overexpression of KLF4 promotes cell senescence through microRNA-203-survivin-p21 pathway. *Oncotarget, 7*(37), 60290-60302. doi:10.18632/oncotarget.11200

Yang, J. X., Rastetter, R. H., & Wilhelm, D. (2016). Non-coding RNAs: an introduction *Non-coding RNA and the Reproductive System* (pp. 13-32): Springer.

Yang, L., Lin, C., & Rosenfeld, M. G. (2011). A lincRNA switch for embryonic stem cell fate. *Cell Research, 21*(12), 1646-1648. doi:10.1038/cr.2011.166

Yang, M., Sun, Y., Xiao, C., Ji, K., Zhang, M., He, N., . . . Wang, Y. (2019). Integrated Analysis of the Altered lncRNAs and mRNAs Expression in 293T Cells after Ionizing Radiation Exposure. *Int J Mol Sci, 20*(12), 2968.

Yang, Y., Pan, F., Lin, G., & Huang, T. (2018, 6-8 Nov. 2018). *Comprehensive Evaluation of Distribution Network Reliability for Power Consumer Based on AHP and Entropy Combination Method.* Paper presented at the 2018 International Conference on Power System Technology (POWERCON).

Yang, Y.-H. K. (2018). Aging of mesenchymal stem cells: Implication in regenerative medicine. *Regenerative therapy, 9*, 120-122.

Yap, K. L., Li, S., Muñoz-Cabello, A. M., Raguz, S., Zeng, L., Mujtaba, S., . . . Zhou, M.-M. (2010). Molecular interplay of the noncoding RNA ANRIL and methylated histone H3 lysine 27 by polycomb CBX7 in transcriptional silencing of INK4a. *Mol Cell, 38*(5), 662-674.

Yoon, J. H., Abdelmohsen, K., Kim, J., Yang, X., Martindale, J. L., Tominaga-Yamanaka, K., . . . Gorospe, M. (2013). Scaffold function of long non-coding RNA HOTAIR in protein ubiquitination. *Nat Commun, 4*, 2939. doi:10.1038/ncomms3939

Yoon, J. H., Abdelmohsen, K., Srikantan, S., Yang, X., Martindale, J. L., De, S., . . . Gorospe, M. (2012). LincRNA-p21 suppresses target mRNA translation. *Mol Cell, 47*(4), 648-655. doi:10.1016/j.molcel.2012.06.027

Yu, K. R., & Kang, K. S. (2013). Aging-related genes in mesenchymal stem cells: a mini-review. *Gerontology, 59*(6), 557-563. doi:10.1159/000353857

Zhang, D.-y., Wang, H.-j., & Tan, Y.-z. (2011). Wnt/β-Catenin Signaling Induces the Aging of Mesenchymal Stem Cells through the DNA Damage Response and the p53/p21 Pathway. *PLoS One, 6*(6), e21397. doi:10.1371/journal.pone.0021397

Zhang, J., Hao, X., Yin, M., Xu, T., & Guo, F. (2019). Long non-coding RNA in osteogenesis: A new world to be explored. *Bone & joint research, 8*(2), 73-80. doi:10.1302/2046-3758.82.BJR-2018-0074.R1

Zhang, L., Zhou, X.-F., Pan, G.-F., & Zhao, J.-P. (2014). Enhanced expression of long non-coding RNA ZXF1 promoted the invasion and metastasis in lung adenocarcinoma. *Biomedicine & Pharmacotherapy, 68*(4), 401-407.

Zhang, P., Wu, W., Chen, Q., & Chen, M. (2019). Non-Coding RNAs and their Integrated Networks. *Journal of integrative bioinformatics, 16*(3), 20190027. doi:10.1515/jib-2019-0027

Zhang, W., Li, J., Suzuki, K., Qu, J., Wang, P., Zhou, J., . . . Belmonte, J. C. (2015). Aging stem cells. A Werner syndrome stem cell model unveils heterochromatin alterations as a driver of human aging. *Science, 348*(6239), 1160-1163. doi:10.1126/science.aaa1356

Zhang, Y.-C., Liao, J.-Y., Li, Z.-Y., Yu, Y., Zhang, J.-P., Li, Q.-F., . . . Chen, Y.-Q. (2014). Genome-wide screening and functional analysis identify a large number of long noncoding RNAs involved in the sexual reproduction of rice. *Genome biology, 15*(12), 512.

Zhu, L., & Xu, P. C. (2013). Downregulated LncRNA-ANCR promotes osteoblast differentiation by targeting EZH2 and regulating Runx2 expression. *Biochem Biophys Res Commun, 432*(4), 612-617. doi:10.1016/j.bbrc.2013.02.036

Zuo, C., Wang, Z., Lu, H., Dai, Z., Liu, X., & Cui, L. (2013). Expression profiling of lncRNAs in C3H10T1/2 mesenchymal stem cells undergoing early osteoblast differentiation. *Mol Med Rep, 8*(2), 463-467. doi:10.3892/mmr.2013.1540

III. Appendices

Appendix A

Full length sequence of transcript 1 (Gm12606)

>Gm12606-202 ENSMUSE00000774036 exon1: lncRNA

GCGAGGCTTAGGCACTTCCTCTCCCATTGAGACCAGACAAGACGGCCGGACAGAGCAGAC

CCCATCTGCTGCACACGTGCGTGCGAGGAAGCCTAGATCCAGCCGGTATATGGTCTTTGG

TTGGTGGTTCAGACTCTTAGAGCCCCATGGGTTCAG

>Gm12606-202 ENSMUSE00000739139 exon2: lncRNA

AGCTGTAACACTTGGGAAGAGATCTCTCCCGAAGAGCCGCGCACGAGTTTTCCTCACTGA

ATTGTCTCACAGAATTGGAGTTACCGAGAGAATTGTCTCACTGAATTGGAGTTACCGAGG

GACCTGGAAGGAGTGGCAGATGCTTCGTCCCCCTGCCTGCACTCACTTCCCTCGCTGGGG

CCTTCCCACCCGGCCTGGATAGAGGTCTCCGTGGAAAACTTCTGGTACCTAGGCCCACAT

CTCCCTAGAAG

>Gm12606-202 ENSMUSE00000732235 exon3: lncRNA

TGATCTCGAGGTGATCTCAAGGTGATCCTGAGGTCCTGTGGCGTGGAGAGTACTCTGGAG

CCCTTAGCGGCCTCTGCTGCGTTCAGACGGAAGATGGCGGAG

>Gm12606-202 ENSMUSE00000816732 exon4: lncRNA

ATAGTGTAGTCTTTATCAAGGAAACCGATGGAGAGAACTACAAAAAAACAGAACCAACAA

ACTGCAGAGTTGTGAAGTCCAGACCCAGCGAATCCATCTACAAAACACTCTCAAACCTAA

GGCTCTGGGGGCATTTGAGAAGAGGGGTGGAAAGACAGTATGAGCCAGAGGATCAGGAAA

TTTGCTGTGCAATTTTGTCTCCTAATGCCAGAAGCTACAACCAGAAAGTCTTCCCAACAT

GACTATCCCAAAATATTGCTGAACAAGAATGACACAGCAGATTTGACAATGTGAACAAGG

AAAAGCCCACGAAGCTTCAACTTTCCAGAAAGAACTACAAGAGTAAAGCCAGGATTGGGA

TAAGGTGGGCTTTTTTTTTTTTTTATAAGGAAGAGCACAACAATTGGTTGTCCAATGCCA

AATGGTCAGCCCTGAAAACATACATACAAATAACATTAGATGGACTGAGCTGGTTGTATT

TAGGAATGCATACAATAACAATTTATGACAAAAGATGCCATGAGTTAGAAGGAGAGGGGG

AAGGGGCATATGGTAGGGTTTGGAGGGAGAAAGGTGAAGAGAAAATATTGTAATTGTATT

ATACTCTCAAAAATAAAAAAAATACATTGTATGAAATTCTCAAAAAACTAATAAAAACGT

TGTTGTTGTTTTTAA

Full length sequence of transcript 2 (Gm12606)

>Gm12606-201 ENSMUSE00000803974 exon1: lncRNA

CTGCCTCCGAGGGTGGAGGCCTTTCCTTGTCATCAACCTCTAGGTTCTGAGGACCATCCT

CGGAAAAGCTGAACTGGAGCTCAGGGTTCAGCACGGCTGCTTACGGAGCAGCCTCGCAAT

GGAAACCTGGTTCGAGCCTCTCGCAGG

>Gm12606-201 ENSMUSE00000739139 exon2: lncRNA

AGCTGTAACACTTGGGAAGAGATCTCTCCCGAAGAGCCGCGCACGAGTTTTCCTCACTGA

ATTGTCTCACAGAATTGGAGTTACCGAGAGAATTGTCTCACTGAATTGGAGTTACCGAGG

GACCTGGAAGGAGTGGCAGATGCTTCGTCCCCCTGCCTGCACTCACTTCCCTCGCTGGGG

CCTTCCCACCCGGCCTGGATAGAGGTCTCCGTGGAAAACTTCTGGTACCTAGGCCCACAT

CTCCCTAGAAG

>Gm12606-201 ENSMUSE00000743427 exon3: lncRNA

ATAGTGTAGTCTTTATCAAGGAAACCGATGGAGAGAACTACAAAAAAACAGAACCAACAA

ACTGCAGAGTTGTGAAGTCCAGACCCAGCGAATCCATCTACAAAACACTCTCAAACCTAA

GGCTCTGGGGGCATTTGAGAAGAGGGGTGGAAAGACAGTATGAGCCAGAGGATCAGGAAA

TTTGCTGTGCAATTTTGTCTCCTAATGCCAGAAGCTACAACCAGAAAGTCTTCCCAACAT

GACTATCCCAAAATATTGCTGAACAAGAATGACACAGCAGATTTGACAATGTGAACAAGG

AAAAGCCCACGAAGCTTCAACTTTCCAGAAAGAACTACAAGAGTAAAGCCAGGATTGGGA

TAAGGTGGGCTTTTTTTTTTTTTTATAAGGAAGAGCACAACAATTGGTTGTCCAATGCCA

AATGGTCAGCCCTGAAAACATACATACAAATAACATTAGATGGACTGAGCTGGTTGTATT

TAGGAATGCATACAATAACAATTTATGACAAAAGATGCCATGAGTTAGAAGGAGAGGGGG

AAGGGGCATATGGTAGGGTTTGGAGGGAGAAAGGTGAAGAGAAAATATTGTAATTGTATT

ATACTCTCAAAAATAAAAAAAATACATTGTATGAAATTCTCAAAAAACTAATAAAAA

Appendix B

2-way ANOVA analysis results

"Table Analyzed"	Short-term expression of Gm12606 in mMSCs (log)				
"Two-way ANOVA"	Ordinary				
" Alpha"	0,05				
"Source of Variation"	"% of total variation"	"P value"	"P value summary"	Significant?	
" Interaction"	15,45	0,0132	*	Yes	
" Days [d]"	53,98	<0.0001	****	Yes	
" 0Gy vs 1 Gy (IR)"	4,752	0,0067	**	Yes	
"ANOVA table"	SS	DF	MS	"F (DFn, DFd)"	"P value"
" Interaction"	22,14	10	2,214	"F (10, 44) = 2.634"	P=0.0132
" Days [d]"	77,35	10	7,735	"F (10, 44) = 9.202"	P<0.0001
" 0Gy vs 1 Gy (IR)"	6,808	1	6,808	"F (1, 44) = 8.100"	P=0.0067
" Residual"	36,98	44	0,8406		
"Difference between column means"					
" Mean of Sham-irradiated (0Gy)"	2,490				
" Mean of Irradiated (2Gy)"	1,848				
" Difference between means"	0,6424				
" SE of difference"	0,2257				
" 95% CI of difference"	"0.1875 to 1.097"				
"Data summary"					
" Number of columns (0Gy vs 1 Gy (IR))"	2				
" Number of rows (Days [d])"	11				

"Table Analyzed"	Time and dose dependency of Gm12606 T1 in X-irradiated mMSCs					
"Two-way ANOVA"	Ordinary					
" Alpha"	0,05					
"Source of Variation"	"% of total variation"	"P value"	"P value summary"	Significant?		
" Interaction"	6,249	0,5432	ns	No		
" Dose"	46,40	0,0027	**	Yes		
" Hours after X-irradiation"	7,986	0,0576	ns	No		
"ANOVA table"	SS	DF	MS	"F (DFn, DFd)"	"P value"	
" Interaction"	0,8401	4	0,2100	"F (4, 20) = 0.7936"	P=0.5432	
" Dose"	6,238	4	1,559	"F (4, 20) = 5.892"	P=0.0027	
" Hours after X-irradiation"	1,074	1	1,074	"F (1, 20) = 4.057"	P=0.0576	
" Residual"	5,293	20	0,2647			
"Difference between column means"						
" Mean of 1.5h"	1,434					
" Mean of 72h"	1,055					
" Difference between means"	0,3784					
" SE of difference"	0,1878					
" 95% CI of difference"	"-0.01349 to 0.7702"					
"Data summary"						
" Number of columns (Hours after X-irradiation)"	2					
" Number of rows (Dose)"	5					
" Number of values"	30					

"Table Analyzed"	Time and dose dependency of T2 in X-irradiated mMSCs				
"Two-way ANOVA"	Ordinary				
" Alpha"	0,05				
"Source of Variation"	"% of total variation"	"P value"	"P value summary"	Significant?	
" Interaction"	28,41	0,0225	*	Yes	
" Dose"	30,98	0,0161	*	Yes	
" Hours after X-irradiation"	1,356	0,4156	ns	No	
"ANOVA table"	SS	DF	MS	"F (DFn, DFd)"	"P value"
" Interaction"	21,27	4	5,317	"F (4, 20) = 3.618"	P=0.0225
" Dose"	23,19	4	5,797	"F (4, 20) = 3.945"	P=0.0161
" Hours after X-irradiation"	1,015	1	1,015	"F (1, 20) = 0.6911"	P=0.4156
" Residual"	29,39	20	1,469		
"Difference between column means"					
" Mean of 1.5h"	2,410				
" Mean of 72h"	2,042				
" Difference between means"	0,3680				
" SE of difference"	0,4426				
" 95% CI of difference"	"-0.5554 to 1.291"				
"Data summary"					
" Number of columns (Hours after X-irradiation)"	2				
" Number of rows (Dose)"	5				
" Number of values"	30				

Parameter

Table Analyzed Proliferation (Presto Blue) of mMSCs (p3)

Two-way ANOVA

Source of Variation	% of total variation	P value
Interaction	15,63	0,0884
wt vs hom (Gm12606)	0,17	0,7386
days after passaging (d)	70,02	0,0007

Source of Variation	P value summary	Significant?
Interaction	ns	No
wt vs hom (Gm12606)	ns	No
days after passaging (d)	***	Yes

Source of Variation	Df	Sum-of-squares	Mean square	F
Interaction	4	9,755e+007	2,439e+007	2,753
wt vs hom (Gm12606)	1	1,043e+006	1,043e+006	0,1177
days after passaging (d)	4	4,371e+008	1,093e+008	12,34
Residual	10	8,857e+007	8,857e+006	

Number of missing values 0

Parameter
Table Analyzed yH2AX- and 53BP1 foci formation in mMSCs (p3)

Two-way ANOVA

Source of Variation	% of total variation	P value
Interaction	2,10	0,0069
wt vs hom (Gm12606)	1,46	0,0032
dose (Gy)	93,18	< 0,0001

Source of Variation	P value summary	Significant?
Interaction	**	Yes
wt vs hom (Gm12606)	**	Yes
dose (Gy)	****	Yes

Source of Variation	Df	Sum-of-squares	Mean square	F
Interaction	3	18,41	6,136	5,146
wt vs hom (Gm12606)	1	12,80	12,80	10,74
dose (Gy)	3	817,6	272,5	228,6
Residual	24	28,62	1,192	

Number of missing values 0

Parameter
Table Analyzed Repair kinetics of yH2AX- and 53BP1 foci
after irradiation in mMSCs (p3)

Two-way ANOVA

Source of Variation	% of total variation	P value
Interaction	4,14	0,0013
wt vs hom (Gm12606)	2,24	0,0022
time after irradiation [min]	89,01	< 0,0001

Source of Variation	P value summary	Significant?
Interaction	**	Yes
wt vs hom (Gm12606)	**	Yes
time after irradiation [min]	****	Yes

Source of Variation	Df	Sum-of-squares	Mean square	F
Interaction	3	0,08359	0,02786	7,201
wt vs hom (Gm12606)	1	0,04524	0,04524	11,69
time after irradiation [min]	3	1,797	0,5988	154,8
Residual	24	0,09287	0,003870	

Number of missing values 0

"Table Analyzed"	Induction of cellular senescence in mMSCs (p3)				
"Two-way ANOVA"	Ordinary				
" Alpha"	0,05				
"Source of Variation"	"% of total variation"	"P value"	"P value summary"	Significant?	
" Interaction"	3,143	0,5272	ns	No	
" Days after seeding [d]"	8,677	0,1888	ns	No	
" wt vs hom (Gm12606)"	45,55	0,0004	***	Yes	
"ANOVA table"	SS	DF	MS	"F (DFn, DFd)"	"P value"
" Interaction"	42,23	2	21,11	"F (2, 18) = 0.6635"	P=0.5272
" Days after seeding [d]"	116,6	2	58,29	"F (2, 18) = 1.832"	P=0.1888
" wt vs hom (Gm12606)"	612,1	1	612,1	"F (1, 18) = 19.23"	P=0.0004
" Residual"	572,8	18	31,82		
"Difference between column means"					
" Mean of wt (Gm12606-1+/+)"	41,13				
" Mean of hom (Gm12606-1-/-)"	31,03				
" Difference between means"	10,10				
" SE of difference"	2,303				
" 95% CI of difference"	"5.262 to 14.94"				
"Data summary"					
" Number of columns (wt vs hom (Gm12606))"	2				
" Number of rows (Days after seeding [d])"	3				
" Number of values"	24				

"Table Analyzed"	Induction of cellular senescence in mMSCs (p7)				
"Two-way ANOVA"	Ordinary				
" Alpha"	0,05				
"Source of Variation"	"% of total variation"	"P value"	"P value summary"	Significant?	
" Interaction"	4,229	0,0334	*	Yes	
" Days after seeding [d]"	2,130	0,1424	ns	No	
" wt vs hom (Gm12606)"	88,09	<0.0001	****	Yes	
"ANOVA table"	SS	DF	MS	"F (DFn, DFd)"	"P value"
" Interaction"	4	30,6	2	215,3 "F (2, 12) = 4.571"	P=0.0334
" Days after seeding [d]"	216,9	2	108,5	"F (2, 12) = 2.303"	P=0.1424
" wt vs hom (Gm12606)"	8969	1	8969	"F (1, 12) = 190.4"	P<0.0001
" Residual"	565,2	12	47,10		
"Difference between column means"					
" Mean of wt (Gm12606-1+/+)"	63,76				
" Mean of hom (Gm12606-1-/-)"	19,11				
" Difference between means"	44,64				
" SE of difference"	3,235				
" 95% CI of difference"	"37.60 to 51.69"				
"Data summary"					
" Number of columns (wt vs hom (Gm12606))"	2				
" Number of rows (Days after seeding [d])"	3				
" Number of values"	18				

Appendix C

Variety of sgRNA7-indueced mutations in mice.

Mouse		InDel [bp]
72	InDel	-256
73	InDel	-23/unknown
74	InDel	-1/-5
75	wt	-
76	InDel	-32/unkown
77	wt	-
78	unknown	unknown
79	InDel	-14/+43
80	InDel	-8
81	wt	-
82	InDel	+4/+9
83	InDel	-5
84	wt	-
85	wt	-
86	wt	-
87	wt	-
88	InDel	-7
89	wt	-
90	wt	-
91	wt	-
92	wt	-
93	wt	-
94	InDel	+1/-6

Sequencing of CRISPR/Cas9 mice reveals different mutations

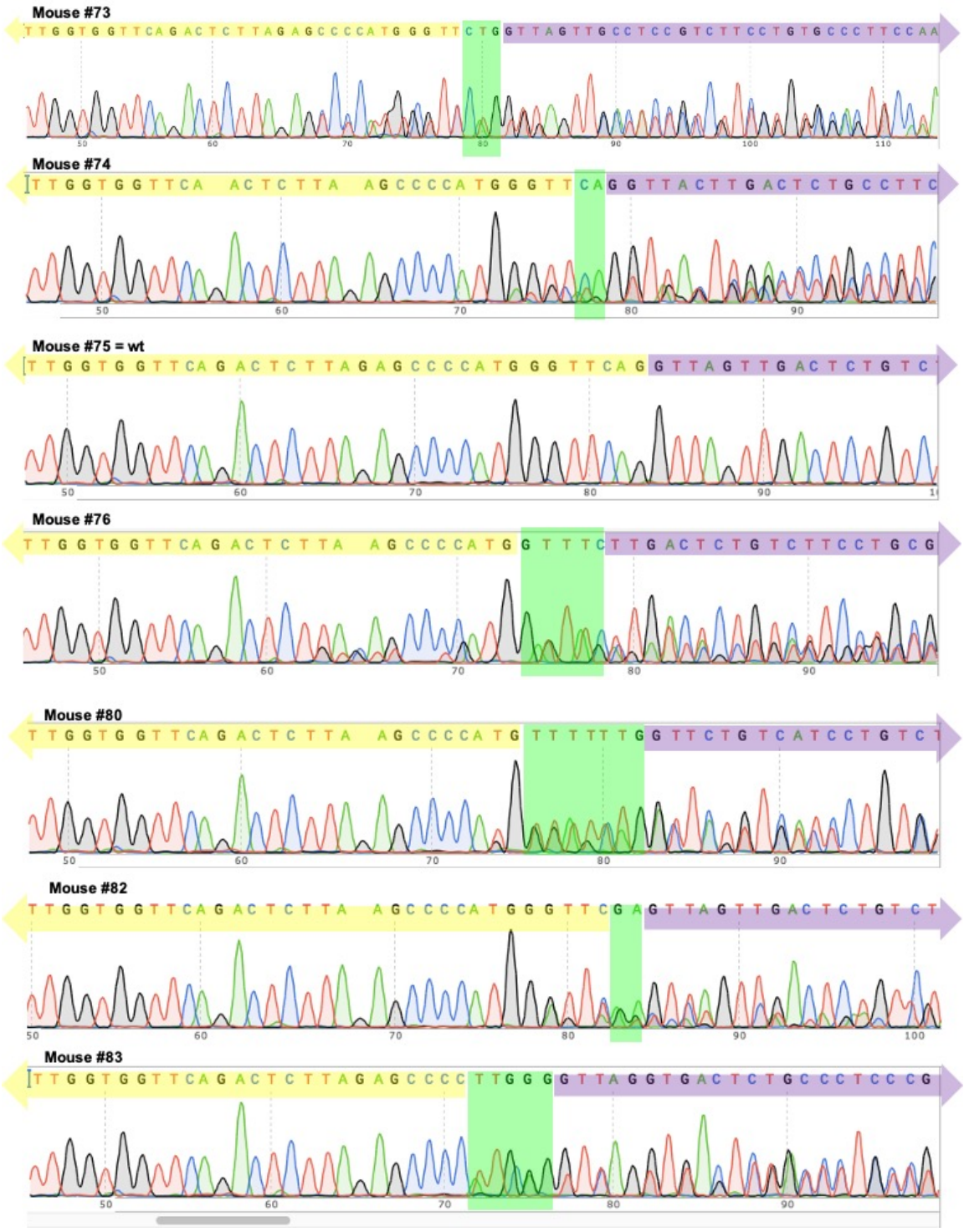

Figure 58: Sequencing results of genomic DNA from CRISPR/Cas9 mice. Sequences show different mutations from CRISPR/Cas9 *in vivo* experiment with sgRNA7. The yellow region represents exon1, while the purple region includes intron1. The green region thus represents the sites where Cas9 induced DSB breaks and where different mutations occurred. All mice presented were mut mice, except for mouse 75.

Compound heterozygosity of mouse 79

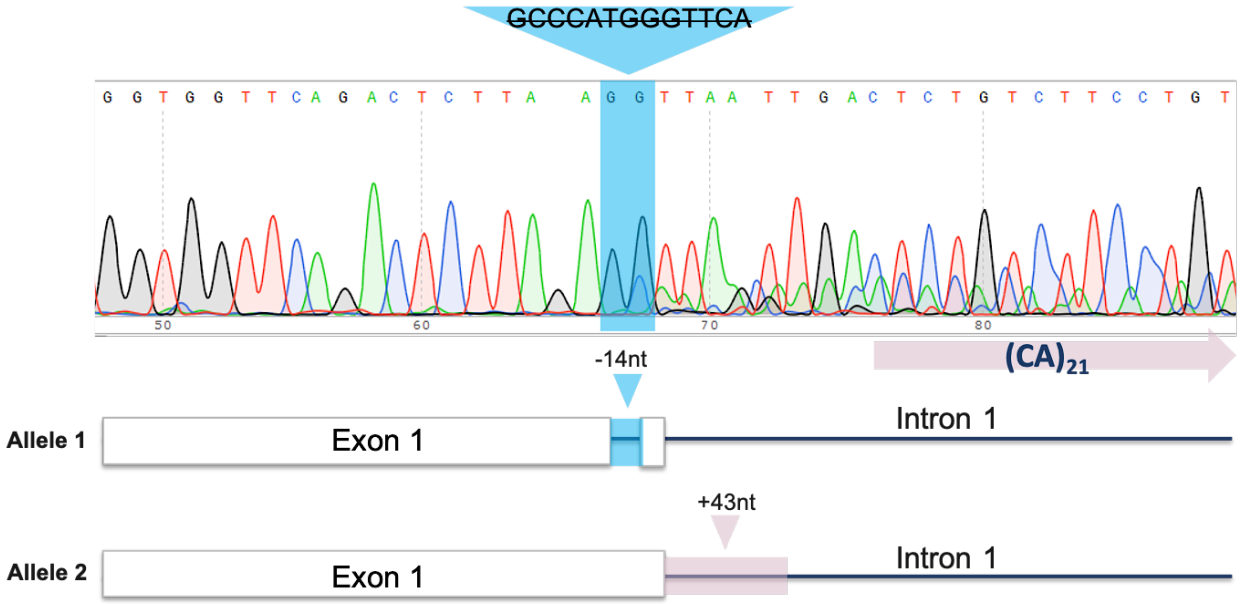

Figure 59: CRISPR/Cas9-mediated knock-in of the homologous repair template. Mouse 79 showed a partial knock-in of the homologous repair template, starting with several CA-repeats but with an interruption after 43 bp (Allele 2). The entire donor construct could not be integrated into the DNA in this study. In addition, the second allele was mutated by a 14 bp deletion (Allele 1). Mouse 79 was classified as compound heterozygous based on two mutated alleles (biallelic).

Appendix D

Secondary structure of Gm12606 transcript 1

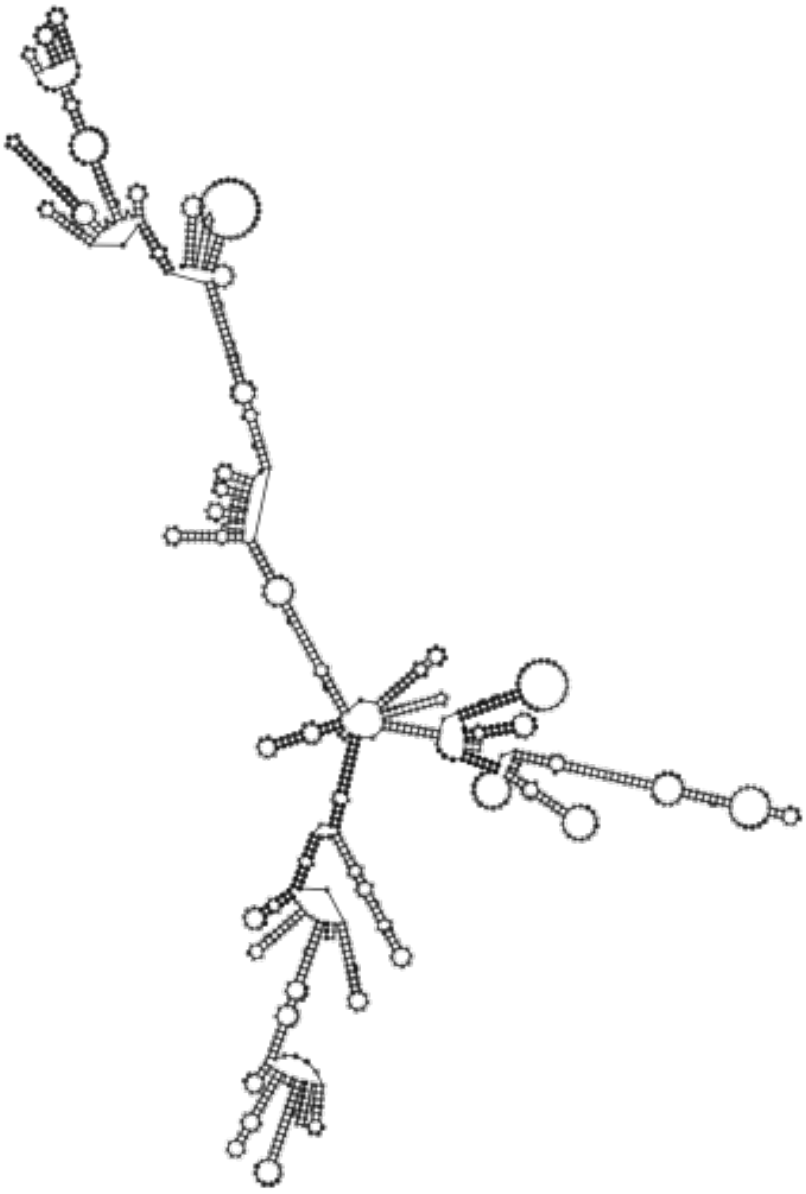

Figure 60: Secondary structure of T1. Graphical output of the predicted secondary structure of T1. Results were generated using the RNAfold webserver RNAfold 2.4.18 (http://rna.tbi.univie.ac.at/).

Secondary structure of Gm12606 transcript 2

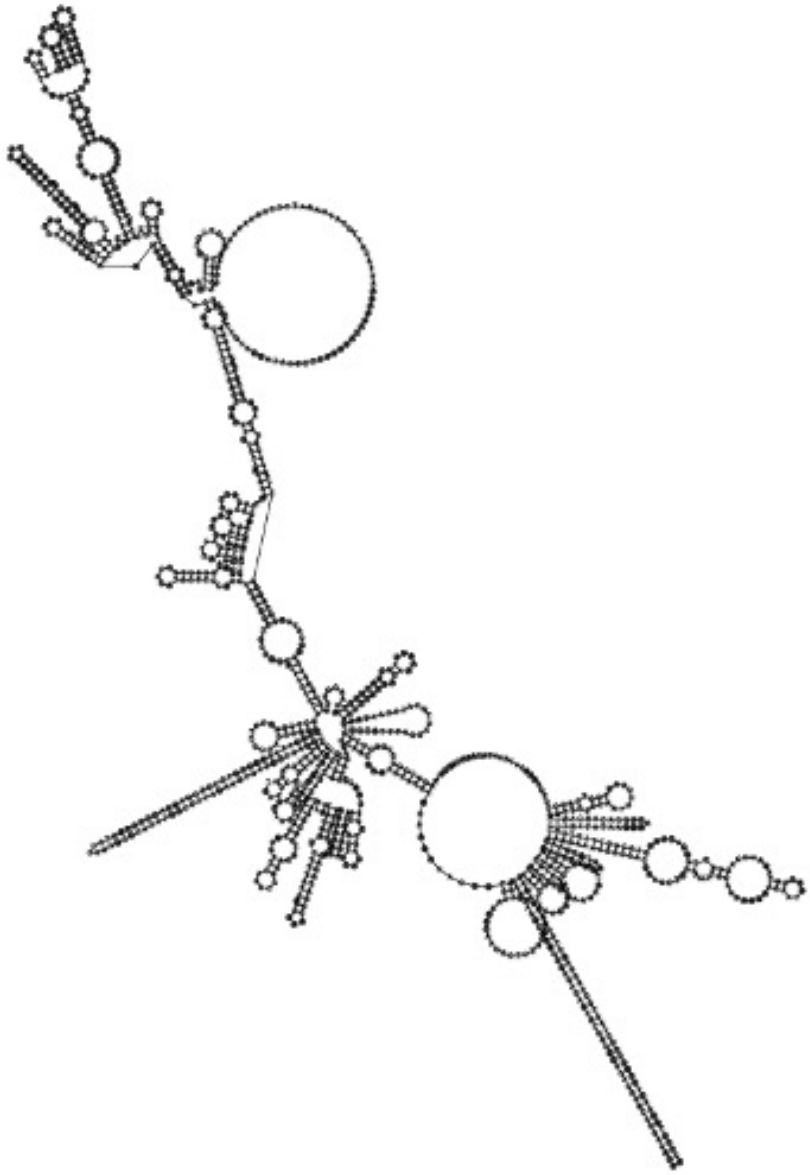

Figure 61: Secondary structure of T2. Graphical output of the predicted secondary structure of T2. Results were generated using the RNAfold webserver RNAfold 2.4.18 (http://rna.tbi.univie.ac.at/).

IV. List of Figures

List of Figures

List of Figures

V. List of Tables

VI. Acknowledgements

First and foremost, I would like to express my sincere gratitude to Dr. Michael Atkinson for his guidance throughout the whole process. His great advice let me to tackle this challenging project. I would also like to thank him for his great support throughout the last five years of my academic career. His guidance and general insights into the field have made this work an inspiring experience for me and expanded my knowledge to a new level.

I would like to say a special thanks to Dr. Michael Rosemann for his mentoring, understanding, patience, and most importantly for his friendship during the period of the research project. He constantly encouraged me and was always willing and enthusiastic to help.

I am also grateful to the members of my thesis committee, Prof. Dr. Michael Atkinson, Prof. Dr. Johannes Beckers, for their feedback and significant contribution to the progress of this project.

I am immensely thankful to all members of the Institute of Radiation Biology, especially my office mates, Daniela, Jos, Bao, Prabal, Michi for the numerous pleasant conversations, great atmosphere, and many fun memories.

I feel obliged to thank Dr. Florian Giesert for his great support in the CRISPR/Cas9 mouse experiments. He deserves a lot of credit for this challenging project.

Finally, and above all, I wholeheartedly thank my husband, parents, and parents-in-law who helped and supported me during the writing of this thesis and never losing their believe in me. Particularly for all the time they spent babysitting while I was writing this thesis.

And most importantly, I would like to thank my baby Caspar. I am so happy that you came into my world.